

Structural and Functional Models for Methane Monooxygenase

by

Xudong Feng

M.S., University of California at Davis (1987)

M.S., Nanjing University, China (1985)

B.S., Nanjing University, China (1982)

SUBMITTED TO THE DEPARTMENT OF CHEMISTRY
IN PARTIAL FULFILLMENT OF THE
REQUIREMENTS FOR THE
DEGREE OF

DOCTOR OF PHILOSOPHY

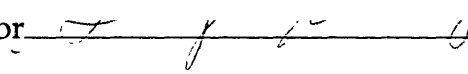
at the

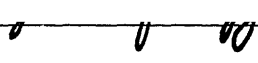
MASSACHUSETTS INSTITUTE OF TECHNOLOGY

September, 1991

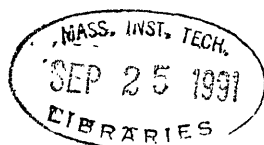
©Massachusetts Institute of Technology 1991

All rights reserved

Signature of Author  _____
Department of Chemistry
August 12, 1991

Certified by  _____
Stephen J. Lippard
Arthur Amos Noyes Professor of Chemistry
Thesis Supervisor

Accepted by _____
Glenn A. Berchtold
Chairman, Departmental Committee on Graduate Students



ARCHIVES

This doctoral thesis has been examined by a committee of the
Department of Chemistry as follows:

Professor Alan Davison _____
Chairman

Professor Stephen J. Lippard _____
Arthur Amos Noyes Professor of Chemistry
Thesis Supervisor

Professor Dietmar Seyferth _____

To

Those Who Died for a Democratic China
on the Streets of Beijing, June 4th, 1989

and to

My Grandparents

Who Taught Me Everything I Need to Know about Life

Structural and Functional Models for Methane Monooxygenase

by

Xudong Feng

Submitted to the Department of Chemistry
on August 12, 1991 in partial fulfillment of the
requirements for the degree of Doctor of Philosophy in
Chemistry

ABSTRACT

Chapter 1

Methane monooxygenase (MMO) catalyzes the conversion of methane to methanol in biological systems. It consists of three proteins, a hydroxylase, a reductase and a regulatory protein B, all of which are required for activity. Hydroxylase is the site of dioxygen activation and substrate hydroxylation. The presence of one or two dinuclear iron clusters on the hydroxylase is suggested by spectroscopic evidence, although the exact structure of these clusters remains ambiguous. Inspired by the knowledge of the enzyme system, efforts have been devoted to develop synthetic model systems by using multinuclear iron complexes to mimic the structure and the function of MMO.

Chapter 2

An oxygen donor tripod ligand, $\{\text{CpCo}[\text{OP}(\text{OEt})_2]_3\}^-$, was used to occupy the terminal coordination sites of a $\{\text{Fe}_2\text{O}(\text{OAc})_2\}^{2+}$ or a $\{\text{Fe}_2(\text{OH})(\text{OAc})_2\}^{3+}$ core, resulting in the formation of novel diiron(III) complexes with exclusive oxygen ligation, $[\text{Fe}_2\text{O}(\text{OAc})_2\{\text{CpCo}[\text{OP}(\text{OEt})_2]_3\}_2]$ and $[\text{Fe}_2(\text{OH})(\text{OAc})_2\{\text{CpCo}[\text{OP}(\text{OEt})_2]_3\}_2]^+$. The structural studies of both complexes revealed very similar core structures to their analogs with exclusive nitrogen terminal coordination except for the shorter Fe-O bonds compared to Fe-N bonds in the latter. Spectroscopic studies of μ -oxo bridged complexes, however, suggest significant effects on the electronic spectra of these complexes by changing the terminal donor atoms from

nitrogen to oxygen. The low energy band around 600 nm shifts significantly due to the variation of the ligand field strength. Resonance Raman studies on the μ -oxo bridged complexes show that the $\nu_s(\text{Fe-O-Fe})$ can be resonance enhanced to the same extent with either the nitrogen or the oxygen terminal ligands. The complex with oxygen terminal ligands is more stable under electrochemical redox conditions than its analogs with nitrogen terminal ligands. These comparisons provide structural information of the possible coordination environments of iron atoms in MMO. The electronic spectra of $[\text{Fe}_2(\text{OH})(\text{OAc})_2\{\text{CpCo}[\text{OP}(\text{OEt})_2]_3\}_2]^+$ compares favorably with that of MMO, suggesting the possibility of a hydroxo bridge in diiron clusters in the protein.

Chapter 3

Bis-chelate mononuclear iron and manganese complexes of the oxygen tripod ligand, $\{\text{CpCo}[\text{OP}(\text{OEt})_2]_3\}^-$, have been synthesized and structurally characterized by X-ray crystallography. The electrochemical studies of these complexes are reported. By comparing the redox potential of the iron complex, $[\text{Fe}\{\text{CpCo}[\text{OP}(\text{OEt})_2]_3\}_2]^+$ to other analogous iron complexes with different oxygen/nitrogen ratio in the coordination sphere, it is demonstrated that the increased oxygen content in the coordination sphere shifts the redox potential of the Fe(II)/Fe(III) couple toward more negative value. This result provides a useful benchmark for studying the ligand environment in metalloproteins.

Chapter 4

Results from detailed selectivity studies for a functional model system of MMO, $(\text{Et}_4\text{N})_2[\text{Fe}_2\text{OCl}_6]/\text{TMRA}$ or $(\text{Et}_4\text{N})_2[\text{Fe}_2\text{OCl}_6]/\text{AA}$, are summarized. Both systems catalyze the air oxidation of cyclic alkanes and benzyl C-H bonds with predominant formation of alcohols. The ratio of tertiary versus secondary C-H bond oxidation is 2.2 to 1. These product distribution patterns are different from that of a classical free radical reaction, even though the limited enantioselectivity and the incorporation of halogens observed in this system do suggest the presence of a caged radical intermediate. The catalytic reaction proceeds much faster in polar

solvents, indicating a possible charged transition state on the reaction pathway. There is no conversion between alcohols and ketones as the reaction products. The possibility of the formation of an alkyl hydroperoxide precursor is discussed.

Chapter 5

As a candidate for the catalytically active species or its precursor in the catalytic alkane oxidation system described in chapter 4, a trinuclear iron complex, $[\text{Fe}_3\text{Cl}_2(\text{TMRA})_2(\text{TMRASQ})_4]$, was isolated and characterized by X-ray crystallography and Mössbauer and other spectroscopic studies. It is a mixed-valent trinuclear iron cluster with one Fe(II) and two Fe(III) ions. The three irons in this cluster form an isosceles triangle with a single alkoxo bridge on its longer edges and two such bridges on its shorter edge. Two chloride are bound to two ferric centers, which provide potential binding sites for dioxygen in the subsequent oxygen activation step. This is the first well characterized iron complex with an analog of ascorbic acid as the ligand. The structure of this trimer serves as a useful analog to the structure of iron ascorbate complexes, which have remained unclear despite an enormous effort devoted to the structural characterization of such complexes. The crystalline iron trimer also demonstrated its catalytic activities toward air oxidation of alkanes, even though a different product distribution was observed. In the presence of excess reductant, it can catalyze the oxidation of alkanes to the same extent as the *in situ* system but with more ketone formation than that in the *in situ* system. The possible role of this complex in the catalytic system was discussed. Also isolated from the catalytic system was a tetranuclear iron-TMRA complex, $[\text{Fe}_4(\text{TMRA})_8(\text{H}_2\text{O})_4]$, whose structure has been determined by X-ray crystallography. An X-ray diffraction study was carried out on the TMRA ligand itself, affording information of the chelate properties of this ligand.

Thesis Supervisor: Stephen J. Lippard

Title: Arthur Amos Noyes Professor of Chemistry

Table of Contents

| | |
|---|------------|
| Dedication..... | 3 |
| Abstract..... | 4 |
| Table of Contents..... | 7 |
| List of Figures..... | 9 |
| List of Tables..... | 13 |
| Acknowledgements..... | 19 |
| | |
| Chapter 1. | |
| Overviews..... | 20 |
| | |
| Chapter 2. Structural Model Complexes with Exclusive Oxygen Coordination..... | 28 |
| Introduction..... | 29 |
| Experimental..... | 34 |
| Results and Discussion..... | 41 |
| Conclusions..... | 52 |
| References..... | 54 |
| Figures..... | 59 |
| Tables..... | 70 |
| | |
| Chapter 3. Mononuclear Iron and Manganese Complexes with Tripod Oxygen Ligation..... | 112 |
| Introduction..... | 113 |
| Experimental..... | 115 |
| Results and Discussion..... | 122 |
| Conclusions..... | 127 |
| References..... | 129 |
| Figures..... | 132 |
| Tables..... | 136 |
| | |
| Chapter 4. Air Oxidation of Alkanes Catalyzed by Iron-Ascorbic and Reductic Acid Complexes..... | 154 |
| Introduction..... | 155 |
| I. Reactivity and Selectivity Studies of $[\text{Fe}_2\text{OCl}_6]^{2-}$ /TMRA or $[\text{Fe}_2\text{OCl}_6]^{2-}$ /AA Catalytic Systems for Air Oxidation of Alkanes.... | 164 |

| | |
|---|------------|
| Experimental..... | 164 |
| Results and Discussion..... | 169 |
| II. Studies of Other Catalytic Systems..... | 180 |
| Experimental..... | 180 |
| Results and Discussion..... | 181 |
| Conclusions..... | 183 |
| References..... | 185 |
| Figures..... | 189 |
| Tables..... | 193 |
| | |
| Chapter 5. Structural and Physical Characterization of A Precursor of the Active Species and Other Complexes Involved in the Catalytic System..... | 201 |
| Introduction..... | 202 |
| I. X-Ray Diffraction Study of Tetramethyl Reductic Acid, C ₉ H ₁₄ O ₃ | 205 |
| Experimental..... | 205 |
| Results and Discussion..... | 207 |
| II. Synthesis and Characterization of [Fe ₃ (TMRA) ₂ (TMRASQ) ₄ CL ₂] and Its Ascorbate Analog | 210 |
| Experimental..... | 210 |
| Results and Discussion..... | 216 |
| III. X-Ray Diffraction Study of a Tetranuclear Iron Complex (Fe ₄ (TMRA) ₈ (H ₂ O) ₄]..... | 229 |
| Experimental..... | 229 |
| Results and Discussion..... | 230 |
| Conclusions..... | 232 |
| References..... | 236 |
| Figures..... | 240 |
| Tables..... | 256 |
| | |
| Appendix. Manometric Measurement of Oxygen Consumption by the Catalytic Alkane Oxidation System..... | 314 |

Chapter 2

| | | |
|--------------|--|----|
| Figure 2.1a. | ORTEP drawing of 4·2CH ₃ CN (25 °C)..... | 59 |
| Figure 2.1b. | ORTEP drawing of 4·2CH ₃ CN (-78.5 °C)..... | 60 |
| Figure 2.2. | PLUTO drawing showing the disordered model for two acetonitrile molecules in the unit cell for 4·2CH ₃ CN at 25 °C..... | 61 |
| Figure 2.3. | ORTEP drawing of 5·CH ₂ Cl ₂ ·0.5C ₇ H ₈ | 62 |
| Figure 2.4. | UV-visible spectrum of 4 in acetonitrile..... | 63 |
| Figure 2.5. | Plot of molar susceptibility (o) and effective moment (Δ) for 4. | 64 |
| Figure 2.6. | Zero field Mössbauer spectrum of 4 at 4.2 K..... | 65 |
| Figure 2.7. | (a) Raman spectrum of 4 in CH ₂ Cl ₂ solution (4.0 x10 ⁻² M). (b) Spectrum of 4 showing the shift of ν _s Fe-O-Fe upon ¹⁸ O substitution..... | 66 |
| Figure 2.8. | Excitation profiles for the methylene chloride solutions of 1 (4.38x10 ⁻² M, o) and 4 (4.29x10 ⁻² M, Δ)..... | 67 |
| Figure 2.9. | Cyclic Voltammogram of (a) 4; (b) 4 and 1 eq. of HBF ₄ ·Et ₂ O; and (c) both 4 and 6 in 0.2 M TBAP methylene chloride solution with scan speed of 200 mV s ⁻¹ | 68 |
| Figure 2.10. | Plot of electrode current versus square root of scan speed from cyclic voltammograms of 4..... | 69 |

Chapter 3

| | | |
|-------------|---------------------------|-----|
| Figure 3.1. | ORTEP drawing of 2c | 132 |
|-------------|---------------------------|-----|

| | | |
|-------------|---|-----|
| Figure 3.2. | ORTEP drawing of 3 | 133 |
| Figure 3.3. | Cyclic Voltammogram of (a) 2 ; and (b) 3 in 0.1 M TBAP acetonitrile solution..... | 134 |
| Figure 3.4. | Plot of electrode current versus square root of scan speed from cyclic voltammograms of 2 | 135 |

Chapter 4

| | | |
|-------------|---|-----|
| Figure 4.1. | Product formation in the air oxidation of cyclohexane catalyzed by the 4 /TMRA system..... | 189 |
| Figure 4.2. | Formation of cyclohexanol as the function of time in the air oxidation of cyclohexane in methylene chloride at 30 °C..... | 190 |
| Figure 4.3. | Substrate concentration effect on the reaction rate of the air oxidation of cyclohexane catalyzed by 4 /AA system at 30 °C. | 191 |
| Figure 4.4. | Comparison of the reaction rates for the halogen incorporation in the catalytic air oxidation of cyclohexane at 30 °C. | 192 |

Chapter 5

| | | |
|--------------|--|-----|
| Figure 5.1a. | ORTEP drawing of molecule 1 of 1 (24 °C)..... | 240 |
| Figure 5.1b. | ORTEP drawing of 1 (-78.5 °C)..... | 241 |
| Figure 5.2a. | Two asymmetric units in the structure of 1 (24 °C) showing the various modes of hydrogen bonding..... | 242 |
| Figure 5.2b. | Part of the packing diagram in the unit cell of 1 showing the hydrogen bonding scheme..... | 243 |
| Figure 5.3a. | Stereoview of the unit cell packing structure of 1 (24°C)..... | 244 |
| Figure 5.3b. | Stereoview of the unit cell packing structure of 1 (-78 °C)..... | 245 |
| Figure 5.4. | Structure of molecule 2 showing the atomic numbering scheme and the model used to define the disordered carbon atoms in the structure of 1 (24 °C)..... | 246 |
| Figure 5.5a. | ORTEP drawing of molecule 1 in the structure of 3 determined from the triclinic data set..... | 247 |
| Figure 5.5b. | ORTEP drawing of 3 determined from the cubic data set..... | 248 |
| Figure 5.6. | ORTEP drawing of two molecules of 3 in the triclinic unit cell showing the packing pattern and hydrogen bonding scheme..... | 249 |
| Figure 5.7. | Packing diagram of 3 in the cubic unit cell..... | 250 |
| Figure 5.8. | Raman spectrum of 3 in chloroform solution..... | 251 |

| | |
|---|-----|
| Figure 5.9. Plot of molar susceptibility (χ) and effective moment (Δ) for 3 | 252 |
| Figure 5.10. Zero field Mössbauer spectra at 80 K for (a) a solid sample and (b) a solution of 3 | 253 |
| Figure 5.11. EPR spectra of 3 in hexane solution at different temperatures..... | 254 |
| Figure 5.12. ORTEP drawing of 8 | 255 |

Chapter 2

| | | |
|--------------|--|----|
| Table 2.1. | Experimental Details of the X-ray Diffraction Studies of $\text{Fe}_2\text{O}(\text{OAc})_2\{\text{CpCo}[\text{OP}(\text{OEt})_2]_3\}_2 \cdot 2\text{CH}_3\text{CN}$ at Different Temperatures..... | 70 |
| Table 2.2. | Experimental Details of the X-ray Diffraction Study of $[\text{Fe}_2(\text{OH})(\text{OAc})_2\{\text{CpCo}[\text{OP}(\text{OEt})_2]_3\}_2][\text{BPh}_4] \cdot \text{CH}_2\text{Cl}_2 \cdot 0.5\text{C}_7\text{H}_8$ | 72 |
| Table 2.3 a. | Final Positional and Equivalent Isotropic Thermal Parameters of Non-Hydrogen Atoms in $\text{Fe}_2\text{O}(\text{OAc})_2\{\text{CpCo}[\text{OP}(\text{OEt})_2]_3\}_2 \cdot 2\text{CH}_3\text{CN}$ at 25 °C..... | 74 |
| Table 2.3 b. | Final Positional and Equivalent Isotropic Thermal Parameters of Non-Hydrogen Atoms for $\text{Fe}_2\text{O}(\text{OAc})_2\{\text{CpCo}[\text{OP}(\text{OEt})_2]_3\}_2 \cdot 2\text{CH}_3\text{CN}$ at -78.5 °C..... | 77 |
| Table 2.4 a. | Final Thermal Parameters of Non-Hydrogen Atoms for $\text{Fe}_2\text{O}(\text{OAc})_2\{\text{CpCo}[\text{OP}(\text{OEt})_2]_3\}_2 \cdot 2\text{CH}_3\text{CN}$ at 25 °C..... | 81 |
| Table 2.4 b. | Final Thermal Parameters of Non-Hydrogen Atoms for $\text{Fe}_2\text{O}(\text{OAc})_2\{\text{CpCo}[\text{OP}(\text{OEt})_2]_3\}_2 \cdot 2\text{CH}_3\text{CN}$ at -78.5 °C..... | 84 |
| Table 2.5 a. | Selected Interatomic Distances (Å) and Angles (deg) for $\text{Fe}_2\text{O}(\text{OAc})_2\{\text{CpCo}[\text{OP}(\text{OEt})_2]_3\}_2 \cdot 2\text{CH}_3\text{CN}$ at 25 °C..... | 88 |
| Table 2.5 b. | Selected Interatomic Distances (Å) and Angles (deg) for $\text{Fe}_2\text{O}(\text{OAc})_2\{\text{CpCo}[\text{OP}(\text{OEt})_2]_3\}_2 \cdot 2\text{CH}_3\text{CN}$ at -78 °C..... | 91 |

| | | |
|-------------|---|-----|
| Table 2.6. | Final Positional and Equivalent Isotropic Thermal Parameters for $[\text{Fe}_2(\text{OH})(\text{OAc})_2\{\text{CpCo}[\text{OP}(\text{OEt})_2]_3\}_2][\text{BPh}_4]\cdot\text{CH}_2\text{Cl}_2\cdot 0.5\text{C}_7\text{H}_8$ | 94 |
| Table 2.7. | Final Thermal Parameters of Non-Hydrogen Atoms for $[\text{Fe}_2(\text{OH})(\text{OAc})_2\{\text{CpCo}[\text{OP}(\text{OEt})_2]_3\}_2][\text{BPh}_4]\cdot\text{CH}_2\text{Cl}_2\cdot 0.5\text{C}_7\text{H}_8$ | 99 |
| Table 2.8. | Selected Interatomic Distances (Å) and Angles (deg) for $[\text{Fe}_2(\text{OH})(\text{OAc})_2\{\text{CpCo}[\text{OP}(\text{OEt})_2]_3\}_2][\text{BPh}_4]\cdot\text{CH}_2\text{Cl}_2\cdot 0.5\text{C}_7\text{H}_8$ | 104 |
| Table 2.9. | Comparison of Selected Structural Features of the Diiron Cores in 1 , 4 and Selected Metalloproteins..... | 107 |
| Table 2.10. | Comparison of Selected Structural Features of Known (μ -hydroxo)bis(μ -carboxylato) Diiron Complexes and MMO..... | 108 |
| Table 2.11. | Comparison of the Features of Electronic Spectra of 1 , 4 , 9 and Selected Metalloproteins..... | 109 |
| Table 2.12. | Temperature Dependence of the Observed and Calculated Molar Magnetic Susceptibilities of $\text{Fe}_2\text{O}(\text{OAc})_2\{\text{CpCo}[\text{OP}(\text{OEt})_2]_3\}_2\cdot 2\text{CH}_3\text{CN}$ | 110 |

Chapter 3

| | | |
|------------|---|-----|
| Table 3.1. | Experimental Details of the X-ray Diffraction Studies of $[\text{Fe}\{\text{CpCo}[\text{OP}(\text{OEt})_2]_3\}_2][\text{BPh}_4]\cdot\text{C}_7\text{H}_8$ and $[\text{Fe}\{\text{CpCo}[\text{OP}(\text{OEt})_2]_3\}_2]\text{ClO}_4$ | 136 |
| Table 3.2. | Final Positional and Equivalent Isotropic Thermal Parameters of Non-Hydrogen Atoms in $[\text{Fe}\{\text{CpCo}[\text{OP}(\text{OEt})_2]_3\}_2]\text{ClO}_4$ | 138 |

| | | |
|-------------|---|-----|
| Table 3.3. | Final Thermal Parameters for Non-Hydrogen Atoms in $[\text{Fe}\{\text{CpCo}[\text{OP}(\text{OEt})_2]_3\}_2]\text{ClO}_4$ | 140 |
| Table 3.4. | Selected Interatomic Distances (Å) and Angles (deg) for $[\text{Fe}\{\text{CpCo}[\text{OP}(\text{OEt})_2]_3\}_2]\text{ClO}_4$ | 142 |
| Table 3.5. | Experimental Details of the X-ray Diffraction Studies of $\text{Mn}\{\text{CpCo}[\text{OP}(\text{OEt})_2]_3\}_2$ | 144 |
| Table 3.6. | Final Positional and Equivalent Isotropic Thermal Parameters of Non-Hydrogen Atoms in $\text{Mn}\{\text{CpCo}[\text{OP}(\text{OEt})_2]_3\}_2$ | 146 |
| Table 3.7. | Final Thermal Parameters of Non-Hydrogen Atoms for $\text{Mn}\{\text{CpCo}[\text{OP}(\text{OEt})_2]_3\}_2$ | 148 |
| Table 3.8. | Selected Interatomic Distances (Å) and Angles (deg) for $[\text{Mn}\{\text{CpCo}[\text{OP}(\text{OEt})_2]_3\}_2]$ | 150 |
| Table 3.9. | Selected Geometric Parameters for Various Iron and Manganese Complexes..... | 152 |
| Table 3.10. | Reduction Potentials of Fe(III)/Fe(II) Couple in Various Iron Complexes..... | 153 |

Chapter 4

| | | |
|------------|--|-----|
| Table 4.1. | The Effect of Excess Cyclohexanol on the Formation of Cyclohexanol in the Air Oxidation of Cyclohexane Catalyzed by 4 | 193 |
| Table 4.2. | Substrates and Oxidation Products in the 4 /TMRA/O ₂ Catalytic Hydroxylation System..... | 194 |
| Table 4.3. | Typical Bond Dissociation Energies..... | 195 |
| Table 4.4. | Product Distribution for the Air Oxidation of Methyl- cyclohexane Catalyzed by 4 /TMRA System..... | 196 |

| | | |
|------------|---|-----|
| Table 4.5. | Regioselectivity of Catalytic Systems for Air Oxidation of Alkanes..... | 197 |
| Table 4.6. | ^{19}F Chemical Shifts of Various Compounds..... | 198 |
| Table 4.7. | Concentration Dependence of the Reaction Rate on 4 and Reductant in Catalytic Air Oxidation of Cyclohexane..... | 199 |
| Table 4.8. | Iron Complexes as Catalysts for Air Oxidation of Alkanes..... | 200 |

Chapter 5

| | | |
|---------------|--|-----|
| Table 5.1. | Experimental Details of the X-ray Diffraction Studies of TMRA and TMRA- CHCl_3 | 256 |
| Table 5. 2 a. | Final Positional and Equivalent Isotropic Thermal Parameters of Non-Hydrogen Atoms in TMRA at 24 °C..... | 258 |
| Table 5. 2 b. | Final Positional and Equivalent Isotropic Thermal Parameters of Non-Hydrogen Atoms in TMRA- CHCl_3 at -70 °C..... | 260 |
| Table 5.3 a. | Final Thermal Parameters of Non-Hydrogen Atoms for TMRA at 24 °C..... | 261 |
| Table 5.3 b. | Final Thermal Parameters of Non-Hydrogen Atoms for TMRA at -70 °C..... | 263 |
| Table 5.4 a. | Selected Interatomic Distances (Å) and angles (°) for TMRA at 24 °C. ^a | 264 |
| Table 5.4 b. | Selected Interatomic Distances (Å) and angles (°) for TMRA- CHCl_3 at -70 °C..... | 267 |
| Table 5.5. | Deviations (Å) of Non-hydrogen Atoms | |

| | | |
|---------------|---|-----|
| | From the Least-squares Planes Through Different Parts of the Molecules of TMRA..... | 268 |
| Table 5.6 | Experimental Details of the X-ray Diffraction Studies of $[\text{Fe}_3\text{Cl}_2(\text{C}_9\text{H}_{12}\text{O}_3)_4(\text{C}_9\text{H}_{13}\text{O}_3)_2]$ | 269 |
| Table 5.7 | Experimental Details of the X-ray Diffraction Study of $(\text{BzPh}_3\text{P})[\text{FeBr}_4]\cdot[\text{BzPh}_3\text{PBr}]$ | 271 |
| Table 5. 8 a. | Final Positional and Equivalent Isotropic Thermal Parameters of Non-Hydrogen Atoms in $[\text{Fe}_3\text{Cl}_2(\text{C}_9\text{O}_3\text{H}_{12})_4(\text{C}_9\text{O}_3\text{H}_{13})_2]\cdot 2\text{CH}_3\text{CN}$ | 273 |
| Table 5. 8 b. | Final Positional and Equivalent Isotropic Thermal Parameters of Non-Hydrogen Atoms in $[\text{Fe}_3\text{Cl}_2(\text{C}_9\text{O}_3\text{H}_{12})_4(\text{C}_9\text{O}_3\text{H}_{13})_2]$ | 279 |
| Table 5.9 a. | Final Thermal Parameters of Non-Hydrogen Atoms for $[\text{Fe}_3\text{Cl}_2(\text{C}_9\text{H}_{12}\text{O}_3)_4(\text{C}_9\text{H}_{13}\text{O}_3)]\cdot 2\text{CH}_3\text{CN}$ | 281 |
| Table 5.9 b. | Final Thermal Parameters of Non-Hydrogen Atoms for $[\text{Fe}_3\text{Cl}_2(\text{C}_9\text{H}_{12}\text{O}_3)_4(\text{C}_9\text{H}_{13}\text{O}_3)]$ | 284 |
| Table 5.10 a. | Selected Interatomic Distances (Å) and Angles (deg) for $[\text{Fe}_3\text{Cl}_2(\text{C}_9\text{H}_{12}\text{O}_3)_4(\text{C}_9\text{H}_{13}\text{O}_3)_2]\cdot 2\text{CH}_3\text{CN}$ | 286 |
| Table 5.10 b. | Selected Interatomic Distances (Å) and Angles (deg) for $[\text{Fe}_3\text{Cl}_2(\text{C}_9\text{H}_{12}\text{O}_3)_4(\text{C}_9\text{H}_{13}\text{O}_3)_2]$ | 290 |
| Table 5. 11. | Final Positional and Equivalent Isotropic Thermal Parameters of Non-Hydrogen Atoms in $[(\text{BzPh}_3\text{P})\text{FeBr}_4]\cdot\text{BzPh}_3\text{PBr}$ | 292 |
| Table 5.12. | Final Thermal Parameters of Non-Hydrogen Atoms in $(\text{BzPh}_3\text{P})[\text{FeBr}_4]\cdot[\text{BzPh}_3\text{PBr}]$ | 294 |
| Table 5.13. | Selected Interatomic Distances (Å) and Angles (deg) for $[(\text{BzPh}_3\text{P})\text{FeBr}_4]\cdot\text{BzPh}_3\text{Br}$ | 297 |

| | | |
|--------------|--|-----|
| Table 5.14. | Reaction Conditions for the Redox Titration Experiment..... | 298 |
| Table 5.15. | Mössbauer Parameters of Solid and Solution Samples of 3 at 80 K and Zero Magnetic Field..... | 299 |
| Table 5.16. | Results from the Redox Titration of Free TMRA and 3 | 300 |
| Table 5.17. | Mössbauer Parameters for the Solution Samples of Analogous Ascorbate Complexes of 3 | 301 |
| Table 5.18 | Experimental Details of the X-ray Diffraction Study of $[\text{Fe}_4(\text{H}_2\text{O})_4(\text{TMRA})_8] \cdot 1.5\text{CH}_3\text{COCH}_3 \cdot \text{H}_2\text{O}$ | 302 |
| Table 5. 19. | Final Positional and Equivalent Isotropic Thermal Parameters of Non-Hydrogen Atoms in $[\text{Fe}_4(\text{H}_2\text{O})_4(\text{C}_9\text{O}_3\text{H}_{12})_6(\text{C}_9\text{O}_3\text{H}_{13})_2] \cdot 1.5\text{CH}_3\text{COCH}_3 \cdot \text{H}_2\text{O}$ | 304 |
| Table 5. 20. | Final Thermal Parameters of Non-Hydrogen Atoms in $[\text{Fe}_4(\text{H}_2\text{O})_4(\text{C}_9\text{O}_3\text{H}_{12})_6(\text{C}_9\text{O}_3\text{H}_{13})_2] \cdot 1.5\text{CH}_3\text{COCH}_3 \cdot \text{H}_2\text{O}$ | 307 |
| Table 5.21. | Selected Interatomic Distances (Å) and Angles (deg) for $[\text{Fe}_4(\text{H}_2\text{O})_4(\text{C}_9\text{O}_3\text{H}_{12})_6(\text{C}_9\text{O}_3\text{H}_{13})_2] \cdot 1.5\text{CH}_3\text{COCH}_3 \cdot \text{H}_2\text{O}$ | 310 |
| Table 5.22. | Assignment of the Oxidation States for Ligands in 8 | 313 |

Appendix

| | | |
|------------|--|-----|
| Table A.1. | Manometric Measurements of Oxygen Uptakes by the Oxygen Binding Reaction of 1 | 319 |
|------------|--|-----|

Acknowledgements

First of all, I would like to thank my thesis supervisor Professor Stephen J. Lippard for his consistent moral support and scientific guidance. I especially appreciate his understanding and patience during the emotionally trying time for me after the 1989, June Fourth Massacre in Beijing. Without his encouragement, support and patience, this thesis would have been simply impossible.

I am deeply indebted to the following people for many helpful suggestions and enlightening discussions: Professors Jack Norton, Avi Bino, Michelle Millar, Steve Koch and Vickie McKee. Drs. M. Roth, W. Tolman, J. Bentsen, G. Whiteker, J. Protasiewicz, R. Beer, P. Turowski, L. Rardin, W. Micklitz, P. Poganiuch. Subgroup mates K. Taft, D. Goldberg, A. Rosenzweig, K. Liu, A. Feig. Special acknowledgement to Dr. W. Tolman, whose suggestion for the use of the tripod oxygen donor ligand has led to most of the works presented in Chapter 2 and 3.

I am also grateful to those coworkers who taught or assisted me with physical measurements: Drs. D. Bancroft, S. Bott, S. Liu and S. Yu (X-ray crystallography); Dr. M. Roth (GC); Dr. G. Papaefthymiou (Mössbauer and magnetic studies); Dr. J. Bentsen (Raman and EPR); Dr. A. Masschelein (Raman); Dr. L. Rardin (Computation); and Steve Bellon (HPLC). I want to thank Dr. L. Taylor at Polaroid for providing TMRA and for interesting discussions. My sincerest thanks to Kingsley Taft, David Golderberg, Andrew Feig and Kathy Liu for proof-reading my thesis.

To all Lippard group members, past and present, I appreciate all the friendship and fun times we spent together. I have especially enjoyed the companionship from the fellow graduate students in my year: Ted Carahan, Mike Keck and Steve Bellon.

Last and the most, I want to thank my husband Zhexi Luo for his constant love and support of my graduate study.

Chapter 1
Overviews

Biological oxidation of organic substrates catalyzed by metal-containing oxygenases has been of great interest to bioinorganic chemists.¹ There are two kinds of oxygenases in biological systems, namely monooxygenases and dioxygenases.^{1,2} Also known as a mixed function oxygenase, monooxygenases catalyze the oxidation reaction in which only one of the two oxygens from the molecular oxygen is incorporated into the substrate while the other oxygen is used for producing water. The best known example of monooxygenases is cytochrome P-450, an ubiquitous heme enzyme which catalyzes the hydroxylation of a large number of nonpolar substrates in both mammalian and bacterial organisms.^{3,4} Only a few monooxygenases are identified as nonheme iron containing enzymes.^{5,6} Among them is methane monooxygenase (MMO).

MMO catalyzes the conversion of methane to methanol (eq. 1.1),



which is the first step of methane assimilation in methanotrophs, a group of bacterial that utilizes methane as their sole carbon and energy source.⁷ The most thoroughly studied MMOs are isolated from two organisms, *Methylococcus capsulatus* (Bath) and *Methylosinus trichosporium* OB3b. Classified as type I and II methanotrophs, respectively, these two organisms differ only in their membrane fine structures and carbon assimilation pathways. The enzymes isolated exhibit little divergence and are considered as having similar structures at their active centers.⁷⁻⁹ The enzyme from *M. capsulatus* exists in both particular and soluble forms, the predominance of which depends on the growth conditions of the cell. These two forms of the enzymes appear to have different properties and polypeptide composition.¹⁰ It is the study of the soluble form of MMO that will be discussed here.

MMO was first identified in the early 1970's but the studies on this enzyme had been limited by the difficulties in isolating the pure and stable enzymes in the following decade.¹¹ Breakthroughs in the purification and stabilization of the enzyme in the early 1980's led to extensive studies on its structural and spectroscopic properties.^{12,13} It was found that MMO is a multiprotein enzyme consisting three proteins, a hydroxylase (A), a reductase (C) and a component B, all of which are required for efficient substrate hydroxylation. The hydroxylase, a 250 kD nonheme iron protein, is the site of oxygen activation and substrate hydroxylation. The reductase (MW 40 kD) is a flavoprotein containing one mole FAD and one Fe₂S₂ cluster per mole of protein. FAD accepts two electrons from the oxidation of NADH and subsequently pass one electron at a time to the Fe₂S₂ cluster, which in turn transfers them one at a time to the hydroxylase.^{14,15} There is no metal or prosthetic groups in component B, the function of which appears to be mainly regulatory. It controls the electron transfer process from the reductase to the hydroxylase by inhibiting the electron transfer in the absence of substrate.¹⁶ Among the three components, the hydroxylase has been the focus of structural investigation. It is a dimer comprised of three subunits, ($\alpha\beta\gamma$)₂, with the site of methane oxidation located on the α subunit.^{17,18} Evidence from Mössbauer, EPR and EXAFS studies are all consistent with the presence of a dinuclear iron cluster,^{8,19,20} similar to those observed for hemerythrin and ribonucleotide reductase but with the absence of a μ -oxo bridge in the diiron center in MMO.²¹ There are approximately two such clusters per mole of hydroxylase.⁸ Each cluster has three oxidation states: oxidized (Fe(III)Fe(III)), mixed valent (Fe(II)Fe(III)) and fully reduced (Fe(II)Fe(II)). The redox potentials of these three oxidation states are reported recently, being 48 mV vs NHE for Fe(III)Fe(III)/Fe(II)Fe(III) couple

and -135 mV for (Fe(II)Fe(III)/Fe(II)Fe(II) couple.²² The oxidized form is diamagnetic and EPR silent, indicating an antiferromagnetic coupling between the high spin Fe(III) ions. The mixed valent state has a multiple line signal below $g = 2$ and the fully reduced form, being ferromagnetically coupled, gives a EPR signal near $g = 15$.^{23,24} For the oxidized form, the optical spectrum exhibits an electronic absorption at 280 nm with no features above 300 nm. A detailed EXAFS study reveals a Fe... Fe distance of 3.42 Å and average Fe-O/N distance of 2.04 Å. The lack of a short Fe-O vector indicates the absence of a μ -oxo tribridged diiron core as observed in hemerythrin.¹⁹ The nature of the bridge between two irons remains ambiguous. The possibility of a hydroxo- or alkoxo bridge is suggested by comparing the structural and spectroscopic data of hydroxylase with that of the discrete model complexes.⁹ An oxygen-rich coordination environment around iron is also suggested by EXAFS study.¹⁹

All three components are required for efficient monooxygenation of the substrates. In a single turnover experiment, however, hydroxylation of both alkanes and alkenes is observed with the presence of the chemically reduced hydroxylase alone (yield, 10% for propane and 40% for propene).⁸ The mixed valent form of the hydroxylase, however, is much less active in the absence of reductase and component B. Yield of only 3% was observed for the hydroxylation of propane. It was discovered, after obtaining the pure enzyme, that MMO not only catalyzes the hydroxylation of alkanes but also a variety of other organic transformations, including the epoxidation of alkenes, the O-dealkylation of ethers, the oxidation and dehalogenation of alkyl halides, and the oxidation of CO to CO₂.^{11,12,25} Using the same approach as for the cytochrome-P450 system,³ a series of substrates were used for probing the reaction mechanism.²⁵ Stereochemical scrambling was

observed for the oxidation of *cis*-1,4-dimethylcyclohexane and *cis*-1,3-dimethylcyclohexane which suggests a nonconcerted reaction mechanism. Allylic rearrangement of the double bond is also demonstrated by the system using methylene cyclohexane. Together with the observation of the ring opening product when cyclopropylbenzene was used as the substrate, these results all points to a nonconcerted radical mechanism for the hydroxylation, similar to that proposed for cytochrome-P450.^{3,26} A detailed stopped-flow kinetic study shows the enzyme follows concerted-substitution mechanism.²⁷ In the catalytic cycle, methane first binds to the enzyme followed by the binding of NADH to form a ternary complex which subsequently produces NAD⁺ and reduced enzyme ternary complex. Another ternary complex is formed by coordinating molecular oxygen to the reduced enzyme-methane complex. This ternary complex breaks down to release water and methanol.

The physical separation of the hydroxylase and the reductase is a very important feature of the MMO system. Chemically, catalytic oxidation of alkane by dioxygen has always been a difficult task because most catalysts that catalyze the alkane oxidation can also accelerate the autoxidation of the reductant required to activate dioxygen. The MMO system circumvent this problem by isolating the hydroxylase, the site of dioxygen activation of dioxygen and substrate hydroxylation, from the reductase. Electrons are only transferred into the hydroxylase when needed. The electron transfer process, regulated by the protein B, is halted in the absence of substrates.

Despite the efforts described above, the structure of the iron centers, as well as catalytic mechanism, remained unclear up to date. To gain further insight of the complicated enzyme system, one valuable approach is to develop synthetic model systems, the structure or the reactivity of which

can mimic the enzyme system. Significant contribution has been made by model studies toward understanding the structure and mechanism of many other metalloproteins such as cytochrome P-450 and hemerythrin.²⁸⁻³⁰ This thesis describes the efforts to develop both structural and functional models for methane monooxygenases by using multinuclear iron complexes. Chapter 2 reports the efforts to develop structural models to study the ligand environment around the iron in the hydroxylase in MMO by synthesizing dinuclear iron complexes with novel exclusive oxygen donating ligand. The effect of the nature of the donors in the coordination sphere to the metal on the redox properties of the metal is elucidated by studying the electrochemical behaviors of several mononuclear iron and manganese complexes in Chapter 3. The fourth chapter presents the study on a functional model system of MMO, including the reactivity and selectivity studies. The isolation and characterization of a precursor of the catalytically active species and other related complexes in the catalytic system are described in Chapter 5.

Reference

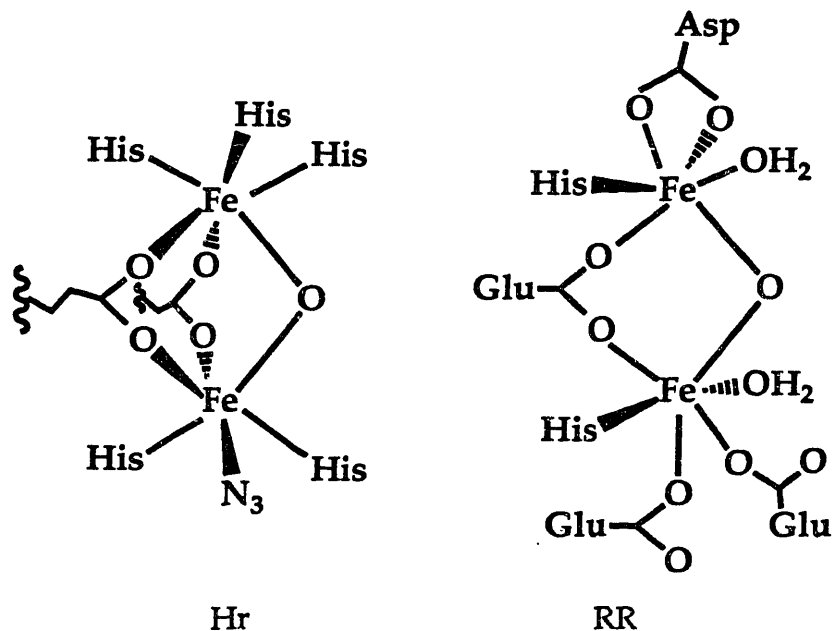
- (1) Hayaishi, O. In *Biological Oxidations*; T. P. Singer, Ed.; Interscience: New York, 1968; pp 581.
- (2) *Oxygenases*; Hayaishi, O., Ed.; Academic: New York and London, 1962.
- (3) Ortiz de Montellano, P. R. In *Cytochrome P-450, Structure, Mechanism and Biochemistry*; P. R. Ortiz de Montellano, Ed.; Plenum Press: New York and London, 1986; pp 217.
- (4) Mansuy, D.; Battioni, P. In *Activation and Functionalization of Alkanes*; C. L. Hill, Ed.; Wiley: New York, 1989; pp 195-218.
- (5) Ruettinger, R. T.; Griffith, G. R.; Coon, M. J. *Arch. Biochem. Biophys.* 1977, 183, 528.
- (6) Dalton, H.; Higgins, I. J. *Antonie van Leeuwenhoek* 1987, 53, 23-28.
- (7) Anthony, C. *The Biochemistry of Methylotrophs*; Academic Press: London, 1982.
- (8) Fox, B. G.; Froland, W. A.; Dege, J. E.; Lipscomb, J. D. *Journal of Biological Chemistry* 1989, 264, 10023-10033.
- (9) Rosenzweig, A. C.; Feng, X.; Lippard, S. J. In 1991.
- (10) Stanley, S. H.; Prior, S. D.; Leak, D. J.; Dalton, H. *Biotechnol. Lett.* 1983, 5, 487.
- (11) Dalton, H. *Oxidation of Hydrocarbons by Methane Monooxygenases form a Variety of Microbes*; Academic Press: 1980; Vol. 26.
- (12) Pilkington, S. J.; Dalton, H. *Methods in Enzymology*; Academic Press: New York, 1990; Vol. 188, pp 181-190.
- (13) Fox, B. G.; Froland, W. A.; Jollie, D. R.; Lipscomb, J. D. *Methods in Enzymology*; Academic Press: New York, 1990; Vol. 188, pp 191-202.
- (14) Lund, J.; Dalton, H. *Eur. J. Biochem.* 1985, 147, 291-296.
- (15) Prince, R. C.; Patel, R. N. *FEBS Lett.* 1986, 203, 127-130.

- (16) Green, J.; Dalton, H. *Journal of Biological Chemistry* 1985, 260, 15795-15801.
- (17) Prior, S. D.; Dalton, H. *FEMS Microbiology Letters* 1985, 29, 105-109.
- (18) Fox, B. G.; Liu, Y.; Dege, J. e.; Lipscomb, J. D. *Journal of Biological Chemistry* 1991, 266, 540-550.
- (19) DeWitt, J. G.; Bentsen, J. G.; Rosenzweig, A. C.; Hedman, B.; Green, J.; Pilkington, S.; Papaefthymiou, G. C.; Dalton, H.; Hodgson, K. O.; Lippard, S. *J. J. Am. Chem. Soc.* 101.
- (20) Fox, B. G.; Lipscomb, J. D. *Biochem. Biophys. Res. Comm.* 1988, 154, 165-170.
- (21) Vincent, J. B.; Olivier-Lilley, G. L.; Averill, B. A. *Chem. Rev.* 1990, 90, 1447.
- (22) Liu, K. E.; Lippard, S. J. *J. Biol. Chem.* 1991, 266, 12836.
- (23) Fox, B. G.; Surerus, K. K.; Münck, E.; Lipscomb, J. D. *Journal of Biological Chemistry* 1988, 263, 1053-1056.
- (24) Hendrich, M. P.; Münck, E.; Fox, B. G.; Lipscomb, J. D. *J. Am. Chem. Soc.* 1990, 112, 5861-5865.
- (25) Green, J.; Dalton, H. *Journal of Biological Chemistry* 1989, 264, 17698-17703.
- (26) Groh, S. E.; Nelson, M. J. In *Alkane Activation* VCH press: New York, 1989.
- (27) Green, J.; Dalton, H. *Biochem. J.* 1989, 259, 167-172.
- (28) Sanders-Loehr, J. In *Iron Carriers and Iron Proteins*; T. M. Loehr, Ed.; VCH: New York, 1989; pp 375-466.
- (29) Lippard, S. J. *Angew. Chem. Int. Ed. Engl.* 1988, 27, 344-361.
- (30) L. Que, J.; Scarrow, R. C. In *Metal Clusters in Proteins*; J. L. Que, Ed.; American Chemical Society: Washington, DC, 1988; pp 152-178.

Chapter 2
Structural Model Complexes with
Exclusive Oxygen Coordination

Introduction

Three non-heme iron containing proteins, namely hemerythrin (Hr), methane monooxygenase (MMO) and ribonucleotide reductase (RR), are known to undergo interesting reactions with dioxygen in biological systems. Hr is an invertebrate dioxygen carrier which binds dioxygen reversibly.^{1,2} RR is involved in the catalytic conversion of ribonucleotides into deoxyribonucleotides, the first step of DNA biosynthesis. It functions by regulating dioxygen-dependent tyrosyl radical generation.^{3,4} MMO catalyzes the hydroxylation of methane to methanol utilizing molecular oxygen.⁵⁻⁷ This group of proteins has attracted great attention among bioinorganic chemists in recent years.⁸⁻¹¹ One of the intriguing aspects about these proteins is that they share an interesting structural motif, oxygen bridged binuclear iron units, at their active site and yet perform diverse functions in their respective biological systems. X-ray crystal structures of Hr¹²⁻¹⁵ and the B2 subunit of RR¹⁶ have revealed that both proteins have an oxo- and carboxylato-bridged diiron core (Scheme 2.1.). A similar binuclear iron center is also believed to exist in MMO based on the favorable comparisons of the spectroscopic properties of MMO and that of Hr and RR.^{6,7} The diversity in the functions of these proteins, therefore, may be attributed to the different coordination environments involving the use of different terminal ligands that connect the binuclear iron cores to the polypeptide chains. It has been demonstrated by X-ray diffraction study that RR has a much more oxygen rich coordination environment around the iron center compared to that of Hr. EXAFS data for MMO also suggest the

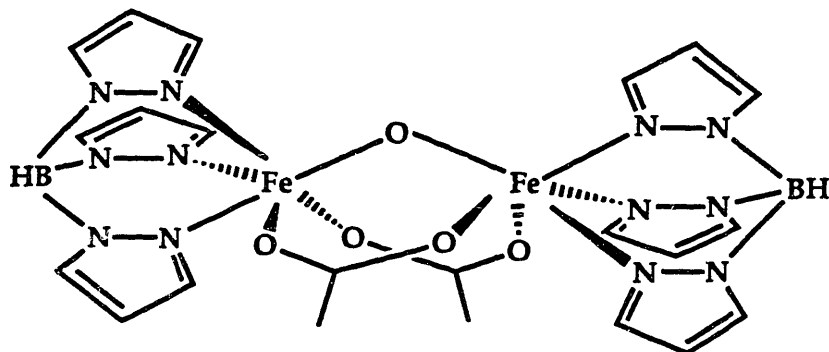


Scheme 2.1. Schematic Drawings of the Structures of
the Active Centers in Hr and RR.

existence of more oxygen coordinations to the iron center than in Hr.^{7,17,18} Oxygen donors are harder ligands compared to their nitrogen donor counterparts so an oxygen rich coordination environment should favor the higher oxidation states of the metal. Thus, the higher oxygen content in the coordination spheres around the iron atoms in RR and MMO may be responsible for their capability of activating dioxygen molecule through intermediates involving high valent iron centers rather than simply binding dioxygen as in Hr.

The synthetic modeling approach has made great contributions toward our current knowledge of the structural features and physical properties of the diiron centers in these proteins. Many (μ -oxo)bis(μ -carboxylato)diiron(III) complexes have been synthesized and characterized as mimics for the structural and spectroscopic properties of these diiron

centers.¹⁹ The first such model compound, $[\text{Fe}_2\text{O}(\text{OAc})_2(\text{HBpz}_3)_2]$ (**1**) (HBpz_3 = tri-1-pyrazolylborate) (Scheme 2.2.), was synthesized and characterized by Armstrong and Lippard in early 1980s. The complex successfully modeled



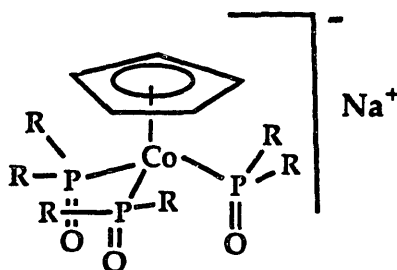
Scheme 2.2. Schematic Representation of the Molecule of **1**

many of the spectroscopic and magnetic properties of Hr.²⁰ A large number of binuclear iron complexes with the $[\text{Fe}_2\text{O}(\text{O}_2\text{CR})_2]^{2+}$ core has been prepared since then with either exclusively nitrogen donor or mixed oxygen-nitrogen donor terminal capping ligands. No compound of this kind, however, has been synthesized using exclusively oxygen donating terminal ligands. The synthesis of structurally well-defined (μ -oxo)bis(μ -carboxylato) diiron(III) complexes with an all oxygen coordination environment, therefore, is of great interest as it would complete the substitution of the all-nitrogen terminal ligand with its all-oxygen counterpart. This will provide a full reference frame for the comparison of the physical properties of the model complexes to those of the aforementioned proteins and thus allow people to obtain a more accurate picture of these diiron centers.

There are several factors which have to be taken into consideration when choosing such an oxygen donor ligand. First of all, the ligand should

have a proper "bite" to allow for comfortable facial coordination to the triply bridged binuclear core. Secondly, the ligand should carry an appropriate charge so that the desired iron complexes will not be highly charged and, therefore, easily isolated and crystallized. Thirdly, the ligand should be innocent under redox conditions so that the redox chemistry of the diiron center can be investigated. Finally, the ligand of choice should be soluble in various organic solvents which affords flexibility in handling and manipulation.

The oxygen tripod ligand, sodium bis(cyclopentadienyl)tris(diethyl phosphito-P)cobaltate, $[\text{CpCo}[\text{OP}(\text{OEt})_2]_3\text{Na}]$ (**2**) (Scheme 2.3.), is an ideal ligand which satisfies almost all the requirements described above. This ligand was synthesized by Kläui and coworkers in the early 1980s and a rich chemistry of the ligand has been developed subsequently in the same laboratory over the last decade.²¹ Ligand **2** is a monoanionic and tridentate oxygen donor with C_{3v} symmetry. The bite distance, i.e., the nonbonding



Scheme 2.3. Schematic Drawing of the Oxygen Tripod Ligand.

R = OEt in the case of **2**.

O ... O distance of the oxygen donor atoms on the P=O groups, ranges from 3.00 to 3.28 Å,²² similar to that found for the nitrogen donor atoms in the HBpz₃⁻ ligand in **1** (2.84 ~ 2.88 Å).²⁰ This geometry suggests that it is

appropriate for facially capping the terminal sites of the $\{\text{Fe}_2\text{O}(\text{OAc})_2\}^{2+}$ core. It has been shown to be an excellent ligand for the formation of complexes with many main group and transition metal ions.²¹⁻²⁵ The ligand is chemically very robust and has virtually no reactivity other than its oxygen donating functionality. Spectroscopic studies of these metal complexes characterizes **2** as having a weak ligand field and being a hard ligand which favors high formal oxidation states on the metals. Compound **2** is also soluble in a variety of solvents, ranging from water to pentane, offering great flexibility in the handling and the studying of metal complexes.

Using **2** as the terminal capping ligand and a preformed μ -oxodiiron(III) core from the starting material, $(\text{Et}_4\text{N})_2[\text{Fe}_2\text{OCl}_6]$ (**3**), the desired complex, $[\text{Fe}_2\text{O}(\text{OAc})_2\{\text{CpCo}[\text{OP}(\text{OEt})_2]_3\}_2]$ (**4**), was successfully synthesized by a spontaneous self-assembly reaction and fully characterized. Comparison of the structural features, spectroscopic properties and reactivities of **4** to that of other known analogs provides new insight into the relationship between the nature of the donor atoms on non-bridging ligands and the physical properties of the compounds. This knowledge will in turn further our understanding about the nature of the non-bridging ligands around the iron centers in metalloproteins.

The protonation of the μ -oxo bridge in **4** led to the isolation and characterization of a μ -hydroxo bridged diiron complex, $[\text{Fe}_2(\text{OH})(\text{OAc})_2\{\text{CpCo}[\text{OP}(\text{OEt})_2]_3\}_2](\text{BPh}_4)$ (**5**). This complex provides a potentially better structural model for the diiron center in MMO, since recent EXAFS studies on the hydroxylase of MMO strongly suggested the lack of oxo bridge in the diiron core at the active center.^{17,18} Viable alternatives for possible bridging ligands in MMO are proposed to be μ -hydroxo, μ -alkoxo or monodentate carboxylato groups.⁷ The unique structural features and spectroscopic

properties of **5** would be especially valuable for evaluating the proposed models of the diiron center in MMO.

Experimental

Materials. All solvents and starting materials were purchased from commercial sources and used as received without further purification unless otherwise specified. Solvents used in the electrochemical studies were special electrochemical grade or freshly distilled. The tripod ligand **2** was synthesized according to the literature procedure.^{22,26} **3** was prepared as described in the literature and recrystallized twice before use.²⁷

General Physical Measurements. UV-visible and IR spectra were recorded on a Perkin-Elmer Lambda 7 spectrophotometer or a Mattson Cygnus 400 Fourier transform spectrometer, respectively. ¹H NMR spectra were obtained using a Bruker WM250 or a Varian XL 300 instrument with tetramethylsilane as the internal standard.

Synthesis

[Fe₂O(OAc)₂(CpCo[OP(OEt)₂]₃)₂], (**4**). A 0.600 g portion of **3** (1.00 mmol) was dissolved in 20 ml of acetonitrile, and 0.400 g of NaO₂CCH₃·3H₂O (2.90 mmol) was then added; the mixture was stirred for 20 minutes. Excess sodium acetate was used to ensure the formation of the (μ-oxo)bis(μ-carboxylato)diiron(III) core. An acetonitrile solution of **2** (1.10 g, 1.97 mmol, 20 ml) was slowly added to the reaction mixture. The brown orange solution changed color to dark red upon stirring for one hour. The reaction mixture was then filtered and concentrated. Slow cooling to -20 °C afforded large red prisms of **4** (0.80 g, 57%). Anal. Calcd. for C₃₈H₇₆P₆O₂₃Co₂Fe₂: C, 34.65; H, 5.82; Fe, 8.48; P, 14.22; N, 0.0; Cl, 0.0. Found

C, 34.03; H, 5.90; Fe, 8.70; P, 13.82; N, 0.0; Cl, 0.0. FTIR (KBr, cm^{-1}): 2978, 2929, 2905, 2860, 1578, 1425, 1389, 1162, 1123, 1096, 1076, 1036, 933, 832, 761, 729, 592. ^1H NMR (250 MHz, 297 K, CDCl_3): δ 10.0 (CH_3 , acetate), 5.10 (C_5H_5), 4.08 (CH_2), 1.26 (CH_3) ppm.

$[\text{Fe}_2(\text{OH})(\text{OAc})_2\{\text{CpCo}[\text{OP}(\text{OEt})_2]_3\}_2](\text{BPh}_4)$, (5). A 13.2 mg portion of 4 (0.01 mmol) was dissolved in acetonitrile and 1 equivalent of toluenesulfonic acid was added to the solution. The orange colored solution turned yellow immediately. Sodium tetraphenylborate (3.45 mg, 0.01 mmol) was subsequently added with stirring. The acetonitrile was then removed from the reaction vessel *in vacuo* and the greenish-yellow residue was redissolved in a mixture of methylene chloride and toluene and recrystallized at $-20\text{ }^\circ\text{C}$. Two different kinds of crystals formed, one green and the other orange in color. Subsequent X-ray diffraction studies revealed that the orange crystals were complex 5 and the green ones were the monomeric complex, $[\text{Fe}\{\text{CpCo}[\text{OP}(\text{OEt})_2]_3\}_2](\text{BPh}_4)$ (6), which will be discussed in Chapter 3.

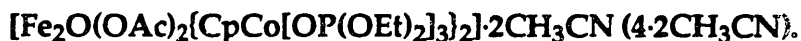
X-ray Diffraction Studies. All data were collected on an Enraf-Nonius CAD4 diffractometer with graphite monochromatized Mo $\text{K}\alpha$ radiation ($\lambda = 0.70926\text{ \AA}$).

X-ray diffraction studies of 4 were carried out at both room temperature ($25\text{ }^\circ\text{C}$) and low temperature ($-78.5\text{ }^\circ\text{C}$). A crystal of dimensions $0.4 \times 0.3 \times 0.4\text{ mm}$ was mounted in a 0.4 mm capillary tube for the room temperature X-ray diffraction study while at $-78.5\text{ }^\circ\text{C}$, a crystal was mounted on the tip of a glass fiber with silicon grease. The crystals isolated from acetonitrile appeared visually to lose solvent slowly at room temperature. No decay in the intensities of three standard reflections was observed in either case during the data collection. Lorentz and polarization corrections

were applied to both data sets. For the room temperature structure, an analytical absorption correction was applied. Experimental details of the X-ray diffraction studies of **4** at both temperatures are recorded in Table 2.1.

The orange crystals of **5** appeared to be stable in air at room temperature. A crystal of dimensions 0.2 x 0.4 x 0.4 mm was mounted on a glass fiber with silicon grease. The data were collected at -78 °C. No decrease in the intensities of three standard reflections was observed. Lorentz and polarization correction were applied to the data, as was an empirical absorption correction calculated from the psi-scan data. Table 2.2 gives the experimental details of the X-ray diffraction study of **5**.

Structure Solution and Refinement. All computations were performed on either a DEC VAXstation II or a DEC VAXstation 3100.



For the data set obtained at 25 °C, the structure of **4** was solved by using the direct method option of SHELX-86.²⁸ The neutral and hydrogen atom scattering factors were taken from the literature.^{29,30} The positions for the iron and cobalt atoms were determined from the initial electron density map. All other non-hydrogen atoms were located on the difference Fourier map. The structure was refined by using the full matrix least-squares program in TEXSAN.³¹ All non-hydrogen atoms were refined anisotropically. Hydrogen atoms were calculated in idealized positions with the C-H distances set equal to 0.95 Å. The thermal parameters of hydrogen atoms were fixed at $1.2 \times B_{\text{eq}}$, where B_{eq} is the equivalent isotropic thermal parameter of the attached carbon atom. The ethyl and Cp groups, as well as two acetonitrile molecules were severely disordered. The disordered acetonitrile molecules were successfully modeled, while the Cp rings and ethyl groups could not be modeled. As a result, the anisotropic thermal

parameters of the carbon atoms on the disordered ethyl groups, such as C222 and C232, in **4** are larger than normal. No hydrogen atoms were assigned to the disordered carbon atoms of the Cp rings or ethyl groups. At convergence, the largest ratio of parameter shift to estimated standard deviation was 0.02. The final R factors are given in Table 2.1. The largest residual peak, $0.73 \text{ e}/\text{\AA}^3$, was located near a phosphorus atom in **4**. Final atomic coordinates and the equivalent isotropic thermal parameters for non-hydrogen atoms are given in Table 2.3 a. Anisotropic thermal parameters for non-hydrogen atoms are listed in Table 2.4 a. Selected bond lengths and angles are collected in Table 2.5 a.

For the data set obtained at $-78.5 \text{ }^\circ\text{C}$, the iron and cobalt atoms were located on the first electron density map generated by the program MITHRIL.³² Other non-hydrogen atoms were found on the difference Fourier map following a scale factor refinement. Hydrogen atoms were calculated in idealized positions with carbon-hydrogen distances of 0.95 \AA . Refinement of the structure was carried out by using the full matrix least-squares program in TEXSAN.³¹ All non-hydrogen atoms were refined anisotropically. The thermal parameters of the hydrogen atoms were fixed at $1.2 \times B_{\text{eq}}$, where B_{eq} is the equivalent isotropic thermal parameter of the attached carbon atom. The solvent molecules were not disordered in this structure. One of the Cp rings was slightly disordered and successfully modeled by using the rigid group option in the TEXSAN program. The ethyl groups, however, were still disordered, and again the disorders could not be modeled except for a single ethyl group. At the convergence, the largest ratio of parameter shift to estimated standard deviation was 0.022. The R factors are listed in Table 2.1. The largest unassigned peak in the final difference map was $1.62 \text{ e}/\text{\AA}^3$, located near one of the cobalt atoms in the

ligand. Final atomic coordinates and the equivalent isotropic thermal parameters for non-hydrogen atoms are given in Table 2.3 b. Anisotropic thermal parameters for non-hydrogen atoms are listed in Table 2.4 b. Selected bond lengths and angles are collected in Table 2.5 b.

$\{\text{Fe}_2(\text{OH})(\text{OAc})_2[\text{CpCo}[\text{OP}(\text{OEt})_2]_3]_2\}[\text{BPh}_4] \cdot \text{CH}_2\text{Cl}_2 \cdot 0.5 \text{C}_7\text{H}_8$ ($5 \cdot \text{CH}_2\text{Cl}_2 \cdot 0.5 \text{C}_7\text{H}_8$). The structure of **5** was solved by using the program MITHRIL.³² All non-hydrogen atoms were found on the difference Fourier map. Hydrogen atoms were calculated, using idealized carbon-hydrogen distances of 0.95 Å and their thermal parameters were fixed at $1.2 \times B_{\text{eq}}$, where B_{eq} is the equivalent isotropic thermal parameter of the attached carbon atom. The refinement for the structure was carried out by using the full matrix least-squares program in TEXSAN.³¹ All non-hydrogen atoms were refined anisotropically except for the carbon atoms on several disordered ethyl groups. The disordered ethyl groups were modeled and refined isotropically. No hydrogen atoms were generated for the carbon atoms on the disordered ethyl groups. The toluene solvent molecule was also disordered and refined by using the rigid group option in the TEXSAN program. At the convergence, the largest ratio of parameter shift to esd was 0.10. The R factors are given in Table 2.2. The largest residual peak on the final difference map, 1.88 e/Å³, was located near a carbon atom of the disordered toluene molecule. Final atomic coordinates and the equivalent isotropic thermal parameters for non-hydrogen atoms are given in Table 2.6. Anisotropic thermal parameters for non-hydrogen atoms are listed in Table 2.7. Selected bond lengths and angles are collected in Table 2.8.

Magnetic Susceptibility Measurement of 4. Solid state magnetic susceptibility measurements on 32.4 mg of crystalline sample were carried out with an S. H. E. Model 905 SQUID-type susceptometer at 10 kG. A total

of 38 data points was taken between 6.0 and 300 K. The silicon-aluminum sample holder used in the experiment was also measured at the same 38 temperature points, and its moment subtracted from that observed with sample present. At four different temperatures the magnetic moment was measured as a function of field between 1.0 and 50.0 kG and no field dependence of the magnetic moment was observed. The solution magnetic susceptibility was measured in CDCl_3 by the Evans NMR method at 298 K.³³⁻³⁶ The mass susceptibility of CDCl_3 was approximated by using the value for CHCl_3 ($-0.497 \times 10^{-6} \text{ emu G}^{-1} \text{ g}^{-1}$).³⁷ A diamagnetic correction for **4** of $-797.5 \times 10^{-6} \text{ emu G}^{-1} \text{ mol}^{-1}$ was calculated by using Pascal's constants and constitutive corrections.^{38,39}

Mössbauer Study of 4. Mössbauer spectra were recorded by Dr. G. Papaefthymiou in Bitter National Magnet laboratory using a conventional constant acceleration spectrometer equipped with a temperature controller maintaining temperatures within ± 0.1 K. A source of ^{57}Co in Rh was employed. Spectra were recorded at zero field and at 4.2 K and 80 K, respectively. There were no major differences in the spectra recorded at different temperatures.

Resonance Raman Studies of 4. Raman spectra were recorded by using a Spex double monochromator with an RCA photomultiplier tube and a Model 1455 photodiode array detector. Laser lines from an argon or krypton Innova laser with wavelengths of 350.7, 356.4, 406.7, 413.1, 457.9, 488.0, 514.5 nm were used. The power of the laser beam was adjusted to 60 mW incident at the sample except for 413.1 nm excitation, where 40 mW power incident at the sample was used. Slits were set for 200/250/200 μm . The sample was prepared as a 0.043 M methylene chloride solution of **4** and sealed in a NMR tube. Relative Raman scattering intensities were calculated

as the ratio of the molar scattering intensities (peak height/concentration) of the ν_s (Fe–O–Fe) mode at 510 cm^{-1} to the molar scattering intensities of the methylene chloride peak at 704 cm^{-1} . ^{18}O substitution into the oxo bridge in **4** was made by stirring an acetonitrile solution of **4** with excess $^{18}\text{OH}_2$ for 24 hours in a Schlenk flask under Argon. The solvent was removed *in vacuo* and the residue redissolved in vigorously dried acetonitrile or methylene chloride. The resulting solution was then sealed in a NMR tube for Raman study. A sample of a 0.043 M methylene chloride solution of **1** was also prepared by the same procedure described above and studied for the purpose of comparison.

Electrochemical Studies of 4. Cyclic voltammetry experiments were performed by using a PAR Model 173 potentiostat and with a Houston Instruments Model 2000 X-Y recorder. Data were recorded in methylene chloride using 0.1M tetrabutylammonium perchlorate (TBAP) as the supporting electrolyte. A glassy carbon working electrode, a platinum wire auxiliary electrode and a Ag/AgCl reference electrode were used in the system. Measurements were made at room temperature under a N_2 flow. The electrode performance was monitored by examining the Fe(II)/Fe(III) couple of ferrocene added to the solution.

Reactivity Studies of 4.

Air oxidation of cyclohexane was attempted with **4** as the catalyst and zinc powder as reductant. Under N_2 atmosphere, 28.4 mg of **4** (2.16×10^{-5} mol) was dissolved in 10 ml of dried acetonitrile, and 0.18 g of zinc powder and 5 ml of cyclohexane were added. Methylbenzoate was used as internal standard. A $5\mu\text{l}$ portion of $\text{HBF}_4 \cdot \text{Et}_2\text{O}$ was added to the mixture before the reaction vessel was opened to dried air. The oxidation reaction was allowed

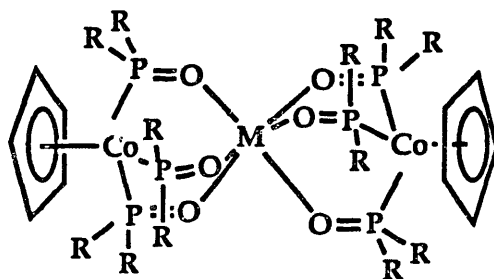
to proceed for several hours and the formation of the products was periodically monitored by GC.

The reaction between **4** and aqueous hydrogen peroxide was studied by using low-T UV-Vis spectroscopy. In a home-made low-T UV-visible cell, 10 μl of H_2O_2 (30% aq.) was added to a methylene chloride solution of **4** at $-78\text{ }^\circ\text{C}$. The system was allowed to warm slowly, whereupon a purple color developed. The UV-Vis spectrum was taken. Further increases in the temperature above $-20\text{ }^\circ\text{C}$ caused the rapid loss of the purple color to form a pale yellow solution.

The reaction between **4** and a strong oxidizing reagent, $(\text{NH}_4)_2\text{Ce}(\text{NO}_3)_6$, was carried out as follows: 37.9 mg of **4** (0.027 mmol) was dissolved in methylene chloride and 14.9 mg of $(\text{NH}_4)_2\text{Ce}(\text{NO}_3)_6$ (1 eq.) was added. No reaction occurred at first because the ceric salt was not soluble in methylene chloride. Addition of a few drops of acetonitrile resulted in the immediate change of the color of the solution from red to yellow. The UV-visible spectrum was recorded and crystallization of the product was attempted at $-20\text{ }^\circ\text{C}$.

Results and Discussion

Synthesis. It is well known that the tripod ligand **2** readily forms bis-chelate complexes (Scheme 2.4.) with many metals.^{21,23,24,40} Attempts to synthesize **4** from mononuclear iron precursors such as $\text{Fe}(\text{ClO}_4)_3 \cdot 3\text{H}_2\text{O}$, together with sodium acetate and **2** in aqueous solution, gave the



Scheme 2.4. Schematic Drawing of the Sandwich-type of Metal Complex Formed Between **2** and Transition Metals.

(M = Fe, Co, Ni, Cu, Zn, Cd, Mg, Sn, Bi, Ga, Ca, Hg, Sr, Ba)

mononuclear complex **6** (see detailed discussion in Chapter 3). To avoid the formation of the monomeric species, it proved necessary to preform the binuclear core before the addition of **2**. Therefore it is very important that excess sodium acetate is used and that the mixture of **3** and sodium acetate is stirred for twenty minutes before the addition of **2**. Attempted ligand exchange reactions between **2** and **1**, as well as another binuclear compound, $[\text{Fe}_2\text{O}(\text{MPDP})(4,4'\text{-Me}_2\text{bipy})_2\text{Cl}_2]$ (MPDP = *m*-phenylene dipropionate),⁴¹ were not successful.

It has been demonstrated that the oxo bridge in binuclear iron complexes can be protonated to form the hydroxo bridge.⁴² The oxo bridge in **4** was found to be susceptible to protonation. Addition of several different proton donors, including toluenesulfonic acid ($\text{pK}_a \sim 4$), 3-[*N*-morpholino]propanesulfonic acid ($\text{pK}_a = 7.2$) and methanol ($\text{pK}_a = 16$), leads to protonation of the oxo bridge. Formation of the byproduct **6**, which results from decomposition of the $[\text{Fe}_2\text{O}(\text{OAc})_2]^{2+}$ core, suggests that trace

amounts of water in the system can act as potential proton source as well. The protonation of the oxo bridge in **4** with weak acids contrasts greatly with its analog **1**, which uses a strong acid for protonation. Given the difference in the coordination sphere of the iron in these two complexes, it appears that the existence of more terminal oxygen donors gives a more basic μ -oxo bridge. A similar phenomenon may be found in the case of MMO, where the oxygen rich environment of the iron centers makes the existence of μ -hydroxo bridge species more feasible, even at relatively high pH (~ 7).

Structural Features of 4. The X-ray diffraction study of **4** was at first carried out at 25 °C. It was found, however, that two acetonitrile solvent molecules in the unit cell were severely disordered at 25 °C. Another data set was then collected at -78.5 °C in the hope of minimizing the disorder problem. No major differences in the structural features of the molecule were observed at the two different temperatures. The molecular structure of **4** determined from the room temperature X-ray diffraction study is shown in Figure 2.1. Features of the (μ -oxo)bis(μ -acetato) core in **4** are similar to those in **1**, the analogous complex with exclusive nitrogen terminal coordination. Table 2.9 gives selected structural features for **4** at both 25 °C and -78.5 °C, as well as for **1** for comparison purposes. Both **1** and **4** exhibit distorted octahedral geometry around the iron atoms. The deviation of the O-Fe-O angles from the ideal of 90° ranges from 90.4° to 96.8°. The Fe-O_{oxo} bond lengths and Fe-O_{oxo}-Fe angles in **4** are very similar to those in **1**. The lengthening of the Fe-ligand bonds trans to the short μ -oxo bridge as a result of the structural "trans effect"⁴³ are clearly demonstrated in **4**. The average Fe-O bond length trans to the μ -oxo bridge is 0.04 ~ 0.07 Å longer than the corresponding average bond length cis to the μ -oxo bridge. The Fe...Fe distance in **4** (3.174 Å) is slightly longer than that in

1 (3.146 Å). In general, change of terminal ligands from nitrogen to oxygen coordination does not greatly affect the $\{\text{Fe}_2\text{O}(\text{OAc})_2\}^{2+}$ core. The average terminal Fe-O bonds in 4 (2.10 Å), however, are significantly shorter than the analogous Fe-N bonds in 1 (2.17 Å). This result agrees with the criterion used to assign oxygen versus nitrogen donor in EXAFS studies of the iron-containing proteins.¹⁰ The composite Fe-O, N bond length in MMO is much shorter than the corresponding bond length in Hr and similar to that in RR (Table 2.9), which suggests the existence of an oxygen-rich coordination environment for the iron centers in MMO.

The two acetonitrile molecule in the unit cell were severely disordered in the room temperature structure. The disorder was modeled as shown in Figure 2.2. The nitrogen and carbon atom occupancies are given in parentheses. The disordered terminal methyl group of the ethyl group connected with O12 (see Figure 2.1. for the labels of the atoms) was modeled to two positions, with a refined occupancy of 0.4 and 0.6, respectively. The structure obtained at -78.5 °C was much better behaved. Two acetonitrile solvent molecules were not disordered. One of the Cp rings was disordered but was successfully refined into two positions, each being assigned an occupancy of 0.5. Several disordered ethyl groups were also modeled.

Structural Features of 5. Protonation of the μ -oxo bridge in 4 dramatically changed several structural features of the binuclear core. Figure 2.3 shows the molecular structure of 5. The Fe-O_{OH} distances (av. 1.963 Å) was much longer than the Fe-O_{oxo} bond length in 4 (1.795 Å). As a result, the Fe...Fe distance in 5 (3.474 Å) was also much longer than that in 4 (3.174 Å). The *trans* effect was no longer unambiguously demonstrated in the structure of 5. The average Fe-O bond length trans to the hydroxo bridge

(2.0018 Å) was only slightly longer than the average Fe-O bond length cis to the hydroxo bridge (1.988 Å). The only other structurally characterized (μ -hydroxo)bis(μ -carboxylato)diiron(III) compound in the literature is $\{[\text{Fe}_2(\text{OH})(\text{OAc})_2(\text{HBpz}_3)_2]\text{ClO}_4\}$ (7), an analog of 5 with exclusive nitrogen terminal coordination.⁴² Comparisons of the structural features of 5, 7 and the diiron center in the hydroxylase of MMO are given in Table 2.10. The features of the $\{\text{Fe}_2(\text{OH})(\text{OAc})_2\}^{3+}$ core in 5 and 7 are very similar. The Fe...Fe distances are quite close to the Fe...Fe distance observed for MMO in EXAFS studies. As found in the cases of 4 and 1, the average terminal Fe-O bonds in 5 are significantly shorter than the average terminal Fe-N bonds in 7.

Electronic Spectra. Compound 4 dissolves in acetonitrile or methylene chloride to give a red solution while a green solution is formed in chloroform. Figure 2.4 gives the UV-vis spectrum of 4 in acetonitrile. Table 2.11 summarizes the UV-vis and near IR data for 4 in the three solvents mention above and, for comparison propose, the corresponding data for two other diiron complexes, 1 and $[\text{Fe}_2\text{O}(\text{O}_2\text{CH})_4(\text{BIPhMe})_2]$ (8) (BIPhMe = 2,2'-bis(1-methylimidazolyl) phenylmethoxymethane),⁴⁴ as well as the data for several proteins. Complexes 1, 4 and 8 all have the same $\{\text{Fe}_2\text{O}(\text{O}_2\text{CR})_2\}^{2+}$ core. Their terminal coordination sites, however, are occupied by the three nitrogen donors, the mixed nitrogen/oxygen donors three oxygen donors, respectively. Thus, 1, 4 and 8 are ideal candidates to evaluate the effect of the terminal ligands on the electronic spectra of the complexes. A significant blue shift occurs for the lowest energy band in the visible region as the oxygen content in the terminal ligands increases. The resonance, assigned as the ${}^6\text{A}_1 \rightarrow {}^4\text{T}_2(4\text{G})$ or a charge transfer transition,²⁰ is found at 695 nm in 1 and shifted to 662 nm in 8 and below 600 nm in 4.

This shift can be attributed to the weaker ligand field strength of the oxygen donor ligands compared to the nitrogen donor ligands upon coordination to high spin iron(III) centers. This result agrees with previous studies on the oxygen tripod ligand, which ranked the ligand among the weakest oxygen donor ligand, similar to F^- in the spectrochemical series.²¹ The same trend is reflected in the electronic spectra of Hr and RR as shown in Table 2.11. This spectroscopic feature, which is closely related to the nature of the non bridging ligands, provides a new benchmark for studying the diiron center in proteins. A weak absorption in near-IR region was observed for **4**, similar to that had been observed in **1**.

Protonation of the oxo bridge in **4** causes the disappearance of all the absorption bands in the visible region. The UV-vis spectrum of **5** in acetonitrile only showed one peak at 330 nm, which is the same energy as the transition observed in the free ligand. It is interesting to note that the UV-vis spectrum of the hydroxylase of MMO also exhibits no absorption bands above 300 nm.⁷ This result suggest that the possibility of a hydroxo bridge in the diiron cluster in MMO cannot be ruled out.

Magnetic Susceptibility Measurement and Mössbauer Studies of 4. The temperature-dependent solid state magnetic susceptibility of **4** was measured between 6 and 300 K, data for which are shown in Figure 2.5. The molar susceptibilities, χ_M (emu G⁻¹ mol⁻¹), and μ_{eff} per iron versus temperature are plotted, with the least-squares fit shown as the solid line. The numerical data are also tabulated in Table 2.12. The expression for the temperature-dependent susceptibility used to fit the data is derived from the general isotropic exchange Hamiltonian $H = -2J S_1 \cdot S_2$ with $S_1=S_2=5/2$, and is given in eq. 2.1, where TIP is the temperature-independent

$$\chi_M = C \frac{2e^{2x} + 10e^{6x} + 28e^{12x} + 60e^{20x} + 110e^{30x}}{1 + 3e^{2x} + 5e^{6x} + 7e^{12x} + 9e^{20x} + 11e^{30x}} + \text{TIP} + \rho \frac{4.40}{T} \quad (2.1)$$

$C = 2Ng^2\mu_B^2/kT$, where N = Avogadro's number, g = magnetogyric ratio, μ_B = Bohr magneton, k = Boltzmann's constant, T = temperature

paramagnetism and p is the mole percentage of a paramagnetic Fe(III) impurity. With g fixed at 2.00, the best fit to the data for **4** gave $J = -108.5$ (4) cm^{-1} , $\text{TIP} = 3.0$ (1) $\times 10^{-4}$ $\text{emu G}^{-1} \text{mol}^{-1}$, $p = 5.94$ (3) $\times 10^{-3}$ with $\text{CC} = 0.999727$. The J value indicates antiferromagnetic coupling between the two iron(III) atoms. This interaction is slightly but significantly weaker than that in complex **1**, which has a J value of -121.3 (2) cm^{-1} .²⁰ Given the longer Fe-O_{oxo} distance in **4** (av. 1.795 Å) compared to that in **1** (1.784 Å), a less negative value of J for **4** is expected. A correlation between the Fe-O_{oxo} distance and the magnitude of J has been identified and an empirical equation relating the Fe-O_{oxo} bond length to the magnitude of J in multi-bridged diiron(III) complexes has been determined.^{45,46} A coupling constant of -113 cm^{-1} is calculated for **4** by using the equation and the average Fe-O_{oxo} distance in **4**, which is in reasonable agreement with the experimental value. The J value of **4** is almost identical with that of **8** ($J = -110.8$ (6) cm^{-1}) which has an average Fe-O_{oxo} bond length of 1.796 Å.⁴⁴ The difference in the degree of magnetic interaction between the ferric centers in **1** and **4** is also reflected in the ambient temperature solution magnetic moments of two complexes, with μ_{eff} per iron being 1.87 μ_B for **4** and 1.71 μ_B for **1**. The TIP term observed for **4** can be attributed to the Co(III) centers in the ligand, which are known to exhibit a large TIP due to a second order Zeeman effect which

mixes the excited states into the ground state.⁴⁷ The contribution of the TIP term to the magnetic susceptibility is usually calculated according to equation 2.2, where $\Delta T_1 = E(^1A_1) - E(^1T_1)$.

$$\chi_{\text{TIP}} = 4/\Delta T_1 \quad (2.2)$$

For $[\text{Co}(\text{NH}_3)_6]^{3+}$, where $^1T_{1g} = 21000 \text{ cm}^{-1}$, a χ_{TIP} term of $1.95 \times 10^{-4} \text{ emu G}^{-1} \text{ mol}^{-1}$ was obtained. A larger χ_{TIP} term observed for **4** ($3.0 \times 10^{-4} \text{ emu G}^{-1} \text{ mol}^{-1}$) suggests a smaller ΔT_1 and thus a weaker ligand field imposed on the cobalt (III) by the Cp ring and the phosphites in the tripod ligand.

The zero field Mössbauer spectrum of **4** at 4.2 K is shown in Figure 2.6. The values of the isomer shift ($0.58 (3) \text{ mm s}^{-1}$) and quadrupole splitting ($1.84 (5) \text{ mm s}^{-1}$) are typical for high-spin iron(III) centers and similar to those observed for **1**.

Solution Resonance Raman Studies of 4. Figure 2.7 a gives a resonance Raman spectrum of a 0.040 M methylene chloride solution of **4** at 406.7 nm laser excitation. The assignment of the peak at 509 cm^{-1} as the ν_s (Fe–O–Fe) was confirmed by the shift of this band to 487 cm^{-1} upon ^{18}O substitution into the oxo bridge (Figure 2.7 b). The excitation profile of **4** and **1** (Figure 2.8), obtained by using laser excitation between 350.7 nm and 647.1 nm, indicates that the ν_s (Fe–O–Fe) band of **4** at 509 cm^{-1} is enhanced to approximately the same extent as that of **1** at their respective enhancement maximum (356.4 nm for **4** and 406.7 nm for **1**). This observation indicates that the change of terminal capping ligands from nitrogen donor to oxygen donor does not significantly affect the extent of resonance enhancement of the ν_s (Fe–O–Fe) band. The possible correlation between the extent of resonance enhancement of the ν_s (Fe–O–Fe) band and the coordination

environment of iron has been of great interest over last several years. The Fe-O-Fe symmetric stretch has been successfully used to confirm the existence of μ -oxo bridged diiron centers in metalloproteins such as hemerythrin and ribonucleotide reductase.^{48,49} A similar oxo-bridged diiron center was also proposed for the purple acid phosphatase (PAP) based on its magnetic properties and Mössbauer spectrum.^{10,50} The resonance Raman study of the protein, however, has failed to generate the supporting evidence for the existence of such a center. The absence of a resonance enhanced ν_s (Fe-O-Fe) band was attributed to the lack of histidine-type of unsaturated nitrogen donor ligands in the coordination sphere, especially in the positions *trans* to the oxo bridge.^{49,51} This hypothesis is proven to be fallacious by the observation of strong resonance enhancement of the Fe-O-Fe symmetric stretch in **4**. The solid state resonance Raman study of **4** has been carried out in Professor Joann Sanders-Loehr's laboratory as part of a collaboration project between our two groups. One of the interesting observations is the discrepancy of the resonance enhancement maxima observed for solid versus solution samples. The excitation profile of a solid sample of **4** shows the maximal enhancement at 410 nm excitation while the maximum was observed at 350 nm excitation for a methylene chloride solution of **4**. Similar discrepancies were observed in at least two other cases. A maximal enhancement was observed at 363.8 nm for a methylene chloride solution of **1** with the intensity ~100 fold higher than in the visible range while the corresponding maximum was found at 407 nm for a solid sample of **1**.^{20,52} For complex $[\text{Fe}_2\text{O}(\text{OAc})_2(\text{TACN})_2]^{2+}$ (**9**), similar discrepancy was observed in the visible range, where the maxima for the resonance enhancement were observed at 550 nm and 520 nm, respectively, for a solid sample and a acetonitrile solution of **9**.^{51,53} Further investigation

is necessary for offering an explanation to this discrepancy between solid and solution samples. One of the possible cause may be the self-absorption problem usually associated with the solid sample.

Electrochemical studies. A cyclic voltammogram of a methylene chloride solution of **4** displays a quasi-reversible reduction wave with $E_{p,c} = -0.55$ V and $E_{p,a} = -0.25$ V vs. Ag/AgCl and a second irreversible reduction wave at $E_{p,c} = -0.8$ V (Figure 2.9a). The current of the quasi-reversible reduction wave was greatly increased upon the addition of the proton source, $\text{HBF}_4 \cdot \text{Et}_2\text{O}$ (Figure 2.9b). This result is attributed to the increased stability of the reduced species upon the protonation of the oxo bridge. The mononuclear complex **6** was prepared in the form of the BF_4^- salt according to the literature procedure⁵⁴ and added into the electrochemical cell together with a methylene chloride solution of **4** (Figure 2.9c). Compound **6** exhibits a $\text{Fe}^{\text{II}}/\text{Fe}^{\text{III}}$ couple at -0.8 V vs. Ag/AgCl, so **4** does not appear to decompose to the mononuclear species **6** during the redox process. This electrochemical behavior is very different from that of **1**, which decomposed to the mononuclear complex $[\text{Fe}(\text{HBpz}_3)_2]^+$ upon electrochemical reduction.²⁰ The quasi-reversibility of the species formed after the addition of acid is also demonstrated by a plot of the electrode currents versus the square root of scan speed (Figure 2.10). The system deviates from the typical reversible ones where a linear i versus $v^{1/2}$ plot should be generated according to the Randles-Sevcik equation.^{55,56}

Catalytic Activity Toward Air Oxidation of Cyclohexane. The addition of the zinc powder to an acetonitrile solution of **4** does not result in any visible color change. Upon addition of $\text{HBF}_4 \cdot \text{Et}_2\text{O}$ to the mixture of zinc and **4**, however, the solution changed color from red-brown to green-yellow. After cyclohexane was added as the substrate, the reaction vessel

was opened to dried air for 6 hr., the color of the solution changed slowly back to reddish orange. During this period of time, 0.47 equivalents of cyclohexanol were produced (based on the amount of catalyst). Addition of another 5 μ l portion of $\text{HBF}_4 \cdot \text{Et}_2\text{O}$ resulted in the formation of the greenish solution again, which slowly turned to orange over four hours. Another 0.42 equivalents of cyclohexanol were obtained. No cyclohexanone was detected. Failure of this system to achieve catalytic air oxidation of alkane may be caused by two factors. One is that zinc may not be the proper reductant to reduce Fe(III) to Fe(II) in **4**, which is a necessary step to promote the further activation of dioxygen. The other is the possibility that the $\{\text{Fe}_2\text{O}(\text{OAc})_2\}^{2+}$ core is decomposed in the presence of a proton source. It has been demonstrated that the oxo bridge in **4** is susceptible even to weak acid.

Reactivity Toward Hydrogen Peroxide. In a methylene chloride solution, complex **4** reacts with H_2O_2 rapidly. At room temperature, the purple color formed upon the addition of H_2O_2 becomes bleached within one minute. At $-20\text{ }^\circ\text{C}$, the purple color remains for more than 30 minutes and quickly disappeared when temperature was raised above $-20\text{ }^\circ\text{C}$. The UV-vis spectrum of this purple species shows two absorption maxima at 506 nm and 462 nm (sh).

Reactivity Toward an Oxidant. As discussed in the introduction part of this chapter, ligand **2** is a hard ligand and can stabilize the high oxidation state of the metal upon coordination. In addition, the ligand itself is very stable under strong oxidizing conditions. For example, it can form Ru^{V} oxo binuclear complexes in the presence of a strong oxidant RuO_4 .⁵⁷ In a preliminary attempt to obtain a higher oxidation state of the iron center (i.e., Fe(IV)), a strong oxidant $(\text{NH}_4)_2\text{Ce}(\text{NO}_3)_6$ was allowed to react with **4**. The red solution of **4** turned to yellow immediately upon the addition of Ce^{4+} .

The UV-visible spectrum of the reaction mixture showed no absorption in the visible region, with only one peak at 320 nm, which is the characteristic band of the tripod ligand. Efforts to crystallize an iron-containing product from this solution have not been successful to date.

Conclusions

The synthesis and study of the physical and, preliminarily, chemical properties of the (μ -oxo)bis(μ -acetato)diiron(III) complex with the exclusive oxygen donor terminal ligand **2** have proven valuable for understanding better the relationship between the structural features and spectroscopic properties of the model compounds and related proteins. Comparisons of **4** to other model complexes with either exclusive nitrogen donor or mixed oxygen/nitrogen donor terminal ligands have revealed that changing the terminal donor atoms from nitrogen to oxygen does not alter the basic structural features of the $\{\text{Fe}_2\text{O}(\text{O}_2\text{CR})_2\}^{2+}$ core. The average iron-ligand bond lengths, however, are significantly shorter for the oxygen donor as compared to its nitrogen donor counterpart. In addition, the different terminal donor atoms greatly affect the electronic spectra of the complexes due to the variation of the ligand field strength. The shift in the visible transition, especially the bands around 600 nm, can be used to identify the terminal ligands at the iron centers in the proteins. The resonance Raman study has demonstrated that the $\nu_s(\text{Fe-O-Fe})$ is resonance enhanced to almost the same extent with either nitrogen or oxygen occupying the position trans to the μ -oxo bridge. The stability of the diiron core under the electrochemical redox condition is improved by using the oxygen tripod ligand **2** as compared to the tris-1-pyrazolylborate ligand.

Finally, the similarity of the electronic spectra and the Fe...Fe distances in **5** and in MMO offers further support for the hypothesis that the bridging ligand in MMO may be a hydroxyl group.

References

- (1) Klotz, I. M.; D. M. Kurtz, J. *Acct. Chem. Res.* 1984, 17, 16-22.
- (2) Wilkins, P. C.; Wilkins, R. G. *Coord. Chem. Rev.* 1987, 79, 195-214.
- (3) Fontecave, M.; Eliasson, R.; Reichard, P. *J. Biol. Chem.* 1989, 264, 9164-9170.
- (4) Sjöberg, B.-M.; Graslund, A. *Adv. Inorg. Biochem.* 1983, 5, 87-110.
- (5) Fox, B. G.; Froland, W. A.; Jollie, D. R.; Lipscomb, J. D. *Methods in Enzymology*; Academic Press: New York, 1990; Vol. 188, pp 191-202.
- (6) Pilkington, S. J.; Dalton, H. *Soluble Methan Monooxygenase from Methylococcus capsulatus (Bath)*; Academic Press: New York, 1990; Vol. 188, pp 181-190.
- (7) Rosenzweig, A. C.; Feng, X.; Lippard, S. J. 1991, manuscript submitted.
- (8) L. Que, J.; True, A. E. In *Progress in Inorganic Chemistry: Bioinorganic Chemistry*; S. J. Lippard, Ed.; Wiley: New York, 1990; Vol. 38; pp 97-200.
- (9) Sanders-Loehr, J. In *Iron Carriers and Iron Proteins*; T. M. Loehr, Ed.; VCH: New York, 1989; pp 375-466.
- (10) L. Que, J.; Scarrow, R. C. In *Metal Clusters in Proteins*; J. L. Que, Ed.; American Chemical Society: Washington, DC, 1988; pp 152-178.
- (11) Lippard, S. J. *Angew. Chem. Int. Ed. Engl.* 1988, 27, 344-361.
- (12) Holmes, M. A.; Trong, I. L.; Turley, S.; Sieker, L. C.; Stenkamp, R. E. *J. Mol. Biol.* 1991, 218, 583-593.
- (13) Sheriff, S.; Hendrickson, W. A.; Smith, J. L. *J. Mol. Biol.* 1987, 197, 273-296.

- (14) Stenkamp, R. E.; Sieker, L. C.; Jensen, L. H. *J. Am. Chem. Soc.* **1984**, *106*, 618-622.
- (15) Stenkamp, R. E.; Sieker, L. C.; Jensen, L. H.; McCallum, J. D.; Sanders-Loehr, J. *Proc. Natl. Acad. Sci. USA* **1985**, *82*, 713-716.
- (16) Nordlund, P.; Sjöberg, B.-M.; Eklund, H. *Nature* **1990**, *345*, 593-598.
- (17) Ericson, A.; Hedman, B.; Hodgson, K. O.; Green, J.; Dalton, H.; Bentsen, J. G.; Beer, R. H.; Lippard, S. J. *J. Am. Chem. Soc.* **1988**, *110*, 2330.
- (18) DeWitt, J. G.; Bentsen, J. G.; Rosenzweig, A. C.; Hedman, B.; Green, J.; Pilkington, S.; Papaefthymiou, G. C.; Dalton, H.; Hodgson, K. O.; Lippard, S. J. *J. Am. Chem. Soc.* **1991**, in press.
- (19) Kurtz, D. M. *Chem. Rev.* **1990**, *90*, 585.
- (20) Armstrong, W. H.; Spool, A.; Papaefthymiou, G. C.; Frankel, R. B.; Lippard, S. J. *J. Am. Chem. Soc.* **1984**, *106*, 3653.
- (21) Kläui, W. *Angew. Chem. Int. Ed. Engl.* **1990**, *29*, 627-637.
- (22) Kläui, W.; Müller, A.; Eberspach, W.; Boese, R.; Goldberg, I. *J. Am. Chem. Soc.* **1987**, *109*, 164-169.
- (23) Kläui, W.; Werner, H. *Angew. Chem. Int. Ed. Engl.* **1976**, *15*, 172-173.
- (24) Kläui, W.; Eberspach, W.; Gütlich, P. *Inorg. Chem.* **1987**, *26*, 3977-3982.
- (25) Kläui, W.; Lenders, B.; Hessner, B.; Evertz, K. *Organometallics* **1988**, *7*, 1357-1363.
- (26) Kläui, W. *Z. Naturforsch* **1979**, *34b*, 1403-1407.
- (27) Roth, M. E. Ph.D. thesis, Massachusetts Institute of Technology, 1988.
- (28) Sheldrick, G. M. In *Crystallographic Computing 3*; G. M. Sheldrick, C. Krüger and R. Goddard, Ed.; Oxford University Press: Oxford, 1985; pp 175-189.
- (29) Ibers, J. A.; Hamilton, W. C. *International Tables for X-ray Crystallography*; Kynoch Press: Birmingham, 1974; Vol. IV, pp 71-98.

- (30) Steward, R. F.; Davison, E. R.; Simpson, W. T. *J. Chem. Phys.* **1965**, *42*, 3175.
- (31) *TEXSAN: Single Crystal Structure Analysis Software Version 5.0*; Molecular Structure Corporation: Woodlands, TX, 1989.
- (32) Gilmore, G. J. *J. Appl. Cryst.* **1984**, *17*, 42.
- (33) Earnshaw, A. *Introduction to Magnetochemistry*; Academic Press: London, 1968, pp 97.
- (34) Evans, D. F. *J. Chem. Soc.* **1959**, 2003-2005.
- (35) Mulay, L. N. In *Physical Methods of Chemistry. Part IV. Determination of Mass, Transport, and Electrical-Magnetic Properties*; A. Weissberger and B. W. Rossiter, Ed.; Wiley-Interscience: New York, 1972; pp Chapter VIII.
- (36) Sur, S. K. *J. Magnet. Resonance* **1989**, *82*, 169-173.
- (37) *Handbook of Chemistry and Physics*; Weast, R. C., Ed.; CRC Press, Inc.: Boca Raton, 1983, pp E-115.
- (38) Carlin, R. L. *Magnetochemistry*; Springer-Verlag: New York, 1986, pp 3-33.
- (39) O'Connor, C. J. *Prog. Inorg. Chem.* **1982**, *29*, 203-283.
- (40) Murr, N. E.; Chaloyard, A.; Kläui, W. *Inorg. Chem.* **1979**, *18*, 2629-2630.
- (41) Beer, R. H.; Tolman, W. B.; Bott, S. G.; Lippard, S. J. *Inorg. Chem.* **1991**, *30*, 2082-2092.
- (42) Armstrong, W. H.; Lippard, S. J. *J. Am. Chem. Soc.* **1984**, *106*, 4632-4633.
- (43) Appleton, T. G.; Clark, H. C.; Manzer, L. E. *Coord. Chem. Rev.* **1973**, *10*, 335-422.
- (44) Tolman, W. B.; Liu, S.; Bentsen, J. G.; Lippard, S. J. *J. Am. Chem. Soc.* **1991**, *113*, 152-164.

- (45) Gorun, S. M.; Lippard, S. J. *Recl. Trav. Chim. Pays-Bas* 1987, 106, 417.
- (46) Turowski, P. N.; Armstrong, W. H.; Roth, M. E.; Lippard, S. J. *J. Am. Chem. Soc.* 1990, 112, 681-690.
- (47) Carlin, R. L. *Magnetochemistry*; Springer-Verlag: Berlin, 1986, pp 12.
- (48) Sanders-Loehr, J. In *Metal Clusters in Proteins*; L. Que Jr., Ed.; American Chemical Society: Washington D.C., 1988; pp 49-67.
- (49) Sanders-Loehr, J. In *Oxidases and Related Redox Systems*; H. S. Mason, T. E. King and M. Morrison, Ed.; Liss: New York, 1988; pp 193-209.
- (50) Averill, B. A.; Davis, J. C.; Burman, S.; Zirino, T.; Sanders-Loehr, J.; Loehr, T.; Sage, J. T.; Debrunner, P. G. *J. Am. Chem. Soc.* 1987, 109, 3760.
- (51) Sanders-Loehr, J.; Wheeler, W. D.; Shiemke, A. K.; Averill, B. A.; Loehr, T. M. *J. Am. Chem. Soc.* 1989, 111, 8084.
- (52) Czernuszewicz, R. S.; Sheats, J. E.; Spiro, T. G. *Inorg. Chem.* 1987, 26, 2063-2067.
- (53) Spool, A.; Williams, I. D.; Lippard, S. J. *Inorg. Chem.* 1985, 24, 2156-2162.
- (54) Kläui, W.; Eberspach, W.; Schwarz, R. J. *J. Organomet. Chem.* 1983, 252, 347-357.
- (55) Van Benschoten, J. J.; Lewis, J. Y.; Heineman, W. R.; Roston, D. A.; Kissinger, P. T. *J. Chem. Ed.* 1983, 60, 772.
- (56) Mabbott, G. A. *J. Chem. Ed.* 1983, 60, 697.
- (57) Power, J. M.; Evertz, K.; Henling, L.; Marsh, R.; Schaefer, W. P.; Labinger, J. A.; Bercaw, J. E. *Inorg. Chem.* 1990, in press.
- (58) Johnson, C. K. *ORTEP-II, A FORTRAN Thermal Ellipsoid Plot Program*; Oak Ridge National Laboratory: Oak Ridge, 1976, pp ORNL-5138.
- (59) Motherwell, S.; Clegg, W. *PLUTO Program for Plotting Molecular and Crystal Structure*; Univ. of Cambridge: England, 1978.

- (60) Reem, R. C.; McCormick, J. M.; Richardson, D. E.; Devlin, F. J.; Stephens, P. J.; Musselman, R. L.; Solomon, E. I. *J. Am. Chem. Soc.* **1989**, *111*, 4688-4704.
- (61) Butcher, K. D.; Gebhard, M. S. *Inorg. Chem.* **1990**, *29*, 2067-2074.
- (62) Schugar, H. J.; Rossman, G. R.; Barraclough, C. G.; Gray, H. B. *J. Am. Chem. Soc.* **1972**, *94*, 2683-2690.

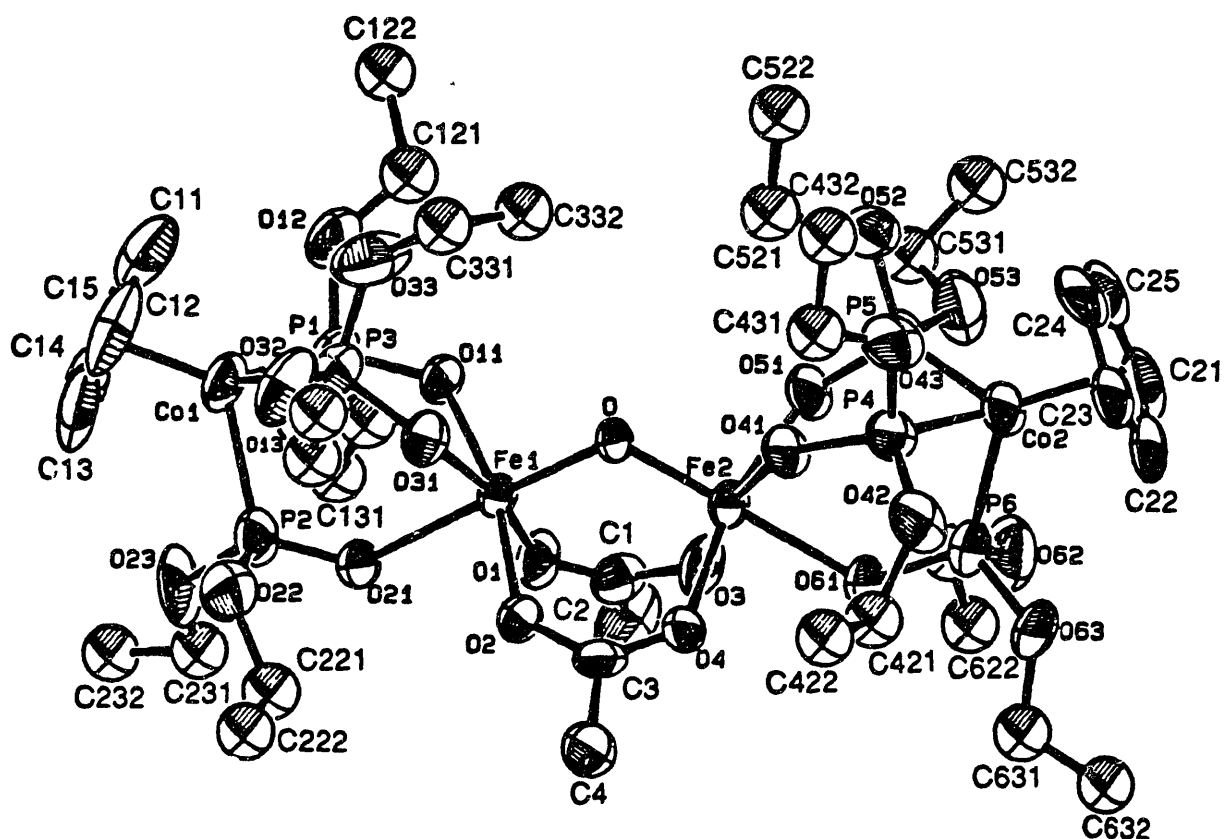


Figure 2.1a. ORTEP⁵⁸ drawing of **4** showing 40% probability thermal ellipsoids and labelling scheme for non-hydrogen atoms. Carbon atoms on ethyl groups are represented as isotropic spheres with $B = 6.0 \text{ \AA}^2$ for clarity. Atom disorder is not shown.

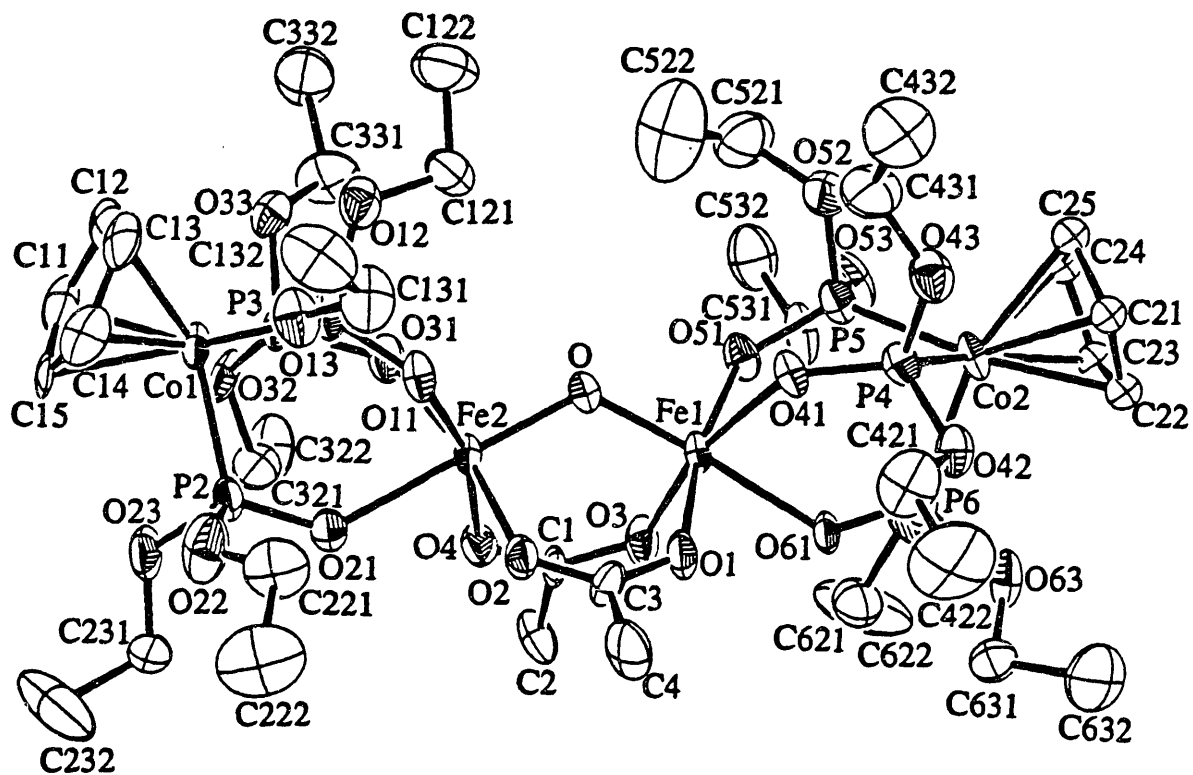


Figure 2.1b. ORTEP⁵⁸ drawing of **4** (-78.5 °C) showing 40% probability thermal ellipsoids and labelling scheme for non-hydrogen atoms. Atom disorder is not shown.

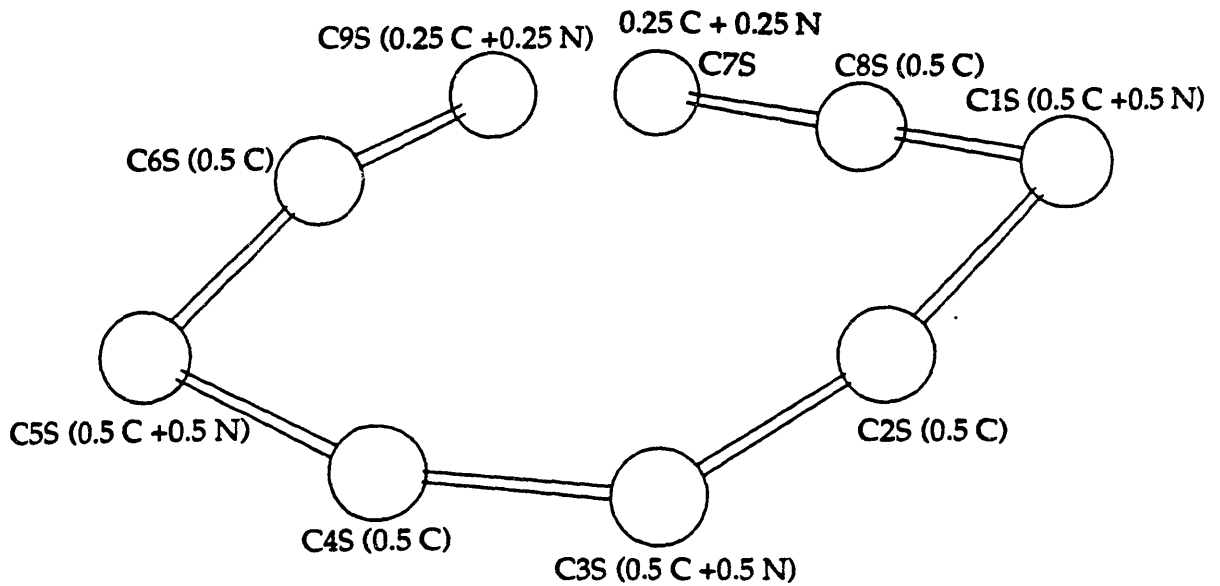


Figure 2.2. PLUTO⁵⁹ drawing showing the disordered model for two acetonitrile molecules in the unit cell for $4 \cdot 2\text{CH}_3\text{CN}$ at 25 °C.

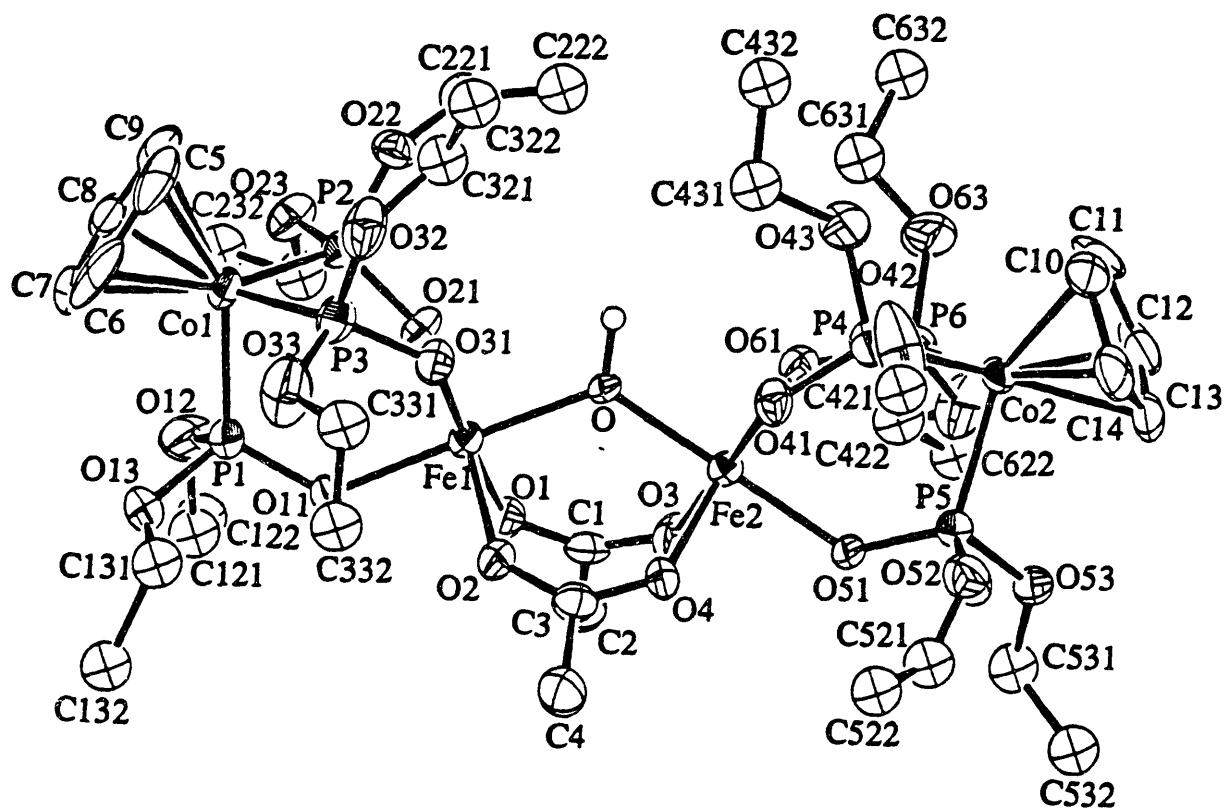


Figure 2.3. ORTEP⁵⁸ drawing of 5 showing 40% probability thermal ellipsoids and labelling scheme for non-hydrogen atoms. Carbon atoms on ethyl groups are represented as isotropic spheres with $B = 4.5 \text{ \AA}^2$ for clarity. Atom disorder is not shown.

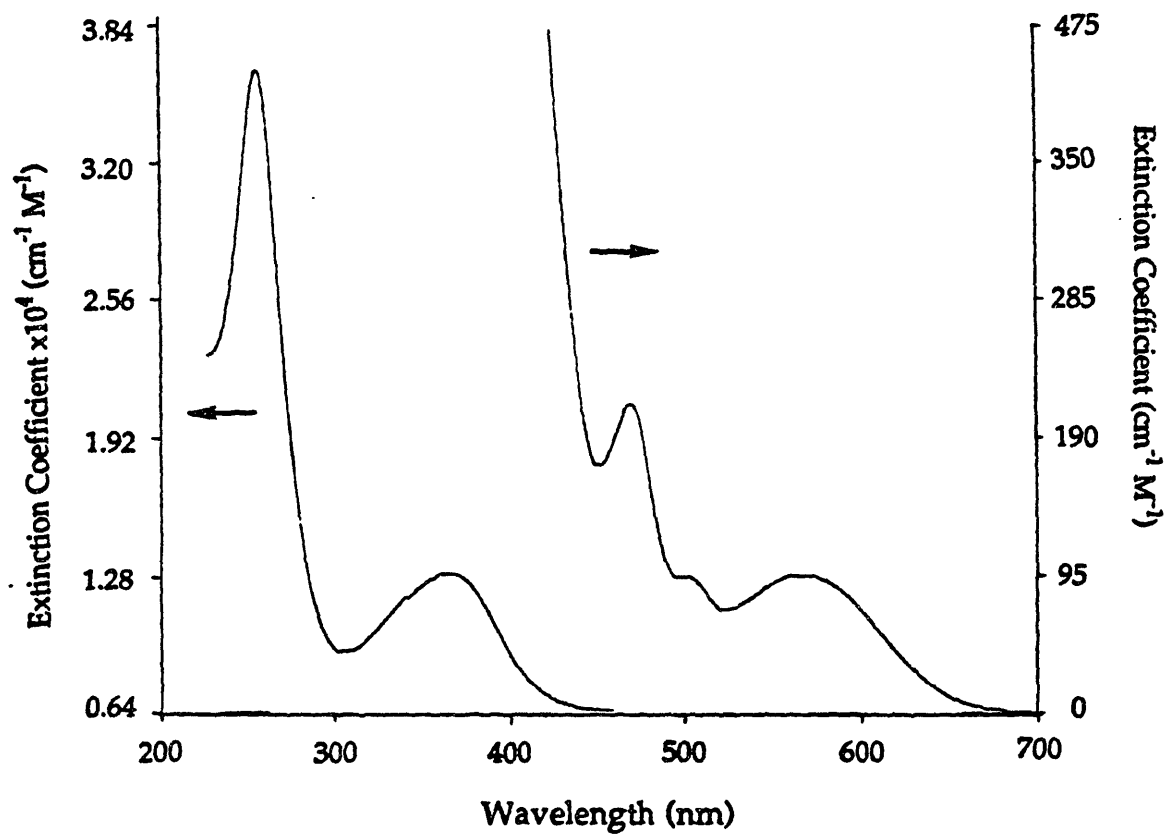


Figure 2.4. UV-visible spectrum of 4 in acetonitrile.

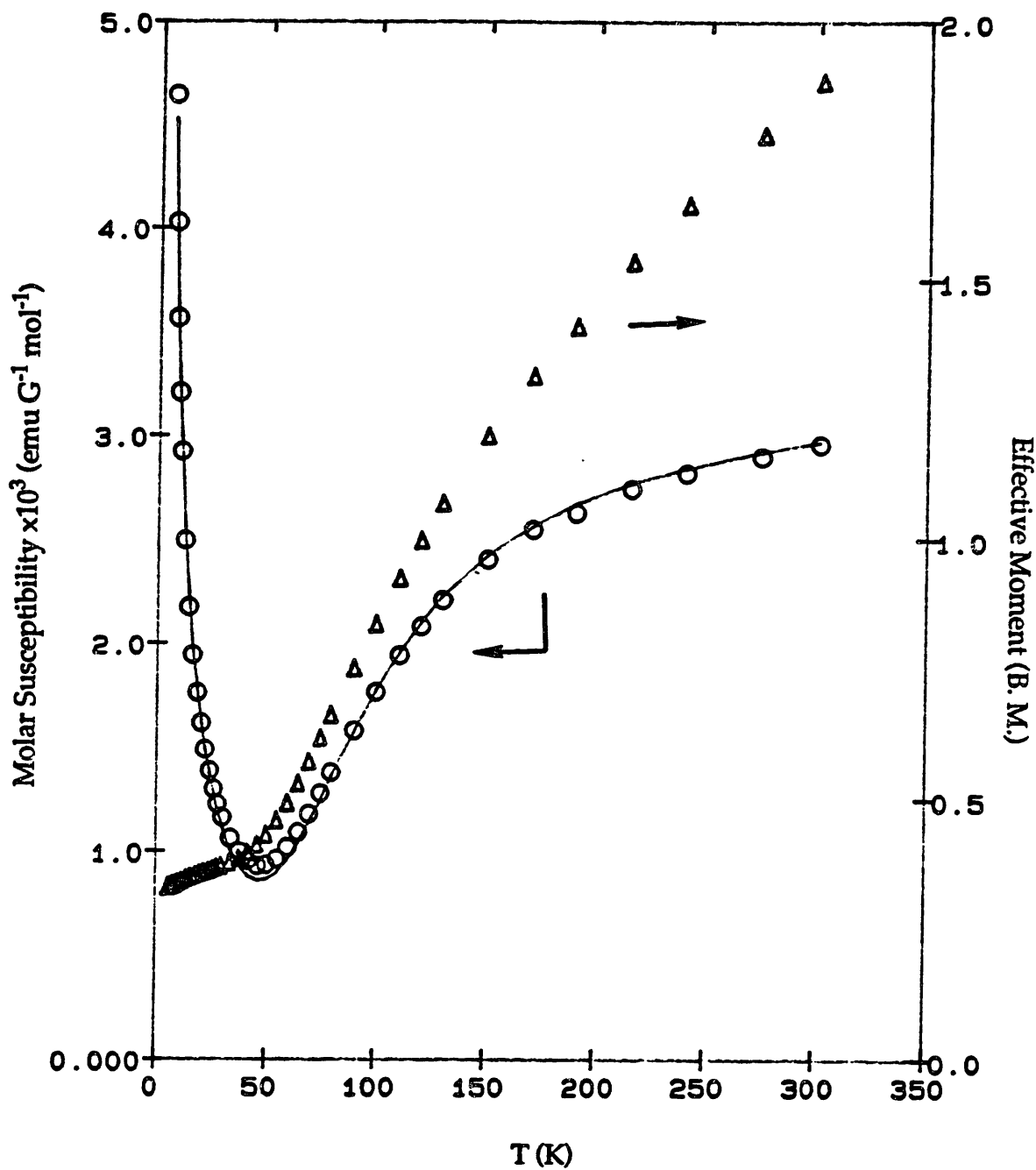


Figure 2.5. Plot of molar susceptibility (o) and effective moment (Δ) for 4. The solid line shows the best result from the least-squares fits of eq. 2.1. to the data with g fixed at 2.0. (See text for details)

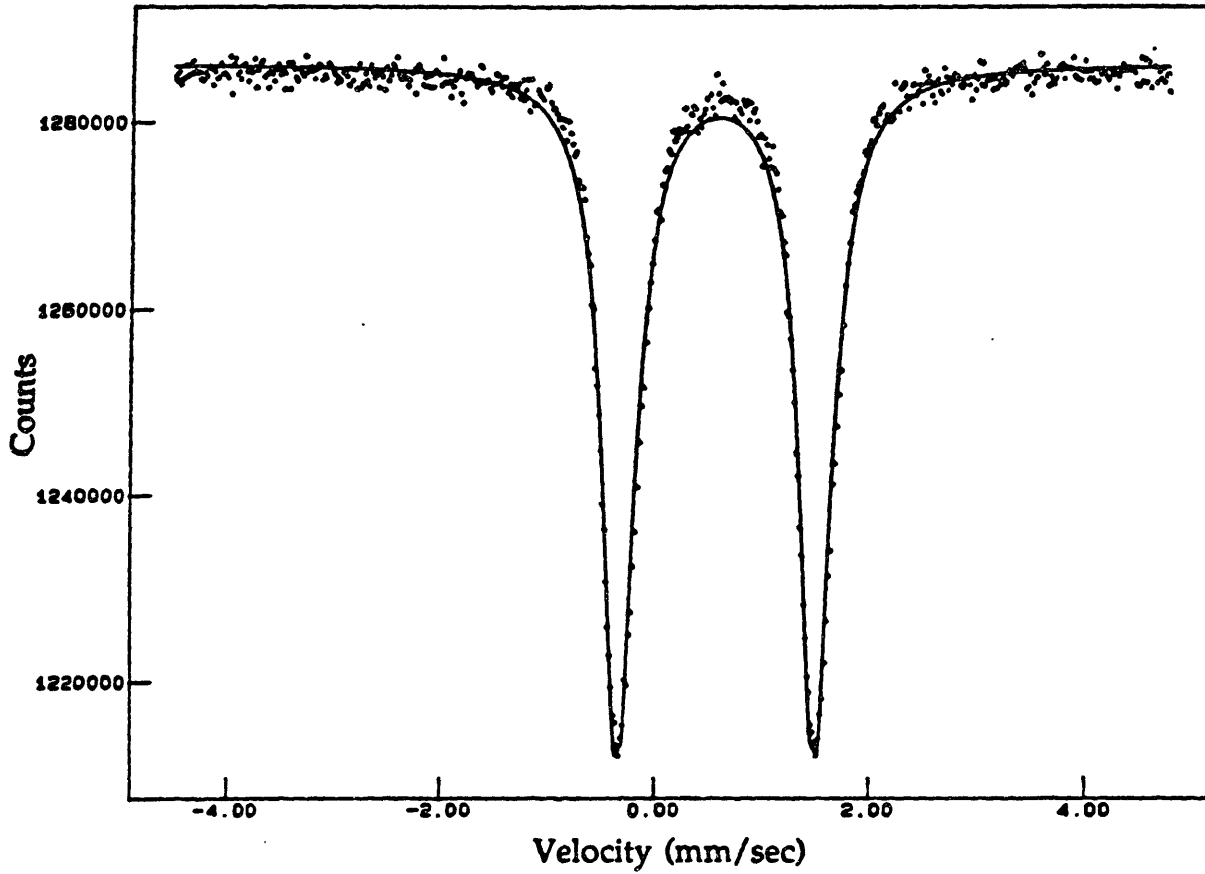


Figure 2.6. Zero field Mössbauer spectrum of 4 at 4.2 K. The solid line is the result of the least-squares fit to the data.

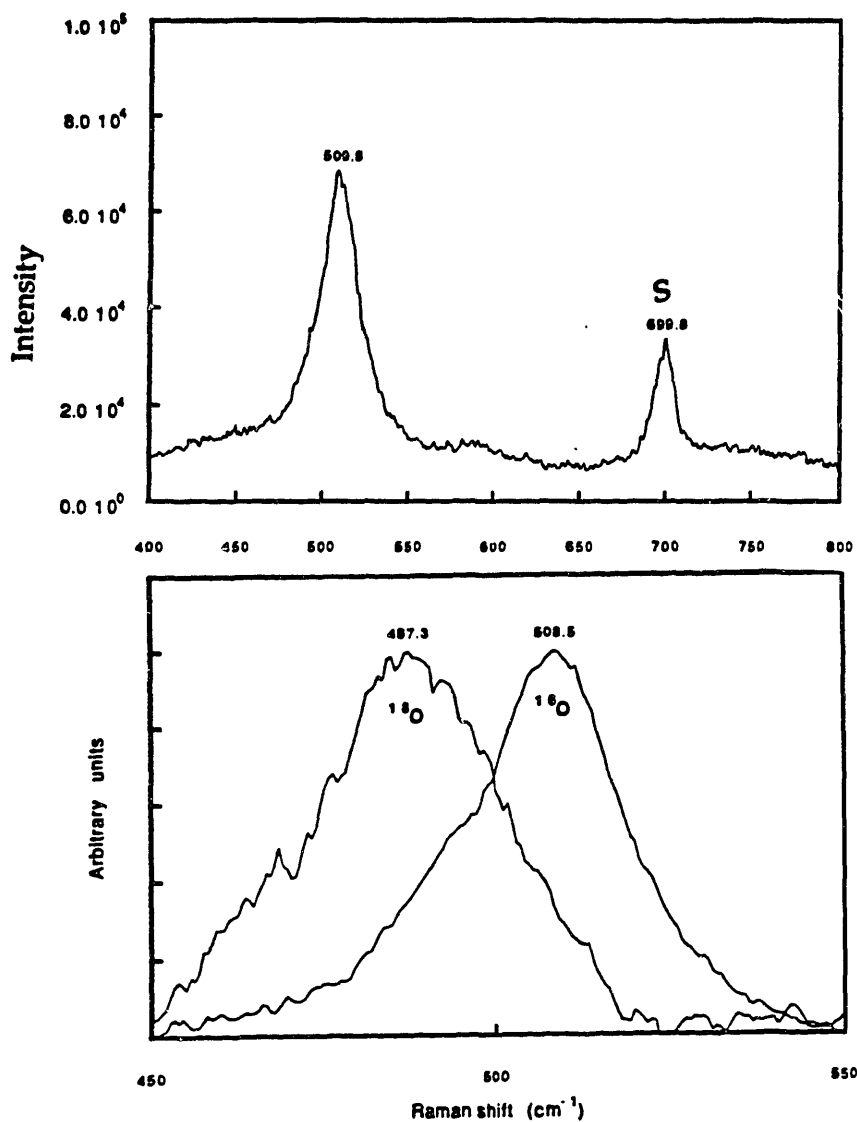


Figure 2.7. (a) Raman spectrum of **4** in CH₂Cl₂ solution (4.0×10^{-2} M). The peak marked as S is the solvent peak. (b) Spectrum of **4** showing the shift of ν_s Fe-O-Fe upon ¹⁸O substitution. Laser line with the wavelength of 406.7 nm and power of 200 mW was used.

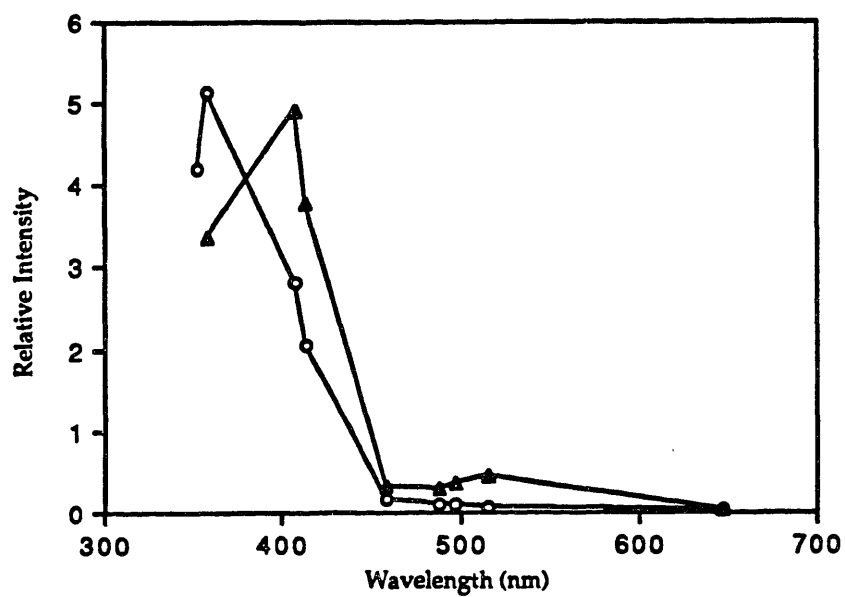


Figure 2.8. Excitation profiles for the methylene chloride solutions of **1** (4.38×10^{-2} M, o) and **4** (4.29×10^{-2} M, Δ).

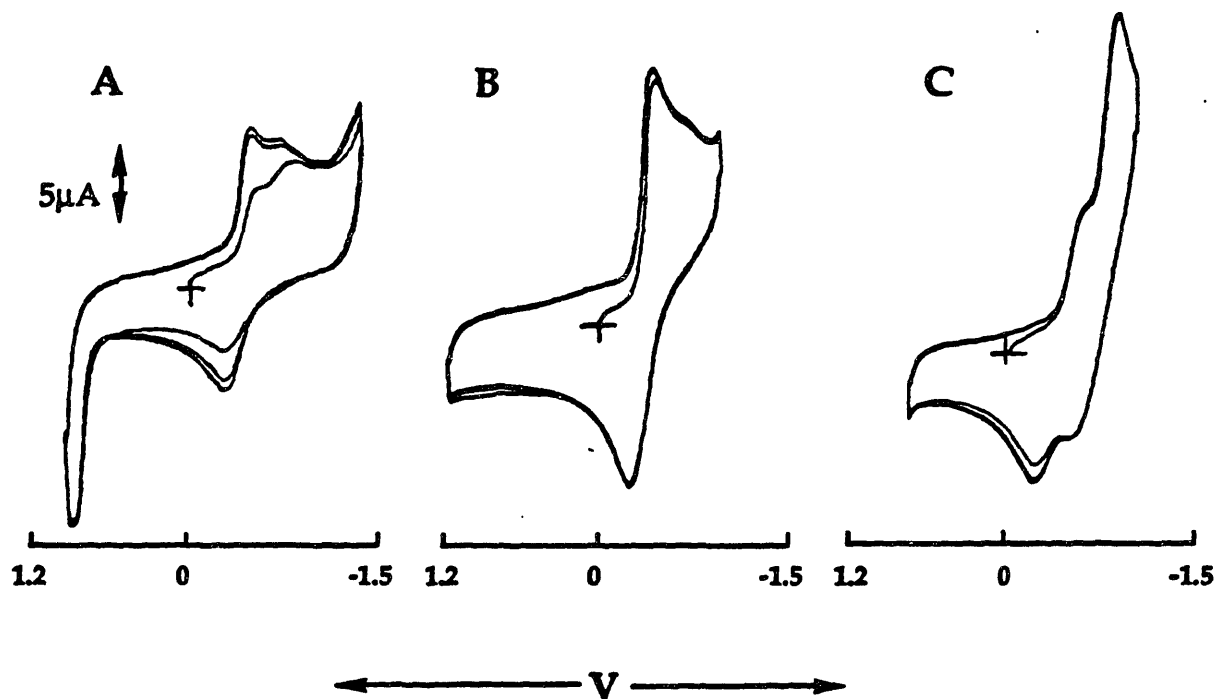


Figure 2.9. Cyclic voltammograms of (a) **4**; (b) **4** and 1 eq. of $\text{HBF}_4 \cdot \text{Et}_2\text{O}$; and (c) both **4** and **6** in 0.2 M TBAP methylene chloride solution with scan speed of 200 mV s^{-1} . Recorded with a glassy carbon electrode with Ag/AgCl as reference.

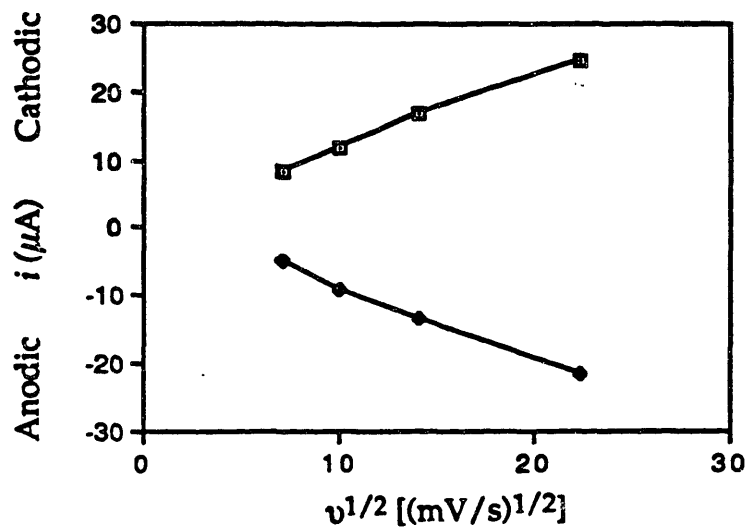


Figure 2.10. Plot of electrode currents versus square root of scan speed from cyclic voltammograms of 4.

Table 2.1. Experimental Details of the X-ray Diffraction Studies of $\text{Fe}_2\text{O}(\text{OAc})_2\{\text{CpCo}[\text{OP}(\text{OEt})_2]_3\}_2 \cdot 2\text{CH}_3\text{CN}$ ($4 \cdot 2\text{CH}_3\text{CN}$) at Different Temperatures.^a

| compound | 1·2CH ₃ CN | 1·2CH ₃ CN |
|---|---|---|
| formula | C ₄₂ H ₈₂ P ₆ O ₂₃ N ₂ Co ₂ Fe ₂ | C ₄₂ H ₈₂ P ₆ O ₂₃ N ₂ Co ₂ Fe ₂ |
| formula weight, g mol ⁻¹ | 1398.52 | 1398.52 |
| crystal system | triclinic | triclinic |
| space group | P $\bar{1}$ | P $\bar{1}$ |
| a, Å | 12.062 (2) | 12.002 (1) |
| b, Å | 15.733 (4) | 15.798 (4) |
| c, Å | 18.667 (6) | 18.471 (3) |
| α, ° | 111.64 (2) | 112.17 (2) |
| β, ° | 96.62 (2) | 98.13 (1) |
| γ, ° | 98.83 (2) | 99.77 (1) |
| V, Å ³ | 3196 | 3114 |
| Z | 2 | 2 |
| temperature, °C | 25 | -78.5 |
| ρ _{calcd} , g cm ⁻³ | 1.453 | 1.491 |
| ρ _{obsd} , g cm ⁻³ | 1.44 (1) | 1.44 (1) |
| transmission factor range | 0.599-1.000 | 0.760-1.000 |
| linear absorption coefficient, cm ⁻¹ | 11.70 | 12.00 |
| 2θ range | 3° ≤ 2θ ≤ 45°, +h,±k, ±l | 2° ≤ 2θ ≤ 45°, +h,±k, ±l |
| total no. of data collected | 8568 | 8580 |
| R _{merge} ^b | 0.288 | 0.038 |

Table 2.1, contd. Experimental Details of the X-ray Diffraction Studies of $\text{Fe}_2\text{O}(\text{OAc})_2[\text{CpCo}[\text{OP}(\text{OEt})_2]_3]_2 \cdot 2\text{CH}_3\text{CN}$ ($4 \cdot 2\text{CH}_3\text{CN}$) at different temperatures.

| compound | 1·2CH ₃ CN | 1·2CH ₃ CN |
|---|-----------------------|-----------------------|
| no. of independent data | 8306 | 8106 |
| no. of unique data with $F > 6\sigma(F)$ | 4719 | 5367 |
| no. of variables | 610 | 661 |
| R^c | 0.070 | 0.077 |
| R_w^d | 0.085 | 0.106 |
| p^d | 0.05 | 0.05 |

^a All measurements were made on an Enraf-Nonius CAD4-F diffractometer with Mo K α radiation ($\lambda = 0.70926 \text{ \AA}$). ^b $R_{(\text{merge})} = \frac{\sum_{i=1}^n \sum_{j=1}^m |\langle F_i^2 \rangle - F_{ij}^2|}{\sum_{i=1}^n m \times \langle F_i^2 \rangle}$ where n = numbers of unique reflections which were measured more than once during data collection, m = number of times a given reflection was measured and $\langle F_i^2 \rangle$ is the average value of F^2 for the reflection. ^c $R = \frac{\sum ||F_o| - |F_c||}{\sum |F_o|}$. ^d $R_w = [\sum w(|F_o| - |F_c|)^2 / \sum w |F_o|^2]^{1/2}$, where $w = 1/\sigma^2(F)$, $\sigma^2(F) = [S^2(C+4B) + (pI)^2] / [(Lp)^2 4F^2]$ with S = scan rate, C = peak count, B = sum of left and right background counts, Lp = Lorentz-polarization factor, and p = fudge factor.

Table 2.2. Experimental Details of the X-ray Diffraction Study of
 $[\text{Fe}_2(\text{OH})(\text{OAc})_2\{\text{CpCo}[\text{OP}(\text{OEt})_2]_3\}_2][\text{BPh}_4]\cdot\text{CH}_2\text{Cl}_2\cdot 0.5\text{C}_7\text{H}_8$
 $(5\cdot\text{CH}_2\text{Cl}_2\cdot 0.5\text{C}_7\text{H}_8)^{\text{a}}$

| compound | $5\cdot\text{CH}_2\text{Cl}_2\cdot 0.5\text{C}_7\text{H}_8$ |
|---|--|
| formula | $\text{C}_{66.5}\text{H}_{103}\text{P}_6\text{O}_{23}\text{Cl}_2\text{BCo}_2\text{Fe}_2$ |
| formula weight, g mol^{-1} | 1767.65 |
| crystal system | triclinic |
| space group | $\text{P}\bar{1}$ |
| a , Å | 12.633 (2) |
| b , Å | 19.462 (5) |
| c , Å | 19.623 (3) |
| α , ° | 113.21 (2) |
| β , ° | 101.00 (1) |
| γ , ° | 93.92 (2) |
| V , Å ³ | 4297 |
| Z | 2 |
| temperature, °C | -78 |
| ρ_{calcd} , g cm^{-3} | 1.366 |
| transmission factor range | 0.922-1.000 |
| linear absorption coefficient, cm^{-1} | 9.45 |
| 2θ range | $3^\circ \leq 2\theta \leq 50^\circ$, $+h, \pm k, \pm l$ |
| total no. of data collected | 16358 |
| R_{merge} | 0.038 |
| no. of independent data | 15028 |

Table 2.2, contd. Experimental Details of the X-ray Diffraction Study of
[Fe₂OH(OAc)₂{CpCo[OP(OEt)₂]₃]₂][BPh₄]·CH₂Cl₂·0.5C₇H₈
(5·CH₂Cl₂·0.5C₇H₈).

| compound | 5·CH ₂ Cl ₂ ·0.5C ₇ H ₈ |
|--|---|
| no. of unique data with $F > 6\sigma(F)$ | 8718 |
| no. of variables | 890 |
| R | 0.075 |
| R _w | 0.096 |
| p | 0.03 |

^a See the footnotes in Table 2.1.

Table 2.3 a. Final Positional and Equivalent Isotropic Thermal Parameters of Non-Hydrogen Atoms in $\text{Fe}_2\text{O}(\text{OAc})_2[\text{CpCo}[\text{OP}(\text{OEt})_2]_3]_2 \cdot 2\text{CH}_3\text{CN}, 4 \cdot 2\text{CH}_3\text{CN}$ at 25 °C.^a

| Atom ^b | X | Y | Z | B(eq) |
|-------------------|------------|-----------|------------|---------|
| Co1 | 0.2403(2) | 0.9490(1) | 0.5758(1) | 5.72(8) |
| Co2 | 0.2401(2) | 0.5967(1) | 0.9626(1) | 6.09(8) |
| Fe1 | 0.2102(1) | 0.7343(1) | 0.64306(9) | 4.15(6) |
| Fe2 | 0.2112(1) | 0.6275(1) | 0.75785(9) | 4.30(7) |
| P1 | 0.3784(3) | 0.9012(2) | 0.6215(2) | 5.5(1) |
| P2 | 0.1621(3) | 0.8055(3) | 0.4998(2) | 5.6(2) |
| P3 | 0.1462(3) | 0.9343(2) | 0.6632(2) | 5.8(2) |
| P4 | 0.1072(3) | 0.6489(2) | 0.9162(2) | 5.6(1) |
| P5 | 0.3670(3) | 0.6795(3) | 0.9293(2) | 6.1(2) |
| P6 | 0.2191(4) | 0.4829(3) | 0.8498(2) | 6.5(2) |
| O | 0.2302(7) | 0.7321(5) | 0.7393(4) | 4.7(3) |
| O1 | 0.2996(7) | 0.6357(6) | 0.5973(4) | 5.5(4) |
| O2 | 0.0596(7) | 0.6404(5) | 0.6020(4) | 5.5(3) |
| O3 | 0.3025(7) | 0.5599(5) | 0.6775(5) | 5.9(4) |
| O4 | 0.0630(7) | 0.5601(5) | 0.6790(4) | 5.3(3) |
| O11 | 0.3537(6) | 0.8364(5) | 0.6630(4) | 4.6(3) |
| O12 | 0.4746(9) | 0.9890(7) | 0.6800(7) | 10.0(5) |
| O13 | 0.4469(8) | 0.8528(7) | 0.5519(6) | 7.6(5) |
| O21 | 0.1874(7) | 0.7313(5) | 0.5269(4) | 5.2(3) |
| O22 | 0.0268(9) | 0.7962(6) | 0.4786(5) | 7.8(5) |
| O23 | 0.199(1) | 0.7830(8) | 0.4154(6) | 9.1(6) |
| O31 | 0.1206(6) | 0.8390(5) | 0.6678(4) | 4.8(3) |
| O32 | 0.028(1) | 0.9662(6) | 0.6544(6) | 8.0(5) |
| O33 | 0.214(1) | 1.0117(6) | 0.7459(6) | 9.4(5) |
| O41 | 0.1207(6) | 0.6742(5) | 0.8464(4) | 5.0(3) |
| O42 | -0.0171(7) | 0.5823(7) | 0.8973(5) | 7.6(4) |
| O43 | 0.091(1) | 0.7403(7) | 0.9867(5) | 7.2(4) |
| O51 | 0.3546(7) | 0.6691(6) | 0.8458(4) | 6.1(4) |
| O52 | 0.3852(9) | 0.7893(7) | 0.9850(5) | 8.1(4) |

Table 2.3 a, contd Final Positional and Equivalent Isotropic Thermal Parameters of Non-Hydrogen Atoms in $\text{Fe}_2\text{O}(\text{OAc})_2[\text{CpCo}[\text{OP}(\text{OEt})_2]_3]_2 \cdot 2\text{CH}_3\text{CN}$ at 25 °C.

| Atom | X | Y | Z | B(eq) |
|------------------|-----------|-----------|-----------|---------|
| O53 | 0.4875(9) | 0.6568(8) | 0.9532(6) | 8.8(5) |
| O61 | 0.1872(7) | 0.5021(5) | 0.7780(4) | 5.5(3) |
| O62 | 0.329(1) | 0.4365(7) | 0.8413(6) | 9.6(6) |
| O63 | 0.124(1) | 0.3989(6) | 0.8479(5) | 9.1(5) |
| C1 | 0.330(1) | 0.5765(9) | 0.6188(7) | 5.3(5) |
| C1S ^c | 0.0477 | 0.2323 | 0.2335 | 9.2(4) |
| C2 | 0.405(1) | 0.516(1) | 0.575(1) | 8.9(8) |
| C2S | 0.1256 | 0.1724 | 0.1763 | 10(1) |
| C3 | 0.016(1) | 0.5780(8) | 0.6258(7) | 4.8(5) |
| C3S | 0.2197 | 0.1385 | 0.1362 | 21(1) |
| C4S | 0.3493 | 0.1694 | 0.1718 | 14(1) |
| C4 | -0.101(1) | 0.522(1) | 0.5824(7) | 6.8(6) |
| C5S | 0.4714 | 0.2335 | 0.2358 | 10.6(5) |
| C6S | 0.4019 | 0.2907 | 0.2830 | 15(1) |
| C7S | 0.2532 | 0.3049 | 0.3404 | 12(1) |
| C8S | 0.1459 | 0.2670 | 0.2822 | 15(2) |
| C9S | 0.3335 | 0.3176 | 0.3377 | 22(2) |
| C11 | 0.1724 | 1.0014 | 0.4976 | 11(1) |
| C12 | 0.288(2) | 0.994(1) | 0.490(1) | 10(1) |
| C13 | 0.355(2) | 1.054(2) | 0.565(2) | 11(1) |
| C14 | 0.284(2) | 1.095(1) | 0.617(1) | 10(1) |
| C15 | 0.1715 | 1.0616 | 0.5725 | 12(1) |
| C21 | 0.206(2) | 0.506(1) | 1.0194(9) | 8.4(9) |
| C22 | 0.154(2) | 0.581(1) | 1.0491(8) | 8.1(8) |
| C23 | 0.239(2) | 0.670(1) | 1.0838(8) | 8.8(8) |
| C24 | 0.344(2) | 0.640(2) | 1.073(1) | 8.7(9) |
| C25 | 0.331(1) | 0.540(2) | 1.032(1) | 8.3(8) |
| C121 | 0.521(2) | 1.008(2) | 0.754(1) | 11.7(6) |
| C122 | 0.506(5) | 1.115(4) | 0.791(3) | 13(2) |
| C123 | 0.611(3) | 1.095(2) | 0.793(2) | 12(1) |

Table 2.3 a, contd Final Positional and Equivalent Isotropic Thermal Parameters of Non-Hydrogen Atoms in $\text{Fe}_2\text{O}(\text{OAc})_2[\text{CpCo}[\text{OP}(\text{OEt})_2]_3]_2 \cdot 2\text{CH}_3\text{CN}$ at 25 °C.

| Atom | X | Y | Z | B(eq) |
|------|-----------|----------|-----------|--------|
| C131 | 0.517(2) | 0.793(1) | 0.557(1) | 11(1) |
| C132 | 0.554(2) | 0.745(2) | 0.493(2) | 15(2) |
| C221 | -0.050(2) | 0.700(1) | 0.447(1) | 12(1) |
| C222 | -0.156(2) | 0.696(1) | 0.430(1) | 13(1) |
| C231 | 0.235(2) | 0.706(1) | 0.372(1) | 11(1) |
| C232 | 0.291(2) | 0.728(1) | 0.310(1) | 12(1) |
| C321 | -0.084(2) | 0.913(2) | 0.643(2) | 13(1) |
| C322 | -0.152(2) | 0.968(2) | 0.694(1) | 14(1) |
| C331 | 0.1763 | 1.0218 | 0.8155 | 15.4 |
| C332 | 0.2523 | 0.9841 | 0.8505 | 15.5 |
| C421 | -0.082(1) | 0.522(1) | 0.8189(7) | 7.5(6) |
| C422 | -0.192(2) | 0.550(1) | 0.806(1) | 11(1) |
| C431 | 0.018(2) | 0.798(2) | 0.971(1) | 11(1) |
| C432 | 0.030(2) | 0.882(2) | 1.043(1) | 15(1) |
| C521 | 0.353(2) | 0.857(1) | 0.955(1) | 9.7(9) |
| C522 | 0.368(2) | 0.944(2) | 1.027(2) | 17(2) |
| C531 | 0.593(2) | 0.705(2) | 0.940(1) | 13(1) |
| C532 | 0.683(2) | 0.723(2) | 1.004(2) | 17(2) |
| C621 | 0.409(2) | 0.445(2) | 0.791(2) | 13(1) |
| C622 | 0.431(3) | 0.363(2) | 0.745(2) | 18(2) |
| C631 | 0.089(2) | 0.314(1) | 0.776(1) | 14(1) |
| C632 | 0.044(2) | 0.239(1) | 0.793(1) | 17(1) |

^aNumbers in parentheses are errors in the last significant digit. ^bSee Figure 2.1a. for atom labelling scheme. ^cC1S, C2S,, C8S, C9S are arbitrarily assigned atom labels for two disordered acetonitrile molecules. See Figure 2.2. for details of the disorder model.

Table 2.3 b. Final Positional and Equivalent Isotropic Thermal Parameters of Non-Hydrogen Atoms for $\text{Fe}_2\text{O}(\text{OAc})_2[\text{CpCo}[\text{OP}(\text{OEt})_2]_3]_2 \cdot 2\text{CH}_3\text{CN}$, 4·2 CH_3CN at -78.5 °C.^a

| Atom ^b | X | Y | Z | B(eq) |
|-------------------|------------|-----------|-----------|---------|
| Co1 | 0.2442(2) | 0.9386(1) | 0.5638(1) | 2.47(7) |
| Co2 | 0.2284(1) | 0.6064(1) | 0.9716(1) | 2.37(6) |
| Fe1 | 0.2152(2) | 0.7351(1) | 0.6443(1) | 1.97(6) |
| Fe2 | 0.2077(2) | 0.6321(1) | 0.7622(1) | 1.96(6) |
| P1 | 0.3862(3) | 0.8942(2) | 0.6143(2) | 2.4(1) |
| P2 | 0.1602(3) | 0.7923(3) | 0.4915(2) | 2.5(1) |
| P3 | 0.1529(3) | 0.9317(2) | 0.6550(2) | 2.6(1) |
| P4 | 0.1004(3) | 0.6638(2) | 0.9232(2) | 2.3(1) |
| P5 | 0.3640(3) | 0.6844(3) | 0.9387(2) | 2.5(1) |
| P6 | 0.1951(3) | 0.4892(2) | 0.8568(2) | 2.4(1) |
| O | 0.2344(7) | 0.7359(6) | 0.7426(5) | 2.1(3) |
| O1 | 0.3061(8) | 0.6353(6) | 0.6021(5) | 2.8(3) |
| O2 | 0.0572(7) | 0.6402(6) | 0.5994(5) | 2.7(3) |
| O3 | 0.3000(8) | 0.5618(6) | 0.6845(5) | 2.6(3) |
| O4 | 0.0533(7) | 0.5660(6) | 0.6813(5) | 2.7(3) |
| O11 | 0.3636(7) | 0.8382(6) | 0.6628(5) | 2.3(3) |
| O12 | 0.4927(8) | 0.9784(7) | 0.6667(6) | 3.5(4) |
| O13 | 0.4408(7) | 0.8392(6) | 0.5417(5) | 2.7(3) |
| O21 | 0.1887(7) | 0.7240(6) | 0.5247(5) | 2.3(3) |
| O22 | 0.0231(7) | 0.7819(6) | 0.4713(5) | 3.1(3) |
| O23 | 0.1883(9) | 0.7622(7) | 0.4036(6) | 3.8(4) |
| O31 | 0.1274(7) | 0.8412(6) | 0.6675(5) | 2.6(3) |
| O32 | 0.0324(8) | 0.9611(7) | 0.6444(7) | 4.0(4) |
| O33 | 0.2226(8) | 1.0165(6) | 0.7362(6) | 3.5(4) |
| O41 | 0.1175(7) | 0.6829(6) | 0.8512(5) | 2.6(3) |
| O42 | -0.0297(7) | 0.6049(7) | 0.9040(5) | 3.1(3) |
| O43 | 0.0974(8) | 0.7595(7) | 0.9951(5) | 3.2(3) |
| O51 | 0.3542(7) | 0.6720(6) | 0.8545(5) | 2.7(3) |
| O52 | 0.3890(8) | 0.7944(7) | 0.9946(5) | 3.6(4) |

Table 2.3 b, contd. Final Positional and Equivalent Isotropic Thermal Parameters of Non-Hydrogen Atoms for $\text{Fe}_2\text{O}(\text{OAc})_2[\text{CpCo}[\text{OP}(\text{OEt})_2]_3]_2 \cdot 2\text{CH}_3\text{CN}, 4 \cdot 2\text{CH}_3\text{CN}$ at $-78.5\text{ }^\circ\text{C}$.

| Atom | X | Y | Z | B(eq) |
|------|-----------|-----------|-----------|--------|
| O53 | 0.480(2) | 0.675(2) | 0.978(1) | 2.3(6) |
| O53A | 0.484(2) | 0.652(2) | 0.960(1) | 2.7(6) |
| O61 | 0.1730(7) | 0.5078(6) | 0.7829(5) | 2.7(3) |
| O62 | 0.290(1) | 0.4316(8) | 0.8510(7) | 4.8(5) |
| O63 | 0.0889(8) | 0.4109(7) | 0.8531(6) | 3.9(4) |
| N1S | 0.735(2) | 0.698(1) | 0.654(1) | 7.4(8) |
| N2S | 0.749(2) | 0.857(1) | 0.877(1) | 8.4(9) |
| C1S | 0.826(2) | 0.728(1) | 0.701(1) | 5.8(9) |
| C1 | 0.333(1) | 0.576(1) | 0.6279(7) | 2.4(5) |
| C2S | 0.938(1) | 0.768(1) | 0.756(1) | 4.7(7) |
| C2 | 0.415(1) | 0.524(1) | 0.588(1) | 4.4(7) |
| C3 | 0.008(1) | 0.5818(9) | 0.6234(7) | 2.1(4) |
| C4 | -0.109(1) | 0.519(1) | 0.5749(9) | 3.2(5) |
| C4S | 0.542(1) | 0.772(2) | 0.774(1) | 7(1) |
| C5S | 0.654(2) | 0.821(1) | 0.833(1) | 5.3(8) |
| C21 | 0.201(1) | 0.514(1) | 1.0291(7) | 2.9(5) |
| C22 | 0.143(1) | 0.586(1) | 1.0561(8) | 3.7(6) |
| C23 | 0.222(1) | 0.673(1) | 1.0911(8) | 4.1(6) |
| C24 | 0.332(1) | 0.659(1) | 1.0881(8) | 3.8(6) |
| C25 | 0.321(1) | 0.562(1) | 1.0481(9) | 4.1(6) |
| C121 | 0.514(1) | 1.026(1) | 0.751(1) | 5.2(7) |
| C122 | 0.622(3) | 1.087(2) | 0.789(2) | 18(2) |
| C131 | 0.525(2) | 0.788(1) | 0.556(1) | 5.5(8) |
| C132 | 0.562(2) | 0.737(2) | 0.491(2) | 10(1) |
| C221 | -0.052(1) | 0.688(1) | 0.4352(9) | 3.6(6) |
| C222 | -0.169(1) | 0.692(1) | 0.414(1) | 7.5(8) |
| C231 | 0.239(1) | 0.684(1) | 0.3676(8) | 3.4(5) |
| C232 | 0.309(2) | 0.711(1) | 0.314(1) | 6.8(9) |

Table 2.3 b, contd. Final Positional and Equivalent Isotropic Thermal Parameters of Non-Hydrogen Atoms for $\text{Fe}_2\text{O}(\text{OAc})_2[\text{CpCo}[\text{OP}(\text{OEt})_2]_3]_2 \cdot 2\text{CH}_3\text{CN}, 4 \cdot 2\text{CH}_3\text{CN}$ at $-78.5\text{ }^\circ\text{C}$.

| Atom | X | Y | Z | B(eq) |
|-------------------|-----------|----------|-----------|--------|
| C321 | -0.081(1) | 0.899(1) | 0.624(1) | 4.0(6) |
| C322 | -0.146(1) | 0.946(1) | 0.688(1) | 4.7(7) |
| C331 | 0.184(2) | 1.029(1) | 0.807(1) | 5.7(8) |
| C332 | 0.255(2) | 0.999(2) | 0.858(1) | 10(1) |
| C421 | -0.095(1) | 0.543(1) | 0.8239(8) | 3.3(5) |
| C422 | -0.210(1) | 0.570(1) | 0.813(1) | 4.4(6) |
| C431 | 0.027(1) | 0.819(1) | 0.979(1) | 4.3(6) |
| C432 | 0.026(2) | 0.896(1) | 1.052(1) | 5.9(8) |
| C521 | 0.365(1) | 0.862(1) | 0.964(1) | 4.1(6) |
| C522 | 0.371(2) | 0.951(1) | 1.030(1) | 6.8(9) |
| C531 | 0.592(2) | 0.694(2) | 0.950(2) | 1.7(6) |
| C531A | 0.582(3) | 0.725(3) | 0.970(2) | 4.0(9) |
| C532 | 0.682(1) | 0.716(1) | 1.020(1) | 6.2(8) |
| C621 | 0.384(2) | 0.441(1) | 0.815(1) | 5.3(7) |
| C622 | 0.413(2) | 0.353(2) | 0.771(1) | 8(1) |
| C631 | 0.040(2) | 0.328(1) | 0.783(1) | 5.7(7) |
| C632 | 0.042(2) | 0.241(1) | 0.800(1) | 9(1) |
| C11 | 0.166(1) | 0.994(2) | 0.491(1) | 2.7(4) |
| C12 | 0.196(2) | 1.061(2) | 0.570(2) | 2.7(4) |
| C13 | 0.317(2) | 1.083(1) | 0.596(1) | 2.7(4) |
| C14 | 0.361(1) | 1.029(2) | 0.533(2) | 2.7(4) |
| C15 | 0.268(2) | 0.973(1) | 0.468(1) | 2.7(4) |
| C11A ^c | 0.165(2) | 1.036(2) | 0.540(2) | 3.6(4) |
| C12A | 0.271(3) | 1.084(1) | 0.595(1) | 3.6(4) |
| C13A | 0.359(1) | 1.051(2) | 0.559(2) | 3.6(4) |
| C14A | 0.307(2) | 0.982(2) | 0.481(1) | 3.6(4) |
| C15A | 0.187(2) | 0.973(2) | 0.470(1) | 3.6(4) |

^aNumbers in parentheses are errors in the last significant digit. ^bSee Figure 2.1 ^b for atom labelling scheme. ^cC11, C12,....., C15 and C11A, C12A,, C15A are two sets of carbon atoms of the disordered Cp ring, each with an occupancy of 0.5.

Table 2.4 a. Final Thermal Parameters of Non-Hydrogen Atoms for
 $\text{Fe}_2\text{O}(\text{OAc})_2\{\text{CpCo}[\text{OP}(\text{OEt})_2]_3\}_2 \cdot 2\text{CH}_3\text{CN}, 4 \cdot 2\text{CH}_3\text{CN}$ at
 25 °C.^a

| Atom | U ₁₁ | U ₂₂ | U ₃₃ | U ₁₂ | U ₁₃ | U ₂₃ |
|------|-----------------|-----------------|-----------------|-----------------|-----------------|-----------------|
| Co1 | 0.070(1) | 0.070(1) | 0.093(1) | -0.003(1) | 0.018(1) | 0.057(1) |
| Co2 | 0.090(1) | 0.088(1) | 0.050(1) | -0.020(1) | 0.007(1) | 0.042(1) |
| Fe1 | 0.067(1) | 0.047(1) | 0.043(1) | -0.0073(8) | 0.0142(8) | 0.0233(8) |
| Fe2 | 0.068(1) | 0.055(1) | 0.045(1) | -0.0020(9) | 0.0193(8) | 0.0280(8) |
| P1 | 0.069(3) | 0.059(2) | 0.082(2) | -0.013(2) | 0.012(2) | 0.041(2) |
| P2 | 0.076(3) | 0.087(3) | 0.064(2) | 0.003(2) | 0.017(2) | 0.048(2) |
| P3 | 0.081(3) | 0.059(2) | 0.089(3) | 0.007(2) | 0.026(2) | 0.039(2) |
| P4 | 0.083(3) | 0.077(2) | 0.046(2) | -0.016(2) | 0.019(2) | 0.027(2) |
| P5 | 0.076(3) | 0.095(3) | 0.064(2) | -0.017(2) | 0.004(2) | 0.050(2) |
| P6 | 0.116(4) | 0.069(2) | 0.070(2) | -0.002(2) | 0.013(2) | 0.045(2) |
| O | 0.096(6) | 0.049(4) | 0.032(4) | -0.006(4) | 0.011(4) | 0.021(3) |
| O1 | 0.100(7) | 0.067(6) | 0.060(5) | 0.021(5) | 0.038(5) | 0.038(5) |
| O2 | 0.079(6) | 0.065(5) | 0.059(5) | -0.024(5) | -0.000(4) | 0.036(4) |
| O3 | 0.112(8) | 0.063(5) | 0.070(5) | 0.025(5) | 0.050(5) | 0.040(5) |
| O4 | 0.082(6) | 0.066(5) | 0.044(5) | -0.019(4) | -0.001(4) | 0.029(4) |
| O11 | 0.055(5) | 0.059(5) | 0.062(5) | -0.008(4) | 0.007(4) | 0.036(4) |
| O12 | 0.12(1) | 0.099(7) | 0.15(1) | -0.059(7) | -0.044(7) | 0.083(7) |
| O13 | 0.089(8) | 0.128(8) | 0.120(8) | 0.037(7) | 0.064(6) | 0.087(7) |
| O21 | 0.096(7) | 0.057(5) | 0.044(4) | -0.004(4) | 0.014(4) | 0.025(4) |
| O22 | 0.099(8) | 0.093(7) | 0.102(7) | 0.002(6) | -0.010(6) | 0.051(6) |
| O23 | 0.17(1) | 0.15(1) | 0.072(7) | 0.048(9) | 0.058(7) | 0.082(7) |
| O31 | 0.060(5) | 0.069(5) | 0.066(5) | 0.011(4) | 0.026(4) | 0.037(4) |
| O32 | 0.095(8) | 0.092(7) | 0.16(1) | 0.034(6) | 0.068(7) | 0.078(7) |
| O33 | 0.15(1) | 0.072(6) | 0.103(8) | -0.010(6) | 0.043(7) | 0.006(6) |
| O41 | 0.077(6) | 0.076(5) | 0.039(4) | -0.001(4) | 0.024(4) | 0.029(4) |
| O42 | 0.086(7) | 0.137(8) | 0.060(6) | -0.027(6) | 0.021(5) | 0.052(6) |
| O43 | 0.119(9) | 0.093(7) | 0.048(5) | 0.002(6) | 0.034(5) | 0.014(5) |
| O51 | 0.086(7) | 0.094(6) | 0.051(5) | -0.016(5) | 0.009(4) | 0.043(5) |
| O52 | 0.123(9) | 0.095(7) | 0.067(6) | -0.038(6) | 0.005(6) | 0.033(6) |
| O53 | 0.093(8) | 0.16(1) | 0.105(8) | -0.001(7) | -0.005(6) | 0.088(7) |

Table 2.4 a,contd Final Thermal Parameters of Non-Hydrogen Atoms for
 $\text{Fe}_2\text{O}(\text{OAc})_2[\text{CpCo}[\text{OP}(\text{OEt})_2]_3]_2 \cdot 2\text{CH}_3\text{CN}, 4 \cdot 2\text{CH}_3\text{CN}$ at
 25 °C.

| Atom | U ₁₁ | U ₂₂ | U ₃₃ | U ₁₂ | U ₁₃ | U ₂₃ |
|------|-----------------|-----------------|-----------------|-----------------|-----------------|-----------------|
| O61 | 0.099(7) | 0.064(5) | 0.052(5) | -0.002(5) | 0.017(4) | 0.036(4) |
| O62 | 0.18(1) | 0.105(8) | 0.109(9) | 0.063(9) | 0.020(8) | 0.064(7) |
| O63 | 0.19(1) | 0.076(6) | 0.082(7) | -0.036(7) | 0.016(7) | 0.054(6) |
| C1 | 0.08(1) | 0.057(8) | 0.064(9) | 0.003(7) | 0.033(7) | 0.019(7) |
| C2 | 0.15(2) | 0.10(1) | 0.14(1) | 0.05(1) | 0.10(1) | 0.06(1) |
| C3 | 0.06(1) | 0.050(7) | 0.045(7) | -0.013(6) | 0.010(7) | 0.006(6) |
| C4 | 0.09(1) | 0.10(1) | 0.068(9) | -0.022(8) | 0.007(8) | 0.040(8) |
| C11 | 0.11(2) | 0.16(2) | 0.20(2) | -0.01(1) | -0.01(2) | 0.16(2) |
| C12 | 0.13(2) | 0.14(2) | 0.17(2) | 0.01(1) | 0.05(2) | 0.13(2) |
| C13 | 0.11(2) | 0.12(2) | 0.27(3) | -0.01(1) | 0.02(2) | 0.17(2) |
| C14 | 0.12(2) | 0.09(1) | 0.19(2) | 0.00(1) | 0.03(2) | 0.09(1) |
| C15 | 0.19(2) | 0.11(2) | 0.22(3) | 0.05(2) | 0.09(2) | 0.13(2) |
| C21 | 0.15(2) | 0.12(1) | 0.06(1) | -0.01(1) | 0.01(1) | 0.07(1) |
| C22 | 0.14(2) | 0.12(1) | 0.05(1) | -0.03(1) | 0.00(1) | 0.06(1) |
| C23 | 0.16(2) | 0.13(2) | 0.032(8) | -0.01(1) | 0.01(1) | 0.037(9) |
| C24 | 0.11(2) | 0.15(2) | 0.06(1) | -0.03(1) | -0.01(1) | 0.07(1) |
| C25 | 0.09(1) | 0.16(2) | 0.08(1) | -0.00(1) | -0.00(1) | 0.09(1) |
| C121 | 0.149(7) | | | | | |
| C122 | 0.16(2) | | | | | |
| C123 | 0.15(1) | | | | | |
| C131 | 0.19(2) | 0.15(2) | 0.16(2) | 0.11(2) | 0.12(2) | 0.08(2) |
| C132 | 0.22(3) | 0.19(2) | 0.22(3) | 0.11(2) | 0.12(2) | 0.09(2) |
| C221 | 0.07(1) | 0.16(2) | 0.22(2) | -0.04(1) | -0.03(1) | 0.11(2) |
| C222 | 0.12(2) | 0.13(2) | 0.19(2) | -0.04(1) | -0.02(2) | 0.04(1) |
| C231 | 0.19(2) | 0.14(2) | 0.08(1) | 0.02(1) | 0.07(1) | 0.04(1) |
| C232 | 0.16(2) | 0.17(2) | 0.12(1) | -0.01(1) | 0.08(1) | 0.06(1) |
| C321 | 0.11(2) | 0.19(2) | 0.27(3) | 0.03(2) | 0.04(2) | 0.16(2) |
| C322 | 0.12(2) | 0.29(3) | 0.15(2) | 0.04(2) | 0.08(1) | 0.10(2) |
| C331 | 0.1981 | | | | | |

Table 2.4 a,contd Final Thermal Parameters of Non-Hydrogen Atoms for
 $\text{Fe}_2\text{O}(\text{OAc})_2[\text{CpCo}[\text{OP}(\text{OEt})_2]_3]_2 \cdot 2\text{CH}_3\text{CN}, 4 \cdot 2\text{CH}_3\text{CN}$ at
 25 °C.

| Atom | U ₁₁ | U ₂₂ | U ₃₃ | U ₁₂ | U ₁₃ | U ₂₃ |
|------------------|-----------------|-----------------|-----------------|-----------------|-----------------|-----------------|
| C332 | 0.1977 | | | | | |
| C421 | 0.09(1) | 0.11(1) | 0.045(8) | -0.05(1) | 0.006(8) | 0.021(8) |
| C422 | 0.11(2) | 0.20(2) | 0.11(1) | -0.00(1) | 0.00(1) | 0.09(1) |
| C431 | 0.15(2) | 0.16(2) | 0.12(2) | 0.09(2) | 0.06(1) | 0.03(1) |
| C432 | 0.22(3) | 0.14(2) | 0.16(2) | 0.03(2) | 0.08(2) | 0.01(2) |
| C521 | 0.19(2) | 0.06(1) | 0.11(1) | 0.01(1) | 0.00(1) | 0.02(1) |
| C522 | 0.27(3) | 0.14(2) | 0.22(3) | 0.04(2) | -0.02(2) | 0.06(2) |
| C531 | 0.06(1) | 0.27(3) | 0.18(2) | -0.03(2) | 0.01(1) | 0.13(2) |
| C532 | 0.09(2) | 0.22(3) | 0.31(3) | -0.02(2) | -0.02(2) | 0.14(2) |
| C621 | 0.18(2) | 0.22(3) | 0.21(2) | 0.13(2) | 0.11(2) | 0.16(2) |
| C622 | 0.25(3) | 0.23(3) | 0.26(3) | 0.16(3) | 0.12(3) | 0.11(3) |
| C631 | 0.30(3) | 0.07(1) | 0.11(1) | -0.06(1) | 0.02(2) | 0.03(1) |
| C632 | 0.32(3) | 0.08(1) | 0.19(2) | -0.03(2) | 0.05(2) | 0.04(1) |
| C1S ^b | 0.1150 | | | | | |
| C2S | 0.1284 | | | | | |
| C3S | 0.2665 | | | | | |
| C4S | 0.1823 | | | | | |
| C5S | 0.1311 | | | | | |
| C6S | 0.1806 | | | | | |
| C7S | 0.1376 | | | | | |
| C8S | 0.1915 | | | | | |
| C9S | 0.1904 | | | | | |

^aNumbers in parentheses are errors in the last significant digit. The anisotropic temperature factors are of the form $\exp[-2\pi^2(U_{11}h^2a^2 + 2U_{12}hkab + \dots)]$. ^bC1S, C2S,, C8S, C9S are arbitrarily assigned atom labels for two disordered acetonitrile molecules. See Figure 2.2. for details of the disorder model.

Table 2.4 b. Final Thermal Parameters of Non-Hydrogen Atoms for
 $\text{Fe}_2\text{O}(\text{OAc})_2[\text{CpCo}[\text{OP}(\text{OEt})_2]_3]_2 \cdot 2\text{CH}_3\text{CN}, 4 \cdot 2\text{CH}_3\text{CN}$ at $-78.5\text{ }^\circ\text{C}$.^a

| Atom ^b | U ₁₁ | U ₂₂ | U ₃₃ | U ₁₂ | U ₁₃ | U ₂₃ |
|-------------------|-----------------|-----------------|-----------------|-----------------|-----------------|-----------------|
| Co1 | 0.029(1) | 0.029(1) | 0.048(1) | 0.0061(8) | 0.0122(9) | 0.028(1) |
| Co2 | 0.028(1) | 0.039(1) | 0.028(1) | 0.0009(8) | 0.0042(8) | 0.024(1) |
| Fe1 | 0.026(1) | 0.026(1) | 0.030(1) | 0.0040(8) | 0.0085(8) | 0.0202(9) |
| Fe2 | 0.027(1) | 0.029(1) | 0.025(1) | 0.0054(8) | 0.0070(8) | 0.0184(9) |
| P1 | 0.027(2) | 0.030(2) | 0.039(2) | 0.004(2) | 0.007(2) | 0.019(2) |
| P2 | 0.031(2) | 0.037(2) | 0.037(2) | 0.009(2) | 0.009(2) | 0.023(2) |
| P3 | 0.033(2) | 0.029(2) | 0.044(2) | 0.010(2) | 0.016(2) | 0.021(2) |
| P4 | 0.026(2) | 0.040(2) | 0.029(2) | 0.004(2) | 0.010(2) | 0.022(2) |
| P5 | 0.026(2) | 0.039(2) | 0.035(2) | -0.000(2) | 0.003(2) | 0.024(2) |
| P6 | 0.038(2) | 0.030(2) | 0.034(2) | 0.009(2) | 0.011(2) | 0.022(2) |
| O | 0.029(5) | 0.027(5) | 0.033(5) | 0.007(4) | 0.011(4) | 0.019(4) |
| O1 | 0.045(6) | 0.034(5) | 0.039(6) | 0.013(5) | 0.019(5) | 0.024(5) |
| O2 | 0.031(5) | 0.042(6) | 0.034(5) | 0.002(4) | -0.000(4) | 0.026(5) |
| O3 | 0.045(6) | 0.033(5) | 0.035(5) | 0.017(4) | 0.018(5) | 0.024(5) |
| O4 | 0.035(5) | 0.032(5) | 0.032(5) | -0.001(4) | 0.001(4) | 0.018(5) |
| O11 | 0.023(5) | 0.028(5) | 0.044(6) | 0.004(4) | 0.006(4) | 0.024(4) |
| O12 | 0.039(6) | 0.049(6) | 0.047(7) | -0.002(5) | 0.002(5) | 0.029(5) |
| O13 | 0.025(5) | 0.046(6) | 0.046(6) | 0.009(4) | 0.012(4) | 0.030(5) |
| O21 | 0.041(5) | 0.026(5) | 0.031(5) | 0.008(4) | 0.017(4) | 0.021(4) |
| O22 | 0.024(5) | 0.041(6) | 0.054(6) | 0.003(4) | 0.000(5) | 0.026(5) |
| O23 | 0.061(7) | 0.058(7) | 0.046(6) | 0.019(6) | 0.018(5) | 0.041(6) |
| O31 | 0.024(5) | 0.035(5) | 0.050(6) | 0.012(4) | 0.013(4) | 0.027(5) |
| O32 | 0.040(6) | 0.041(6) | 0.097(9) | 0.019(5) | 0.038(6) | 0.044(6) |
| O33 | 0.060(7) | 0.034(6) | 0.045(6) | 0.017(5) | 0.021(5) | 0.015(5) |
| O41 | 0.028(5) | 0.038(6) | 0.039(6) | 0.004(4) | 0.010(4) | 0.023(5) |
| O42 | 0.028(5) | 0.067(7) | 0.026(5) | 0.000(5) | 0.010(4) | 0.028(5) |
| O43 | 0.047(6) | 0.047(6) | 0.036(6) | 0.014(5) | 0.019(5) | 0.020(5) |
| O51 | 0.024(5) | 0.042(6) | 0.048(6) | 0.006(4) | 0.010(4) | 0.031(5) |
| O52 | 0.038(6) | 0.054(7) | 0.040(6) | -0.011(5) | 0.003(5) | 0.026(5) |
| O53 | 0.030(7) | | | | | |

Table 2.4 b, contd. Final Thermal Parameters of Non-Hydrogen Atoms for
 $\text{Fe}_2\text{O}(\text{OAc})_2[\text{CpCo}[\text{OP}(\text{OEt})_2]_3]_2 \cdot 2\text{CH}_3\text{CN}, 4 \cdot 2\text{CH}_3\text{CN}$ at
 -78.5 °C.

| Atom | U_{11} | U_{22} | U_{33} | U_{12} | U_{13} | U_{23} |
|------|----------|----------|----------|-----------|-----------|----------|
| O53A | 0.035(7) | | | | | |
| O61 | 0.041(6) | 0.029(5) | 0.029(5) | 0.003(4) | 0.005(4) | 0.012(4) |
| O62 | 0.067(8) | 0.089(9) | 0.067(8) | 0.050(7) | 0.034(6) | 0.056(7) |
| O63 | 0.055(7) | 0.051(7) | 0.043(6) | -0.014(5) | 0.007(5) | 0.033(6) |
| N1S | 0.08(1) | 0.11(2) | 0.11(2) | 0.02(1) | 0.01(1) | 0.07(1) |
| N2S | 0.08(1) | 0.10(2) | 0.10(2) | 0.00(1) | 0.01(1) | 0.01(1) |
| C1S | 0.10(2) | 0.09(2) | 0.07(1) | 0.05(1) | 0.06(1) | 0.05(1) |
| C1 | 0.038(8) | 0.038(9) | 0.024(7) | 0.017(7) | 0.013(6) | 0.016(7) |
| C2S | 0.05(1) | 0.11(1) | 0.08(1) | 0.05(1) | 0.04(1) | 0.07(1) |
| C2 | 0.08(1) | 0.04(1) | 0.07(1) | 0.04(1) | 0.04(1) | 0.035(9) |
| C3 | 0.036(8) | 0.029(8) | 0.023(7) | 0.007(6) | 0.006(6) | 0.018(6) |
| C4 | 0.032(8) | 0.037(9) | 0.06(1) | -0.005(7) | -0.007(7) | 0.032(8) |
| C4S | 0.02(1) | 0.17(2) | 0.11(2) | 0.01(1) | 0.01(1) | 0.09(2) |
| C5S | 0.09(2) | 0.05(1) | 0.08(1) | 0.04(1) | 0.04(1) | 0.02(1) |
| C21 | 0.05(1) | 0.040(9) | 0.021(8) | -0.007(8) | 0.003(7) | 0.026(7) |
| C22 | 0.04(1) | 0.07(1) | 0.034(9) | 0.001(9) | 0.007(7) | 0.030(9) |
| C23 | 0.06(1) | 0.06(1) | 0.029(9) | -0.01(1) | -0.009(8) | 0.032(8) |
| C24 | 0.04(1) | 0.07(1) | 0.027(9) | -0.012(8) | -0.012(7) | 0.031(9) |
| C25 | 0.04(1) | 0.08(1) | 0.04(1) | 0.016(9) | -0.017(7) | 0.03(1) |
| C121 | 0.06(1) | 0.05(1) | 0.06(1) | -0.02(1) | 0.01(1) | 0.01(1) |
| C122 | 0.31(4) | 0.14(3) | 0.10(2) | -0.16(3) | -0.01(2) | 0.02(2) |
| C131 | 0.06(1) | 0.10(2) | 0.07(1) | 0.06(1) | 0.02(1) | 0.04(1) |
| C132 | 0.14(2) | 0.14(2) | 0.13(2) | 0.12(2) | 0.07(2) | 0.05(2) |
| C221 | 0.04(1) | 0.04(1) | 0.04(1) | -0.001(7) | 0.000(7) | 0.018(8) |
| C222 | 0.03(1) | 0.05(1) | 0.15(2) | -0.009(9) | -0.01(1) | -0.00(1) |
| C231 | 0.05(1) | 0.04(1) | 0.04(1) | 0.017(8) | 0.021(8) | 0.013(8) |
| C232 | 0.10(2) | 0.09(2) | 0.08(1) | 0.02(1) | 0.06(1) | 0.04(1) |
| C321 | 0.05(1) | 0.05(1) | 0.07(1) | 0.010(8) | 0.009(9) | 0.05(1) |
| C322 | 0.05(1) | 0.07(1) | 0.08(1) | 0.021(9) | 0.02(1) | 0.04(1) |

Table 2.4 b, contd. Final Thermal Parameters of Non-Hydrogen Atoms for $\text{Fe}_2\text{O}(\text{OAc})_2[\text{CpCo}[\text{OP}(\text{OEt})_2]_3]_2 \cdot 2\text{CH}_3\text{CN}, 4 \cdot 2\text{CH}_3\text{CN}$ at $-78.5\text{ }^\circ\text{C}$.

| Atom | U_{11} | U_{22} | U_{33} | U_{12} | U_{13} | U_{23} |
|-------------------|----------|----------|----------|-----------|----------|----------|
| C331 | 0.07(1) | 0.07(1) | 0.06(1) | 0.01(1) | 0.02(1) | 0.01(1) |
| C332 | 0.10(2) | 0.23(3) | 0.13(2) | 0.10(2) | 0.04(2) | 0.12(2) |
| C421 | 0.032(8) | 0.05(1) | 0.04(1) | -0.005(7) | 0.004(7) | 0.019(8) |
| C422 | 0.04(1) | 0.08(1) | 0.06(1) | 0.013(9) | 0.001(8) | 0.05(1) |
| C431 | 0.06(1) | 0.06(1) | 0.05(1) | 0.03(1) | 0.017(9) | 0.016(9) |
| C432 | 0.10(2) | 0.06(1) | 0.08(1) | 0.05(1) | 0.04(1) | 0.03(1) |
| C521 | 0.07(1) | 0.032(9) | 0.05(1) | 0.005(8) | 0.008(9) | 0.017(8) |
| C522 | 0.13(2) | 0.05(1) | 0.07(1) | 0.02(1) | 0.00(1) | 0.02(1) |
| C531 | 0.022(7) | | | | | |
| C531A | 0.05(1) | | | | | |
| C532 | 0.04(1) | 0.07(1) | 0.12(2) | 0.01(1) | -0.00(1) | 0.03(1) |
| C621 | 0.06(1) | 0.07(1) | 0.08(1) | 0.04(1) | 0.01(1) | 0.03(1) |
| C622 | 0.07(1) | 0.10(2) | 0.12(2) | 0.04(1) | 0.01(1) | 0.04(1) |
| C631 | 0.13(2) | 0.03(1) | 0.04(1) | -0.02(1) | 0.02(1) | 0.011(8) |
| C632 | 0.11(2) | 0.05(1) | 0.15(2) | -0.00(1) | 0.00(2) | 0.04(1) |
| C11 | 0.034(5) | | | | | |
| C12 | 0.034(5) | | | | | |
| C13 | 0.034(5) | | | | | |
| C14 | 0.034(5) | | | | | |
| C15 | 0.034(5) | | | | | |
| C11A ^c | 0.045(5) | | | | | |
| C12A | 0.045(5) | | | | | |
| C13A | 0.045(5) | | | | | |
| C14A | 0.045(5) | | | | | |
| C15A | 0.045(5) | | | | | |

^aNumbers in parentheses are errors in the last significant digit. The anisotropic temperature factors are of the form $\exp[-2\pi^2(U_{11}h^2a^2 + 2U_{12}hkab + \dots)]$. ^bSee Figure 2.1b for the atom labelling scheme. ^cC11-C15

and C11A-C15A are two sets of carbon atoms of the disordered Cp ring, each at 0.5 occupancy.

Table 2.5 a. Selected Interatomic Distances (Å) and Angles (deg) for $\text{Fe}_2\text{O}(\text{OAc})_2\{\text{CpCo}[\text{OP}(\text{OEt})_2]_3\}_2 \cdot 2\text{CH}_3\text{CN}, 4 \cdot 2\text{CH}_3\text{CN}$ at 25 °C.

| <u>Coordination Sphere</u> | | | |
|----------------------------|------------|-------------|-------------|
| Fe1- O | 1.799(6) | Fe2- O | 1.791(6) |
| Fe1- O1 | 2.012(9) | Fe2- O3 | 2.039(8) |
| Fe1- O2 | 2.023(7) | Fe2- O4 | 2.036(8) |
| Fe1- O31 | 2.048(8) | Fe2- O41 | 2.057(7) |
| Fe1- O11 | 2.066(6) | Fe2- O51 | 2.079(8) |
| Fe1- O21 | 2.137(7) | Fe2- O61 | 2.125(7) |
| Fe1... Fe2 | 3.174(2) | | |
| O-Fe1-O1 | 95.4(3) | O-Fe2-O4 | 96.8(3) |
| O-Fe1-O2 | 95.5(3) | O-Fe2-O3 | 95.7(3) |
| O-Fe1-O31 | 96.7(3) | O-Fe2-O41 | 95.6(3) |
| O-Fe1-O11 | 96.9(3) | O-Fe2-O51 | 96.8(3) |
| O-Fe1-O21 | 177.7(3) | O-Fe2-O61 | 179.1(3) |
| O1-Fe1-O2 | 92.6(3) | O4-Fe2-O3 | 90.4(3) |
| O1-Fe1-O31 | 167.7(3) | O4-Fe2-O41 | 90.5(3) |
| O1-Fe1-O11 | 89.4(3) | O4-Fe2-O51 | 166.3(3) |
| O1-Fe1-O21 | 82.5(3) | O4-Fe2-O61 | 82.4(3) |
| O2-Fe1-O31 | 88.5(3) | O3-Fe2-O41 | 168.5(3) |
| O2-Fe1-O11 | 167.2(3) | O3-Fe2-O51 | 89.8(3) |
| O2-Fe1-O21 | 83.6(3) | O3-Fe2-O61 | 83.9(3) |
| O31-Fe1-O11 | 86.9(3) | O41-Fe2-O51 | 86.6(3) |
| O31-Fe1-O21 | 85.4(3) | O41-Fe2-O61 | 84.9(3) |
| O11-Fe1-O21 | 84.1(3) | O51-Fe2-O61 | 84.0(3) |
| Fe1-O-Fe2 | 124.4(4) | | |
| <u>Carboxylate Group</u> | | | |
| | <i>Min</i> | <i>Max</i> | <i>Mean</i> |
| C-C | 1.50(2) | 1.51(2) | 1.51(2) |

Table 2.5 a, contd. Selected Interatomic Distances (Å) and Angles (deg) for $\text{Fe}_2\text{O}(\text{OAc})_2[\text{CpCo}[\text{OP}(\text{OEt})_2]_3]_2 \cdot 2\text{CH}_3\text{CN}$, $4 \cdot 2\text{CH}_3\text{CN}$ at 25 °C.

| <u>Carboxylate Group, contd</u> | | | |
|---|------------|------------|-------------|
| | <i>Min</i> | <i>Max</i> | <i>Mean</i> |
| O-C | 1.23(1) | 1.29(1) | 1.26(1) |
| O-C-O | 114(1) | 120(1) | 117(1) |
| <u>Ligand Geometry</u> | | | |
| | <i>Min</i> | <i>Max</i> | <i>Mean</i> |
| Co-P | 2.144(5) | 2.162(4) | 2.153(5) |
| Co-C | 2.07(1) | 2.13(1) | 2.09(1) |
| P=O | 1.491(8) | 1.520(7) | 1.504(8) |
| P-O _{Et} | 1.59(1) | 1.63(1) | 1.61(1) |
| O-C _{Et} | 1.33(2) | 1.51(2) | 1.43(2) |
| C _{Cp} -C _{Cp} | 1.3713(5) | 1.49(3) | 1.43(3) |
| C _{Et} -C _{Et} | 1.27(2) | 1.61(2) | 1.43(5) |
| P-Co-P | 89.0(1) | 91.0(2) | 90.0(2) |
| O=P-Co | 117.4(3) | 119.2(3) | 118.4(4) |
| O-P-Co | 106.9(4) | 112.8(4) | 109.2(4) |
| O=P-O | 107.3(5) | 110.7(5) | 108.5(6) |
| O-P-O | 100.4(5) | 102.4(6) | 101.6(6) |
| P-O-C _{Et} | 119(1) | 128(1) | 123(1) |
| C _{Cp} -C _{Cp} -C _{Cp} | 102(2) | 114(2) | 108(2) |
| O-C _{Et} -C _{Et} | 98(2) | 118(2) | 110(2) |
| <u>Solvent Geometry</u> | | | |
| C1S ^b - C8S | 1.3102(4) | C4S- C5S | 1.6921(6) |
| C1S- C2S | 1.6334(4) | C5S- C6S | 1.4518(4) |
| C2S- C3S | 1.4908(3) | C6S- C9S | 1.3727(4) |

Table 2.5 a, contd. Selected Interatomic Distances (Å) and Angles (deg) for
 $\text{Fe}_2\text{O}(\text{OAc})_2[\text{CpCo}[\text{OP}(\text{OEt})_2]_3]_2 \cdot 2\text{CH}_3\text{CN}, 4 \cdot 2\text{CH}_3\text{CN}$ at
 25 °C.

| <u>Solvent Geometry, contd</u> | | | |
|--------------------------------|------------|-------------|------------|
| C3S- C4S | 1.5528(4) | C7S- C8S | 1.4734(5) |
| C8S-C1S-C2S | 82.02(2) | C6S-C5S-C4S | 87.49(2) |
| C3S-C2S-C1S | 165.676(5) | C9S-C6S-C5S | 157.888(8) |
| C2S-C3S-C4S | 126.35(2) | C1S-C8S-C7S | 176.86(2) |
| C3S-C4S-C5S | 158.624(9) | | |

^aNumbers in parentheses are errors in the last significant digit(s). See Figure 2.1a for atom labelling scheme. ^bC1S, C2S,, C8S, C9S are arbitrarily assigned atom labels for two disordered acetonitrile molecules. See Figure 2.2 for details of the disorder model.

Table 2.5 b. Selected Interatomic Distances (Å) and Angles (deg) for $\text{Fe}_2\text{O}(\text{OAc})_2\{\text{CpCo}[\text{OP}(\text{OEt})_2]_3\}_2 \cdot 2\text{CH}_3\text{CN}, 4 \cdot 2\text{CH}_3\text{CN}$ at $-78\text{ }^\circ\text{C}.$ ^a

| <u>Coordination Sphere</u> | | | |
|----------------------------|------------|--------------|-------------|
| Fe1- O | 1.79(1) | Fe2- O | 1.80(1) |
| Fe1- O1 | 2.04(1) | Fe2- O3 | 2.046(9) |
| Fe1- O2 | 2.045(8) | Fe2- O4 | 2.035(8) |
| Fe1- O11 | 2.089(8) | Fe2- O41 | 2.079(9) |
| Fe1- O21 | 2.12(1) | Fe2- O51 | 2.088(8) |
| Fe1- O31 | 2.07(1) | Fe2- O61 | 2.12(1) |
| Fe1... Fe2 | 3.174(3) | | |
| O- Fe1- O1 | 94.6(4) | O- Fe2- O3 | 95.3(4) |
| O- Fe1- O2 | 95.6(4) | O- Fe2- O4 | 96.9(4) |
| O- Fe1- O11 | 99.2(4) | O- Fe2- O41 | 96.3(4) |
| O- Fe1- O21 | 176.1(3) | O- Fe2- O51 | 97.7(4) |
| O- Fe1- O31 | 96.2(4) | O- Fe2- O61 | 178.6(3) |
| O1- Fe1- O2 | 94.2(3) | O3- Fe2- O4 | 93.2(3) |
| O1- Fe1- O11 | 88.5(3) | O3- Fe2- O41 | 167.9(4) |
| O1- Fe1- O21 | 82.9(4) | O3- Fe2- O51 | 87.9(3) |
| O1- Fe1- O31 | 168.7(4) | O3- Fe2- O61 | 84.5(4) |
| O2- Fe1- O11 | 164.7(4) | O4-Fe2-O41 | 89.0(3) |
| O2- Fe1- O21 | 81.7(4) | O4-Fe2-O51 | 165.2(4) |
| O2- Fe1- O31 | 87.8(4) | O4-Fe2-O61 | 81.8(4) |
| O11- Fe1- O21 | 83.7(3) | O41-Fe2-O51 | 87.0(3) |
| O11- Fe1- O31 | 86.7(3) | O41-Fe2-O61 | 84.1(4) |
| O21- Fe1- O31 | 86.5(4) | O51-Fe2-O61 | 83.6(4) |
| Fe1-O-Fe2 | 124.4(4) | | |
| <u>Carboxylate Group</u> | | | |
| | <i>Min</i> | <i>Max</i> | <i>Mean</i> |
| C-C | 1.50(2) | 1.51(2) | 1.51(2) |

Table 2.5 b, contd. Selected Interatomic Distances (Å) and Angles (deg) for $\text{Fe}_2\text{O}(\text{OAc})_2[\text{CpCo}[\text{OP}(\text{OEt})_2]_3]_2 \cdot 2\text{CH}_3\text{CN}, 4 \cdot 2\text{CH}_3\text{CN}$ at $-78\text{ }^\circ\text{C}$.

| <u>Carboxylate Group, contd</u> | | | |
|---|------------|------------|-------------|
| | <i>Min</i> | <i>Max</i> | <i>Mean</i> |
| O-C | 1.25(2) | 1.27(2) | 1.26(2) |
| O-C-O | 125(1) | 125(1) | 125(1) |
| <u>Ligand Geometry</u> | | | |
| | <i>Min</i> | <i>Max</i> | <i>Mean</i> |
| Co-P | 2.151(4) | 2.172(5) | 2.162(5) |
| Co-C | 2.06(3) | 2.12(3) | 2.09(3) |
| P=O | 1.48(1) | 1.52(1) | 1.50(1) |
| P-O _{Et} | 1.53(3) | 1.65(3) | 1.59(3) |
| O-C _{Et} | 1.40(2) | 1.53(4) | 1.44(4) |
| C _{Cp} -C _{Cp} | 1.40(3) | 1.40(4) | 1.40(4) |
| C _{Et} -C _{Et} | 1.35(3) | 1.54(2) | 1.46(3) |
| P-Co-P | 88.5(2) | 91.1(2) | 89.9(2) |
| O=P-Co | 116.3(3) | 120.3(3) | 118.5(3) |
| O-P-Co | 106.4(4) | 114.0(5) | 109.1(5) |
| O=P-O | 106.3(6) | 115(1) | 109(1) |
| O-P-O | 93.4(9) | 106.1(8) | 100.1(9) |
| P-O-C _{Et} | 100(1) | 125(1) | 119(1) |
| C _{Cp} -C _{Cp} -C _{Cp} | 108(2) | 108(2) | 108(2) |
| O-C _{Et} -C _{Et} | 104(1) | 111(2) | 110(2) |
| <u>Solvent Geometry</u> | | | |
| C-N | 1.19(3) | 1.20(3) | 1.20(3) |
| C-C | 1.45(3) | 1.47(3) | 1.46(3) |

Table 2.5 b, contd. Selected Interatomic Distances (Å) and Angles (deg) for
 $\text{Fe}_2\text{O}(\text{OAc})_2[\text{CpCo}[\text{OP}(\text{OEt})_2]_3]_2 \cdot 2\text{CH}_3\text{CN}, 4 \cdot 2\text{CH}_3\text{CN}$ at
-78 °C.

Solvent Geometry, contd

| | | | |
|-------|--------|--------|--------|
| C-C-N | 176(2) | 177(3) | 177(3) |
|-------|--------|--------|--------|

^aNumbers in parentheses are errors in the last significant digit(s). See
Figure 2.1b for atom labelling scheme.

Table 2.6. Final Positional and Equivalent Isotropic Thermal Parameters for $[\text{Fe}_2(\text{OH})(\text{OAc})_2(\text{CpCo}[\text{OP}(\text{OEt})_2]_3)_2][\text{BPh}_4] \cdot \text{CH}_2\text{Cl}_2 \cdot 0.5\text{C}_7\text{H}_8$, $5\text{CH}_2\text{Cl}_2 \cdot 0.5\text{C}_7\text{H}_8$.^a

| Atom ^b | X | Y | Z | B(eq) |
|-------------------|------------|------------|------------|---------|
| Co1 | 0.1109(1) | 0.05011(7) | 0.38470(7) | 2.97(4) |
| Co2 | 0.0248(1) | 0.42653(7) | 0.13337(7) | 3.09(5) |
| Fe1 | 0.0883(1) | 0.24971(7) | 0.39142(7) | 2.77(4) |
| Fe2 | 0.0577(1) | 0.37615(7) | 0.30681(7) | 2.82(5) |
| Cl1 | 0.2509(3) | 0.3831(2) | 0.8647(2) | 6.9(1) |
| Cl2 | 0.3211(3) | 0.3325(2) | 0.9836(2) | 7.7(2) |
| P1 | 0.1622(2) | 0.1542(1) | 0.4860(1) | 3.27(9) |
| P2 | 0.1847(2) | 0.0970(1) | 0.3192(2) | 3.6(1) |
| P3 | -0.0404(2) | 0.0892(2) | 0.3582(1) | 3.6(1) |
| P4 | 0.1575(2) | 0.3754(2) | 0.1692(2) | 3.3(1) |
| P5 | 0.0340(3) | 0.5067(1) | 0.2489(2) | 4.0(1) |
| P6 | -0.0930(2) | 0.3501(1) | 0.1462(1) | 2.83(8) |
| O | 0.0540(5) | 0.2730(3) | 0.3023(3) | 2.8(2) |
| O1 | 0.2158(6) | 0.3350(3) | 0.4449(4) | 3.9(2) |
| O2 | -0.0102(6) | 0.3207(4) | 0.4420(3) | 4.0(3) |
| O3 | 0.1971(6) | 0.4162(4) | 0.3906(4) | 3.9(2) |
| O4 | -0.0280(6) | 0.4029(3) | 0.3877(3) | 3.7(2) |
| O11 | 0.1267(5) | 0.2261(3) | 0.4822(3) | 3.1(2) |
| O12 | 0.2904(6) | 0.1670(4) | 0.5137(5) | 5.3(3) |
| O13 | 0.1228(6) | 0.1448(4) | 0.5552(3) | 4.4(3) |
| O21 | 0.1887(5) | 0.1813(3) | 0.3399(3) | 3.2(2) |
| O22 | 0.1234(9) | 0.0507(4) | 0.2293(4) | 7.3(4) |
| O23 | 0.3023(8) | 0.0774(5) | 0.3174(7) | 8.9(5) |
| O31 | -0.0323(5) | 0.1614(3) | 0.3448(3) | 3.2(2) |
| O32 | -0.1244(8) | 0.0254(5) | 0.2876(5) | 7.0(4) |
| O33 | -0.1025(6) | 0.0999(5) | 0.4250(4) | 5.4(3) |
| O41 | 0.1461(5) | 0.3450(3) | 0.2284(3) | 3.2(2) |
| O42 | 0.2666(6) | 0.4344(5) | 0.1999(5) | 6.5(4) |
| O43 | 0.1908(6) | 0.3086(5) | 0.1025(4) | 5.1(3) |

Table 2.6, contd. Final Positional and Equivalent Isotropic Thermal
Parameters for $[\text{Fe}_2(\text{OH})(\text{OAc})_2(\text{CpCo}[\text{OP}(\text{OEt})_2]_3)_2][\text{BPh}_4]$
 $\cdot \text{CH}_2\text{Cl}_2 \cdot 0.5\text{C}_7\text{H}_8$, $5\text{CH}_2\text{Cl}_2 \cdot 0.5\text{C}_7\text{H}_8$.

| Atom | X | Y | Z | B(eq) |
|------|------------|------------|-----------|--------|
| O51 | 0.0715(6) | 0.4805(3) | 0.3129(3) | 3.7(2) |
| O52 | -0.0807(7) | 0.5343(4) | 0.2531(4) | 5.8(3) |
| O53 | 0.1069(8) | 0.5858(4) | 0.2741(5) | 6.3(4) |
| O61 | -0.0778(5) | 0.3475(3) | 0.2249(3) | 2.9(2) |
| O62 | -0.2120(5) | 0.3664(4) | 0.1240(4) | 3.8(2) |
| O63 | -0.0975(5) | 0.2666(3) | 0.0833(3) | 3.5(2) |
| C1 | 0.2452(7) | 0.3937(5) | 0.4372(5) | 3.2(3) |
| C2 | 0.351(1) | 0.4430(6) | 0.4909(7) | 5.6(5) |
| C3 | -0.0474(8) | 0.3759(5) | 0.4341(5) | 3.2(3) |
| C4 | -0.117(1) | 0.4167(6) | 0.4870(6) | 4.7(4) |
| C5 | 0.156(1) | -0.0552(6) | 0.3246(6) | 5.0(5) |
| C6 | 0.221(1) | -0.0203(6) | 0.3993(7) | 4.9(5) |
| C7 | 0.152(1) | -0.0105(6) | 0.4505(6) | 5.0(5) |
| C8 | 0.046(1) | -0.0376(6) | 0.4063(8) | 5.4(5) |
| C8S | 0.353(1) | 0.3421(8) | 0.9042(7) | 6.4(6) |
| C9 | 0.047(1) | -0.0643(5) | 0.3264(7) | 5.1(5) |
| C10 | -0.049(1) | 0.3905(7) | 0.0186(6) | 4.5(4) |
| C11 | 0.061(1) | 0.4031(9) | 0.0294(7) | 6.1(6) |
| C12 | 0.101(1) | 0.483(1) | 0.0809(9) | 7.9(7) |
| C13 | 0.006(1) | 0.5128(7) | 0.0984(7) | 5.9(6) |
| C14 | -0.081(1) | 0.4563(6) | 0.0604(6) | 4.0(4) |
| C40 | 0.6074(9) | 0.2979(5) | 0.8493(6) | 3.7(4) |
| C41 | 0.542(1) | 0.3189(6) | 0.7974(6) | 4.4(4) |
| C42 | 0.526(1) | 0.3946(7) | 0.8160(7) | 5.2(5) |
| C43 | 0.571(1) | 0.4502(7) | 0.8870(8) | 5.3(5) |
| C44 | 0.632(1) | 0.4303(6) | 0.9402(7) | 5.2(5) |
| C45 | 0.6517(9) | 0.3572(6) | 0.9211(6) | 4.3(4) |
| C46 | 0.5967(9) | 0.1735(6) | 0.8834(7) | 4.6(4) |
| C47 | 0.5506(9) | 0.2091(7) | 0.9445(7) | 5.1(5) |

Table 2.6, contd. Final Positional and Equivalent Isotropic Thermal
Parameters for $[\text{Fe}_2(\text{OH})(\text{OAc})_2(\text{CpCo}[\text{OP}(\text{OEt})_2]_3)_2][\text{BPh}_4]$
 $\cdot \text{CH}_2\text{Cl}_2 \cdot 0.5\text{C}_7\text{H}_8$, $5 \cdot \text{CH}_2\text{Cl}_2 \cdot 0.5\text{C}_7\text{H}_8$.

| Atom | X | Y | Z | B(eq) |
|-------|-----------|-----------|-----------|---------|
| C48 | 0.518(1) | 0.174(1) | 0.9862(9) | 6.5(6) |
| C49 | 0.528(1) | 0.102(1) | 0.971(1) | 8.5(8) |
| C50 | 0.575(1) | 0.0631(9) | 0.912(1) | 8.2(7) |
| C51 | 0.607(1) | 0.0960(7) | 0.8661(8) | 5.9(5) |
| C52 | 0.566(1) | 0.1568(7) | 0.7387(7) | 6.1(5) |
| C53 | 0.457(1) | 0.1259(8) | 0.7254(9) | 8.2(7) |
| C54 | 0.446(2) | 0.074(1) | 0.594(1) | 11(1) |
| C55 | 0.394(2) | 0.083(1) | 0.651(1) | 11(1) |
| C56 | 0.542(2) | 0.099(1) | 0.602(1) | 14(1) |
| C57 | 0.606(1) | 0.142(1) | 0.6786(7) | 8.9(7) |
| C58 | 0.767(1) | 0.2181(5) | 0.8362(5) | 3.9(4) |
| C59 | 0.838(1) | 0.1815(6) | 0.8698(5) | 4.1(4) |
| C60 | 0.946(1) | 0.1891(7) | 0.8735(6) | 4.8(4) |
| C61 | 0.996(1) | 0.2326(7) | 0.8448(7) | 5.5(5) |
| C62 | 0.821(1) | 0.2642(7) | 0.8088(7) | 5.5(5) |
| C63 | 0.930(1) | 0.2697(6) | 0.8117(7) | 5.8(6) |
| C121 | 0.348(1) | 0.229(1) | 0.571(1) | 6.1(4) |
| C121A | 0.356(4) | 0.234(3) | 0.525(3) | 4(1) |
| C122 | 0.440(2) | 0.261(1) | 0.552(1) | 9.4(6) |
| C122A | 0.388(4) | 0.298(3) | 0.595(3) | 6(1) |
| C131 | 0.093(2) | 0.2020(7) | 0.616(1) | 10.4(9) |
| C132 | 0.160(2) | 0.210(2) | 0.687(1) | 22(2) |
| C221 | 0.133(2) | 0.077(1) | 0.1744(9) | 13(1) |
| C222 | 0.094(2) | 0.017(1) | 0.101(1) | 11(1) |
| C231 | 0.399(3) | 0.126(2) | 0.323(2) | 8.8(9) |
| C231A | 0.392(2) | 0.110(1) | 0.360(1) | 3.2(4) |
| C232 | 0.492(1) | 0.087(1) | 0.325(1) | 9.1(8) |
| C321 | -0.155(2) | 0.022(1) | 0.217(2) | 9.6(6) |
| C321A | -0.226(4) | 0.013(3) | 0.251(3) | 5(1) |

Table 2.6, contd. Final Positional and Equivalent Isotropic Thermal
Parameters for $[\text{Fe}_2(\text{OH})(\text{OAc})_2\{\text{CpCo}[\text{OP}(\text{OEt})_2\}_3\}_2][\text{BPh}_4]$
 $\cdot \text{CH}_2\text{Cl}_2 \cdot 0.5\text{C}_7\text{H}_8$, $5 \cdot \text{CH}_2\text{Cl}_2 \cdot 0.5\text{C}_7\text{H}_8$.

| Atom | X | Y | Z | B(eq) |
|-------|-----------|-----------|-----------|---------|
| C322 | -0.252(2) | -0.040(2) | 0.173(1) | 17(1) |
| C331 | -0.192(1) | 0.148(1) | 0.434(1) | 8.9(8) |
| C332 | -0.157(5) | 0.195(4) | 0.516(4) | 8(1) |
| C332A | -0.254(2) | 0.141(1) | 0.480(1) | 8.3(5) |
| C421 | 0.366(1) | 0.416(1) | 0.227(1) | 10(1) |
| C422 | 0.430(2) | 0.471(1) | 0.297(1) | 12(1) |
| C431 | 0.147(1) | 0.2313(8) | 0.0744(7) | 6.7(6) |
| C432 | 0.211(1) | 0.180(1) | 0.031(1) | 11(1) |
| C521 | -0.102(2) | 0.585(1) | 0.330(1) | 14(1) |
| C522 | -0.159(4) | 0.554(3) | 0.362(3) | 10(1) |
| C522A | -0.211(3) | 0.578(2) | 0.334(2) | 9(1) |
| C531 | 0.223(2) | 0.600(1) | 0.305(1) | 12(1) |
| C532 | 0.240(2) | 0.680(2) | 0.372(1) | 10.6(7) |
| C532A | 0.289(6) | 0.623(4) | 0.385(5) | 10(2) |
| C621 | -0.281(2) | 0.397(2) | 0.177(2) | 5.3(6) |
| C621A | -0.301(2) | 0.363(2) | 0.166(2) | 4.8(6) |
| C622 | -0.363(2) | 0.432(1) | 0.149(1) | 4.8(5) |
| C622A | -0.397(3) | 0.387(2) | 0.136(2) | 7.2(7) |
| C631 | -0.181(1) | 0.2052(7) | 0.0711(6) | 5.3(5) |
| C632 | -0.133(1) | 0.1446(9) | 0.083(1) | 10(1) |
| B | 0.636(1) | 0.2098(7) | 0.8278(6) | 3.9(4) |
| C1S | 0.634(1) | 0.247(1) | 0.280(1) | 8.9(3) |
| C2S | 0.553(2) | 0.209(1) | 0.213(1) | 8.9(3) |
| C3S | 0.444(2) | 0.214(1) | 0.2134(8) | 8.9(3) |
| C4S | 0.415(1) | 0.2577(8) | 0.2810(9) | 8.9(3) |
| C5S | 0.496(2) | 0.296(1) | 0.3482(8) | 8.9(3) |
| C6S | 0.606(1) | 0.291(1) | 0.348(1) | 8.9(3) |
| C7S | 0.295(1) | 0.263(1) | 0.282(1) | 8.9(3) |

^aNumbers in parentheses are errors in the last significant digit. ^bSee Figure 2.3. for atom labelling scheme. ^cC1S,C2S, C3S, C4S, C7S, C8S, and C9S are the carbon atoms on the toluene molecule while C6S is the carbon atom of the methylene chloride molecule.

Table 2.7. Final Thermal Parameters of Non-Hydrogen Atoms for
 $[\text{Fe}_2(\text{OH})(\text{OAc})_2\{\text{CpCo}[\text{OP}(\text{OEt})_2]_3\}_2][\text{BPh}_4]\cdot\text{CH}_2\text{Cl}_2\cdot 0.5\text{C}_7\text{H}_8$,
 $5\cdot\text{CH}_2\text{Cl}_2\cdot 0.5\text{C}_7\text{H}_8$.^a

| Atom ^b | U ₁₁ | U ₂₂ | U ₃₃ | U ₁₂ | U ₁₃ | U ₂₃ |
|-------------------|-----------------|-----------------|-----------------|-----------------|-----------------|-----------------|
| Co1 | 0.0609(9) | 0.0242(6) | 0.0282(7) | 0.0053(6) | 0.0180(6) | 0.0084(5) |
| Co2 | 0.0533(8) | 0.0403(8) | 0.0324(7) | 0.0108(6) | 0.0117(6) | 0.0227(6) |
| Fe1 | 0.0502(8) | 0.0296(7) | 0.0260(7) | 0.0076(6) | 0.0084(6) | 0.0120(6) |
| Fe2 | 0.0532(9) | 0.0312(7) | 0.0259(7) | 0.0110(6) | 0.0106(6) | 0.0137(6) |
| C11 | 0.079(2) | 0.090(3) | 0.076(2) | 0.013(2) | 0.006(2) | 0.023(2) |
| C12 | 0.095(3) | 0.124(3) | 0.107(3) | 0.035(2) | 0.057(2) | 0.064(3) |
| P1 | 0.064(2) | 0.029(1) | 0.030(1) | 0.005(1) | 0.009(1) | 0.013(1) |
| P2 | 0.061(2) | 0.040(1) | 0.047(2) | 0.014(1) | 0.028(1) | 0.020(1) |
| P3 | 0.051(2) | 0.047(2) | 0.036(1) | -0.004(1) | 0.012(1) | 0.013(1) |
| P4 | 0.043(2) | 0.051(2) | 0.046(2) | 0.008(1) | 0.017(1) | 0.031(1) |
| P5 | 0.080(2) | 0.033(1) | 0.038(2) | 0.013(1) | 0.007(1) | 0.017(1) |
| P6 | 0.042(1) | 0.042(1) | 0.027(1) | 0.012(1) | 0.011(1) | 0.016(1) |
| O | 0.059(4) | 0.027(3) | 0.018(3) | 0.010(3) | 0.007(3) | 0.009(3) |
| O1 | 0.067(5) | 0.030(4) | 0.046(4) | -0.002(3) | -0.007(4) | 0.022(3) |
| O2 | 0.086(5) | 0.048(4) | 0.035(4) | 0.034(4) | 0.030(4) | 0.022(3) |
| O3 | 0.062(5) | 0.041(4) | 0.039(4) | -0.002(3) | -0.006(3) | 0.022(3) |
| O4 | 0.074(5) | 0.039(4) | 0.033(4) | 0.025(4) | 0.021(4) | 0.015(3) |
| O11 | 0.066(4) | 0.029(3) | 0.023(3) | 0.009(3) | 0.008(3) | 0.010(3) |
| O12 | 0.061(5) | 0.045(4) | 0.080(6) | -0.002(4) | -0.015(4) | 0.026(4) |
| O13 | 0.108(6) | 0.035(4) | 0.026(4) | 0.017(4) | 0.023(4) | 0.009(3) |
| O21 | 0.048(4) | 0.042(4) | 0.045(4) | 0.011(3) | 0.023(3) | 0.026(3) |
| O22 | 0.19(1) | 0.054(5) | 0.037(5) | 0.002(6) | 0.058(6) | 0.012(4) |
| O23 | 0.093(7) | 0.088(7) | 0.23(1) | 0.046(6) | 0.099(9) | 0.109(8) |
| O31 | 0.040(4) | 0.042(4) | 0.040(4) | 0.004(3) | 0.003(3) | 0.020(3) |
| O32 | 0.115(8) | 0.071(6) | 0.052(5) | -0.043(5) | -0.020(5) | 0.026(5) |
| O33 | 0.062(5) | 0.098(6) | 0.080(6) | 0.022(5) | 0.048(5) | 0.057(5) |
| O41 | 0.047(4) | 0.044(4) | 0.043(4) | 0.016(3) | 0.017(3) | 0.024(3) |
| O42 | 0.048(5) | 0.101(7) | 0.117(8) | -0.005(5) | 0.004(5) | 0.075(6) |
| O43 | 0.082(6) | 0.079(6) | 0.070(5) | 0.038(5) | 0.049(5) | 0.052(5) |
| O51 | 0.082(5) | 0.026(3) | 0.031(4) | 0.010(3) | 0.012(3) | 0.013(3) |

Table 2.7, contd Final Thermal Parameters of Non-Hydrogen Atoms for
 $[\text{Fe}_2(\text{OH})(\text{OAc})_2[\text{CpCo}[\text{OP}(\text{OEt})_2]_3]_2][\text{BPh}_4]\cdot\text{CH}_2\text{Cl}_2\cdot 0.5\text{C}_7\text{H}_8$,
 $5\cdot\text{CH}_2\text{Cl}_2\cdot 0.5\text{C}_7\text{H}_8$.

| Atom | U ₁₁ | U ₂₂ | U ₃₃ | U ₁₂ | U ₁₃ | U ₂₃ |
|------|-----------------|-----------------|-----------------|-----------------|-----------------|-----------------|
| O52 | 0.104(7) | 0.060(5) | 0.047(5) | 0.051(5) | 0.013(4) | 0.007(4) |
| O53 | 0.126(8) | 0.039(5) | 0.060(5) | -0.010(5) | -0.011(5) | 0.025(4) |
| O61 | 0.040(4) | 0.053(4) | 0.025(3) | 0.012(3) | 0.010(3) | 0.022(3) |
| O62 | 0.046(4) | 0.064(5) | 0.039(4) | 0.020(4) | 0.014(3) | 0.024(4) |
| O63 | 0.053(4) | 0.036(4) | 0.038(4) | 0.005(3) | 0.013(3) | 0.007(3) |
| C1 | 0.033(5) | 0.042(6) | 0.040(6) | 0.004(4) | 0.003(4) | 0.013(5) |
| C2 | 0.076(8) | 0.055(7) | 0.068(8) | -0.013(6) | -0.013(7) | 0.030(6) |
| C3 | 0.047(6) | 0.036(5) | 0.027(5) | 0.004(5) | 0.005(4) | 0.001(4) |
| C4 | 0.083(8) | 0.053(7) | 0.049(7) | 0.027(6) | 0.034(6) | 0.016(6) |
| C5 | 0.12(1) | 0.033(6) | 0.040(7) | 0.033(7) | 0.034(7) | 0.010(5) |
| C6 | 0.089(9) | 0.037(6) | 0.076(8) | 0.033(6) | 0.031(7) | 0.031(6) |
| C7 | 0.12(1) | 0.035(6) | 0.052(7) | 0.027(7) | 0.033(8) | 0.027(6) |
| C8 | 0.11(1) | 0.024(6) | 0.08(1) | 0.007(6) | 0.053(9) | 0.020(6) |
| C8S | 0.08(1) | 0.11(1) | 0.08(1) | 0.030(8) | 0.032(8) | 0.058(9) |
| C9 | 0.10(1) | 0.019(5) | 0.060(8) | -0.012(6) | 0.034(7) | -0.005(5) |
| C10 | 0.073(8) | 0.077(8) | 0.033(6) | 0.015(7) | 0.007(6) | 0.036(6) |
| C11 | 0.11(1) | 0.11(1) | 0.065(8) | 0.06(1) | 0.058(9) | 0.071(9) |
| C12 | 0.07(1) | 0.17(2) | 0.09(1) | -0.06(1) | -0.023(8) | 0.11(1) |
| C13 | 0.14(1) | 0.045(7) | 0.049(7) | 0.015(8) | 0.009(8) | 0.035(6) |
| C14 | 0.083(8) | 0.051(7) | 0.032(6) | 0.027(6) | 0.013(6) | 0.027(5) |
| C40 | 0.061(7) | 0.039(6) | 0.039(6) | 0.012(5) | 0.018(5) | 0.012(5) |
| C41 | 0.079(8) | 0.041(6) | 0.045(6) | 0.018(6) | 0.014(6) | 0.014(5) |
| C42 | 0.09(1) | 0.063(8) | 0.066(8) | 0.035(7) | 0.033(7) | 0.041(7) |
| C43 | 0.068(8) | 0.056(8) | 0.08(1) | 0.019(6) | 0.016(7) | 0.027(7) |
| C44 | 0.063(8) | 0.049(7) | 0.064(8) | -0.003(6) | 0.015(6) | 0.003(6) |
| C45 | 0.059(7) | 0.036(6) | 0.050(7) | 0.004(5) | 0.007(5) | 0.004(5) |
| C46 | 0.049(7) | 0.051(7) | 0.067(8) | -0.005(5) | -0.013(6) | 0.033(6) |
| C47 | 0.049(7) | 0.082(9) | 0.065(8) | 0.013(6) | 0.009(6) | 0.036(7) |
| C48 | 0.064(9) | 0.11(1) | 0.10(1) | 0.013(8) | 0.015(8) | 0.08(1) |
| C49 | 0.06(1) | 0.16(2) | 0.12(1) | -0.01(1) | 0.02(1) | 0.10(1) |

Table 2.7, contd Final Thermal Parameters of Non-Hydrogen Atoms for
 $[\text{Fe}_2(\text{OH})(\text{OAc})_2\{\text{CpCo}[\text{OP}(\text{OEt})_2]_3\}_2][\text{BPh}_4]\cdot\text{CH}_2\text{Cl}_2\cdot 0.5\text{C}_7\text{H}_8,$
 $5\cdot\text{CH}_2\text{Cl}_2\cdot 0.5\text{C}_7\text{H}_8.$

| Atom | U ₁₁ | U ₂₂ | U ₃₃ | U ₁₂ | U ₁₃ | U ₂₃ |
|-------|-----------------|-----------------|-----------------|-----------------|-----------------|-----------------|
| C332A | 0.106(7) | | | | | |
| C421 | 0.05(1) | 0.18(2) | 0.20(2) | 0.00(1) | 0.01(1) | 0.13(2) |
| C422 | 0.11(1) | 0.22(2) | 0.15(2) | -0.03(2) | -0.04(1) | 0.13(2) |
| C431 | 0.09(1) | 0.09(1) | 0.052(8) | 0.021(9) | 0.033(7) | 0.005(7) |
| C432 | 0.13(1) | 0.11(1) | 0.22(2) | 0.08(1) | 0.12(1) | 0.09(1) |
| C521 | 0.19(2) | 0.12(2) | 0.10(1) | 0.12(2) | -0.05(1) | -0.05(1) |
| C522 | 0.13(2) | | | | | |
| C522A | 0.12(1) | | | | | |
| C531 | 0.19(2) | 0.06(1) | 0.20(2) | -0.02(1) | -0.00(2) | 0.06(1) |
| C532 | 0.134(9) | | | | | |
| C532A | 0.12(2) | | | | | |
| C621 | 0.067(8) | | | | | |
| C621A | 0.061(7) | | | | | |
| C622 | 0.061(6) | | | | | |
| C622A | 0.09(1) | | | | | |
| C631 | 0.074(8) | 0.061(8) | 0.049(7) | -0.006(7) | 0.012(6) | 0.010(6) |
| C632 | 0.12(1) | 0.07(1) | 0.23(2) | 0.02(1) | 0.04(1) | 0.08(1) |
| B | 0.061(8) | 0.040(7) | 0.027(6) | 0.008(6) | -0.004(6) | 0.000(5) |
| C1S | 0.113(4) | | | | | |
| C2S | 0.113(4) | | | | | |
| C3S | 0.113(4) | | | | | |
| C4S | 0.113(4) | | | | | |
| C5S | 0.113(4) | | | | | |
| C6S | 0.113(4) | | | | | |
| C7S | 0.113(4) | | | | | |

^aNumbers in parentheses are errors in the last significant digit. The anisotropic temperature factors are of the form $\exp[-2\pi^2(U_{11}h^2a^2 + 2U_{12}hkab + \dots)]$. ^bSee Figure 2.3 for atom labelling scheme. ^cC1S, C2S, C3S,

C4S, C7S, C8S, and C9S are the carbon atoms on the toluene molecule while C6S is the carbon atom of the methylene chloride molecule.

Table 2.8. Selected Interatomic Distances (Å) and Angles (deg) for
 $[\text{Fe}_2(\text{OH})(\text{OAc})_2\{\text{CpCo}[\text{OP}(\text{OEt})_2]_3\}_2][\text{BPh}_4]\cdot\text{CH}_2\text{Cl}_2\cdot 0.5\text{C}_7\text{H}_8$,
 $5\cdot\text{CH}_2\text{Cl}_2\cdot 0.5\text{C}_7\text{H}_8$.^a

| <u>Coordination Sphere</u> | | | |
|----------------------------|------------|-------------|-------------|
| Fe1- O | 1.953(7) | Fe2- O | 1.971(6) |
| Fe1- O1 | 2.016(6) | Fe2- O3 | 2.028(6) |
| Fe1- O2 | 2.017(7) | Fe2- O4 | 2.011(8) |
| Fe1- O11 | 1.990(7) | Fe2- O41 | 1.998(7) |
| Fe1- O21 | 2.016(7) | Fe2- O51 | 1.979(7) |
| Fe1- O31 | 1.996(6) | Fe2- O61 | 1.984(5) |
| Fe1... Fe2 | 3.474(2) | | |
| O-Fe1-O1 | 92.9(3) | O-Fe2-O3 | 92.5(3) |
| O-Fe1-O2 | 90.7(3) | O-Fe2-O4 | 90.2(3) |
| O-Fe1-O11 | 178.8(3) | O-Fe2-O41 | 86.8(3) |
| O-Fe1-O21 | 88.0(3) | O-Fe2-O51 | 176.4(3) |
| O-Fe1-O31 | 91.9(3) | O-Fe2-O61 | 93.4(3) |
| O1-Fe1-O2 | 89.4(3) | O3-Fe2-O4 | 88.8(3) |
| O1-Fe1-O11 | 86.2(3) | O3-Fe2-O41 | 89.8(3) |
| O1-Fe1-O21 | 89.4(3) | O3-Fe2-O51 | 84.5(3) |
| O1-Fe1-O31 | 174.9(3) | O3-Fe2-O61 | 174.1(3) |
| O2-Fe1-O11 | 90.2(3) | O4-Fe2-O41 | 176.6(3) |
| O2-Fe1-O21 | 178.2(3) | O4-Fe2-O51 | 91.7(3) |
| O2-Fe1-O31 | 92.1(3) | O4-Fe2-O61 | 91.5(3) |
| O11-Fe1-O21 | 91.1(3) | O41-Fe2-O51 | 91.2(3) |
| O11-Fe1-O31 | 88.9(3) | O41-Fe2-O61 | 90.2(2) |
| O21-Fe1-O31 | 89.2(2) | O51-Fe2-O61 | 89.6(3) |
| Fe1-O-Fe2 | 124.5(2) | | |
| <u>Carboxylate Group</u> | | | |
| | <i>Min</i> | <i>Max</i> | <i>Mean</i> |
| C-C | 1.51(2) | 1.52(1) | 1.52(2) |

Table 2.8. Selected Interatomic Distances (Å) and Angles (deg) for
 $[\text{Fe}_2(\text{OH})(\text{OAc})_2\{\text{CpCo}[\text{OP}(\text{OEt})_2]_3\}_2][\text{BPh}_4]\cdot\text{CH}_2\text{Cl}_2\cdot 0.5\text{C}_7\text{H}_8$,
 $5\cdot\text{CH}_2\text{Cl}_2\cdot 0.5\text{C}_7\text{H}_8$.

| <u>Carboxylate Group, contd</u> | | | |
|---|------------|------------|-------------|
| | <i>Min</i> | <i>Max</i> | <i>Mean</i> |
| O-C | 1.24(1) | 1.25(1) | 1.25(1) |
| O-C-O | 125.9(9) | 127.0(8) | 126.5(9) |
| <u>Ligand Geometry</u> | | | |
| | <i>Min</i> | <i>Max</i> | <i>Mean</i> |
| Co-P | 2.150(4) | 2.162(3) | 2.153(4) |
| Co-C | 2.05(1) | 2.10(1) | 2.07(1) |
| P=O | 1.521(7) | 1.541(8) | 1.529(8) |
| P-O _{OEt} | 1.56(1) | 1.628(8) | 1.59(1) |
| O-C _{Et} | 1.23(2) | 1.53(2) | 1.41(2) |
| C _{Cp} -C _{Cp} | 1.36(2) | 1.46(2) | 1.40(2) |
| C _{Et} -C _{Et} | 1.30(6) | 1.57(3) | 1.44(8) |
| P-Co-P | 88.7(1) | 92.7(1) | 91.0(1) |
| O=P-Co | 116.5(3) | 118.0(3) | 117.4(3) |
| O-P-Co | 108.5(4) | 115.4(3) | 110.5(4) |
| O=P-O | 105.5(5) | 110.0(5) | 108.2(5) |
| O-P-O | 98.7(5) | 102.5(5) | 100.8(5) |
| P-O-C _{Et} | 120(1) | 140(2) | 126(2) |
| C _{Cp} -C _{Cp} -C _{Cp} | 104(1) | 111(1) | 108(1) |
| O-C _{Et} -C _{Et} | 100(3) | 131(4) | 113(4) |
| <u>Anion Geometry</u> | | | |
| | <i>Min</i> | <i>Max</i> | <i>Mean</i> |
| B-C | 1.63(2) | 1.68(2) | 1.66(2) |
| C-C | 1.23(4) | 1.43(2) | 1.37(4) |

Table 2.8, contd. Selected Interatomic Distances (Å) and Angles (deg) for
 $[\text{Fe}_2(\text{OH})(\text{OAc})_2[\text{CpCo}[\text{OP}(\text{OEt})_2]_3]_2][\text{BPh}_4] \cdot \text{CH}_2\text{Cl}_2 \cdot 0.5\text{C}_7\text{H}_8,$
 $5 \cdot \text{CH}_2\text{Cl}_2 \cdot 0.5\text{C}_7\text{H}_8.$

| <u>Anion Geometry, contd</u> | | | |
|--|------------|------------|-------------|
| | <i>Min</i> | <i>Max</i> | <i>Mean</i> |
| C-B-C | 104.9(8) | 113(1) | 110(1) |
| C-C-C | 113(1) | 126(2) | 120(2) |
| <u>Solvent Geometry (CHCl₃)</u> | | | |
| Cl-C | 1.76(2) | 1.77(2) | 1.77(2) |
| Cl-C-Cl | | | 109.9(8) |
| <u>Solvent Geometry (Toluene)</u> | | | |
| C-C | | | 1.53(2) |
| C=C | 1.23(4) | 1.43(2) | 1.37(4) |
| C-C-C (ring) | | | 120(2) |

^aNumbers in parentheses are errors in the last significant digit(s). See Figure 2.3 for atom labelling scheme.

Table 2.9. Comparison of Selected Structural Features of the Diiron Cores in **1**, **4** and Selected Metalloproteins.^a

| | 4·2CH ₃ CN | | 1 | Hr ^b | RR | MMO |
|------------------------------------|-----------------------|-----------|-----------|-----------------|------|------|
| | 25 °C | -78.5 °C | | | | |
| ∠ Fe—O—Fe, deg | 124.4 (4) | 124.3 (4) | 123.6 (1) | 125.4 | 130 | 105 |
| Fe-O _{oxo} , Å | 1.799 (6) | 1.80 (1) | 1.788 (2) | | | |
| | 1.791 (6) | 1.79 (1) | 1.780 (2) | | | |
| av. Fe-O _{oxo} , Å | 1.795 | 1.795 | 1.784 | 1.84 | 1.78 | |
| Fe···Fe, Å | 3.174 (2) | 3.174 (3) | 3.146 (1) | 3.27 | 3.22 | 3.42 |
| av. Fe-O _{OAc} , Å | 2.028 | 2.041 | 2.043 | | | |
| av. Fe-L cis to μ-oxo, Å | 2.06 | 2.089 | 2.15 | | | |
| av. Fe-L trans to μ-oxo, Å | 2.13 | 2.12 | 2.19 | | | |
| av. Fe-O _N ^c | | | | 2.14 | 2.06 | 2.04 |

^a From X-ray crystallographic data for all model complexes and Hr and from EXAFS data for RR and MMO. ^b Data for metmyohemerythrin azide.¹²

^cThese values are for proteins only.

Table 2.10. Comparison of Selected Structural Features of Known (μ -hydroxo)bis(μ -carboxylato) Diiron Complexes and MMO.^a

| | 5 | 7 | MMO |
|--|-----------|-----------|------|
| $\angle \text{Fe}-(\text{OH})-\text{Fe}, ^\circ$ | 124.6 (2) | 123.1 (2) | |
| $\text{Fe}-\text{OOH}, \text{\AA}$ | 1.954 (7) | 1.952 (4) | |
| | 1.971(6) | 1.960 (4) | |
| av. $\text{Fe}-\text{OOH}, \text{\AA}$ | 1.963 | 1.955 | |
| $\text{Fe}\cdots\text{Fe}, \text{\AA}$ | 3.474 (2) | 3.439 (1) | 3.4 |
| av. $\text{Fe}-\text{OOAc}, \text{\AA}$ | 2.022 | 1.999 | |
| av. $\text{Fe}-\text{L}, \text{\AA}$ | 1.994 | 2.102 | 2.04 |
| reference | This work | 42 | 18 |

^a Data for complexes are from X-ray diffraction studies and for MMO, from EXAFS study.

Table 2.11. Comparison of the Features of Electronic Spectra of 1, 4, 9 and Selected Metalloprotein.^a

| assign- ment ^b | | LMCT (O ²⁻ →Fe) | ⁶ A ₁ → [⁴ T ₂] (⁴ D) | ⁶ A ₁ → [⁴ A ₁ , ⁴ E] (⁴ G) | ⁶ A ₁ → [⁴ T ₂] (⁴ G), CT | | |
|---|--------------------------------|-------------------------------|--|---|---|-----------|--|
| 4 in CH ₂ Cl ₂ | 240 (3.18x10 ⁴) | 353 (8050) | 467 (226) | 493 (sh) | 554 (112) | | |
| 4 in CH ₃ CN | 247 (2.91x10 ⁴) | 357 (6630) | 471 (208) | 501 (sh) | 569 (95) | | |
| 4 in CHCl ₃ | 243 (3.26x10 ⁴) | 341 (6170) | 466 (205) | 500 (sh) | 591 (78) | 905 (1.6) | |
| 1 | 262 (3375) | 339 (4635) | 457 (505) | 492 (460) | 695 (70) | 993 (3.5) | |
| 8 | | 329 (3400) | 448 (370) | 478 (sh) | 662 (70) | | |
| OxyHr | | 330 (6800) | | 500 (1100) | 750 (200) | 990 (10) | |
| | | 360 (5500) | | | | | |
| RR | | 325 (4700) | | 500 (400) | 600 (150) | | |
| | | 370 (3600) | | | | | |

^a Numbers in parentheses are the extinction coefficient per iron atom. ^b See reference 60-62.

Table 2.12. Temperature Dependence of the Observed and Calculated
Molar Magnetic Susceptibilities of
 $\text{Fe}_2\text{O}(\text{OAc})_2[\text{CpCo}[\text{OP}(\text{OEt})_2]_3]_2 \cdot 2\text{CH}_3\text{CN}, 4 \cdot 2\text{CH}_3\text{CN}.$ ^a

| T(K) | $\chi_{\text{obs}} \times 10^3(\text{emu}/\text{G}\cdot\text{mol})$ | $\chi_{\text{calc}} \times 10^3(\text{emu}/\text{G}\cdot\text{mol})$ |
|-------|---|--|
| 6.00 | 4.648 | 4.660 |
| 7.00 | 4.028 | 4.037 |
| 8.00 | 3.565 | 3.570 |
| 9.00 | 3.209 | 3.207 |
| 10.00 | 2.924 | 2.917 |
| 12.00 | 2.493 | 2.481 |
| 14.00 | 2.177 | 2.169 |
| 16.00 | 1.945 | 1.936 |
| 18.00 | 1.763 | 1.754 |
| 20.00 | 1.615 | 1.609 |
| 22.00 | 1.491 | 1.490 |
| 24.00 | 1.387 | 1.391 |
| 26.00 | 1.299 | 1.308 |
| 28.00 | 1.226 | 1.237 |
| 30.00 | 1.164 | 1.176 |
| 34.00 | 1.064 | 1.079 |
| 38.00 | 1.000 | 1.011 |
| 42.00 | 0.955 | 0.966 |
| 46.00 | 0.934 | 0.942 |
| 50.00 | 0.938 | 0.939 |
| 55.00 | 0.965 | 0.960 |

Table 2.12, contd. Temperature Dependence of the Observed and Calculated Molar Magnetic Susceptibilities of $\text{Fe}_2\text{O}(\text{OAc})_2[\text{CpCo}[\text{OP}(\text{OEt})_2]_3]_2 \cdot 2\text{CH}_3\text{CN}$, $4 \cdot 2\text{CH}_3\text{CN}$.

| T(K) | $\chi_{\text{obs}} \times 10^3 (\text{emu/G}\cdot\text{mol})$ | $\chi_{\text{calc}} \times 10^3 (\text{emu/G}\cdot\text{mol})$ |
|--------|---|--|
| 59.99 | 1.020 | 1.005 |
| 65.00 | 1.092 | 1.070 |
| 69.95 | 1.180 | 1.150 |
| 75.00 | 1.279 | 1.241 |
| 80.00 | 1.379 | 1.338 |
| 90.05 | 1.582 | 1.540 |
| 99.95 | 1.769 | 1.732 |
| 110.45 | 1.946 | 1.917 |
| 120.25 | 2.086 | 2.068 |
| 130.20 | 2.214 | 2.200 |
| 150.40 | 2.408 | 2.411 |
| 170.40 | 2.550 | 2.562 |
| 190.40 | 2.628 | 2.676 |
| 215.70 | 2.743 | 2.783 |
| 240.80 | 2.818 | 2.864 |
| 274.60 | 2.899 | 2.947 |
| 301.45 | 2.958 | 2.998 |

^aThe data was collected at 10 kG magnetic field on a SQUID susceptometer.

Chapter 3
Mononuclear Iron and Manganese Complexes
with Tripod Oxygen Ligation

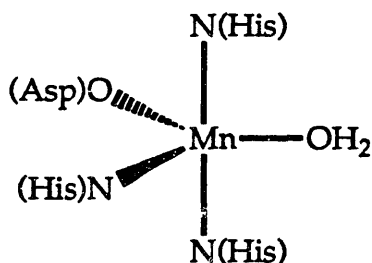
Introduction

The coordination chemistry of the tridentate, facial coordinating oxygen ligands $\{\text{CpCo}[\text{OP}(\text{OR})_2]_3\}^-$ (see Scheme 2.3 in Chapter 2 for a schematic representation of the ligand) has been well established through extensive spectroscopic studies of the metal complexes of the ligands.¹⁻⁵ This ligand class is capable of forming stable mononuclear bis chelate complexes of the form $[\{\text{CpCo}[\text{OP}(\text{OR})_2]_3\}_2\text{M}]^{n+}$ ($n = 0$ for M^{2+} and $n = 1$ for M^{3+}) with various divalent and, to a less extent, trivalent transition metal ions. Relatively few of these complexes have been structurally characterized by X-ray diffraction studies.⁶⁻⁸ Synthetic, spectroscopic and electrochemical studies are documented in the literature for iron and manganese complexes, namely $[\text{Fe}\{\text{CpCo}[\text{OP}(\text{OR})_2]_3\}_2]^{n+}$ ($n = 0, (1); n = 1, (2)$) and $[\text{Mn}\{\text{CpCo}[\text{OP}(\text{OR})_2]_3\}_2] (3)$.^{1,2} No crystal structures of these complexes, however, have been reported to date.

Recently, our laboratory has become interested in these complexes, as well as their hydrotris(pyrazolyl)borate analogues with exclusive nitrogen ligation, in part because of their reversible redox behaviors revealed by electrochemical studies.⁹ As a result, they are ideal systems for studying the relative effects of nitrogen versus oxygen ligation on the redox properties of the metal centers. It has been proposed that different coordination environments around the metal centers in metalloproteins may affect the redox potential as well as the functions of the metal center.¹⁰ Comparison of the redox properties of structurally well-defined model complexes with different ligand environments around the metal could offer a better understanding of this relationship. Although our principal focus is on dinuclear, carboxylate bridged iron and manganese model complexes,

electrochemical studies of these systems have encountered major difficulties due to the instability of the dinuclear iron cores under the redox conditions. The reduction or oxidation of the dinuclear iron complexes in an electrochemical cell is often irreversible, resulting from decomposition of the $\{\text{Fe}_2\text{O}(\text{O}_2\text{CCR})_2\}^{2+}$ core and formation of stable mononuclear complexes.^{9,11} The only exception reported to date is $[\text{Fe}_2\text{O}(\text{OAc})_2(\text{Me}_3\text{TACN})_2]\text{PF}_6$ (**4**) (Me_3TACN = 1,4,7-trimethyl-1,4,7-triazacyclononane),¹² where the diiron(III) core undergoes reversible reduction to form a mixed-valent $\text{Fe}_2(\text{III}, \text{II})$ core. Simple mononuclear complexes with different ligand environments, therefore, offer valuable alternatives for studying the effects of the ligands on the redox properties of the metal centers.

The mononuclear manganese complex **3** is also of interest as a potential model complex for enzymes, such as pyruvate carboxylase, manganese catalase and pseudocatalase, and manganese superoxide dismutase (SOD). All of these proteins contain mononuclear manganese centers.^{13,14} Among them, SOD has been studied most extensively.¹⁵ The crystal structure of the SOD isolated from *Thermus thermophilus* HB8 contains an Mn^{III} center surrounded by three nitrogen donors from the histidine ligands of the polypeptide side chain and two oxygen donors, one from aspartate and the other from a water molecule as indicated in Scheme 3.1.^{16,17} A series of mononuclear manganese complexes with different oxidation states and exclusive nitrogen donor ligands has been synthesized and structurally characterized.^{11,18} Comparison of the structural features and spectroscopic properties of **3** and its analogs with different ligands can offer valuable insight about coordination environments around manganese centers in manganese-containing proteins.



Scheme 3.1. Schematic drawing of the active site of SOD
from *Thermus thermophilus* bacteria

Experimental

Materials and Methods. All solvents and starting materials were purchased from commercial sources and used as received without further purification unless otherwise specified. Solvents used in the electrochemical studies were special electrochemical grade or freshly distilled. The supporting electrolyte, tetrabutylammonium perchlorate (TBAP), was recrystallized three times from ether before use. The tripod ligand **2** was synthesized according to the literature procedure.^{19,20}

UV-visible and IR spectra were recorded on a Perkin-Elmer Lambda 7 spectrophotometer and a Mattson Cygnus 400 Fourier transform spectrometer, respectively. ¹H NMR spectra were obtained using a Bruker WM250 or a Varian XL 300 instrument with tetramethylsilane as the internal standard.

Cyclic voltammetry experiments were performed by using a Princeton Applied Research Model 173 potentiostat and with a Houston Instruments Model 2000 X-Y recorder. Details of assembling the

electrochemical cell are discussed elsewhere.* Measurements were made either in methylene chloride (0.2 M tetrabutylammonium perchlorate (TBAP)) or acetonitrile (0.1 M TBAP) solution at room temperature under argon. Redox potentials were referenced to a Ag/AgCl electrode. The electrode performance was monitored by examining the Fe(II)/Fe(III) couple of ferrocene. The $E_{1/2}$ of the couple was found to be 0.471 V in 0.1 M TBAP acetonitrile solution with $\Delta E_p = 73$ mV. The reversibility of the couple was improved by raising the concentration of electrolyte; the ΔE_p value becoming 68 mV in 0.2 M TBAP acetonitrile solution. It is less reversible in 0.2 M TBAP methylene chloride solution, the ΔE_p value being 94 mV.

Synthesis

$[\text{Fe}\{\text{CpCo}[\text{OP}(\text{OEt})_2]_3\}_2]\text{X}$, (X = BPh₄, 2a; X = BF₄, 2b; X = ClO₄, 2c).

Compound 2a was obtained as a byproduct of the protonation reaction of the oxo bridge ligand in Fe₂O(OAc)₂{CpCo[OP(OEt)₂]₃}₂ (5) (details see Chapter 2, experimental section). The yellow-green crystals formed from a mixture of toluene and methylene chloride at the same time as those of yellow-orange crystals of [Fe₂(OH)(OAc)₂{CpCo[OP(OEt)₂]₃}₂]BPh₄ (6) and were manually separated under a microscope. Anal. Calcd. for C₅₈H₉₀P₆BO₁₈Co₂Fe: C: 48.19; H: 6.27; N: 0.0. Found C: 47.98; H: 6.43; N: 0.0. FTIR (KBr, cm⁻¹): 3054 (m), 2980 (s), 2928 (m), 2901 (m), 1581 (m), 1478 (m), 1441 (m), 1435 (m), 1426 (m), 1400 (m), 1385 (m), 1162 (m), 1118 (s), 1101 (s), 1070 (s), 1033 (s), 941 (s), 845 (s), 774 (s), 739 (s), 729 (s), 702 (s), 609 (s), 492 (w), 456 (w).

Compound 2b was synthesized by a procedure analogous to that previously reported for [Fe{CpCo[OP(OEt)₂]₃}₂]PF₆.²¹ A portion of Fe(NO)₃·9H₂O (120 mg, 0.30 mmol) was added into an aqueous solution of

* See the experimental part of the first section in chapter 2.

$\text{Na}[\{\text{OP}(\text{OEt})_2\}_3\text{Co}(\text{C}_5\text{H}_5)\}$ (300 mg, 0.56 mmol in 10 ml of distilled water). A orange homogeneous solution was obtained after slow addition of ethanol until the solution was clear. A portion of NaBF_4 (50 mg, 0.45 mmol) was added subsequently. The reaction mixture was concentrated by partially removal of the solvent. A yellow precipitate was formed, which is collected by filtration and washed several times with distilled water. After dried under vacuum, compound **2b** (165 mg, 45% yield) was obtained. Anal. Calcd. for $\text{C}_{34}\text{H}_{70}\text{P}_6\text{BF}_4\text{O}_{18}\text{Co}_2\text{Fe}$: C: 33.66; H: 5.82. Found C: 33.38; H: 5.83. FTIR (KBr, cm^{-1}): 2990 (sh), 2985 (m), 2979 (m), 2934 (m), 2932 (m), 2909 (m), 1480 (m), 1472 (w), 1465 (w), 1457 (w), 1436 (w), 1426 (w), 1387 (m), 1158 (m), 1117 (sh), 1103 (s), 1089 (sh), 1056, 1042 (sh), 1031 (s), 949 (s), 929 (s), 844 (m), 777 (m), 730 (m), 612 (s), 520 (s), 490 (w), 456 (w).

Compound **2c** was isolated from a reaction mixture prepared in the following manner. An aqueous solution of $\text{Na}[\{\text{OP}(\text{OEt})_2\}_3\text{Co}(\text{C}_5\text{H}_5)\}$ (136 mg, 0.24 mmol) was added slowly into a stirred aqueous solution of 154 mg of $\text{Fe}(\text{ClO}_4)_3$ (0.43 mmol) and 118 mg of $\text{NaOAc}\cdot 3\text{H}_2\text{O}$ (0.86 mmol). A yellow-orange precipitate formed immediately. The reaction mixture was stirred for another half hour and the precipitate was collected by filtration. The solid was redissolved in a small portion of methylene chloride and several small drops of residual water were carefully removed by pipette from the bulk of the solution. Compound **2c** (72 mg) was then recrystallized from a mixture of methylene chloride and toluene at $-20\text{ }^\circ\text{C}$. Yield was 14 %. Anal. Calcd. for $\text{C}_{34}\text{H}_{70}\text{P}_6\text{ClO}_{22}\text{Co}_2\text{Fe}$: C: 33.30; H: 5.77. Found C: 33.29; H: 5.70. FTIR (KBr, cm^{-1}): 2977 (m), 2930 (m), 2906 (m), 2866 (w), 1593 (m), 1436 (m), 1387 (m), 1320 (w), 1300 (w), 1160 (m), 1104 (s), 1095 (sh), 1069 (s), 1032 (s), 1014 (sh), 947 (s), 932 (sh), 843 (m), 777 (m), 730 (m), 610 (s).

$\text{Mn}(\text{CpCo}[\text{OP}(\text{OEt})_2]_3)_2$, (3). Compound 3 was synthesized by using either of the two methods described as follows.

Method A. A 0.5 g portion of $\text{Mn}(\text{O}_2\text{CCH}_3)_2 \cdot 4\text{H}_2\text{O}$ (2 mmol) and 0.16 g KMnO_4 (1 mmol) were added to 10 ml of glacial acetic acid. The mixture was heated to 80 °C for 50 min with stirring and then cooled to room temperature. A brown solution was obtained. After the addition of 1.12 g (2 mmol) of $\text{Na}[\{\text{OP}(\text{OEt})_2\}_3\text{Co}(\text{C}_5\text{H}_5)]$, the solution was stirred for 15 min and filtered. The red filtrate was evaporated to dryness under vacuum at elevated temperature (60 °C) and the residue dissolved in methylene chloride. Filtration gave a red filtrate and tan powder. Finally, the filtrate was concentrated and layered with a small amount of acetonitrile. Slow cooling to -20 °C gave red crystals.

Method B. An acetonitrile solution of $\text{Na}[\{\text{OP}(\text{OEt})_2\}_3\text{Co}(\text{C}_5\text{H}_5)]$ (0.53 g, 0.95 mmol) was added to an acetonitrile solution of $\text{Mn}(\text{O}_2\text{CCH}_3)_3 \cdot 2\text{H}_2\text{O}$ (0.255 g, 0.95 mmol). The reaction mixture was heated to 65 °C for 2 hr. Filtration gave a red solution and green brown precipitate. After removing the solvent from the filtrate, the residue was extracted by ether. A yellow solution and black insoluble material were obtained. Orange yellow crystals (85 mg, 16 % yield) were obtained from the solution at -20 °C. Anal. Calcd. for $\text{C}_{34}\text{H}_{70}\text{P}_6\text{O}_{18}\text{Co}_2\text{Mn}$: C: 36.27; H: 6.28. Found C: 36.26; H: 6.16. FTIR (KBr, cm^{-1}): 2973 (s), 2922 (s), 2895 (s), 2863 (m), 1476 (m), 1475 (m), 1457 (m), 1453 (m), 1441 (s), 1427 (m), 1386 (s), 1162 (sh), 1129 (s), 1117 (sh), 1041 (s), 1028 (sh), 923 (s), 835 (s), 764 (s), 716 (s), 613 (sh), 585 (s), 497 (w), 441 (w).

X-ray Diffraction Studies. All data were collected on an Enraf-Nonius CAD4 diffractometer with graphite monochromatized Mo $\text{K}\alpha$ radiation ($\lambda = 0.70926 \text{ \AA}$). X-ray diffraction studies of both 2a and 2c were carried out at -78 °C. Only a preliminary study was made on a crystal of 2a in order to confirm

its chemical composition. A green crystal of **2a** was mounted on the tip of a glass fiber with silicon grease. The crystals isolated from a mixture of toluene and methylene chloride appeared to be stable at room temperature. The data set was collected by using a set of parameters designed for fast data collection.²² No decay of the intensities of three standard reflections was observed during the data collection. Lorentz and polarization, but not absorption corrections were applied to the data set. A more detailed study was carried out on a crystal of **2c** to obtain accurate geometric information about this compound. A crystal of **2c** was mounted on the tip of a glass fiber with silicon grease. No notable intensity changes were recorded during the data collection. Lorentz and polarization corrections were applied to the data sets. An empirical absorption correction was applied based on the data calculated from the psi-scan data. Experimental details of the X-ray diffraction studies of both **2a** and **2c** are recorded in Table 3.1.

An X-ray diffraction study was carried out on a crystal of **3**, prepared by using the method B, at -38 °C. The crystal (0.20 x 0.18 x 0.24 mm) was mounted on a glass fiber with silicon grease. No decay of the intensities of the standard reflections was observed during the data collection. Lorentz and polarization corrections were applied to the data sets. Experimental details of the X-ray diffraction study of **3** are recorded in Table 3.5.

Structure Solution and Refinement. The structure of **2c** was solved by using the direct methods option of SHELX-86.²³ Neutral and hydrogen atom scattering factors were taken from the literature.^{24,25} The positions for the iron and cobalt atoms were determined from the initial electron density map. All other non-hydrogen atoms were located either through the DIRDIF program²⁶ or on a difference Fourier map following least-squares refinement. The structure was refined by using the full matrix least-squares

program in TEXSAN,²⁷ All non-hydrogen atoms were refined anisotropically except the carbon atoms on both Cp rings. Hydrogen atoms were calculated in idealized positions with the carbon-hydrogen distances set equal to 0.95 Å for the non-disordered carbon atoms. The thermal parameters of hydrogen atoms were fixed at $1.2 \times \text{Beq}$, where Beq is the equivalent isotropic thermal parameter of the attached carbon atom. The ethyl and Cp groups were disordered. The disorder in the Cp rings was successfully modeled while the disordered ethyl groups were not modeled. The five carbon atoms on both Cp rings are disordered into three sets of positions, each with 0.33 occupancy. These three sets of positions are symmetry related through a three fold axis centered at the Cp ring. All carbons are in the same plane and the average distances between Cs and C's is 0.51 Å. No hydrogen atoms were assigned to the disordered carbon atoms of the Cp rings. At the convergence, the largest ratio of parameter shift to estimated standard deviation was 0.84. The final R factors are given in Table 3.1. The largest residual peak contained 0.797 e/Å³ and was located near one of the disordered Cp rings in 2c. Final atomic coordinates and the equivalent isotropic thermal parameters for non-hydrogen atoms are given in Table 3.2. Anisotropic thermal parameters for non-hydrogen atoms are listed in Table 3.3. Selected bond lengths and angles are collected in Table 3.4.

The structure solution of 2a was also obtained and the refinement carried out as described for compound 2c. All non hydrogen atoms were located on difference Fourier maps. The refinement of the structure was carried out by using the full matrix least-squares program in TEXSAN.²⁷ The neutral and hydrogen atom scattering factors were taken from the literature.^{24,25} All phenyl rings on the BPh₄⁻, both Cp rings as well as the

toluene solvent molecule were refined by using the rigid group option in the TEXSAN program to reduce the number of parameters needed for the refinement due to the limited number of reflections available. The current R factors are given in Table 3.1. No attempt was made to model the disorder on some ethyl groups and the refinement of the structure has not been carried out to completion due to the lack of reflections with high intensities.

$\text{Mn}\{\text{CpCo}[\text{OP}(\text{OEt})_2]_3\}_2$, **3**. The structure of **3** was solved by using the direct method option of SHELX-86.²³ The neutral and hydrogen atom scattering factors were taken from the literature.^{24,25} The position for the manganese atom was determined from the initial electron density map. Half of the non-hydrogen atoms were located on difference Fourier maps following least-squares refinement. Since the manganese atom was sitting on an inversion center, the atoms on the other half of the molecule were generated by symmetry operation. The structure was refined by using the full matrix least-squares program in TEXSAN.²⁷ All non-hydrogen atoms were refined anisotropically. Hydrogen atoms were calculated in idealized positions so that the carbon-hydrogen distances equalled to 0.95 Å. The thermal parameters of hydrogen atoms were fixed at $1.2 \times \text{Beq}$, where Beq is the equivalent isotropic thermal parameter of the attached carbon atom. No hydrogen atoms were assigned to the carbon atoms on Cp rings. At the convergence, the largest ratio of parameter shift to estimated standard deviation was 0.21. The final R factors are given in Table 3.5. The largest residual peak contained $1.26 \text{ e}/\text{Å}^3$ and was located near one of the cobalt atoms in **3**. Final atomic coordinates and the equivalent isotropic thermal parameters for non-hydrogen atoms are given in Table 3.6. Anisotropic thermal parameters for non-hydrogen atoms are listed in Table 3.7. Selected bond lengths and angles are collected in Table 3.8.

Results and Discussion

Synthesis. All but one of the synthetic routes to compounds **2** and **3** were designed to prepare dinuclear triply bridged μ -oxo or μ -hydroxo iron complexes.^{28,29} Only the procedure for preparing **2b** was optimized for synthesizing a mononuclear bis-chelate complex. As a result, the yields of these synthetic routes are very low (<20%). The fact that monomers were isolated from all the reaction mixtures is a testimonial to their thermodynamic stability, under the reaction condition, compared to the formation of their binuclear counterparts. Moreover, the coordination of the all-oxygen tripod ligands may render the oxo bridge in dinuclear complexes more susceptible to the attack by even weak acid (see discussion, Chapter 2), facilitating their decomposition to stable monomers. It is also interesting that in no case was a mixed tripod ligand/acetate complex isolated, even in the presence of large excess of acetate. This result indicates that the tripod ligand competes favorably with acetate for binding to ferric ions.

In method B for the synthesis of **3**, a Mn(III) starting material was used. Disproportionation apparently occurred, generating **3** and Mn(IV) byproduct obtained as a black insoluble material.

Structural Features of 2c. Figure 3.1. shows the molecular structure of the cation of **2c**. It is a linear mixed-metal trinuclear complex with average Co-Fe distance of 3.882 Å and Co-Fe-Co angle of 180°. The iron coordination environment is almost ideally octahedral with Fe-O distances ranging from 1.992 Å to 2.003 Å and cis O-Fe-O angles between 89.2° and 90.8°. Table 3.9 compares selected geometric parameters at the metal centers in various iron

and manganese model complexes. The distortion from octahedral geometry at the iron center is much more severe in **5** than in **2c**, reflected by a much smaller O-Fe-O angle (av. 85.3°) in **5** versus that observed in **2c** (av. 90.0°). The ligand was, therefore, much less sterically constrained in the monomer **2c**. The mean Fe-O bond length is shorter in **2c** compared to that of **5** (2.00 Å in **2c** and 2.10 Å in **5**), which in turn gives rise to the larger cis O-Fe-O angle in **2c** (av. 90.0 ° in **2c** and 85.3 ° in **5**). Thus, the steric constraint of the ligand was released by allowing the relatively rigid ligand to move closer toward the iron atom. A similar constraint release mechanism is also clearly shown in the case of nitrogen tripod ligand, tri-1-pyrazolylborate.⁹ A longer Fe-N distance was observed in the binuclear complex, [Fe₂O(OAc)₂(HBpz₃)₂] (**7**), compared to its mononuclear counterpart, [Fe(HBpz₃)₂]⁺, (**8**) (2.160 Å vs. 1.957 Å). As a result, **7** has a more distorted octahedral geometry around iron than **8** ($\langle\langle\angle\text{N-Fe-N}\rangle\rangle = 82.9^\circ$ vs. 88.5 °). It seems that the existence of the exceptionally long Fe-L bonds due to the *trans-influence* of the short Fe-O_{oxo} bond in binuclear complexes prevents the capping ligand from moving closer to the iron centers and causes more steric constraint of the ligand. Another example of how this steric constraint could be released by shortening of Fe-N bonds is a low spin Fe(II) complex [(HBpz₃)₂Fe] (**9**), where the mean Fe-N bond length is much shorter than that observed in **8** (1.973 Å) and thus the cis N-Fe-N angle is closer to the 90° value ($\langle\langle\angle\text{N-Fe-N}\rangle\rangle = 88.3$).³⁰

Comparison of the structural features of mononuclear complexes **2c** and **8** is also very interesting. A slightly longer Fe-O distance ($\langle\langle\text{Fe-O}\rangle\rangle = 1.994$ Å) was obtained compared to the Fe-N bonds in **8** ($\langle\langle\text{Fe-N}\rangle\rangle = 1.957$ Å). This result agrees with what was observed for the binuclear complexes **5** and **7**. The oxygen tripod ligand has a larger bite distance which results in a larger

O-Fe-O angle ($\langle\text{O-Fe-O}\rangle = 90.0^\circ$) compared to the N-Fe-N angle in its nitrogen donor counterpart ($\langle\text{N-Fe-N}\rangle = 88.5^\circ$). Other ligand geometric parameters in **2c**, $\langle\text{P=O}\rangle$ (1.518 Å), $\langle\text{P-O}\rangle$ (1.588 Å), $\langle\text{Co-P}\rangle$ (2.160 Å) and $\langle\text{Co-C}\rangle$ (2.08 Å), are similar to those of the free ligand.²⁰

Structural features of 3. The molecular structure of **3** is shown in Figure 3.2. The molecule of **3** contains two cobalt atoms and one manganese atom which are in a linear arrangement with a Mn-Co distance of 3.989 Å. The manganese atom sits on an inversion center and surrounded by an array of six oxygen donor atoms adapting a distorted octahedral geometry. The O-Mn-O angles deviate from the ideal 90° value, ranging from 87.3 to 87.8° , reflecting the significant steric constraint of the tripod ligand. The trans O-Mn-O angles are required to be 180° owing to the crystallographic inversion center. An even more severe distortion was observed in an analog of **3** with nitrogen donors, $\text{Mn}(\text{HB}(3,5\text{-Me}_2\text{pz})_3)_2$ (**10**) ($\text{HB}(3,5\text{-Me}_2\text{pz})_3 = \text{hydrotris}\{1\text{-}(3,5\text{-dimethyl})\text{ pyrazolyl}\}\text{borate}$).¹¹ The N-Mn-N angle between the nitrogen donors within the ligand was 84.5° in **10**. The Mn-O bond lengths ($\langle\text{Mn-O}\rangle = 2.156$ Å) are on the average 0.1 Å longer than the Fe-O bonds in **2c**, presumably due to the larger ionic radius of Mn(II) vs. Fe(III) (0.80 Å pm vs. 0.64 Å). The correlation between the M-L bond lengths and the steric constraint of the ligand is again demonstrated in this case. The shorter the M-L bond, the less constrained the ligand is. An even shorter Mn-O bond length (2.132 (5) Å) was observed in another mononuclear manganese complex, $\text{Mn}(\text{OAc})_2(\text{BIPhMe})_2$ (**11**) (BIPhMe = 2,2'-bis(1-methylimidazolyl) phenylmethoxymethane), where the steric constraint of the oxygen donor ligand was absent.³¹

Spectroscopic Properties of 2c and 3. The electronic spectra of both **2c** and **3** in acetonitrile are featureless in the visible region. The only

transition is a band at 340 nm, which is the same as observed in the free ligand. Both compounds are high spin d^5 and thus paramagnetic. The ^1H NMR spectrum of **2** in CDCl_3 showed only a single broad resonance at 1.58 ppm, which can be assigned to phosphite ethyl CH_3 group. The same resonance was observed for **3** as a broad signal at 1.27 ppm.

Electrochemical Studies of 2 and 3. A cyclic voltammogram of an acetonitrile solution of **2b** with 0.1 M TBAP as supporting electrolyte at a scan speed of 50 mV/s is shown in Figure 3.3 a. It displays a quasi-reversible wave for the $\text{Fe}^{\text{II}}/\text{Fe}^{\text{III}}$ couple with $E_{p,c} = -0.652$ V and $E_{p,a} = -0.566$ V vs. Ag/AgCl. The peak-to-peak separation changed slightly under different scan speeds, ranging from 86 mV at 50 mV/s to 124 mV at 500 mV/s. Figure 3.4 displays a plot of the anodic and cathodic currents versus the square roots of scan speeds. Both anodic and cathodic currents increase as $v^{1/2}$ increases, as described by the Randles-Sevcik equation.^{32,33} The redox potential of this couple is solvent dependent, $E_{1/2}$ shifting to -0.70 V (vs. Ag/AgCl) in methylene chloride with TBAP as supporting electrolyte. It was also reported to be -0.48V vs. SCE or -0.47 V vs. Ag/AgCl in tetrahydrofuran, with $[\text{Bu}_4\text{N}]\text{PF}_6$ as supporting electrolyte.³⁴ As has been discussed in the introduction part of this chapter, the nature of the donor atoms coordinated to iron may play a major role in fine-tuning its redox properties. Table 3.10 lists the redox potentials determined for several iron complexes with different oxygen/nitrogen donor ligand ratios in their coordination spheres. It is clear that replacement of oxygen with nitrogen donors in the coordination sphere results in a shift of the redox potential of iron toward more positive values. In other word, substitution of the "softer" nitrogen for a "harder" oxygen donor in the ligand environment makes the iron center harder to be oxidized, stabilizing its lower oxidation

state. Complex 4, in which the iron center has three nitrogen and three oxygen donors, provides the only example among triply bridged dinuclear iron complexes that undergoes a reversible redox reaction. Taking the difference of the solvent system into consideration, the redox potential of Fe(III,III)/ Fe(III,II) couple in 4 (-0.374 V vs. SCE or -0.138 V vs. NHE) still fits in favorably with the general trend expressed in Table 3.10. It appears that the redox properties of the metal centers correlate more closely with the electronic properties of the ligand than with the geometry of the complex. This correlation, thus, facilitates identification of the ligand environment, and changes in this environment, in proteins. By monitoring the redox potential changes during a reaction, insights into structural changes might be obtained. For example, the redox potential of the diferric form of the hydroxylase protein of MMO shifts toward a more positive value by 0.25 mV upon substrate binding.³⁵ This result indicates a substantial change of the coordination environment around iron centers during the substrate binding, for example, loss of one of the original oxygen ligands or addition of a nitrogen donor ligand in the coordination sphere of the iron center(s).

A preliminary study of the redox properties of 3 has also been carried out. Figure 3.3 b. shows a cyclic voltammogram of a methylene chloride solution of 3 with 0.2 M TBAP as supporting electrolyte and a scan speed of 50 mV/s. There is a pair of totally irreversible peaks, with the cathodic wave at -0.081 V and the anodic wave at + 0.692 V. The two waves are clearly related to one another. When the switching potentials were set between +0.5 V and -1.5 V, both peaks were absent. So the peak observed at -0.081 V is due to reduction of an oxidized species formed at +0.692 V. The redox process appears to be repeatable as indicated by the occurrence of identical CV traces during multiple scans. The observed $E_{p,c}$ and $E_{p,a}$ values

shift further apart as the scan rate increases, with $E_{p,c}$ being -0.196 V and $E_{p,a}$ being +0.809 V, respectively at a scan rate of 500 mV/s. The anodic current (4.6 μ A at 50 mV/s) is significantly larger than the cathodic current (1.6 μ A at 50 mV/s). The nature of the oxidized species, i.e., the number of electrons transferred, could be established by using the controlled potential coulometry. It could be either the 1e⁻ oxidation product (Mn^{III}) or the 2e⁻ oxidation product (Mn^{IV}). Comparison of the reversibility of the redox processes involving **2** and **3** indicates that the redox reaction of Fe^{II}/Fe^{III} couple is much faster than that of Mn^{II}/Mn^{III} or Mn^{II}/Mn^{IV} couples in the same ligand environment.

Conclusions

Bis-chelate mononuclear iron and manganese complexes of the oxygen tripod ligand, $\{[\text{OP}(\text{OEt})_2]_3\text{Co}(\text{C}_5\text{H}_5)\}^-$, have been synthesized and structurally characterized by X-ray diffraction. The ubiquity of the mononuclear complexes in various synthetic routes is indicative of their high thermodynamic stability. Comparison of the structural features of mononuclear complexes with either their binuclear counterparts or other mononuclear complexes with different ligands offers some interesting insights about the flexibility of the ligand. In general, the steric constraint of the ligand experienced in binuclear complexes due to the restricted geometry of the capping sites is released in the mononuclear complexes. The coordination sphere of the metal center, therefore, is much closer to the ideal octahedral geometry. The release of the constraint is usually accomplished by moving the ligand closer to the metal center. Thus, a larger L-M-L angle is usually accompanied by a shorter metal-ligand bond

length. The mean Fe-O bond length is longer than the mean Fe-N bond length in the mononuclear complexes with oxygen and nitrogen donor ligands, respectively.

The iron complex is fairly well-behaved in the electrochemical study. The comparison of the redox properties of this complex and that of other iron analogs with different ligands allows for a detailed investigation of the relationship between the redox properties of the metal centers and their coordination environments. A better understanding of this relationship certainly helps to expand our knowledge about the coordination environments of the metal centers in metalloproteins. By studying the redox properties of the proteins and comparing them with that of the structurally characterized model complexes, one could make better assessment about the structural proposals of the metal centers in the proteins. By examining the redox potentials of the iron complexes with different oxygen/nitrogen ratio in the coordination sphere, it is clearly evident that the increase of the oxygen content in the coordination sphere shift the redox potential of the Fe(III)/Fe(II) couple toward more negative values. The iron center, therefore, becomes easier to be oxidized. This result is consistent with the knowledge that a oxygen donor ligand is a harder ligand which prefers higher oxidation state of the metal upon coordination.

References

- (1) Kläui, W.; Werner, H. *Angew. Chem. Int. Ed. Engl.* 1976, 15, 172-173.
- (2) Kläui, W.; Dehnicke, K. *Chem. Ber.* 1978, 111, 451-468.
- (3) Kläui, W.; Eberspach, W.; Gütlich, P. *Inorg. Chem.* 1987, 26, 3977-3982.
- (4) Kläui, W.; Lenders, B.; Hessner, B.; Evertz, K. *Organometallics* 1988, 7, 1357-1363.
- (5) Kläui, W. *Angew. Chem. Int. Ed. Engl.* 1990, 29, 627-637.
- (6) Dubler, E.; Linowsky, L.; Kläui, W. *Transition Met. Chem.* 1979, 4, 191-198.
- (7) Harder, V.; Dubler, E.; Werner, H. *J. Organomet. Chem.* 1974, 71, 427.
- (8) Kamenar, B.; Hergold-Brundic, A.; Bruvo, M. *Z. Kristallogr.* 1988, 184, 103-110.
- (9) Armstrong, W. H.; Spool, A.; Papaefthymiou, G. C.; Frankel, R. B.; Lippard, S. J. *J. Am. Chem. Soc.* 1984, 106, 3653.
- (10) Rosenzweig, A. C.; Feng, X.; Lippard, S. J. 1991, manuscript submitted.
- (11) Beer, R. H. Thesis, Massachusetts Institute of Technology, 1990.
- (12) Hartman, J. R.; Rardin, R. L.; Chaudhuri, P.; Pohl, K.; Wieghardt, K.; Nuber, B.; Weiss, J.; Papaefthymiou, G. C.; Frankel, R. B.; Lippard, S. J. *J. Am. Chem. Soc.* 1987, 109, 7387-7396.
- (13) Gärtner, A.; Weser, U. *Top. Curr. Chem.* 1986, 132, 1.
- (14) *Manganese in Metabolism and Enzyme Function*; Schramm, V. L.; Wedler, F. C., Ed.; Academic Press: Orlando, Florida, 1986.
- (15) *Superoxide Dismutase*; Oberley, L. W., Ed.; CRC: Boca Raton, Florida, 1982; Vol. I+II.
- (16) Wieghardt, K. *Angew. Chem. Int. Ed. Engl.* 1989, 28, 1153-1172.

- (17) Stallings, W. C.; Pattridge, K. A.; Strong, R. K.; Ludwig, M. L. *J. Biol. Chem.* **1985**, *260*, 16424.
- (18) Chan, M. K.; Armstrong, W. H. *Inorg. Chem.* **1989**, *28*, 3777-3779.
- (19) Kläui, W. Z. *Naturforsch* **1979**, *34b*, 1403-1407.
- (20) Kläui, W.; Müller, A.; Eberspach, W.; Boese, R.; Goldberg, I. J. *Am. Chem. Soc.* **1987**, *109*, 164-169.
- (21) Kläui, W.; Eberspach, W.; Schwarz, R. J. *J. Organomet. Chem.* **1983**, *252*, 347-357.
- (22) Bott, S. G. *A Primer for the CAD4*; Massachusetts Institute of Technology: Cambridge, 1989.
- (23) Sheldrick, G. M. In *Crystallographic Computing 3*; G. M. Sheldrick, C. Krüger and R. Goddard, Ed.; Oxford University Press: Oxford, England, 1985; pp 175-189.
- (24) Ibers, J. A.; Hamilton, W. C. *International Tables for X-ray Crystallography*; Kynoch Press: Birmingham, 1974; Vol. IV, pp 71-98.
- (25) Steward, R. F.; Davison, E. R.; Simpson, W. T. *J. Chem. Phys.* **1965**, *42*, 3175.
- (26) Parthasarathi, V.; Beurskens, P. T.; Slot, J. J. *Acta Cryst.* **1983**, *A39*, 860.
- (27) *TEXSAN: Single Crystal Structure Analysis Software Version 5.0*; Molecular Structure Corporation: Woodlands, TX, 1989.
- (28) Sheats, J. E.; Czernuszewicz, R. S.; Dismukes, G. C.; Rheingold, A. L.; Petrouleas, V.; Stubbe, J.; Armstrong, W. H.; Beer, R. H.; Lippard, S. J. *Am. Chem. Soc.* **1987**, *109*, 1435.
- (29) Armstrong, W. H.; Lippard, S. J. *J. Am. Chem. Soc.* **1984**, *106*, 4633.
- (30) Oliver, J. D.; Mullica, D. F.; Hutchinson, B. B.; Milligan, W. O. *Inorg. Chem.* **1980**, *19*, 165-169.
- (31) Goldberg, D. P.; Lippard, S. J. unpublished result.

- (32) Mabbott, G. A. *J. Chem. Ed.* **1983**, *60*, 697-701.
- (33) Van Benschoten, J. J.; Lewis, J. Y.; Heineman, W. R.; Roston, D. A.; Kissinger, P. T. *J. Chem. Ed.* **1983**, *60*, 772-776.
- (34) Murr, N. E.; Chaloyard, A.; Kläui, W. *Inorg. Chem.* **1979**, *18*, 262-264.
- (35) Liu, K. E.; Lippard, S. J. *J. Biol. Chem.* **1991**, *266*, 12836.
- (36) Feng, X.; Bott, S. G.; Lippard, S. J. *J. Am. Chem. Soc.* **1989**, *111*, 8046-8047.
- (37) Cofré, P.; Richert, S. A.; Sobkowjak, A.; Sawyer, D. T. *Inorg. Chem.* **1990**, *29*, 2645.
- (38) Johnson, C. K. *ORTEP-II, A FORTRAN Thermal Ellipsoid Plot Program*; Oak Ridge National Laboratory: Oak Ridge, 1976, pp ORNL-5138.

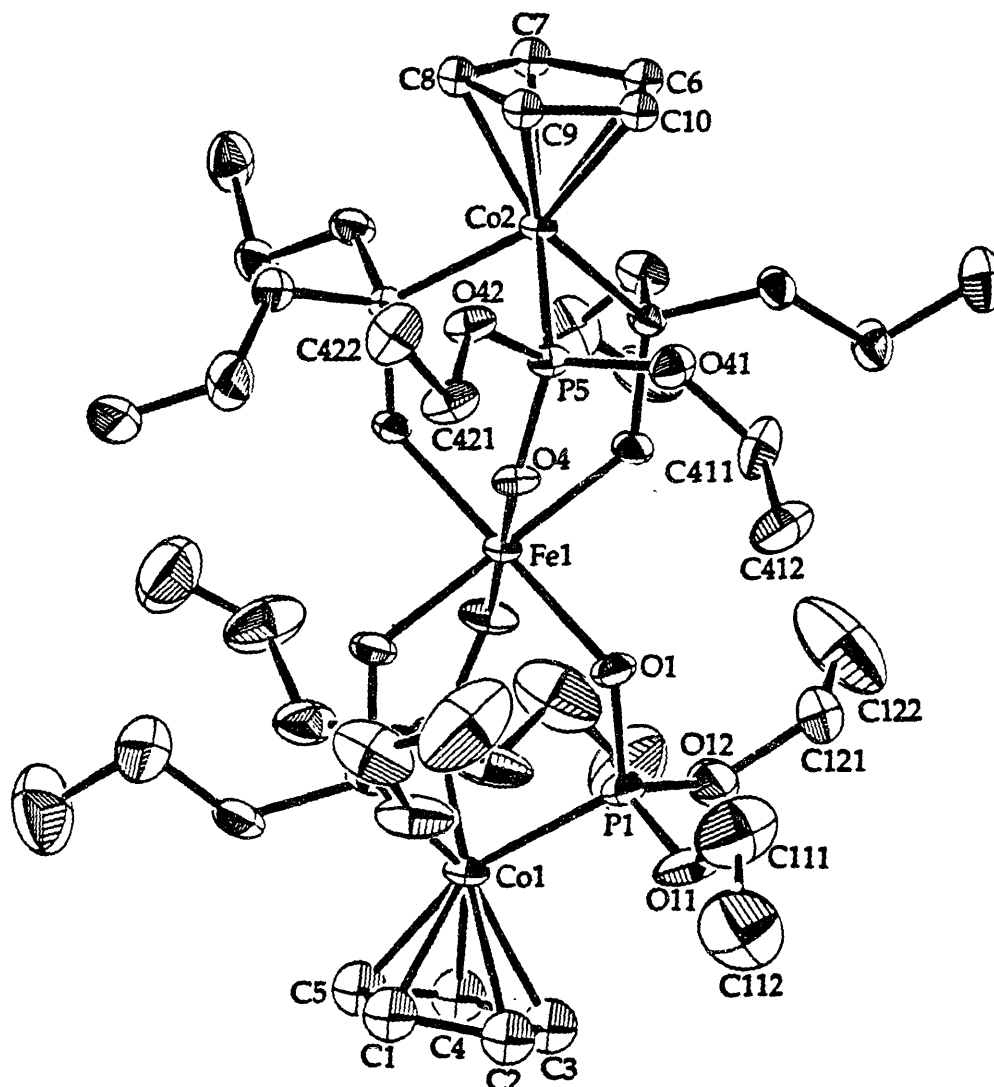


Figure 3.1. ORTEP³⁸ drawing of 2c showing 40% probability thermal ellipsoids and labelling scheme for non-hydrogen atoms. Atom disorder is not shown.

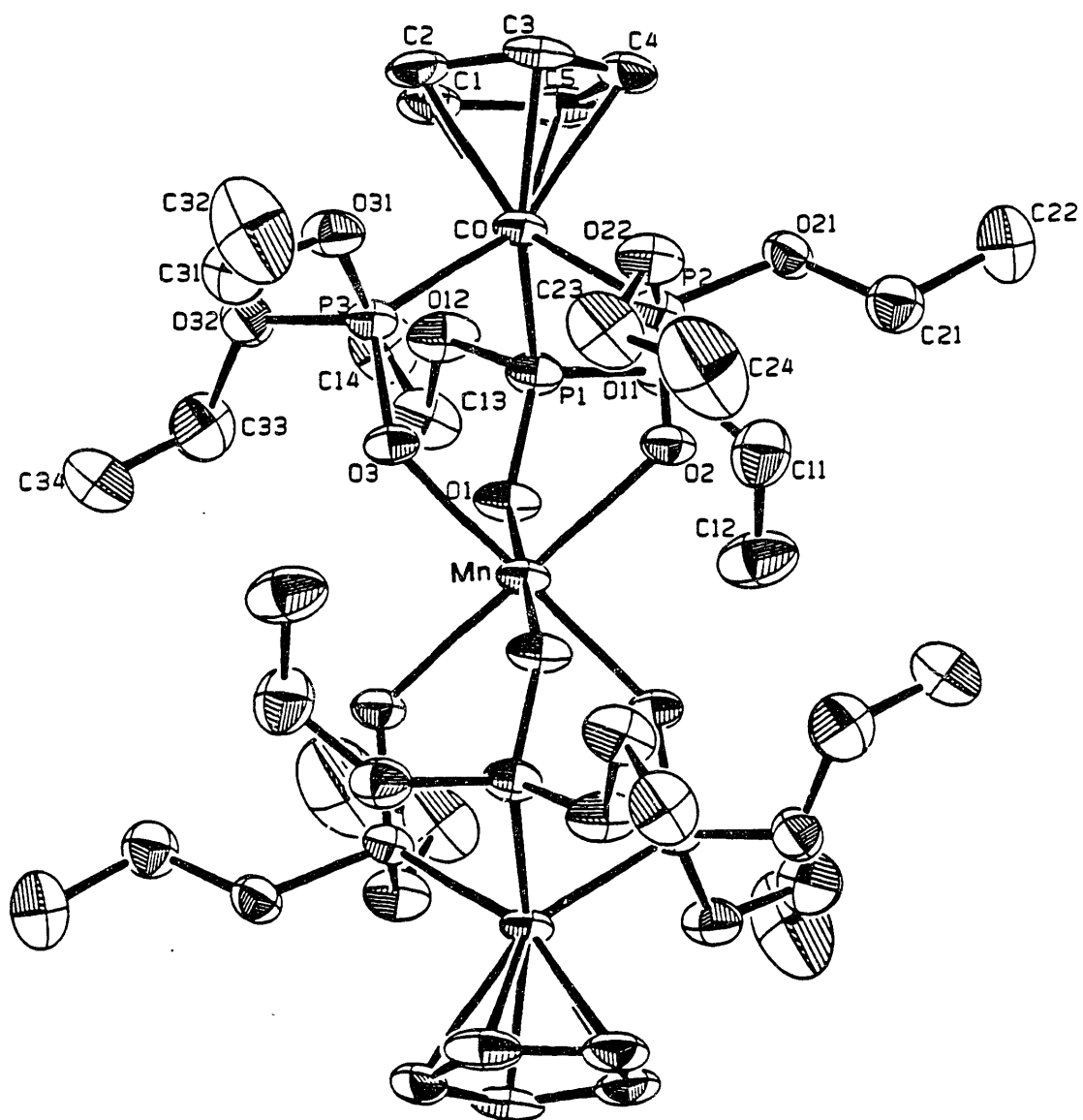
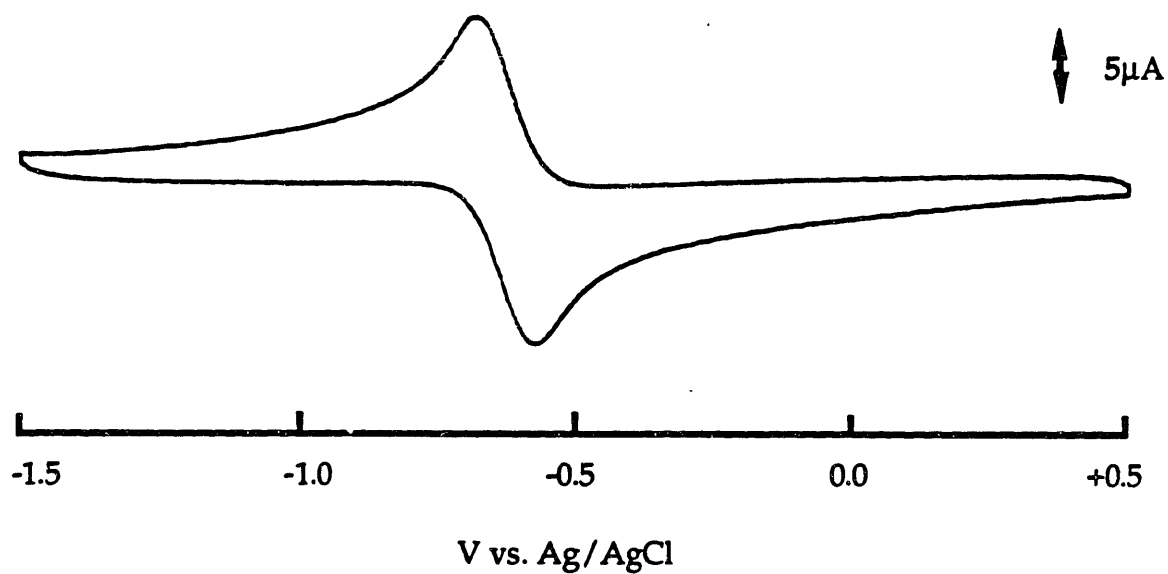
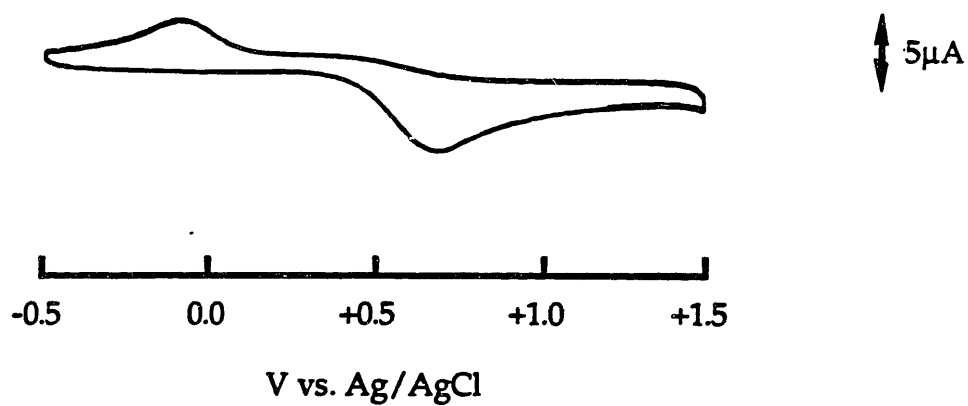


Figure 3.2. ORTEP³⁶ drawing of 3 showing 50% probability thermal ellipsoids and labelling scheme for non-hydrogen atoms. Atom disorder is not shown.



(A)



(B)

Figure 3.3. Cyclic Voltammograms of (a) **2** in 0.1 M TBAP acetonitrile solution; and (b) **3** in 0.2 M TBAP methylene chloride solution. Scan speed: 50 mV s^{-1} . Recorded with a glassy carbon electrode vs. Ag/AgCl reference electrode.

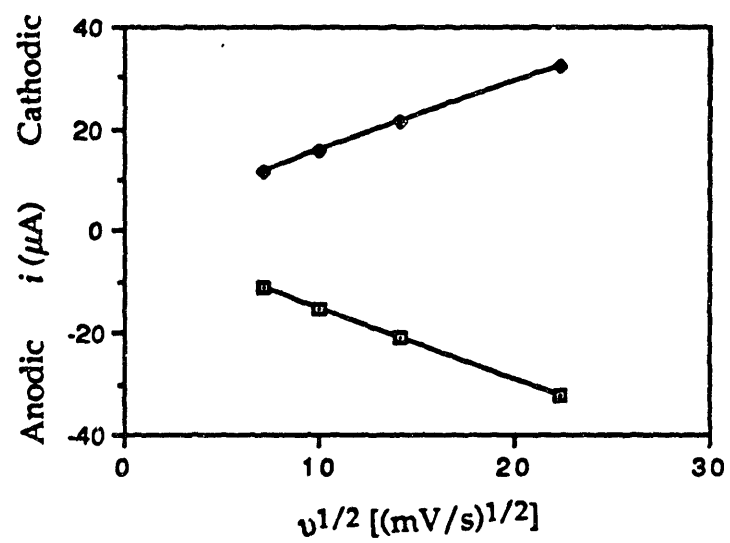


Figure 3.4. Plot of cathodic and anodic currents versus square root of scan speed from voltammograms of 2.

Table 3.1. Experimental Details of the X-ray Diffraction Studies of
 $[\text{Fe}[\text{CpCo}[\text{OP}(\text{OEt})_2]_3]_2][\text{BPh}_4] \cdot \text{C}_7\text{H}_8$, $2\text{a} \cdot \text{C}_7\text{H}_8$ and
 $[\text{Fe}[\text{CpCo}[\text{OP}(\text{OEt})_2]_3]_2]\text{ClO}_4$, 2c^{a}

| compound | 2a·C ₇ H ₈ | 2c |
|---|--|---|
| formula | C ₆₅ H ₉₈ P ₆ BO ₁₈ Co ₂ Fe | C ₃₄ H ₇₀ P ₆ ClO ₂₂ Co ₂ Fe |
| formula weight, g mol ⁻¹ | 1537.84 | 1225.92 |
| crystal system | triclinic | rhombohedral |
| space group | P $\bar{1}$ | R $\bar{3}$ |
| a, Å | 18.379(3) | 12.169(2) |
| b, Å | 18.945(4) | 12.172(2) |
| c, Å | 12.205(3) | 61.397(95) |
| α, ° | 105.95(2) | |
| β, ° | 100.09(2) | |
| γ, ° | 88.50(2) | |
| V, Å ³ | 4022 | |
| Z | 2 | 6 |
| temperature, °C | -78 | -78 |
| ρ _{calcd} , g cm ⁻³ | 1.270 | 1.551 |
| transmission factor range | | 0.948 ~ 1.000 |
| linear absorption coefficient, cm ⁻¹ | | 11.97 |
| 2θ range | 3° ≤ 2θ ≤ 40°, ±h, ±k, +l | 3° ≤ 2θ ≤ 51°, ±h, ±k, +l |
| total no. of data collected | 8214 | 10735 |
| R _{merge} ^b | 0.047 | 0.016 |
| no. of independent data | 7499 | 9742 |

Table 3.1, contd. Experimental Details of the X-ray Diffraction Studies of
 $[\text{Fe}\{\text{CpCo}[\text{OP}(\text{OEt})_2]_3\}_2][\text{BPh}_4]\cdot\text{C}_7\text{H}_8$, **2a** $\cdot\text{C}_7\text{H}_8$ and
 $[\text{Fe}\{\text{CpCo}[\text{OP}(\text{OEt})_2]_3\}_2]\text{ClO}_4$, **2c**.

| compound | 2a $\cdot\text{C}_7\text{H}_8$ | 2c |
|---|---------------------------------------|-----------|
| no. of unique data with $F > 6\sigma(F)$ | 3793 | 4197 |
| no. of variables | 496 | 183 |
| R^c | 0.116 | 0.044 |
| R_w^d | 0.166 | 0.061 |
| p^d | 0.05 | 0.03 |

^a All measurements were made on an Enraf-Nonius CAD4-F diffractometer with Mo $K\alpha$ radiation ($\lambda = 0.70926 \text{ \AA}$). For **2a**, the data were collected using parameters for rapid data collection.²² ^b $R_{(\text{merge})} = \frac{\sum_{i=1}^n \sum_{j=1}^m | \langle F_i^2 \rangle - F_{ij}^2 |}{\sum_{i=1}^n m \times \langle F_i^2 \rangle}$ where n = numbers of unique reflections which were measured more than once during data collection, m = number of times a given reflection was measured and $\langle F_i^2 \rangle$ is the average value of F^2 for the reflection. ^c $R = \frac{\sum | |F_o| - |F_c| |}{\sum |F_o|}$. ^d $R_w = [\sum w (|F_o| - |F_c|)^2 / \sum w |F_o|^2]^{1/2}$, where $w = 1/\sigma^2(F)$, $\sigma^2(F) = [S^2(C+4B) + (pI)^2] / [(Lp)^2 4F^2]$ with S = scan rate, C = peak count, B = sum of left and right background counts, Lp = Lorentz-polarization factor, and p = fudge factor.

Table 3.2. Final Positional and Equivalent Isotropic Thermal Parameters of Non-Hydrogen Atoms in [Fe{CpCo[OP(OEt)₂]₃]₂]ClO₄, 2c.^a

| Atom ^b | X | Y | Z | B(eq) |
|-------------------|------------|------------|------------|---------|
| Co1 | 0.6667 | 0.3335 | 0.14674(1) | 1.77(2) |
| Co2 | 0.6666 | 0.3334 | 0.02031(1) | 2.50(2) |
| Fe1 | 0.6667 | 0.3333 | 0.08350(1) | 1.86(2) |
| Cl1 | 0.3331 | 0.6667 | 0.08453(3) | 4.62(6) |
| P1 | 0.70257(8) | 0.20829(8) | 0.12683(1) | 1.94(3) |
| P5 | 0.6135(1) | 0.4437(1) | 0.04068(2) | 2.97(4) |
| O1 | 0.6801(2) | 0.2071(2) | 0.10250(3) | 2.21(9) |
| O4 | 0.6531(2) | 0.4591(2) | 0.06453(4) | 3.0(1) |
| O11 | 0.8403(2) | 0.2254(2) | 0.13026(4) | 3.0(1) |
| O12 | 0.6158(2) | 0.0696(2) | 0.13620(4) | 2.7(1) |
| O41 | 0.4639(3) | 0.3854(3) | 0.03931(4) | 4.9(1) |
| O42 | 0.6662(4) | 0.5821(3) | 0.03102(4) | 5.6(1) |
| O70 | 0.3321(4) | 0.7774(3) | 0.09232(6) | 6.6(2) |
| O72 | 0.3333 | 2/3 | 0.0614(1) | 6.8(2) |
| C111 | 0.9448(3) | 0.2985(4) | 0.11543(7) | 4.1(2) |
| C112 | 0.9845(4) | 0.2150(5) | 0.10470(7) | 5.0(2) |
| C121 | 0.6090(4) | -0.0398(3) | 0.12515(6) | 3.2(1) |
| C122 | 0.5432(4) | -0.1512(4) | 0.14041(8) | 4.1(2) |
| C411 | 0.4032(6) | 0.4335(6) | 0.05430(8) | 6.3(3) |
| C412 | 0.2948(6) | 0.3334(7) | 0.0638(1) | 10.4(4) |
| C421 | 0.7279(6) | 0.6961(5) | 0.0422(1) | 7.7(3) |
| C422 | 0.8104(6) | 0.8007(6) | 0.0273(1) | 8.7(3) |
| C1 | 0.675(3) | 0.239(2) | 0.1752(2) | 2.22(8) |
| C2 | 0.7710(6) | 0.366(3) | 0.1758(2) | 2.22(8) |
| C3 | 0.714(3) | 0.4416(7) | 0.1747(2) | 2.22(8) |
| C4 | 0.583(2) | 0.361(2) | 0.1733(2) | 2.22(8) |
| C5 | 0.558(1) | 0.236(1) | 0.1736(2) | 2.22(8) |
| C6 | 0.766(1) | 0.335(3) | -0.0079(4) | 4.0(1) |
| C7 | 0.646(3) | 0.225(1) | -0.0094(2) | 4.0(1) |
| C8 | 0.5546(7) | 0.262(3) | -0.0081(3) | 4.0(1) |

Table 3.2, contd. Final Positional and Equivalent Isotropic Thermal Parameters of Non-Hydrogen Atoms in [Fe{CpCo[OP(OEt)₂]₃]₂]ClO₄, 2c.

| Atom | X | Y | Z | B(eq) |
|------|----------|----------|------------|--------|
| C9 | 0.617(3) | 0.394(3) | -0.0058(3) | 4.0(1) |
| C10 | 0.748(2) | 0.439(1) | -0.0057(2) | 4.0(1) |

^aNumbers in parentheses are errors in the last significant digit. ^bSee Figure 3.1. for atom labelling scheme. ^cCl1 and O72 are atoms on the anion.

Table 3.3. Final Thermal Parameters for Non-Hydrogen Atoms in
 $[\text{Fe}\{\text{CpCo}[\text{OP}(\text{OEt})_2]_3\}_2]\text{ClO}_4, 2c.^a$

| Atom ^b | U ₁₁ | U ₂₂ | U ₃₃ | U ₁₂ | U ₁₃ | U ₂₃ |
|-------------------|-----------------|-----------------|-----------------|-----------------|-----------------|-----------------|
| Co1 | 0.0268(3) | 0.0268 | 0.0136(4) | 0.0134 | 0 | 0 |
| Co2 | 0.0406(3) | 0.0407 | 0.0137(5) | 0.0203 | 0 | 0 |
| Fe1 | 0.0280(3) | 0.0281 | 0.0144(3) | 0.0140 | 0 | 0 |
| Cl1 ^c | 0.0634(8) | 0.0635 | 0.048(1) | 0.032 | 0 | 0 |
| P1 | 0.0307(5) | 0.0273(5) | 0.0192(5) | 0.0169(4) | 0.0025(3) | 0.0026(4) |
| P5 | 0.0570(7) | 0.0491(6) | 0.0190(6) | 0.0355(5) | -0.0040(4) | 0.0017(4) |
| O1 | 0.041(1) | 0.031(1) | 0.017(1) | 0.022(1) | 0.005(1) | 0.000(1) |
| O4 | 0.066(2) | 0.043(1) | 0.019(1) | 0.037(1) | -0.005(1) | 0.000(1) |
| O11 | 0.037(1) | 0.052(2) | 0.034(1) | 0.030(1) | 0.003(1) | 0.005(1) |
| O12 | 0.049(2) | 0.029(1) | 0.026(1) | 0.020(1) | 0.011(1) | 0.005(1) |
| O41 | 0.066(2) | 0.112(3) | 0.034(2) | 0.065(2) | -0.006(1) | -0.004(2) |
| O42 | 0.146(3) | 0.054(2) | 0.027(2) | 0.061(2) | -0.014(2) | 0.003(1) |
| O70 | 0.094(3) | 0.069(2) | 0.098(3) | 0.048(2) | 0.008(2) | -0.010(2) |
| O72 | 0.110(3) | 0.110 | 0.039(3) | 0.055 | 0.000 | 0.000 |
| C111 | 0.030(2) | 0.056(3) | 0.070(3) | 0.022(2) | 0.011(2) | 0.015(2) |
| C112 | 0.065(3) | 0.098(4) | 0.047(3) | 0.055(3) | 0.021(2) | 0.022(3) |
| C121 | 0.057(2) | 0.031(2) | 0.040(2) | 0.027(2) | 0.013(2) | 0.003(2) |
| C122 | 0.054(3) | 0.036(2) | 0.071(3) | 0.026(2) | 0.015(2) | 0.008(2) |
| C411 | 0.101(4) | 0.128(5) | 0.061(3) | 0.094(4) | 0.025(3) | 0.021(3) |
| C412 | 0.072(4) | 0.139(6) | 0.142(7) | 0.020(4) | 0.031(4) | -0.058(5) |
| C421 | 0.145(6) | 0.056(3) | 0.087(4) | 0.047(4) | -0.026(4) | -0.011(3) |
| C422 | 0.105(5) | 0.068(4) | 0.131(6) | 0.023(4) | 0.041(4) | 0.028(4) |
| C1 | 0.028(1) | | | | | |
| C3 | 0.028(1) | | | | | |
| C4 | 0.028(1) | | | | | |
| C5 | 0.028(1) | | | | | |
| C6 | 0.051(1) | | | | | |
| C7 | 0.051(1) | | | | | |
| C8 | 0.051(1) | | | | | |
| C9 | 0.051(1) | | | | | |

Table 3.3, contd. Final Thermal Parameters for Non-Hydrogen Atoms
in $[\text{Fe}(\text{CpCo}[\text{OP}(\text{OEt})_2]_3)_2]\text{ClO}_4$, **2c**.

| Atom | U_{11} | U_{22} | U_{33} | U_{12} | U_{13} | U_{23} |
|------|----------|----------|----------|----------|----------|----------|
| C10 | 0.051(1) | | | | | |

^aNumbers in parentheses are errors in the last significant digit. The anisotropic temperature factors are of the form $\exp[-2\pi^2(U_{11}h^2a^2 + 2U_{12}hka^*b^* + \dots)]$. ^bSee Figure 3.1 for the atom labelling scheme. ^cCl1 and O72 are atoms on the anion.

Table 3.4. Selected Interatomic Distances (Å) and Angles (deg) for
 $[\text{Fe}(\text{CpCo}[\text{OP}(\text{OEt})_2]_3)_2]\text{ClO}_4, 2\text{c}^{\text{a}}$

| <u>Coordination Sphere</u> | | | |
|----------------------------------|------------|---------------|-------------|
| Fe1- O1 | 2.003(3) | Fe1- O4 | 1.999(3) |
| Fe1- O1 | 1.997(3) | Fe1- O4 | 1.992(3) |
| Fe1- O1 | 1.999(3) | Fe1- O4 | 1.995(3) |
| Fe1...Co1 | 3.883(1) | Fe1...Co2 | 3.880(1) |
| O1- Fe1- O1 | 89.4(1) | O1- Fe1- O4 | 179.93(9) |
| O1- Fe1- O1 | 89.3(1) | O1- Fe1- O4 | 179.92(9) |
| O1- Fe1- O1 | 89.5(1) | O1- Fe1- O4 | 90.7(1) |
| O1- Fe1- O4 | 90.6(1) | O1- Fe1- O4 | 90.5(1) |
| O1- Fe1- O4 | 179.93(9) | O4- Fe1- O4 | 89.2(1) |
| O1- Fe1- O4 | 90.8(1) | O4- Fe1- O4 | 89.3(1) |
| O1- Fe1- O4 | 90.7(1) | O4- Fe1- O4 | 89.5(1) |
| O1- Fe1- O4 | 90.5(1) | Co1- Fe1- Co2 | 180.0 |
| <u>Ligand Geometry</u> | | | |
| | <u>Min</u> | <u>Max</u> | <u>Mean</u> |
| Co-P | 2.153(1) | 2.163(2) | 2.159(2) |
| Co-C _{Cp} ^b | 1.97(1) | 2.19(2) | 2.08(2) |
| P=O | 1.518(2) | 1.523(3) | 1.521(3) |
| P-O _{Et} | 1.587(2) | 1.596(3) | 1.591(3) |
| O _{Et} -C _{Et} | 1.382(6) | 1.470(8) | 1.441(8) |
| C _{Cp} -C _{Cp} | | | 1.40(4) |
| C _{Et} -C _{Et} | 1.401(8) | 1.510(5) | 1.468(8) |
| P-Co-P | 89.78(5) | 92.0(5) | 90.8(5) |
| Co-P=O | 117.2(2) | 117.6(1) | 117.4(2) |
| Co-P-O | 106.4(1) | 113.8(1) | 110.0(1) |
| O-P=O | 107.2(1) | 109.2(1) | 108.3(2) |

Table 3.4, contd. Selected Interatomic Distances (Å) and Angles (deg) for
 $[\text{Fe}(\text{CpCo}[\text{OP}(\text{OEt})_2]_3)_2]\text{ClO}_4, 2c$.

| <u>Ligand Geometry, contd</u> | | | |
|---|------------|------------|-------------|
| | <u>Min</u> | <u>Max</u> | <u>Mean</u> |
| O-P-O | 100.8(2) | 102.6(2) | 101.7(2) |
| Fe-O=P | 127.7(2) | 130.7(2) | 129.2(2) |
| P-O _{Et} -C _{Et} | 118.7(3) | 127.4(3) | 122.3(3) |
| C _{Cp} -C _{Cp} -C _{Cp} | | | 108(2) |
| O _{Et} -C _{Et} -C _{Et} | 107.2(3) | 110.9(6) | 109.7(6) |
| <u>Anion Geometry</u> | | | |
| Cl-O | 1.420(6) | 1.440(4) | 1.433(6) |
| Cl-O-Cl | 109.3(2) | 109.7(2) | 109.5(2) |

^a Numbers in parentheses are errors in the last significant digit(s). See Figure 3.1 for atom labelling scheme. ^bThe footnotes, "Cp" and "Et", are used for atoms on Cp rings and ethyls of the phosphite group, respectively.

Table 3.5. Experimental Details of the X-ray Diffraction Studies of
 $\text{Mn}(\text{CpCo}[\text{OP}(\text{OEt})_2]_3)_2$, **3**.^a

| compound | 3 |
|---|---|
| formula | $\text{C}_{34}\text{H}_{70}\text{P}_6\text{O}_{18}\text{Co}_2\text{Mn}$ |
| formula weight, g mol^{-1} | 1125.56 |
| crystal system | triclinic |
| space group | $\text{P}\bar{1}$ |
| a, Å | 11.648(4) |
| b, Å | 11.723(3) |
| c, Å | 12.285(2) |
| α , ° | 116.50(2) |
| β , ° | 91.24(2) |
| γ , ° | 118.67(2) |
| V, Å ³ | 1256 |
| Z | 1 |
| temperature, °C | -78 |
| ρ_{calcd} , g cm^{-3} | 1.49 |
| ρ_{obsd} , g cm^{-3} | 1.46(1) |
| crystal dimensions, mm | 0.20 × 0.18 × 0.24 |
| linear absorption coefficient, cm^{-1} | 11.40 |
| 2 θ range | $3^\circ \leq 2\theta \leq 48^\circ$, +h, ±k, ±l |
| total no. of data collected | 4235 |
| $R_{\text{merge}}^{\text{b}}$ | 0.025 |
| no. of independent data | 3533 |
| no. of unique data with $F > 6\sigma(F)$ | 3338 |

Table 3.5, contd. Experimental Details of the X-ray Diffraction Studies of 3.

| compound | 3 |
|-----------------------------|----------|
| no. of variables | 277 |
| R ^c | 0.057 |
| R _w ^d | 0.075 |
| p ^d | 0.05 |

^a See footnotes of Table 3.1.

Table 3. 6. Final Positional and Equivalent Isotropic Thermal Parameters of Non-Hydrogen Atoms in $\text{Mn}[\text{CpCo}[\text{OP}(\text{OEt})_2]_3]_2$, **3**.^a

| Atom ^b | X | Y | Z | B(eq) |
|-------------------|------------|------------|------------|---------|
| Co | 0.35185(6) | 0.22150(7) | 0.12210(6) | 1.97(2) |
| Mn | 1/2 | 1/2 | 1/2 | 1.89(3) |
| P(1) | 0.5247(1) | 0.4576(1) | 0.2203(1) | 2.18(4) |
| P(2) | 0.2333(1) | 0.2823(1) | 0.2429(1) | 2.08(4) |
| P(3) | 0.4295(1) | 0.1778(1) | 0.2511(1) | 2.19(4) |
| O(1) | 0.5919(3) | 0.5426(4) | 0.3613(3) | 2.4(1) |
| O(2) | 0.3063(3) | 0.4142(4) | 0.3788(3) | 2.4(1) |
| O(3) | 0.4571(3) | 0.2726(4) | 0.3915(3) | 2.3(1) |
| O(11) | 0.4926(4) | 0.5618(4) | 0.1907(3) | 3.1(1) |
| O(12) | 0.6369(4) | 0.4577(4) | 0.1463(3) | 3.1(1) |
| O(21) | 0.1453(4) | 0.3159(4) | 0.1725(3) | 2.7(1) |
| O(22) | 0.1108(4) | 0.1367(4) | 0.2415(3) | 3.1(1) |
| O(31) | 0.3225(4) | 0.0014(4) | 0.2042(3) | 3.0(1) |
| O(32) | 0.5628(4) | 0.1741(5) | 0.2260(4) | 3.3(1) |
| C(1) | 0.4084(6) | 0.1366(7) | -0.0400(5) | 3.2(2) |
| C(2) | 0.3076(6) | 0.0141(6) | -0.0305(5) | 3.3(2) |
| C(3) | 0.1906(6) | 0.0189(6) | -0.0321(5) | 3.3(2) |
| C(4) | 0.2148(6) | 0.1406(7) | -0.0465(5) | 3.2(2) |
| C(5) | 0.3503(6) | 0.2167(6) | -0.0494(5) | 3.3(2) |
| C(11) | 0.4618(7) | 0.6653(7) | 0.2805(6) | 4.0(2) |
| C(12) | 0.5877(8) | 0.8230(7) | 0.3565(6) | 4.7(2) |
| C(13) | 0.7673(6) | 0.5964(7) | 0.1919(6) | 3.6(2) |
| C(14) | 0.8266(6) | 0.5800(8) | 0.0830(6) | 4.2(2) |
| C(21) | 0.0692(6) | 0.3749(7) | 0.2391(6) | 3.2(2) |
| C(22) | 0.0023(7) | 0.4032(8) | 0.1587(7) | 4.0(2) |
| C(23) | 0.1105(7) | 0.1181(8) | 0.3489(7) | 4.6(2) |
| C(24) | 0.013(1) | 0.140(2) | 0.411(1) | 9.2(5) |
| C(31) | 0.3525(7) | -0.0587(7) | 0.2731(6) | 3.9(2) |
| C(32) | 0.2276(9) | -0.176(1) | 0.274(1) | 7.5(4) |
| C(33) | 0.6975(6) | 0.2965(7) | 0.3124(7) | 4.1(2) |

Table 3.6, contd. Final Positional and Equivalent Isotropic Thermal Parameters of Non-Hydrogen Atoms in $\text{Mn}[\text{CpCo}[\text{OP}(\text{OEt})_2]_3]_2$, 3.^a

| Atom | X | Y | Z | B(eq) |
|-------|-----------|----------|-----------|--------|
| C(34) | 0.7442(8) | 0.253(1) | 0.3917(8) | 6.0(3) |

^aNumbers in parentheses are errors in the last significant digit. ^bSee Figure 3.2. for atom labelling scheme.

Table 3.7. Final Thermal Parameters of Non-Hydrogen Atoms for
 $\text{Mn}[\text{CpCo}[\text{OP}(\text{OEt})_2]_3]_2$, **3**.^a

| Atom ^b | U ₁₁ | U ₂₂ | U ₃₃ | U ₁₂ | U ₁₃ | U ₂₃ |
|-------------------|-----------------|-----------------|-----------------|-----------------|-----------------|-----------------|
| Co | 0.0249(4) | 0.0260(4) | 0.0141(4) | 0.0094(3) | 0.0038(3) | 0.0083(3) |
| Mn | 0.0223(6) | 0.0249(5) | 0.0145(5) | 0.0074(4) | 0.0042(4) | 0.0087(4) |
| P(1) | 0.0282(7) | 0.0296(7) | 0.0189(7) | 0.0104(6) | 0.0082(5) | 0.0137(6) |
| P(2) | 0.0218(7) | 0.0290(7) | 0.0197(7) | 0.0094(6) | 0.0041(5) | 0.0111(6) |
| P(3) | 0.0287(7) | 0.0276(7) | 0.0204(7) | 0.0124(6) | 0.0058(5) | 0.0108(6) |
| O(1) | 0.026(2) | 0.028(2) | 0.019(2) | 0.004(2) | 0.006(1) | 0.012(1) |
| O(2) | 0.025(2) | 0.035(2) | 0.020(2) | 0.013(2) | 0.005(1) | 0.009(2) |
| O(3) | 0.035(2) | 0.029(2) | 0.018(2) | 0.014(2) | 0.008(1) | 0.011(1) |
| O(11) | 0.047(2) | 0.034(2) | 0.030(2) | 0.017(2) | 0.007(2) | 0.018(2) |
| O(12) | 0.034(2) | 0.042(2) | 0.028(2) | 0.012(2) | 0.017(2) | 0.017(2) |
| O(21) | 0.032(2) | 0.043(2) | 0.026(2) | 0.021(2) | 0.007(2) | 0.016(2) |
| O(22) | 0.030(2) | 0.034(2) | 0.035(2) | 0.006(2) | 0.010(2) | 0.019(2) |
| O(31) | 0.048(2) | 0.027(2) | 0.030(2) | 0.014(2) | 0.003(2) | 0.013(2) |
| O(32) | 0.041(2) | 0.058(2) | 0.030(2) | 0.033(2) | 0.011(2) | 0.018(2) |
| C(1) | 0.040(3) | 0.049(3) | 0.017(3) | 0.023(3) | 0.007(2) | 0.007(2) |
| C(2) | 0.058(4) | 0.038(3) | 0.015(3) | 0.025(3) | 0.002(2) | 0.003(2) |
| C(3) | 0.037(3) | 0.035(3) | 0.017(3) | 0.006(3) | -0.005(2) | 0.004(2) |
| C(4) | 0.048(3) | 0.051(3) | 0.016(3) | 0.029(3) | 0.002(2) | 0.009(2) |
| C(5) | 0.052(4) | 0.040(3) | 0.016(3) | 0.015(3) | 0.005(2) | 0.012(2) |
| C(11) | 0.056(4) | 0.045(3) | 0.061(4) | 0.028(3) | 0.020(3) | 0.032(3) |
| C(12) | 0.089(5) | 0.045(4) | 0.035(3) | 0.030(4) | 0.016(3) | 0.021(3) |
| C(13) | 0.033(3) | 0.055(4) | 0.042(3) | 0.014(3) | 0.016(3) | 0.030(3) |
| C(14) | 0.044(4) | 0.073(4) | 0.059(4) | 0.030(3) | 0.029(3) | 0.047(4) |
| C(21) | 0.037(3) | 0.047(3) | 0.041(3) | 0.024(3) | 0.014(3) | 0.023(3) |
| C(22) | 0.047(4) | 0.068(4) | 0.072(5) | 0.037(3) | 0.032(3) | 0.052(4) |
| C(23) | 0.048(4) | 0.072(5) | 0.070(5) | 0.025(4) | 0.023(3) | 0.054(4) |
| C(24) | 0.101(7) | 0.24(1) | 0.090(7) | 0.110(9) | 0.067(6) | 0.119(9) |
| C(31) | 0.056(4) | 0.042(3) | 0.052(4) | 0.022(3) | 0.012(3) | 0.030(3) |
| C(32) | 0.065(5) | 0.092(6) | 0.16(1) | 0.025(5) | 0.024(6) | 0.101(7) |
| C(33) | 0.030(3) | 0.053(4) | 0.064(4) | 0.019(3) | 0.018(3) | 0.027(3) |
| C(34) | 0.065(5) | 0.074(5) | 0.062(5) | 0.040(4) | -0.011(4) | 0.015(4) |

^aNumbers in parentheses are errors in the last significant digit. The anisotropic temperature factors are of the form $\exp[-2\pi^2(U_{11}h^2a^2 + 2U_{12}hka^*b^* + \dots)]$. ^bSee Figure 3.2. for the atom labelling scheme.

Table 3.8. Selected Interatomic Distances (Å) and Angles (deg) for
[Mn{CpCo[OP(OEt)₂]₃}]₂, 3.^a

| <u>Coordination Sphere</u> | | | |
|---|------------|------------|-------------|
| Mn-O1 | 2.150(3) | Mn-O3 | 2.158(3) |
| Mn-O2 | 2.159(3) | Mn...Co | 3.989(2) |
| O1-Mn-O2 | 87.6(1) | O1-Mn-O3 | 87.7(1) |
| O2-Mn-O3 | 87.3(1) | | |
| <u>Ligand Geometry</u> | | | |
| | <u>Min</u> | <u>Max</u> | <u>Mean</u> |
| Co-P | 2.167(2) | 2.177(2) | 2.171(2) |
| Co-C _{Cp} ^b | 2.075(5) | 2.095(5) | 2.085(5) |
| P=O | 1.495(3) | 1.508(4) | 1.502(4) |
| P-O _{Et} | 1.607(4) | 1.616(4) | 1.610(4) |
| O _{Et} -C _{Et} | 1.430(7) | 1.446(7) | 1.435(7) |
| C _{Cp} -C _{Cp} | 1.391(8) | 1.435(8) | 1.410(8) |
| C _{Et} -C _{Et} | 1.44(1) | 1.50(1) | 1.48(1) |
| P-Co-P | 90.68(6) | 92.01(6) | 91.37(6) |
| Co-P=O | 119.4(2) | 120.3(1) | 119.9(2) |
| Co-P-O | 105.4(1) | 112.2(2) | 109.0(2) |
| O-P=O | 107.9(2) | 109.5(2) | 108.7(2) |
| O-P-O | 99.4(2) | 99.9(2) | 99.7(2) |
| Mn-O=P | 127.2(2) | 128.4(2) | 127.7(2) |
| P-O _{Et} -C _{Et} | 117.8(3) | 122.8(4) | 120.5(4) |
| C _{Cp} -C _{Cp} -C _{Cp} | 106.8(5) | 108.9(5) | 108.0(5) |
| O _{Et} -C _{Et} -C _{Et} | 107.5(5) | 112.7(6) | 110.3(6) |

^a Numbers in parentheses are errors in the last significant digit(s). See Figure 3.2 for atom labelling scheme. ^bThe footnotes, "Cp" and "Et", are used for atoms on Cp rings and ethyls of the phosphite group, respectively.

Table 3.9. Selected Geometric Parameters for Various Iron and Manganese Complexes

| Compound | $\langle M-O \rangle$ Å | $\langle M-N \rangle$ Å | $\langle O-M-O \rangle$ deg | $\langle N-M-N \rangle$ deg | ref. |
|---|----------------------------|----------------------------|--------------------------------|--------------------------------|------|
| [Fe(CpCo[OP(OEt) ₂] ₃) ₂] ⁺ , 2 | 1.994 | | 90.0 | | b |
| Fe ₂ O(OAc) ₂ (CpCo[OP(OEt) ₂] ₃) ₂ , 5 | 2.085 | | 85.3 | | 36 |
| [Fe(HBpz ₃) ₂] ⁺ , 8 | | 1.957 | | 88.5 | 9 |
| [Fe ₂ O(OAc) ₂ (HBpz ₃) ₂], 7 | | 2.160 | | 82.9 | 9 |
| [Fe(HBpz ₃) ₂], 9 | | 1.973 | | 88.3 | 30 |
| Mn(CpCo[OP(OEt) ₂] ₃) ₂ , 3 | 2.156 | | 87.6 | | b |
| Mn(HB(3,5-Me ₂ pz) ₃) ₂ , 10 | | 1.972 | | 84.5 | 11 |
| Mn(OAc) ₂ (BIPhMe) ₂ , 11 | 2.132 | | | | 31 |

^aAbbreviations used: HBpz₃ = hydrotris(1-pyrazolyl)borate; HB(3,5-Me₂pz)₃ = hydrotris{1-(3,5-dimethyl) pyrazolyl}borate; BIPhMe = 2,2'-bis(1-methylimidazolyl) phenylmethoxymethane. ^bThis work.

Table 3.10. Reduction Potentials of Fe(III)/Fe(II) Couple in Various Iron Complexes

| Compound | Coord. Sphere | $E_{1/2}$ (V vs. NHE) | Solvent | Ref. |
|--|--------------------------|-----------------------|--------------------------|------|
| $[\text{Fe}(\text{HBpz}_3)_2]^+$, 8 | FeN_6 | +0.47 | CH_3CN | 9 |
| $[\text{Fe}(\text{PA})_3]$ | FeO_3N_3 | +0.21 | DMF | 37 |
| $[\text{Fe}_2\text{O}(\text{OAc})_2(\text{Me}_3\text{TACN})_2]^{2+}$, 4 | FeO_3N_3 | -0.13 | CH_2Cl_2 | 12 |
| $[\text{Fe}(\text{DPA})_2]^-$ | FeO_4N_2 | -0.07 | DMF | 37 |
| $[\text{Fe}[\text{CpCo}[\text{OP}(\text{OEt})_2]_3]_2]^+$, 2 | FeO_6 | -0.40 | CH_3CN | b |

^aAbbreviations used: HBpz₃ = hydrotris(1-pyrazolyl)borate; PA = picolinate; Me₃TACN = N, N', N''-methyl-1,4,7-triazacyclononane; DPA = 2,6-pyridinedicarboxylate. ^bThis work.

Chapter 4
Air Oxidation of Alkanes Catalyzed by
Iron-Ascorbic and Reductic Acid Complexes

Introduction

The catalytic oxidation of saturated hydrocarbons using molecular oxygen as sole oxygen source under ambient conditions remains a great challenge to chemists. Despite the fact that the reactions between molecular oxygen and organic substrates are thermodynamically favorable, they are kinetically restricted due to spin conservation. Dioxygen has a triplet ground state while saturated hydrocarbon molecules have singlet ground states. This difference makes the direct reaction between the two species very difficult without proper activation of one or both of the reactants.

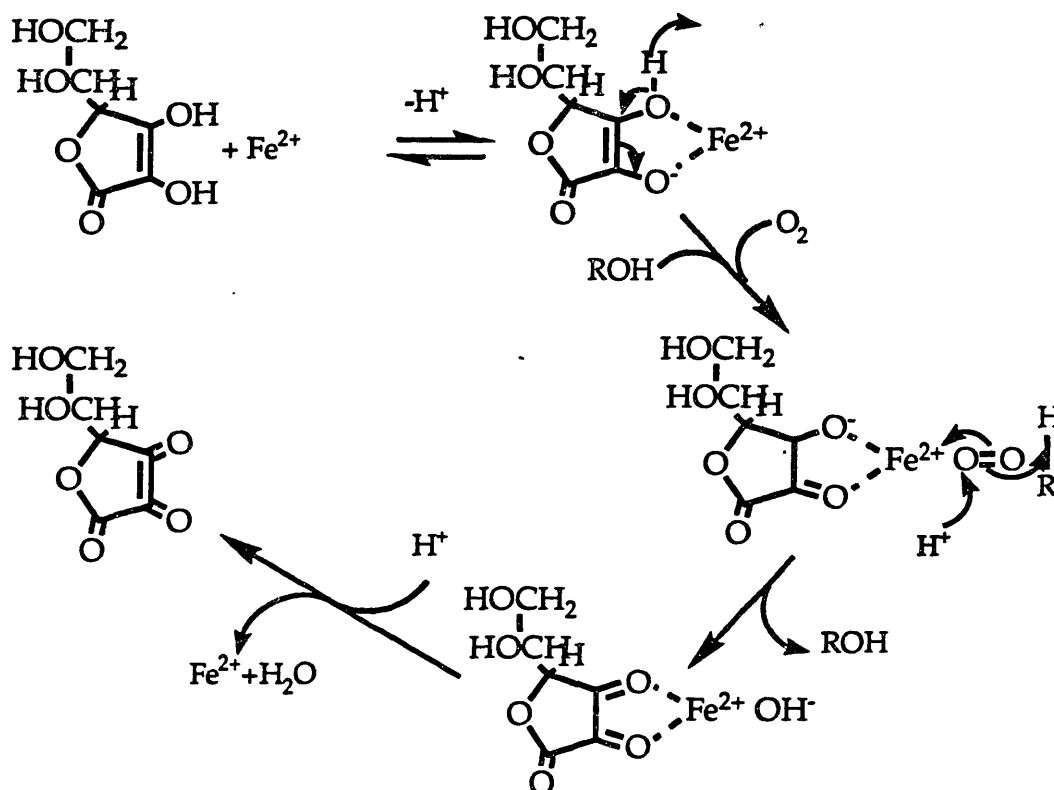
This reaction, however, is readily carried out in biological systems with the help of various mono- and dioxygenases.¹ The aforementioned difficulties are overcome either by activating the molecular oxygen with a metal center that can receive unpaired electrons to generate an activated singlet oxygen or by promoting the formation of hydrocarbon radicals that further react with dioxygen. In the latter case, the active sites of enzymes can also act as a template to channel the radical reaction to form specific products instead of a random distribution of products as is produced in a free radical reaction. Two of the best known examples of monooxygenases are the heme enzyme cytochrome P-450 and its non-heme counterpart methane monooxygenase. Both enzymes catalyze the reaction described in equation 4.1. A detailed discussion of these two enzymes has been given in Chapter 1.



Great interest in the development of chemical model systems that mimic the function of these enzymes has emerged over last several decades for two main reasons: first, to provide a better understanding of the mechanism of the enzymatic oxidation reaction and, second, to develop catalytic systems that can process naturally abundant saturated hydrocarbons selectively under mild conditions. This task, however, has been proven a rather difficult one. One of the major obstacles encountered in such a chemical system is the autoxidation of the reductant, which not only wastes a large amount of reductant, resulting in low yields based on the reductant, but also competes with the substrate for the activated oxidizing intermediate(s). In the enzyme, nature has cleverly avoided this situation by separating the active center, where highly oxidizing species are generated, from the electron source (reductase). The electrons required for the reduction are only transferred to the metal when needed (see Chapter 1 for detailed discussion). Despite the inherent difficulties, much effort has been devoted to the study of functional model systems that utilize iron or manganese complexes as the catalyst.

Among the earliest developed models for oxygenases were systems using mononuclear iron as catalyst and molecular oxygen as oxidant in the presence of a suitable reductant. The first such system was discovered by Udenfriend and co-workers.^{2,3} It was observed that a mixture of Fe(II)-EDTA-ascorbic acid can hydroxylate aromatic compounds. The system was further explored by Hamilton and found to hydroxylate saturated hydrocarbons and epoxidize alkenes, but only in low yield (<3%).⁴ In aqueous solution with cyclohexane as the substrate, the system can produce 2.1 turnovers of cyclohexanol and 0.7 turnovers* of cyclohexanone. The active species in this system was at first proposed to be free hydroxyl radical,

the same active species in Fenton chemistry ($\text{Fe}^{2+} + \text{H}_2\text{O}_2 \rightarrow \text{Fe}^{3+} + \cdot\text{OH} + \text{OH}^-$).^{5,6} Reexamination of the system by Hamilton and co-workers, however, led to a different proposal that suggests a single oxygen transfer (oxenoid) mechanism (Scheme 4.1).⁷



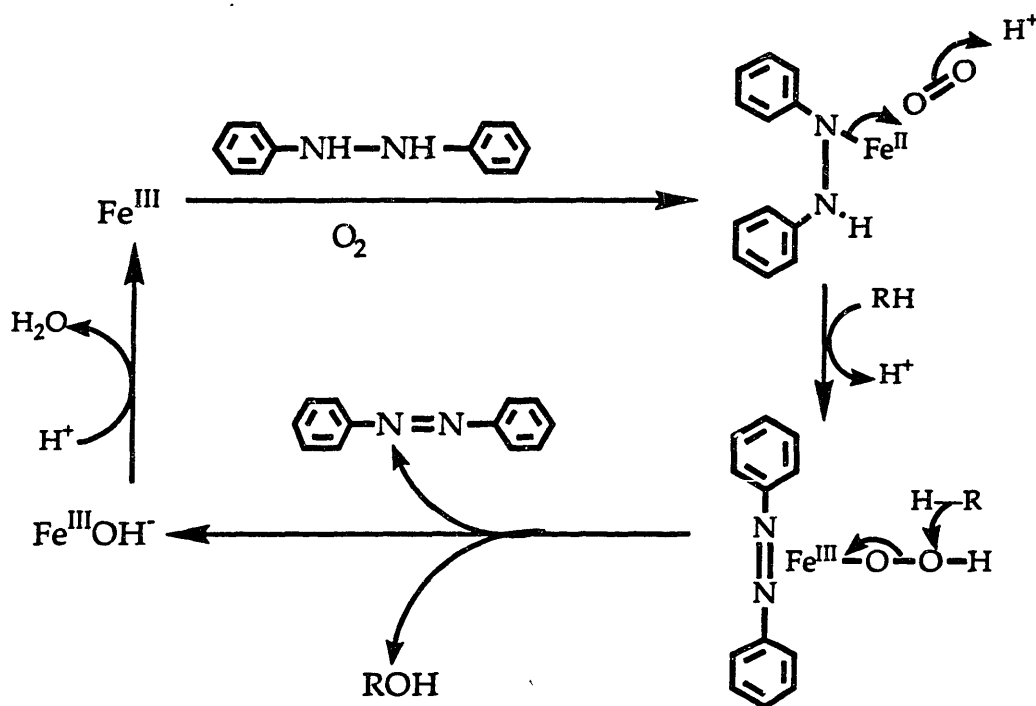
Scheme 4.1.

*In this chapter, the number of turnovers is defined as the number of moles of product per moles of catalyst. Yield (%) is calculated based on the reductant.

Several years later, Ullrich developed another system using Fe(II)-2-mercaptobenzoic acid-NaOH as the catalyst and molecular oxygen as the oxidant. The system was able to oxidize alkane to a mixture of alcohol and

ketone with similar selectivity compared to that of the Udenfriend system⁸. An oxenoid intermediate, therefore, was also proposed by the author.

In 1975, Mimoun and Seree de Roch reported another system using ferric or ferrous salt as the catalyst, 1,2-diphenylhydrazine as the reductant and molecular oxygen as the oxidant.⁹ In the presence of an organic acid, such as benzoic acid or propionic acid, the system can produce four moles of cyclohexanol from cyclohexane with only a trace amount of cyclohexanone. A further study on this system later appeared in 1987.¹⁰ Both authors suggested an iron-hydroperoxide complex as the active species (Scheme 4.2).



Scheme 4.2

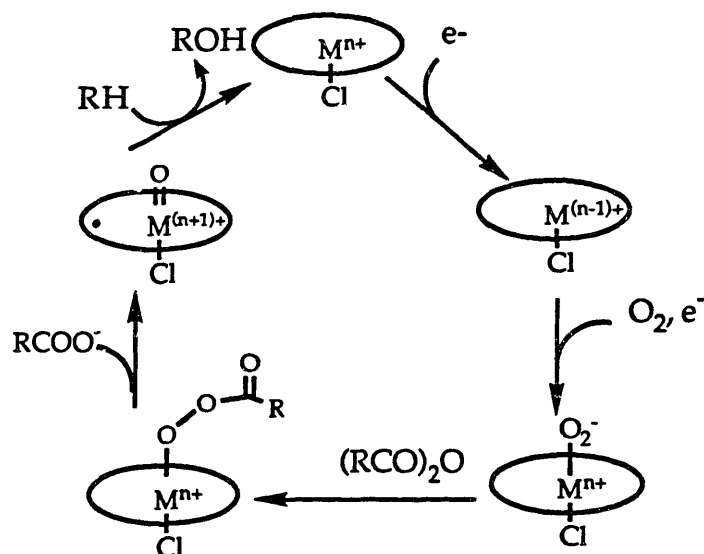
This system, however, is not metal ion specific. Similar yields and product distributions can be obtained by using ferric, ferrous, manganous or vanadyl salts as the catalyst, results which raise serious questions about the integral role of iron in the catalytic cycle. In general, the nature of the active species

in these mononuclear iron systems remains ambiguous due to their complexity.

In contrast, another group of model systems, those using iron or manganese porphyrin complexes as catalysts and O_2 as the oxygen source for mimicking functions of heme monooxygenase cytochrome P-450,¹¹ has been very well defined owing to the extensive studies in many research groups over the last two decades. Upon addition of the proper reducing agent, Mn- or Fe-porphyrin complexes can catalyze the O_2 -dependent oxidation of hydrocarbons. The rate and selectivity are dependent on the reductant. Among the first reducing agents used were borohydrides. With $NaBH_4$ as the reductant and $Mn(TPP)Cl$ (TPP = tetraphenylporphyrin) as the catalyst, cyclohexene is oxidized to cyclohexanol and cyclohexenol. The former is believed to arise from reduction of cyclohexene oxide.¹² The yield of epoxide can be greatly increased by using hydrogen as the reductant in the presence of a catalytic amount of colloidal platinum.¹³ This system catalyzes the oxidation of adamantane with the predominant formation of tertiary alcohol (*tert:sec* = 100:1).¹³ When sodium ascorbate was used as the reductant, $Mn(TPP)Cl$ catalyzed the O_2 -dependent oxidation of cyclohexene exclusively to cyclohexene oxide and the oxidation of cyclohexane preferably to cyclohexanone (ketone:alcohol = 7.5:1).¹⁴ All these systems, which mimic the main reaction of cytochrome P-450 in a quantitative manner, suffer from very low yields based on the reductant (< 5% for alkene oxidation and < 0.5% for alkane oxidation).

Two new systems were subsequently developed which give good yields based on the reducing agent, comparable to that of the cytochrome P-450 system. One system uses a mixture of $Mn(TPP)Cl$, N-methylimidazole, zinc and CH_3COOH to catalyze epoxidation of alkenes and hydroxylation of

alkanes with yields of up to 50% based on zinc.¹⁵ Another system uses zinc amalgam as the reductant and Fe(TPP)Cl as the catalyst.¹⁶ In the presence of an electron-transfer reagent (methyl viologen) and an acylating agent (acetic anhydride), the system catalyzes the hydroxylation of cyclic hydrocarbons with a rate up to 1.1 cycle per minute. The acetic anhydride plays an important role in facilitating the O-O bond cleavage as indicated by the fact that labelled oxygen was incorporated in both the product and the acetate from anhydride when $^{18}\text{O}_2$ was used. This system also has a high kinetic isotope effect ($k_{\text{H}}/k_{\text{D}} = 7$) that is very similar to the cytochrome P-450 system. The ability of the systems mentioned above to hydroxylate alkanes and epoxidize alkenes is very similar to the cytochrome P-450 system except for the case of the Mn(TPP)Cl-N-methylimidazole-Zn-O₂ system where the



Scheme 4.3.

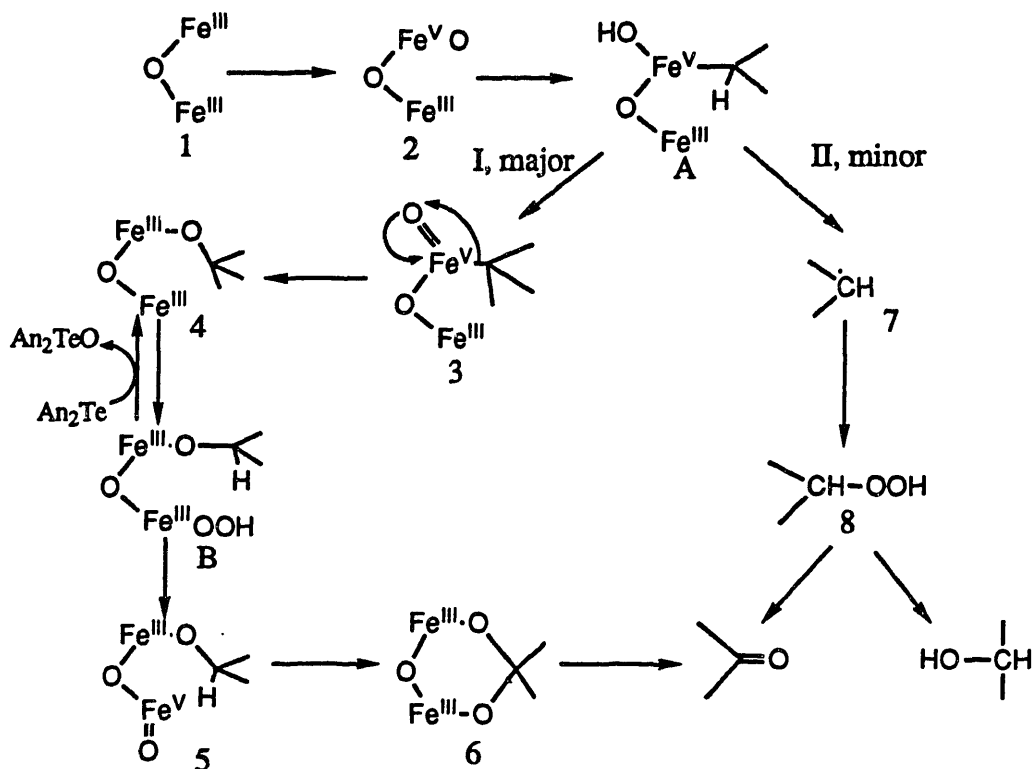
ketone was the major product. It is plausible that these systems react by a similar mechanism to that of cytochrome P-450 (Scheme 4.3).^{11,17,18}

As information about the nature of the active center of the non-heme iron monooxygenase MMO emerged, systems were investigated using

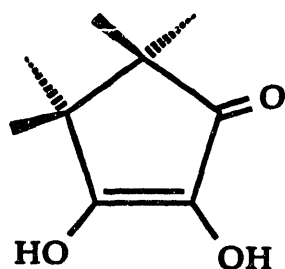
multinuclear iron complexes as the catalyst. Kitajima and co-workers reported that the use of the dinuclear complex $[\text{Fe}_2\text{O}(\text{OAc})_2(\text{HBpz}_3)_2]$ (1) as the catalyst and zinc as reductant.¹⁹ In the presence of acetic acid, saturated hydrocarbons, such as cyclohexane and adamantane, can be oxidized by molecular oxygen to the corresponding alcohols and ketones. When cyclohexane was used as the substrate, equal amounts of cyclohexanol and cyclohexanone were formed. Another group reported use of a similar dinuclear iron complex $[\text{Fe}_2\text{O}(\text{OAc})_2\text{Cl}_2(\text{bipy})_2]$ (2) and reaction conditions identical to those as that used by Kitajima group.²⁰ When cyclohexane was used as the substrate, cyclohexanone was the only product. Both of these systems suffer from low yield (~1.5%) and poor selectivity for alcohol formation.

Another catalyst extensively studied by Barton and his co-workers is the so-called *Gif* and related systems.²¹ This chemistry originally used Fe^0 , Zn, py and acetic acid, which catalyses the air oxidation of saturated hydrocarbons selectively to ketones and demonstrated an unusual selectivity for secondary > tertiary > primary carbon atoms (*Gif*^{III}).²² A mixed-valent trinuclear iron species, $[\text{Fe}_3\text{O}(\text{OAc})_6(\text{py})_3] \cdot 0.5 \text{ py}$ (3), was later isolated from the reaction mixture and a new system was developed by using the trinuclear complex as the catalyst under the same reaction conditions (*Gif*^{IV}).²³ Several modifications have been reported recently. In *Gif*-Orsay system, the chemical reductant zinc was replaced by an electrode.²⁴ Molecular oxygen has also been replaced by KO_2 (*GOAgg*^I) and hydrogen peroxide (*GoAgg*^{II}).²⁵ One intriguing property of these systems is that pyridine is essential to the reactivity of the catalyst. This result has been considered by some investigators as evidence for the existence of a pyridine radical.²⁶ Pyridine was, indeed, not innocent in the catalytic reaction. It

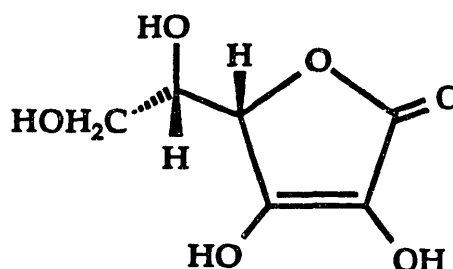
formed a coupling product with adamantane on the tertiary position. The formation of alkyl radical on the tertiary position was proposed.^{25,27} The preference for the formation of secondary oxidation products versus the tertiary products was attributed to a compromise between C-H bond strengths (*prim* > *sec* > *tert*) and the steric hindrance to the insertion of activated oxygen (*tert* > *sec* > *prim*).²¹ An iron-carbene intermediate (A in Scheme 4.4) was proposed. The predominance of the ketone formation was altered by the presence of an oxygen transfer reagent, dianisyl telluride (An_2Te). With the increase amount of An_2Te present in the catalytic system, the ratio of secondary alcohol to ketone was dramatically increased.²⁸ The formation of more alcohol was explained by the author as a result of the reduction of the iron peroxide species (4 in Scheme 4.4) to another intermediate B by An_2Te and subsequent hydrolysis of B, which, in the absence of An_2Te , would be transformed into ketone.^{27,28} A more plausible intermediate, however, is the alkyl hydroperoxide (8 in Scheme 4.4). It has been shown that hydroperoxide is reduced by An_2Te to the corresponding alcohol almost quantitatively under the reaction conditions of *Gif* system.²⁸ Recently, the same research group did report the detection of a cyclohexyl hydroperoxide intermediate in the oxidation of cyclohexane by *Gif* system.²⁹



All the model systems described so far are poorly defined. Furthermore, none of them exhibit the high selectivity for alcohol formation observed in the enzyme systems, not to mention their low yields. The goal of developing a better model system, especially for the non-heme enzyme MMO, was initiated several years ago. Our ultimate goal is to develop catalytic systems for air oxidation of hydrocarbons under ambient conditions using multinuclear iron complexes as catalysts and biologically relevant reductants. A novel catalytic system using a simple dinuclear iron salt, $(\text{NEt}_4)_2[\text{Fe}_2\text{OCl}_6]$ (4), as the catalyst and ascorbic acid (AA) or tetramethyl reductic acid (TMRA) (Scheme 4.5) as the reductant was first discovered by Mary Roth in 1987.³⁰



Tetramethyl Reductic Acid (TMRA)



L-Ascorbic Acid (AA)

Scheme 4.5

Upon reacting **4** with a 20-fold excess of AA or TMRA under an inert atmosphere, a purple species formed which can catalyze the air oxidation of alkanes selectively to alcohols with fairly high yield. When cyclohexane was used as the substrate, the ratio of cyclohexanol to cyclohexanone formation was as high as 55 to 1. The highest yield observed is 17%. The high selectivity for alcohol formation, the significant deuterium isotope effect ($k_H/k_D \sim 2.5$) and the fact that the catalytic reaction was not inhibited by the use of a free radical trap distinguishes this system from the typical free radical system such as the Fenton system.³⁰

Extensive study on the selectivities and reactivities of the aforementioned system has been carried out over the last three years. This chapter summarizes the results from those studies. The mechanistic implications of these results are discussed in relation to the other systems, the mechanisms of which were reviewed at the beginning of this chapter.

I. Reactivity and Selectivity Studies of **4**/TMRA or **4**/AA Catalytic Systems for Air Oxidation of Alkanes.

Experimental

Materials. All organic compounds and solvents were purchased from commercial sources unless otherwise specified. Tetramethyl reductic acid (TMRA) was obtained from Polaroid Corporation, Cambridge, MA. Complex 4 was prepared according to the literature procedure³⁰ and recrystallized from a mixture of acetonitrile and tetrahydrofuran at least twice before use. The complex $(\text{BzPh}_3\text{P})_2[\text{Fe}_2\text{OBr}_6]$ (5) was prepared by Professor Michelle Millar according to a literature procedure.³¹

S-(+)- α -Methoxy- α -trifluoromethylphenylacetyl chloride (Mosher's chloride) was prepared according to the following procedure. A 5.0 g portion of R-(+)- Mosher's acid (Aldrich, 21.4 mmol) was transferred into a 25 ml round bottom flask equipped with a stir bar and a reflux condenser. The acid is a solid at room temperature (m.p. 46 ~ 49 °C) so it has to be heated slightly before the transfer. A portion of 5.6 ml of oxalyl chloride (64.2 mmol) was subsequently added. The dropwise addition of 1 ml of pentane containing one drop of dimethylformamide initiated a vigorous reaction. After the addition, the reaction mixture was heated to 70 °C for 4 hours and subsequently cooled down to room temperature. The volatile components of the reaction mixture were removed by vacuum. The product was vacuum-distilled at 35 °C (0.5 mm Hg) as a clear oil. The optical purity of the product was examined by the formation of Mosher's ester with optically pure (S)-(+)-1-phenylethanol. The ¹⁹F NMR spectrum of the ester proved the formation of only one diastereomer.

The treatment of organic compounds and solvents was as follows. All solvents were treated according to literature procedures.³² All saturated hydrocarbons, except cyclohexane and adamantane, were shaken with concentrated sulfuric acid a few times, 5 - 10 ml each time, until the H₂SO₄

layer was colorless. The organic layer was neutralized with Na_2CO_3 aq. solution and washed with water, then dried by MgSO_4 , refluxed with sodium and finally distilled immediately before use. Cyclohexanol was purified by distillation from sodium metal. Adamantane was used without further purification. The TMRA was recrystallized three times from chloroform before use. The purity of L-ascorbic acid (L-AA, Aldrich, 99%) was examined by determining the optical rotation of a 1% aqueous solution of L-AA at 26 °C. The result, +23.8°, was comparable to the literature value of +24°.³³ Thus, L-AA was used without further purification. Oxygen and compressed air were obtained from Airco. The latter was passed through a drying tube filled with CaSO_4 drying agent. For GC analyses, the internal standard (methylbenzoate or anisole) and various authentic samples of the oxidation products were obtained from commercial sources and used as received.

Physical Measurements. All proton NMR spectra were recorded on either a Bruker WM250 or Varian XL 300 spectrometers. ^{19}F NMR spectra were recorded on Varian XL 300 spectrometer with CFCl_3 or CF_3COOH as external standard. The oxidation products were analyzed by using a Hewlett-Packard 5890 gas chromatograph interfaced with a Model 3393A integrator. In all but one experiment, the GC column used for separating various oxidation products was an HP FFAP column (530 μ x 10 m). Only in the case of the oxidation of adamantane was an HP methyl silica column used. For quantitating the products, an internal standard was used. A response ratio, C , of the products to be quantitated versus the internal standard was determined by using authentic samples of known concentration as indicated in eq. 4.2, where $[X]$ and $[\text{Std}]$ are the concentrations of the sample and internal standard, respectively, and X_{int}

and Std_{int} are the integrals on the GC trace for samples and internal standard.

$$\frac{[X]}{[\text{Std}]} = \frac{C \cdot X_{\text{int}}}{\text{Std}_{\text{int}}} \quad (4.2)$$

A phenylglycine Piracle I-A chiral column (Regis) was used to separate the enantiomeric products and determine the enantiomeric excess values by HPLC.

Protocol 1: Standard Procedure for Air Oxidation of Saturated Hydrocarbons with 1 as Catalyst. In a typical experiment, a portion of **4** (15.0 mg, 2.5×10^{-5} mol) was dissolved in 10 ml of solvent. The reductant (TMRA or AA) (5.0×10^{-4} mol) was added. A purple species formed immediately. Methylbenzoate (1.6×10^{-5} mol) was then added as internal GC standard except in the cases of isopentane and adamantane, in which anisole (1.84×10^{-5} mol) was used. Finally, substrate (~180-fold excess based on the catalyst) was added. In the case of oxidation of methane, methane gas was slowly bubbled into the reaction mixture. The foregoing solutions were prepared in the dry box and kept carefully under nitrogen or argon before being open to air. The reaction vessel was then put under a positive pressure of dried air at 30°C in a constant temperature shaker bath. Product was monitored periodically by taking an aliquot from the reaction mixture and injecting it into a GC. The identification of the products on a GC trace was usually done by either the injection of an authentic sample of the corresponding product or by GC-mass spectrometry.

Protocol 2: Determination of the Enantiomeric Excess for the Oxidation Products of Ethylbenzene. The oxidation of ethylbenzene was carried out as described in protocol 1. After 48 hours, the reaction mixture was filtered and the solvent was removed from the filtrate by rotary

evaporation. The residue was extracted with ether and a fair amount of green-yellow solid was discarded. Ether was then removed from the solution and the residue redissolved in a very small amount of methylene chloride (~ 0.5 ml). This solution was passed through a 20 cm silica gel column saturated with hexane. The products, acetophenone and 1-phenylethanol, as well as methylbenzoate, were separated on the column by gradually increasing the polarity of the solvent. The content of each band collected was monitored by GC. The solvent mixture used was either hexane/methylene chloride or a methylene chloride/THF with various ratios of two components. It was found that by using 10% THF in methylene chloride as the solvent, one can obtain a band that contains mainly 1-phenylethanol with a very small portion of acetophenone and methylbenzoate.

The amount of the alcohol formed was determined quantitatively relative to the internal standard (methylbenzoate) before the chromatographic separation. 1-Phenylethanol isolated by chromatography was then converted to either diastereomeric Mosher's ester or to the enantiomeric acetate. To prepare the Mosher's ester of 1-phenylethanol, the alcohol was transferred into an NMR tube containing 0.5 ml of CDCl_3 . The addition of 2 equivalents of Et_3N was followed by the addition of a small crystal of dimethylaminepyridine (DMAP) and 1 equivalent of Mosher's chloride. The NMR tube was then sealed and the reaction allowed to proceed overnight. For the ^{19}F NMR spectroscopic study, the reaction mixture can be used directly for quantitation. The ^{19}F NMR spectrum was determined on the 300 XL spectrometer with CFCl_3 or CF_3COOH as external standard. Authentic samples were prepared by using optically pure S- and R-1-phenylethanol as described above and were employed for chemical shift

assignments. For the ^1H NMR spectroscopic study, the reaction mixture was loaded on a short silica column and flash chromatographed with 20% CH_2Cl_2 in ethylacetate to remove any excess amine. ^1H NMR spectra were recorded on either an XL300 or a Varian 500 NMR spectrometer. In addition, 1-phenylethanol was converted to the acetate ester by standard literature procedures and purified by a short flash silica column.³⁴ The enantiomeric acetate was separated on HPLC by using a Pirkel chiral column. Isopropyl alcohol, 0.5% in hexane, was used as the solvent with a flow rate of 3 ml/min.

Results and Discussion

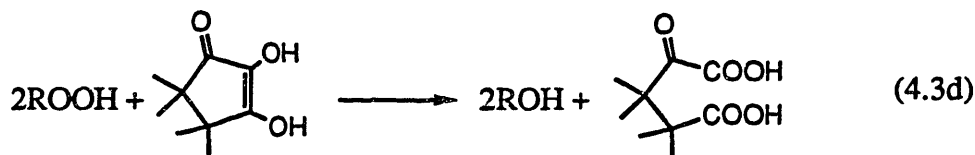
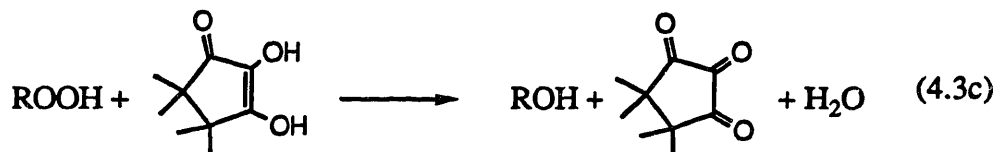
Oxidation of Cyclohexane. It was previously established that, in the presence a proper reductant, **4** can catalyze the air oxidation of cyclohexane selectively to form cyclohexanol and a small amount of cyclohexanone.³⁰ Under optimized reaction conditions, up to 3.5 turnovers of cyclohexanol and about 0.07 turnovers of cyclohexanone were observed in 4 hours. The purple color of the solution which developed when **4** reacted with TMRA slowly faded to brown within eight hours. Repetitive addition of TMRA could regenerate the purple color of the solution, restoring reactivity to that of the original system. Figure 4.1 shows the formation of both cyclohexanol and cyclohexanone as functions of time in an experiment where TMRA was added several times repetitively. It shows that the catalytic system can be regenerated repeatedly, although with partial loss of the activity after each addition of TMRA compared to the previous addition. The second addition reproduced almost quantitatively the yield obtained during the first. The yields in the subsequent additions decreased gradually and the reaction

became very sluggish after 48 hours. The purple color of the solution was also regenerated at each addition of more TMRA, although the intensity of the color decreased with increasing reaction time. Two interesting observations were obtained. One is that the selectivity of the system, i.e. the ratio of cyclohexanol versus cyclohexanone, did not change significantly over the long period of time. The second one is that the regenerated system was still much more active than that formed from the mononuclear iron complexes FeCl_2 or $(\text{NEt}_4)\text{FeCl}_4$.³⁰ This latter results suggests the preservation of some kind of multinuclear iron cluster in solution, even when the purple color is discharged. In other words, it not only indicates that the active species is multinuclear but also that degradation to mononuclear iron species does not occur during the reaction period. This result also suggests a new exciting possibility for a better catalytic system. If the electrons can be provided separately from the reaction mixture through other means, such as by using an electrode, it maybe possible to recycle the catalytically active species completely. This alternative also would avoid the autoxidation of the reductant, which accounts for a large portion of reductant consumption and competes with substrate for the oxidant as well.

Chemo- and Regioselectivities. One of the most interesting aspects of this system is the high selectivity for the formation of cyclohexanol versus cyclohexanone. As much as 55 fold excess of cyclohexanol was formed versus cyclohexanone. The implication of this result is very significant. First of all, it excludes a free radical mechanism as the major mechanism operating in this system. One of the characteristics of free hydroxyl radical attack on hydrocarbons, as seen in a typical Fenton reaction, is the loss of selectivity of alcohol versus ketone formation. The ratio of cyclohexanol to cyclohexanone in the Fenton system, when cyclohexane was used as the

substrate, was 1 to 1.⁴ None of the multinuclear iron catalysts investigated so far (see introduction for detailed discussion) has such a high selectivity for the alcohol formation.

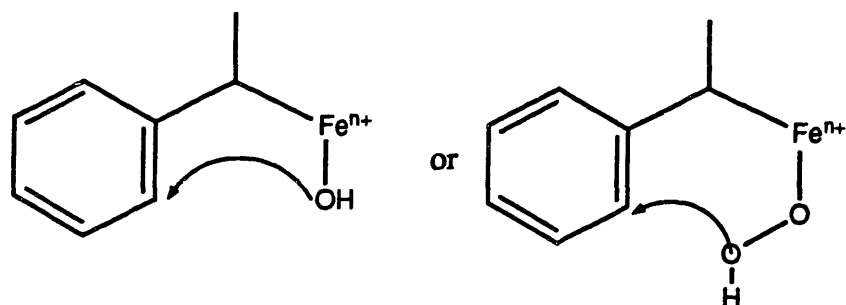
Attempts have been made to extend our understanding toward this remarkable selectivity. One interesting control reaction was to carry out reaction by using cyclohexanol or cyclohexanone as the sole substrate. Neither oxidation of cyclohexanol to cyclohexanone nor reduction of cyclohexanone to cyclohexanol was observed under the typical reaction conditions. Mechanistically, this implies either that formation of cyclohexanol and cyclohexanone occurs via two different pathways which do not cross or they are derived from a common intermediate, as postulated for the *Gif* system (see the last step of path 2 in Scheme 4.4). The possibility of alkyl peroxide formation cannot be excluded in our system. Alkyl hydroperoxide, ROOH, could undergo decomposition either through a homolytic cleavage of the O-O bond to form ketone (eq. 4.3a) or, in the presence of metal ions, heterolytic cleavage to form alcohol (eq. 4.3b).³⁵ The preference for the formation of alcohol observed in our system could also be attributed to the presence of a large excess of TMRA in the solution. It can function as An_2Te reported in *Gif* system (see the introduction section of this chapter for detailed information). Upon reaction with TMRA, the alkyl hydroperoxide would be reduced to form alcohol and water (eq. 4.3c). On the other hand, TMRA, or any other good oxygen acceptor, can also react with peroxide to remove single oxygen atom (eq. 4.3d), so the formation of ketone (eq. 4.3a) will be inhibited.³⁶ Recently, cyclohexyl hydroperoxide was reported as the intermediate in a number of cyclohexane oxidation systems catalyzed by iron complexes using hydrogen peroxide and oxygen as the oxidant.^{29,37}



In another study, both cyclohexanol and cyclohexane were added at the beginning of the reaction, the experimental results of which are shown in Table 4.1. The presence of excess cyclohexanol reduced the reaction rate. Further investigation, especially detailed kinetic studies, must be carried out to understand fully how each of these products formed and why the system favors the formation of alcohol over that of ketone.

The system, 4/TMRA or 4/AA, can also catalyze the oxidation of a variety of other substrates. Table 4.2 lists various saturated hydrocarbons used as substrates and the products formed during the oxidation. In general, aromatic C-H bonds are stable under the oxidation conditions. No oxidation of aromatic C-H bonds was observed for methylbenzoate, anisole, benzene or toluene. The only exception is the oxidation which occurred at the *ortho* position to the ethyl group on the aromatic ring of ethylbenzene. One possible explanation for the formation of this product is that an intermediate involving an iron carbon bond at the benzyl position exists, as shown in Scheme 4.6. This type of intermediate was proposed by Barton and coworkers (Scheme 4.4). This iron center, at the same time, could have

an activated oxygen ligand that might attack the *ortho* position by forming a five- or six-membered ring (Scheme 4.6).



Scheme 4.6

As indicated in Table 4.2, non-strained acyclic alkanes such as isopentane or octane are not good substrates. This unusual specificity cannot be fully explained by the difference in bond energies because the bond dissociation energy of C-H bonds in cyclohexane is not significantly smaller than that of other secondary C-H bonds in acyclic alkanes (Table 4.3). One possible explanation is that the system may be shape selective. If substrate binding site in the active species forms a pocket with a certain shape, then steric effects becomes important. Only those substrates which fit in the pocket nicely, for example, five- or six-membered rings, can access the activated oxygen sufficiently to form products. Examples of such shape selective catalysts are common in iron porphyrin systems.³⁸ The only non-strained C-H bond oxidation occurs at the benzyl position, in which the C-H bond is highly activated by the phenyl ring. Much more ketone was formed at this position (Table 4.2), also consistent with the high reactivity at this particular position.

This system has also demonstrated interesting regioselectivities. To determine the selectivity of the catalyst toward the oxidation of primary,

secondary and tertiary saturated C-H bonds, methylcyclohexane was chosen as a substrate. Table 4.4 gives the product distribution for the oxidation of methylcyclohexane. Under the same reaction conditions, the rate of oxidation of methylcyclohexane is much slower than that of cyclohexane (Table 4.2). Very small amounts of ketone (<0.02 turnovers in 8h.) are formed. No oxidation occurs at the primary position. The ratio of secondary versus tertiary oxidation is 1:2.2 after statistical correction for the number of C-H bonds at each position. This result again indicates a non-radical reaction mechanism, because in a typical reaction, the rate of attack at the tertiary positions by a free hydroxyl radical is 175-fold faster than at secondary sites.³⁹

The tertiary versus secondary oxidation ratio is one of the characteristics which distinguishes this system from other iron oxidation catalyst. Table 4.5. shows the ratio of tertiary versus secondary oxidation in various enzyme and model systems. The Fenton system, iron porphyrins and many other iron-based oxidation catalysts have generally shown great preference for the tertiary oxidation compared to the secondary oxidation. MMO, on the other hand, only demonstrates moderate selectivity ($2^\circ/3^\circ = 2.0$) for tertiary/secondary oxidation. The 4/TMRA system, therefore, acts very similarly to MMO. The only other case where a similar selectivity was observed is the *Gif* system.^{21,27} The amount of tertiary product reported, however, includes a large amount of coupling product formed between the substrate (adamantane) and the solvent (pyridine). It is also interesting to notice the preference for the formation of 3-methyl, and 4-methyl-cyclohexanol over 2-methyl-cyclohexanol. It indicates that steric effects do play an important role in the catalytic reaction. The "*ortho*" position on the

methylcyclohexane ring is presumably less active due to the greater steric hindrance at this position.

Enantioselectivity and its Mechanistic Implications. One of the intriguing aspects of catalytic systems for the oxidation of hydrocarbons is the possibility of enantioselectivity. Ethylbenzene was chosen as the prochiral substrate for the study of enantioselectivity not only because it was known to be a good substrate in our system but also because extensive studies on this substrate in cytochrome P-450 and iron porphyrin systems would allow for valuable comparisons.^{40,41}

The major task involved in this work was to separate the enantiomeric 1-phenylethanols from the reaction mixture and to convert them into diastereomers for NMR quantitation, or into acetates for HPLC quantitation. The formation of both Mosher's esters and acetates can be readily achieved by following the procedures described in the experimental section. The major problem encountered was separation of either the alcohols from the oxidation reaction mixture or the esters from the esterification reaction mixture. The alcohols were separated from the reaction mixture by column chromatography. ¹⁹F NMR spectroscopy was used exclusively for the quantitation of Mosher's esters due to the cleanness of its spectrum and the high sensitivity of ¹⁹F nuclei. Table 4.6 lists the chemical shifts of the various compounds present in the system, using CFC1₃ and CF₃COOH as the external standard, respectively. It was discovered, however, that the residual ascorbic acid in the reaction mixture could not be separated from alcohols on a silica column. Its presence caused a nasty problem because AA also forms its Mosher's ester in the subsequent step and this ester has the same chemical shift as the Mosher's ester of R-1-phenylethanol (Table 4.6)!

¹H NMR spectroscopy was used to quantitate the relative amounts of both enantiomers. The existence of a large amount of amine, necessary for the formation of Mosher's ester, interfered with the accurate integration of the two well resolved ethyl resonances from the esters. A flash silica column was used to remove the amine and other unwanted components after esterification. The results were quite satisfactory. Another problem, however, surfaced at this stage. It was found that the esters of both enantiomeric alcohols did not migrate on the silica column at the same rate. The ester of one of the enantiomers tails more on the column. Therefore, caution had to be taken to elute all of the esters from the column and to collect them carefully to ensure the reliability of the results.

To circumvent the aforementioned problem with the flash column after the formation of diastereomeric esters, a slightly modified procedure was later developed. The alcohols were converted into enantiomeric acetate esters and the esters were then separated on a HPLC chiral column. In this procedure, the "tailing" is avoided because the acetate esters are still enantiomers so their interaction with the column should be the same.

A small enantiomeric excess was observed in all experiments ($5\pm 1\%$), a result that is very similar to what was observed in cytochrome P-450 systems.⁴⁰ An alkane oxidation system displays enantioselectivity when both substrate and activated oxygenation reagent are properly oriented in the transition state so that C-H bond fission and C-O bond formation can occur on the same face of the molecule.⁴⁰ Depending on the size and the shape of the substrate-binding pocket formed in the transition state, small molecules like ethylbenzene might overcome the steric restriction and rotate freely, gaining equal excess to the oxygenation reagent on both faces of the C-H bond, resulting in the formation of a racemic mixture of products.

This hypothesis could be tested by using a substrate having bulkier substituents around the potential chiral center to prevent such free rotation. On the other hand, if the oxygen transfer proceeds by a caged radical recombination mechanism as in the case of cytochrome P-450 (see Scheme 4.3), then the enantiomeric excess will depend on the relative rate of radical recombination and the internal rotation of the alkyl radical formed. At least two things can happen to a caged radical before it diffusively escapes the initial cage. One is recombination with the other radicals available in the cage. The other is internal rotation in the cage which allows subsequent reaction to occur on both faces of the molecule. If recombination of the hydroxyl and alkyl radicals does not occur before rotation of the radical, a small enantiomeric excess of the product could occur. This possibility cannot be excluded for the 4/TMRA system.

Factors which Affect the Reaction Rate and Product Distribution.

Solvent Effects. The dependences of this catalytic system, both its reaction rate and product distribution, on solvent were noticed previously by M. Roth³⁰ who mainly attributed them to the different solubilities of reactants in different solvents. Further investigation revealed that solubility is not the ultimate cause of solvent dependence. In particular, the oxidation reaction went much slower in methylene chloride, benzene and methylbenzoate than in acetone or acetonitrile. Similar reactivities were observed for the reactions carried out in benzene and methylbenzoate, with 0.25 and 0.33 turnovers, respectively, of cyclohexanol formed in 5 hours.

Figure 4.2 shows the profile of cyclohexanol formation in the air oxidation of cyclohexane in methylene chloride. Despite the fact that the purple species formed between 4 and TMRA is as soluble in methylene chloride as it is in acetone, the reaction in methylene chloride is much

slower than in acetone. The interesting feature of the reaction in methylene chloride is that product continues to form for as long as 55 hours with a reasonably steady rate. By contrast, in acetone or acetonitrile, TMRA was almost completely consumed after 8 hours, largely by the autoxidation reaction, thus halting the oxidation of the substrate. This observation suggests that in methylene chloride, not only is the rate of the substrate oxidation diminished, but the rate of autoxidation is also decreased. Similar observations were made for the reactions in benzene or methylbenzoate, where the purple color of the solution lasted much longer than what observed in acetone or acetonitrile. Generally speaking, oxidation reactions tend to go faster in polar solvents. This observation implies the existence of a charged transition state, the kinetic barrier of which could be reduced by better charge separation in a polar solvent. The solvent effect, thus, could be attributed to a combination of at least two factors, the polarity of the solvent and the solubility of the reactant in the solvent.

Concentration Effects. Previous study shows that a large excess of substrate is needed for optimize the yield.³⁰ Usually the reaction was started with 5 ml of substrate, an approximately 2800 fold excess over the catalyst. A preliminary study indicated that the reaction rate was affected by varying the concentration of the substrate. Figure 4.3 demonstrates the effect of substrate concentration on the reaction rate and the total yield of cyclohexanol in a 4/AA system. The rate of the oxidation reaction and the total yield of the products both decrease as the concentration of the substrate decreases. One plausible explanation for this observation is that a large excess of the substrate is needed so that it can compete more efficiently with the autoxidation of the reductant.

The preliminary data in Table 4.7 provide some information about the effect of varying the concentration of **4** and/or reductant on the rate of the oxidation reaction. When the concentration of **4** was reduced to half, while the catalyst/reductant ratio kept the same, a decrease on the amount of products formed was observed. If the reductant concentration remains the same, the change of the concentration of **4** seems have little effect on the amount of products formed. In either case, the yield remains constant. These results suggests that the reductant might be the limiting reagent. More kinetic studies, however, are necessary to reach any quantitative conclusion about the concentration dependence of the reaction rate in this system.

Halogen Incorporation. Figure 4.4 displays the formation of various cyclohexyl halides in the catalytic system. Incorporation of various halides into the substrate competes with the oxidation of the substrate, presumably because of the formation of an alkyl radical intermediate. Bromide is much faster than chloride incorporation, which is indicative of the radical nature of this reaction because bromine radical is much more stable than chloride radical. The formation of cyclohexanol, on the other hand, is much slower with **5** as the catalyst. Only about 2 equivalents of cyclohexanol were formed over 5 hours compared to 3.5 in **4**/TMRA system. It seems that the more incorporation of halogen into the substrate occurred, the less the oxidation products were formed. It is conceivable that some radicals formed in the cage, as in the case of cytochrome P-450 (Scheme 4.3), reacts with the halogen ion to generate the halogen radical and then recombined with the alkyl radical in site. The reason that iodine incorporation is much slower could be due to the lower effective concentration of I^- due to the limited solubility of KI used. Another reason is that the I^- is not bound to the iron

starting material. The majority of I⁻ is in the bulk of the solution. Iodine radical can only be generated by diffusively exchanging into the cage and reacting with radicals in the cage.

II. Studies of Other Catalytic Systems

Experimental

Materials. The purification of TMRA and AA was described in the part I of this chapter. The alternative reductant, zinc amalgam was prepared in the following manner. After washing with 10% aqueous HCl solution and then water, 4 g of granular zinc was stirred with 1% HgCl₂ solution for about 5 minutes. The supernatant was decanted and the resulting amalgam was washed with water, dried in a vacuum oven at 110 °C for 2 hours, and stored under N₂. Methyl viologen dichloride (MVCl₂), a mediator used for facilitating electron transfer, was used without further purification.

The iron complex (BzPh₃P)₃{[Fe(C₆H₄O₂)₂]₂(OAc)] (6), where C₆H₄O₂²⁻ is catecholate, and basic iron acetate [Fe₃O(OAc)₆(H₂O)₃](OAc) (7) were synthesized according to literature procedures.^{42,43} The preparation of [Fe₂O(OAc)₂{CpCo[OP(OEt)₂]₃}]₂ (8) was described elsewhere.⁴⁴ The tetrametalated peroxide complex, [Fe₆(O)₂(O₂)₂(O₂CPh)₁₂(H₂O)₂] (9) was provided by Dr. Wolfgang Micklicz.⁴⁵

Protocol 1: Oxidation of Cyclohexane by Using the Non-coordinating Reductant Zinc. Under an inert atmosphere, a portion of the iron catalyst (1.0-2.5 x10⁻⁵ mol) was dissolved in 10 ml of acetonitrile. 20 equivalents of either zinc powder or zinc amalgam was added, together with 10 equivalents of the mediator methyl viologen. After the addition of

substrate (5 ml) and internal standard, the reaction vessel was opened to air. The formation of products was checked periodically by GC.

Protocol 2: Oxidation of Cyclohexane by Using t-BuOOH as Oxidant and 4 as Catalyst. An acetonitrile solution of 4/cyclohexane (2.5×10^{-5} mol/ 5.0×10^{-3} mol) was prepared in the same way as described in protocol 1. Under Ar, a portion of 2 ml t-BuOOH/CH₂Cl₂ solution (6.8 mmol, t-BuOOH/catalyst ratio: 272/1) was added. In one run, the standard (1.6×10^{-5} mol methylbenzoate) was added immediately following the addition of t-BuOOH and in another run, the standard was added before injection into the GC. The same results were obtained for both cases, indicating that no interaction occurred between the standard and t-BuOOH. Addition of second or third portion of the standard was necessary for the quantitation of the large amount of the products produced with time. The products were quantitated by GC.

Results and Discussion.

To help understand the role of the reductate ligand AA or TMRA, the non-coordinating reducing agent zinc, both in the form of powder or zinc amalgam, was employed. Methyl viologen (MVCl₂) was used as an electron transfer mediator. With 4 as catalyst and cyclohexane as substrate, no oxidation products were detected. There are two possible reasons for the failure of zinc to function as a reductant in this system. One is that zinc does not have the appropriate redox potential (-0.7618 V vs. NHE) to reduce iron(III) center in the active species. The other is that the formation of the active species in the catalytic cycle requires the proper coordination environment provided by reductic acid ligand, which cannot be supplied by

zinc. As discussed before, TMRA and AA are not acting simply as a reducing agent in the system. They are also excellent ligands which bind the iron atoms to form the catalytically active species or their precursor(s).

Table 4.8 lists various iron complexes, ranging from mononuclear to hexanuclear, tested for the ability to catalyze air oxidation of saturated hydrocarbons. Two multinuclear iron complexes, 6 and 7, showed interesting reactivities. The total yields of the oxidation products in both systems, however, were much lower than that of 4/TMRA system. The selectivity for the alcohol formation was very poor. The formation of a purple-colored species was observed in the case of basic iron acetate as the catalyst. The limited catalytic capabilities of these compounds may be due to the fact that TMRA or AA is not coordinated to the iron. The iron atoms in most of the complexes tested were chelated by nitrogen donor ligands or by carboxylates, both of which seem to be better ligands for iron than TMRA or AA. Perhaps more importantly, the iron centers in all multinuclear complexes studied were coordinately saturated, making it more difficult to form TMRA or AA-iron complexes.

When *t*-BuOOH was used as an oxygen source to replace molecular oxygen, much more efficient oxygen transfer to substrate was observed. After 24 hours, 51 equivalents of cyclohexanol and 53 of cyclohexanone per mole of 4 were produced. A control reaction was carried out by using the mononuclear iron salt $\text{NEt}_4[\text{FeCl}_4]$. In the latter case, only 24 equivalents of cyclohexanol and 25 of cyclohexanone were observed. The formation of almost equal amounts of alcohol and ketone could be indicative of a free radical reaction, as observed in the Fenton chemistry.⁴ It also could be due to the formation and subsequent decomposition of cyclohexyl hydroperoxide.

As discussed before, the absence of TMRA or other good oxygen acceptor such as Ph_3P could result in the formation of larger amount of ketone.

Conclusions

Detailed studies of the selectivities of the 4/TMRA and 4/AA systems, as well as factors that affect the catalytic capabilities of both systems, have been carried out. Both systems can catalyze the air oxidation of cyclic alkanes and benzyl C-H bonds, whereas non-strained alkanes and aromatic C-H bonds are generally unreactive under the reaction conditions. The catalytic reaction proceeds at different rates in different solvents, proceeding faster in polar solvents. The fact that the reaction is favored in polar solvents seems to suggest the existence of some kind of charged transition state which is stabilized by better charge separation under the reaction conditions. The catalytically active species is gradually consumed during the course of the reaction and can be regenerated by addition of extra reductant. The high selectivity for alcohol formation in the hydroxylation of alkanes, and the low ratio of tertiary versus secondary oxidation, are indicative of a non-free radical mechanism. While the exact nature of the catalytically active species in the system remains ambiguous, it is plausible to propose the multinuclear iron complexes with reductant as the ligand. This hypothesis is supported by the fact that non-coordinating reductants, such as zinc, do not act as proper electron source for this system. The possibility that a substrate-based peroxide is an intermediate could not be ruled out. The caged radical mechanism for the oxygen transfer step is supported by the observation of the small enantioselectivity and the incorporation of halogens into the substrate. The lack of the

interconversion between cyclohexanol and cyclohexanone under the reaction conditions may suggest the existence of separate synthetic pathways for their formation, although the existence of excess cyclohexanol does decrease the overall reaction rate. Detailed kinetic studies are necessary to provide more mechanistic insight of this unique catalytic system.

References

- (1) Hayaishi, O. In *Biological Oxidations*; T. P. Singer, Ed.; Interscience: New York, 1968; pp 581.
- (2) Udenfriend, S.; Clark, C. T.; Axelrod, J.; Brodie, B. B. *J. Biol. Chem.* **1954**, *208*, 731-739.
- (3) Brodie, B. B.; Axelrod, J.; Shore, P. A.; Udenfriend, S. *J. Biol. Chem.* **1954**, *208*, 741-750.
- (4) Hamilton, G. A.; Workman, R. J.; Woo, L. *J. Am. Chem. Soc.* **1964**, *86*, 3390-3391.
- (5) Fenton, H. J. H. *J. Chem. Soc.* **1894**, *65*, 899.
- (6) Walling, C. *Accoun. Chem. Res.* **1975**, *8*, 125-131.
- (7) Hamilton, G. A. In *Molecular Mechanism of Oxygen Activation*; O. Hayaishi, Ed.; Academic: New York, 1974; pp 405-451.
- (8) Ullrich, V. Z. *Naturforschg.* **1969**, *24b*, 699-704.
- (9) Mimoun, H.; Roch, I. S. d. *Tetrahedron* **1975**, *31*, 777-784.
- (10) Davis, R.; Durrant, J. L. A.; Khan, M. A. *Polyhedron* **1988**, *7*, 425-438.
- (11) Mansuy, D.; Battioni, P. In *Activation and Functionalization of Alkanes*; C. L. Hill, Ed.; Wiley: New York, 1989; pp 195-218.
- (12) Tabushi, I.; Koga, N. *J. Am. Chem. Soc.* **1979**, *101*, 6456.
- (13) Tabushi, I.; Yazaki, A. *J. Am. chem. Soc.* **1981**, *103*, 7371.
- (14) Mansuy, D.; Fontecave, M.; Bartoli, J. F. *J. CHem. Soc., Chem. Commun.* **1983**, *26*, 253.
- (15) Battioni, P.; Bartoli, J. F.; Leduc, P.; Fontecave, M.; Mansuy, D. *J. Chem. Soc., Chem. Commun.* **1987**, 791.

- (16) Karasevich, E. I.; Khenkin, A. M.; Shilov, A. E. *J. Chem. Soc., Chem. Commun.* **1987**, 731.
- (17) McMurry, T. J.; Groves, J. T. In *Cytochrome P-450: Structure, Mechanism, and Biochemistry*; P. R. Ortiz de Montellano, Ed.; Plenum: New York, 1986; pp 1.
- (18) au Point, M. *Bull. Soc. Chem. Fr.* **1986**, *4*, 578-594.
- (19) Kitajima, N.; Fukui, H.; Moro-oka, Y. *J. Chem. Soc. Chem. Commun.* **1988**, 485-486.
- (20) Vincent, J. B.; Huffman, J. C.; Christou, G.; Li, Q.; Nanny, M. A.; Hendrickson, D. N.; Fong, R. H.; Fish, R. H. *J. Am. Chem. Soc.* **1988**, *110*, 6898-6900.
- (21) Barton, D. H. R. *Aldrichimica Acta* **1990**, *23*, 3-10.
- (22) Barton, D. H. R.; Gastiger, M. J.; Motherwell, W. B. *J. Chem. Soc., Chem. Commun.* **1983**, 41-43.
- (23) Barton, D. H. R.; Gastiger, M. J.; Motherwell, W. B. *J. Chem. Soc., Chem. Commun.* **1983**, 731-733.
- (24) Balavoine, G.; Barton, D. H. R.; Boivin, J.; Gref, A.; Coupanec, P. L.; Ozbalik, N.; Pestana, J. A. X.; Riviere, H. *Tetrahedron* **1988**, *44*, 1091-1105.
- (25) Barton, D. H. R.; Halley, F.; Ozbalik, N.; Young, E.; Balavoine, G.; Gref, A. *New J. Chem.* **1989**, *13*, 177-182.
- (26) Shilov, A. E.; Shul'pin, G. B. *Russ. Chem. Rev.* **1987**, *56*, 442-464.
- (27) Barton, D. F. R.; Csuhai, E.; Doller, D.; Ozbalik, N.; Balavoine, G. *Proc. Natl. Acad. Sci., USA* **1990**, *87*, 3401-3404.
- (28) Barton, D. H. R.; Csuhai, E.; Ozbalik, N. *Tetrahedron Lett.* **1990**, *131*, 2817-2820.
- (29) Barton, D. H. R.; Csuhai, E.; Doller, D.; Balavoine, G. *J. Chem. Soc., Chem. Commun.* **1991**, 1787.

- (30) Roth, M. E. Thesis, Mass. Institute of Technology, 1988.
- (31) Petridis, D.; Terzis, A. *Inorg. Chim. Acta* 1986, 118, 129-134.
- (32) Perrin, D. D.; Armbrages, W. L. F.; Perrin, D. R. *Purification of Laboratory Chemicals*; 2nd ed.; Pergamon: Oxford, 1980.
- (33) *Dictionary of Organic Compounds*; 5th ed.; Chapman and Hall: New York, 1982.
- (34) Kasai, M.; Frousson, C.; Ziffer, H. J. *Organ. Chem.* 1983, 48, 459.
- (35) *Organic Peroxides*; Swern, D., Ed.; Interscience: New York, 1971.
- (36) Tolman, C. A.; Druliner, J. D.; Nappa, M. J.; Herron, N. In *Activation and Functionalization of Alkanes*; C. L. Hill, Ed.; Wiley: New York, 1989; pp 303.
- (37) Fish, R. H.; Konings, M. S.; Oberhausen, K. J.; Fong, R. H.; Yu, W. M.; Christou, G.; Vincent, J. B.; Coggin, D. K.; Buchanan, R. M. *Inorg. Chem.* 1991, 30, 3002-3006.
- (38) Suslick, K. S. In *Activation and Functionalization of Alkanes*; C. L. Hill, Ed.; Wiley: New York, 1989; pp 219-241.
- (39) Russel, G. A. In *Free Radicals*; J. K. Kochi, Ed.; Wiley: New York, 1973; Vol. I; pp 275.
- (40) White, R. E.; Miller, J. P.; Favreau, L. V.; Behattacharyya, A. *J. Am. Chem. Soc.* 1986, 108, 6024.
- (41) Groves, J. T.; Viski, P. *J. Am. Chem. Soc.* 1989, 111, 8537.
- (42) Anderson, B. F.; Webb, J.; Buckingham, D. A.; Robertson, G. B. *J. Inorg. Biochem.* 1982, 16, 21-32.
- (43) Weinland, R. F.; Gussman, E. Z. *An. Chem.* 1910, 66, 157.
- (44) Feng, X. Thesis, Massachusetts Institute of Technology, 1991.
- (45) Micklitz, W.; Bott, S. G.; Bentsen, J. G.; Lippard, S. J. *J. Am. Chem. Soc.* 1989, 111, 372.

- (46) Shilov, A. E. *Activation of Saturated Hydrocarbons by Transition Metal Complexes*; D. Reidel: Dordrecht, 1984.
- (47) Dalton, H.; Leak, D. J. *Mechanistic Studies on the Mode of Action of Methane Monooxygenase*; D. Reidel Publishing Co.: London, 1985, pp 169-186.
- (48) Green, J.; Dalton, H. *Journal of Biological Chemistry* 1989, 264, 17698-17703.

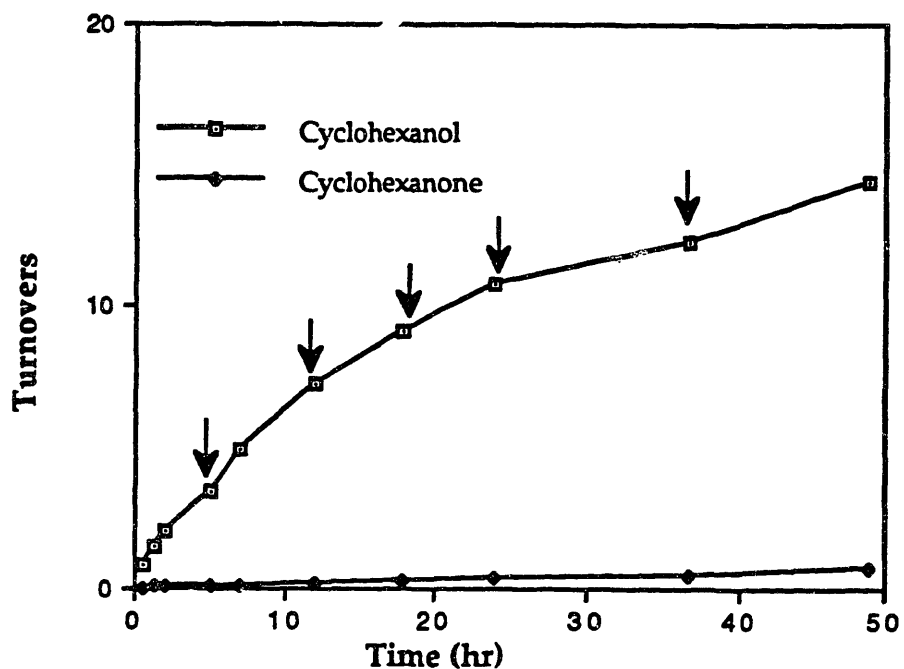


Figure 4.1. Product formation in the air oxidation of cyclohexane catalyzed by the 4/TMRA system. The reaction was carried out in acetone at 30 C with 2.5×10^{-5} mol of 4. Arrows indicate the points at which more TMRA (5.0×10^{-5} mol each time) was added.

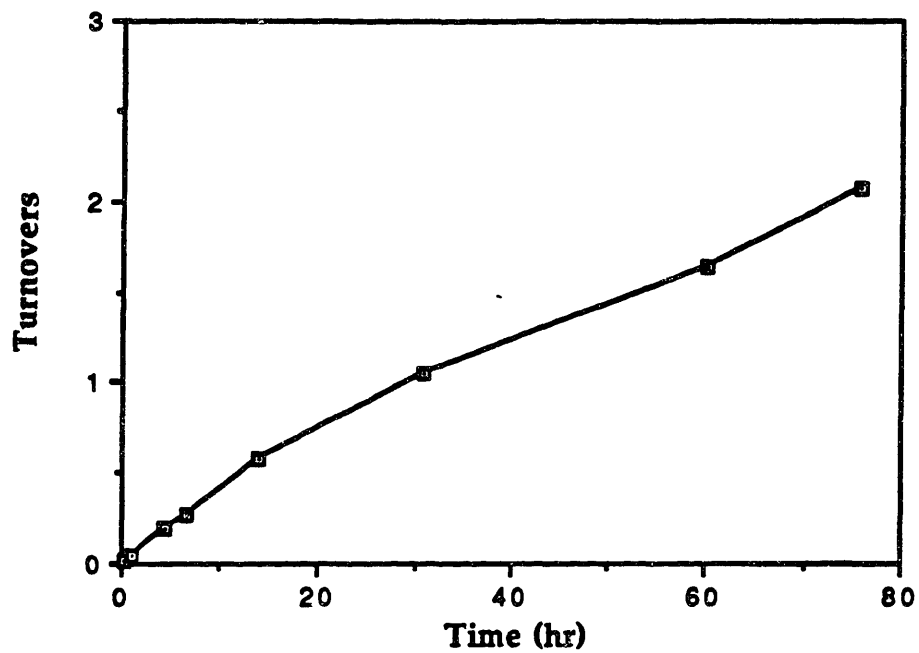


Figure 4.2. Formation of cyclohexanol as the function of time in the air oxidation of cyclohexane in methylene chloride at 30 °C.

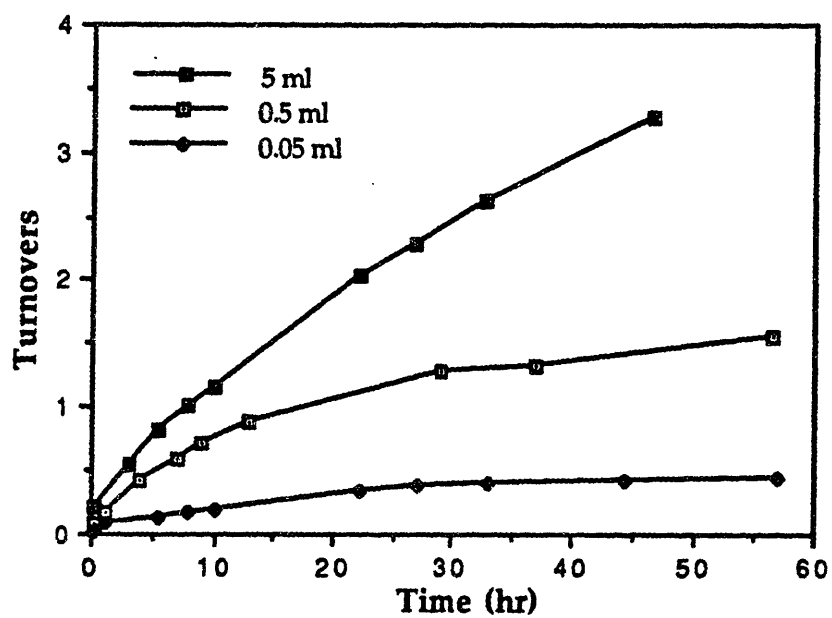


Figure 4.3. Substrate concentration effect on the reaction rate of the air oxidation of cyclohexane catalyzed by 4/AA system at 30 °C. Figure legends show the amount of substrate (ml) added at the beginning of the reaction.

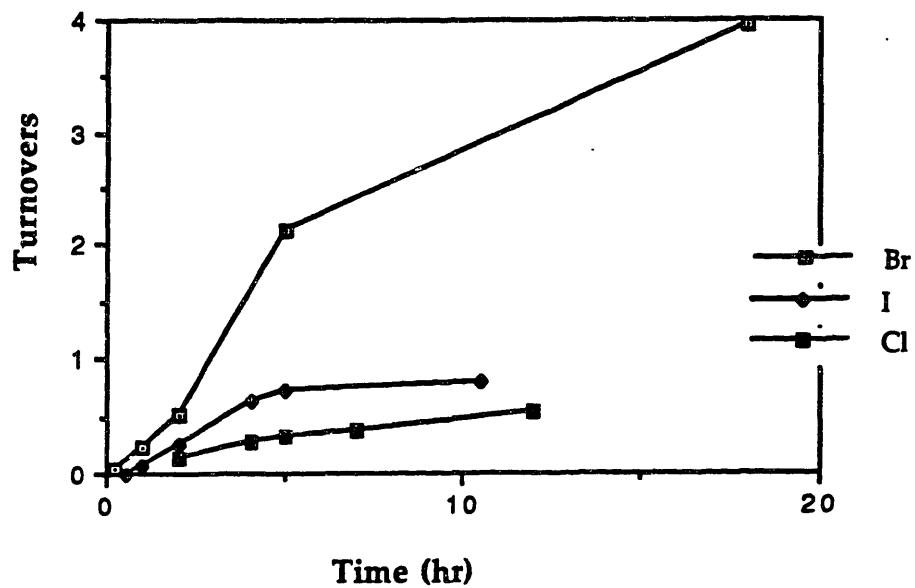


Figure 4.4. Comparison of the reaction rates for the halogen incorporation in the catalytic air oxidation of cyclohexane at 30 °C. The catalyst used is (a) 4; (b) 5; and (c) 4 and KI.

Table 4.1. The Effect of Excess Cyclohexanol on the Formation of Cyclohexanol in the Air Oxidation of Cyclohexane Catalyzed by 4.

| Experiment ^a | Reductant | C ₆ H ₁₁ OH _{added} (ml/r) ^b | Time (hr) ^c | Turnovers |
|-------------------------|-----------|---|------------------------|-----------|
| 2Al | AA | 0.01/39 | 55 | 1.86 |
| 11AC | AA | 0.0 | 55 | 4.33 |
| 1Tl | TMRA | 0.001/390 | 11 | 2.73 |
| 6T | TMRA | 0.0 | 11 | 5.58 |

^aAll reactions were carried out in acetone at 30 °C. ^br is the molar ratio of cyclohexane to cyclohexanol added. ^cReaction time at which the turnover numbers listed were obtained. The turnover numbers reported here are the number of moles of product per mole of 4.

Table 4.2. Substrates and Oxidation Products in the 4/TMRA/O₂ Catalytic Hydroxylation System^a

| Substrate | Time (hr) ^b | Turnover | Yield(%) | Product (% total yield) |
|----------------|------------------------|----------|----------|--|
| cyclohexane | 5 | 4.3 | 21.5 | cyclohexanol (98) cyclohexanone (2) |
| Me-cyclohexane | 4 | 1.5 | 8.0 | 1-Me-cyclohexanol (19) 2-Me-cyclohexanol (8) 3-Me-cyclohexanol and 4-Me-cyclohexanol (72) |
| ethylbenzene | 4 | 3.2 | 15.9 | 1-phenylethanol (71) 2-phenylethanol (trace) acetophenone (29) |
| octane | 22 | trace | | |
| isopentane | 20 | 0.59 | 3.0 | 2-Me-2-butanol (50) 2-Me-1-butanol (41) 3-Me-2-butanol (8) 3-Me-2-butanone (trace) |

^aAll reactions were carried out in acetone at 30 °C. ^bReaction time at which the turnover numbers and yields listed were obtained. The turnover numbers reported here are the number of moles of product per mole of 4 and the yields are the number of moles of product per mole of TMRA.

Table 4.3. Typical Bond Dissociation Energies.^a

| Bond | D (kcal/mol) |
|--|--------------|
| <i>cyclo</i> -C ₆ H ₁₁ -H | 94 |
| C ₂ H ₅ -H | 98 |
| <i>sec</i> -C ₄ H ₉ -H | 95 |
| <i>tert</i> -C ₄ H ₉ -H | 91 |
| C ₆ H ₅ CH ₂ -H | 85 |
| C ₆ H ₅ -H | 104 |

^aTaken from Kerr, J. A., *Chem. Rev.* 1966, 66, 465.

Table 4.4. Product Distribution for the Air Oxidation of Methylcyclohexane Catalyzed by 4/TMRA System.

| Exp. | Product (Turnovers) ^a | | |
|------------------|----------------------------------|-------------------|--|
| | 1-Me-cyclohexanol | 2-Me-cyclohexanol | 3-Me-cyclohexanol 4-Me-cyclohexanol |
| <u>t = 4 hrs</u> | | | |
| 12T | 0.32 | 0.13 | 1.22 |
| 13T | 0.27 | 0.15 | 1.08 |
| 14T | 0.22 | 0.15 | 0.92 |
| 65T | 0.36 | 0.18 | 1.40 |
| 66T | 0.24 | 0.11 | 0.93 |
| <u>t = 8 hrs</u> | | | |
| 12T | 0.42 | 0.22 | 1.71 |
| 13T | 0.41 | 0.28 | 1.58 |

^a The numbers reported here are the number of moles of product formed per mole of 4.

Table 4.5. Regioselectivity of Catalytic Systems for Air Oxidation of Alkanes

| System | Substrate | Product Distribution | | | ref |
|---|----------------|----------------------|-----------|-----------|-----------|
| | | <u>1°</u> | <u>2°</u> | <u>3°</u> | |
| 4+TMRA+O ₂ | Me-cyclohexane | | 1 | 2.1 | This work |
| FeCl ₂ +PhNHNHPh+O ₂ | Me-cyclohexane | 1 | 5.0 | 25.0 | 9 |
| FeCl ₂ +O ₂ | isopentane | 1 | 4.1 | 13.0 | 46 |
| [Fe ₂ O(OAc) ₂ (HBpz ₃) ₂]+O ₂ | adamantane | | 1 | 5.0 | 19 |
| Fe+O ₂ +AcOH+py (Gif) | adamantane | | 1 | 3 | 21 |
| MMO | adamentane | | 11 | 3 | 47,48 |
| | isopentane | 1 | 2.7 | | |

Table 4.6. ^{19}F Chemical Shifts of Various Compounds in CDCl_3 .

| Compound | δ vs. CFCl_3 (ppm) | δ vs. CF_3COOH (ppm) |
|----------------------------------|------------------------------------|---|
| (S)-ester of (S)-1-phenylethanol | -71.98 | 4.15 |
| (S)-ester of (R)-1-phenylethanol | -72.18 | 3.95 |
| (S)-ester of 2-phenylethanol | -72.08 | |
| (S)-ester of L-ascorbic acid | | 3.96 |
| Mosher's acid | -70.50 | 5.64 |
| Mosher's chloride | -71.50 | 5.08 |

Table 4.7. Concentration Dependence of the Reaction Rate on 4 and Reductant in Catalytic Air Oxidation of Cyclohexane.^a

| [4] (M) | [Red] (M) | Reductant | Time (hr) | Product(mol) | Turnover | Yield(%) |
|----------------------|----------------------|-----------|-----------|----------------------|----------|----------|
| 2.5×10^{-3} | 5.0×10^{-2} | AA | 26 | 5.7×10^{-5} | 2.93 | 11 |
| 1.0×10^{-3} | 2.0×10^{-2} | AA | 25 | 2.5×10^{-5} | 2.45 | 12 |
| 2.5×10^{-3} | 5.0×10^{-2} | TMRA | 4 | 6.5×10^{-5} | 2.60 | 13 |
| 5.0×10^{-5} | 5.0×10^{-5} | TMRA | 4 | 7.2×10^{-5} | 1.43 | 14 |

^aNumbers listed are for cyclohexanol formation. All reactions were carried out in acetone at 30 °C.

Table 4.8. Iron Complexes as Catalysts for Air Oxidation of Alkanes.^a

| Complex | Reductant | Time (hr) | Solvent | Product (turnovers) | |
|---------|-------------------------------|-----------|--------------|---------------------|--------------|
| | | | | cyclohexanol | cydohexanone |
| 6 | AA | 23 | acetone | 1.7 | 0.1 |
| 7 | TMRA | 3 | acetone | 1.7 | 0.5 |
| 8 | Zn/MVCl ₂ | 10 | acetonitrile | 0.8 | - |
| 9 | Zn/MVCl ₂ /AcOH | 7 | acetone | 1.1 | 0.4 |

^aAll reactions were carried out at 30 °C using cyclohexane as the substrate.

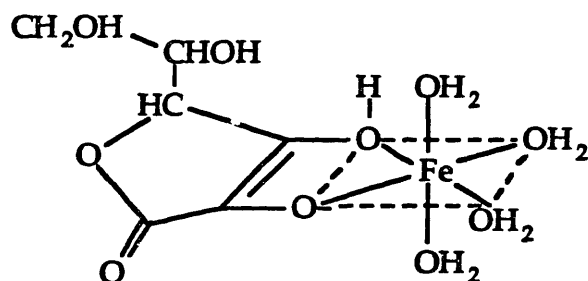
Chapter 5

Structural and Physical Characterization of A Precursor of the Active Species and Other Complexes Involved in the Catalytic System

Introduction

Ascorbic acid (AA, Scheme 4.5) is widely distributed in both the plant and animal kingdoms. It is commonly used pharmaceutically to counteract scurvy and in the food industry functions as an anti-oxidant.¹⁻⁴ Its ability to coordinate metals as a ligand, however, is not as well recognized as its role as a biological reductant. Only a few scattered reports are available in the literature on the formation of AA complexes with metals.⁵ A review of the history of ascorbic acid, however, reveals that many important biological functions of AA are closely related to the availability of metal ions, such as iron and copper, in the system.⁶⁻¹³ Its relationship with iron, for example, can be traced back to half a century ago when ascorbic acid was found to assist the iron uptake in human body.⁹ Further investigation led to the proposal that the antiscorbutic property of ascorbate is related to the formation and dissociation of some kind of iron ascorbate complexes.¹⁴ More detailed studies were carried out to examine the effect of ascorbic acid on the bioavailability of iron in food in the early 1950's,^{4,15} and the isolation of a purple complex between ascorbic acid and iron was first reported in 1968.¹⁶

Detailed kinetic studies by Taqui Khan and coworkers on the mechanism of autoxidation of AA catalyzed by iron and iron complexes led to a proposed structure for the iron AA complex (Scheme 5.1).^{17,18} Efforts have been made to characterize the complex formed between AA



Scheme 5.1

and iron. The first spectroscopic evidence appeared in 1967. Ferrous ion forms a complex with AA which has absorption maxima at 500 and 380 nm in aqueous solution at pH = 9.¹⁹ A more detailed study later described a transient species formed in the reaction of ferric ion with AA ($\text{Fe}^{3+}:\text{AA} = 1:2$) which has an absorption maxima at 560 nm.²⁰ A "polynuclear mixed-valent compound" was proposed as the species formed between iron and AA based on UV-Vis and redox potential measurements.²¹ In a study by Martinez et al, the blue complex formed between FeCl_3 and AA in aqueous solution was isolated by ethanol precipitation.²² The complex has an optical band at 560 nm as reported by previously. The result from Mössbauer spectroscopy, however, revealed a single high spin iron(III) site in the complex. Elemental analysis provided additional evidence for a mononuclear bis complex. The results are somewhat ambiguous because the reaction may not have been carried out anaerobically, and the Mössbauer spectrum of the complex at $-78\text{ }^\circ\text{C}$ contains an additional peak at $\delta \sim 2.7\text{ mm s}^{-1}$ which was not explained. Recently, Wilson and coworkers reported use of Mössbauer and optical spectroscopy to show that, in the absence of oxygen, little Fe(II)-AA complex is formed when $\text{FeCl}_2 \cdot 4\text{H}_2\text{O}$ is used as the starting material.²³ A blue intermediate, detected by stopped-flow spectrophotometry, was formed in the presence of oxygen at pH 6-7. The Mössbauer spectrum of this species revealed two iron sites, one iron(II)

and one iron(III), in a ratio of 3:1. Despite these efforts, the nature and the coordination geometry of the iron-AA complex remains ambiguous. There are few structurally characterized metal complexes of AA except for several $[M^{n+}-(AA^-)]^{(n-1)+}$ metal salts.^{24,25} The only structurally characterized metal derivative of AA is a platinum complex in which one of the carbon atoms on the lactone ring is coordinated to the platinum.²⁶ In general, the structure of iron-AA complexes remains a mystery after almost half century of investigation.

Interest in iron ascorbate chemistry arose in this laboratory following the discovery that ascorbic acid, together with an μ -oxo dinuclear salt, form a catalytic system for the air oxidation of saturated hydrocarbons (see chapter 4 for a detailed discussion). The catalytic activity depends on the existence of a purple species, possibly the catalyst itself or an immediate precursor, formed between the iron salt and AA or a related analog, particularly tetramethyl reductic acid (TMRA, see scheme 4.5). It was therefore of interest to isolate and characterize of this purple species to help unravel the mechanism of the catalytic reaction. At the same time, such a structure would resolve a long-standing problem as discussed above. The task of crystallizing an iron-AA complex is very difficult owing to its short lifetime in aqueous solution and insolubility in most non-aqueous solvents. The isolation and crystallization proved successful, however, for the purple complexes formed between the iron salt and TMRA. This chapter presents the structural information obtained from X-ray diffraction studies of two different purple complexes isolated from the iron-TMRA system. The results from spectroscopic and reactivity studies of these complexes are also summarized, and their possible roles in the catalytic oxidation chemistry are discussed. In addition, the X-ray diffraction study of TMRA itself, is included.

I. X-Ray Diffraction Study of Tetramethyl Reductic Acid, C₉H₁₄O₃, (1)

Experimental

Materials. Compound 1 (tetramethyl reductic acid, C₉H₁₄O₃) was obtained from Polaroid Corp and purified by repetitive recrystallization from chloroform or acetonitrile at -20 °C. Anal Calcd, for C₉H₁₄O₃: C, 63.50; H, 8.31. Found C, 63.32; H, 8.26. ¹H NMR (300 M Hz, 297 K, CDCl₃): δ 1.02 ppm. FTIR (KBr, cm⁻¹): 3200 (broad, s), 1688 (s), 1668 (s), 1611 (s), 1608 (sh), 1566 (s), 1564 (sh), 1504 (s), 1485 (m), 1474 (m), 1461 (m), 1448 (m), 1422 (m), 1410 (m), 1375 (m), 1334 (s), 1291 (s), 1235 (m), 1207 (w), 1147 (m), 1007 (w), 974 (w), 940 (w), 877 (m), 787 (m), 774 (m), 680 (w), 601 (w), 536 (m). UV-Vis (CH₃CN, nm): 265.

Physical Measurements. UV-visible and IR spectra were recorded on a Perkin-Elmer Lambda 7 spectrophotometer or a Mattson Cygnus 400 Fourier transform spectrometer, respectively. ¹H NMR spectra were obtained with a Bruker WM250 or a Varian XL 300 instrument and tetramethylsilane as the internal standard.

X-ray Diffraction Studies. Colorless transparent needles grown from either acetonitrile or chloroform at -20 °C were suitable for X-ray diffraction studies. The data set was first collected at room temperature (24 °C) with a crystal grown from acetonitrile. The severe disorder found for carbon atoms on the five membered ring and the attached methyl groups in the room temperature structure made refinement very difficult. Another data set was therefore collected at -70 °C, using a crystal grown from chloroform, to resolve the disorder problem. For the room temperature structure, one colorless, transparent needle of approximate dimensions 0.30 x 0.35 x 0.50

mm was mounted in a capillary tube. For the low-temperature study, a needle of dimensions 0.12 x 0.18 x 0.25 mm was mounted with silica grease on the tip of a glass fiber. X-ray data were collected on an Enraf-Nonius CAD-4 diffractometer with Ni-filtered Cu K α radiation for the room temperature data set and a graphite monochromated Mo K α radiation for the low temperature structure. Three standard reflections measured after every 3600 seconds of exposure time showed no significant decay in either case. Lorentz and polarization corrections were applied to both data sets. No corrections for extinction or absorption were applied. Experimental details of the X-ray diffraction studies of **1** at both temperatures are given in Table 5.1.

Structure Solution and Refinement. All computations were performed on either a DEC VAXstation II or a DEC VAXstation 3100.

The structures were solved by direct methods and difference Fourier syntheses in TEXSAN.²⁷ Scattering factors for non-hydrogen atoms were taken from the literature.^{28,29} The refinement was carried out by using the full matrix least-squares program in TEXSAN. All non-hydrogen atoms were refined with anisotropic thermal parameters. For the room temperature data set, a sufficient number of hydrogen atoms was located on a difference Fourier map to allow the remainder to be generated by geometry. All hydrogens were constrained to ride on the appropriate carbon [$B(H) = 1.2B_{eq}(C)$], except for the hydrogens of the hydroxyl groups, whose coordinates and isotropic thermal parameters were refined. In the low temperature structure, all hydrogen atoms were generated in idealized positions with the C-H distances set equal to 0.95 Å. In the room temperature structure, the methyl groups in one of two crystallographically independent molecules were disordered over two positions and refined

with relative occupancies of 1:1. The final refinement converged at $R = 0.051$ and $R_w = 0.069$. In the final difference map, the largest residual peak was $0.202 \text{ e } \text{\AA}^{-3}$ and was located near one of the disordered carbon atoms on the five membered ring. The ratio of parameter shift to estimated standard deviation was less than 0.004. The disorder of the five-membered ring diminished in the low temperature structure. The final refinement gave $R = 6.3\%$ and $R_w = 8.4\%$. At convergence, the largest ratio of parameter shift to estimated standard deviation was 0.008. The largest residual peak, $0.65 \text{ e } / \text{\AA}^3$, was located near one of the chlorides on the solvent in **1**. Atomic coordinates and isotropic thermal parameters are listed in Tables 5.2a and b for the room and low temperature structures. Corresponding anisotropic thermal parameters are listed in Tables 5.3a and b. Selected bond lengths and angles obtained from these two studies are listed in Tables 5.4a and b, respectively.

Results and Discussion

There are two molecules in the asymmetric unit of **1** for the room temperature structure. The structure of one of the unique molecules (molecule **1**) is shown in Figure 5.1a. The two molecules differ primarily through their hydrogen bonding interactions (Figure 5.2a). In molecule **1**, the hydroxyl protons are hydrogen-bonded to the carbonyl and one hydroxyl oxygen of molecule **2**, while both hydroxyl protons of molecule **2** interact with carbonyl oxygen of another molecule **1**. This particular hydrogen bonding scheme generates sheets of molecules which lie virtually parallel to the *ac* plane, as illustrated in the packing diagram (Figure 5.3a). One of the ring carbon atoms and its attached methyl groups in molecule **2** are

disordered as shown in Figure 5.4. The disordered methyl groups lie in the grooves separating these sheets. The disordered ring carbons (C(15) and C(15A)), separated by 0.625(7) Å, were refined at 0.5 occupancy.

An ORTEP drawing of a molecule of **1** from the low temperature structure is shown in Figure 5.1b. There are no major differences in the bond lengths and angles in the five membered ring between the two structures. The disorder of the methyl groups has diminished, even though the methyl carbons have slight larger thermal ellipsoids. The hydrogen bonding scheme, however, is completely different from the one observed for the room temperature structure (Figure 5.2b). Both hydroxyl protons of each molecule interact with the carbonyl oxygen of a different molecule, while its own carbonyl group hydrogen-bonds to a third molecule. The intermolecular O...O distances of the carbonyl oxygen to the hydroxyl oxygen are 2.568 (5) Å and 2.732 (4) Å. The packing diagram (Figure 5.3b) shows the formation of chains through intermolecular hydrogen bonding network along y axis.

It is interesting to note that the hydrogen bonding schemes observed for **1** are very different from those found for the parent compound, reductic acid (RA, 2-cyclopentene-2,3-diol-1-one, **2**).³⁰ In the structure of **2**, the carbonyl group forms hydrogen bonds to two hydroxyl groups of two different neighboring molecules. In the low-temperature structure of **1**, however, the carbonyl group accepts the two hydroxyl group protons from only one neighboring molecule. In the structure of **1**, the carbonyl group of molecule **1** hydrogen-bonds to two hydroxyl groups from one of its neighbors while the carbonyl group of molecule **2** only accepts one hydrogen bond from the hydroxyl group of its neighboring molecule (Figure 5.2a). In addition, the hydroxyl groups in **2** only act as hydrogen bond

donors while one of the hydroxyl groups in molecule 2 in the room temperature structure of 1 is both a hydrogen bond donor and acceptor.

Table 5.5 gives the deviations from the best least-squares planes through portions of the TMRA molecule calculated for both structures. For the room temperature structure, the five-membered ring in molecule 1 is nearly planar while only four of the five carbon atoms of the ring in molecule 2 are coplanar. The fifth carbon atom lies ~ 0.25 Å out of the plane. The carbon atoms in the ring in the low-temperature structure are coplanar, with the largest deviation from the plane being only 0.029 Å, which is comparable to that observed for 2 (< 0.031 Å).³⁰ The larger deviation from planarity observed in the room temperature structure, therefore, may arise from crystal packing forces. Nevertheless, the conjugated portions of the molecule, O(1) - C(1) - C(2) - C(3) - O(3) in molecule 1 and O(11) - C(11) - C(12) - C(13) - O(13) in molecule 2 in the room temperature structure, are planar, reflecting electron delocalization. As a consequence, the C-O bonds of terminal hydroxyl groups, C(3)-O(3) in molecule 1 or C(13) - O(13) in molecule 2, are shorter than those of the central hydroxyl groups, C(2) - O(2) in molecule 1 and C(12) - O(12) in molecule 2 (Table 5.4). The same trend can be observed for the low-temperature structure as well, and a similar phenomenon was observed for reductic acid 2. The difference between the C-O bond lengths was used to rationalize the higher acidity of the terminal, versus the central, hydroxyl group.³⁰ In addition, the C(1) - C(2) distance in molecule 1 and the C(11) - C(12) distance in molecule 2 of the room temperature structure and C(1) - C(2) in the low temperature structure of 1 are shorter than other carbon-carbon single bonds in the molecule (Table 5.4a and b) due to the electron delocalization.

II. Synthesis and Characterization of $[\text{Fe}_3(\text{TMRA})_2(\text{TMRASQ})_4\text{Cl}_2]$ (3) and Its Ascorbate Analog

Experimental

Material. Solvents were dried according to literature procedures.³¹ All reagents used in the redox titrations were commercially available and used as received except as indicated below. The primary standard for the redox titration, $\text{FeSO}_4 \cdot \text{C}_2\text{H}_4(\text{NH}_3)_2\text{SO}_4 \cdot 4\text{H}_2\text{O}$ (4), was prepared as described in the literature.³² Another primary standard, As_2O_3 , was commercially available and dried at 120 °C overnight before use. The synthesis of $(\text{NEt}_4)_2[\text{Fe}_2\text{OCl}_6]$ (5) and $(\text{BzPh}_3\text{P})_2[\text{Fe}_2\text{OBr}_6]$ (6) was described in chapter 4 of this thesis.

Synthesis. A portion of 630 mg (1.05 mmol) of 5 was dissolved in 30 ml of acetone under nitrogen and 357 mg (2.10 mmol) of 1 was added. The solution turned purple immediately and was allowed to stand under nitrogen for half an hour. The solvent was removed in vacuo and the purple residue was extracted with ether. Subsequent filtration gave a purple solution and a green-yellow precipitate (470 mg). The ether was removed and the residue was redissolved in pentane. After standing for more than 24 hours at -20 °C, purple needle-like crystals deposited (207 mg, yield 47.4%). Anal. Calcd. for $\text{C}_{54}\text{H}_{74}\text{Fe}_3\text{Cl}_2\text{O}_{18}$: C, 51.90; H, 5.97; Fe, 5.68; Cl, 13.41. Found C, 51.42; H, 6.24; Fe, 5.18; Cl, 12.95.

An attempt was made to synthesize the analogous complex with bromide in place of chloride, in order to obtain crystals of better quality, by using 6 as the starting material via the aforementioned procedure. A purple solution and a deep red precipitate were obtained after ether extraction.

Efforts to crystalize the purple species have not succeeded while recrystallization of the red species from a mixture of acetonitrile, ether and methylene chloride gave red crystals of $(\text{BzPh}_3\text{P})[\text{FeBr}_4]$ (**7**) that were suitable for X-ray diffraction study.

Physical Measurements. All measurements were performed under inert atmosphere on microcrystalline **3**, which was recrystallized at least twice. Electronic spectra were recorded in acetonitrile on a Perkin-Elmer Lambda 7 UV-Vis spectrometer, and the near IR region was recorded on a Perkin-Elmer 330 spectrometer. The resonance Raman study was carried out on a solution sample of **3** in chloroform in a sealed NMR tube, which was slowly rotated during the measurement. Laser line of 406.7 nm was used for excitation with a power of 60 mW incidented on the sample. The back-scattering method was used to avoid severe absorption problems. Magnetic susceptibility measurements on a 26.7 mg solid sample were carried out with an S.H.E. Model 905 SQUID-type susceptometer at 5 KG. A total of 36 data points were taken between 6.0-300 K. The magnetism of the teflon sample holder used in the experiment was measured at the same temperature points, and its moment subtracted from the observed moment with sample present. At 6.0 K, the magnetic moment of the sample was measured as a function of field between 1.0 - 50.0 KG to check for saturation effects. EPR spectra were recorded on a Bruker 300 ESR spectrometer on a frozen sample of **3** in pentane with 1 mW power. Mössbauer spectra for both solid and solution samples of **3** was recorded by Georgia Papaefthymiou in the Francis Bitter Magnet Laboratory at 4.2 K and 80 K with zero magnetic field. The solution sample of **3** used for the Mössbauer study was prepared anaerobically in acetonitrile according to the aforementioned synthetic procedure, transferred into a sample holder by

syringe and immediately frozen in liquid nitrogen.

X-ray Diffraction Studies of 3. Purple crystals grown from acetonitrile or pentane were obtained and found to be suitable for X-ray diffraction studies. In the first X-ray diffraction study of **3**, a thin plate crystal grown from CD₃CN in a NMR tube at -20 °C was mounted on a glass fiber with silicon grease under a cold nitrogen stream. The data set was collected at -78.5 °C. A second crystal (0.35 mm x 0.2 mm x 0.1 mm) was needed to complete the data collection owing to the severe decay of the first crystal (26.2 % loss of intensities for the three standards monitored after completion of the data collection for the first shell.). The data from $2\theta = 2^\circ$ to 32° were collected on the first crystal and the data set (to $2\theta = 44^\circ$) was completed by using the second crystal. Due to the poor quality of the first data set, another data set was collected on a crystal (0.4 mm x 0.3 mm x 0.3 mm block) obtained from pentane at -79 °C. The crystal obtained from pentane decayed much slower than the ones from acetonitrile (7.7% loss of intensities throughout the data collection for the three standards monitored). The data collections were carried out on an Enraf-Nonius CAD-4 diffractometer with graphite monochromated Mo K α radiation. Both data sets were corrected for absorption by using psi scan data and for crystal deterioration. Lorentz and polarization corrections were applied to both data sets. Experimental details of the X-ray diffraction studies of **3** are given in Table 5.6.

X-ray Diffraction Studies of 7. A crystal of **7** (0.3 mm x 0.3 mm x 0.3 mm), crystallized from a mixture of acetonitrile, ether and methylene chloride, was mounted on a glass fiber with silicon grease under a cold nitrogen stream. The data set was collected at -78 °C on an Enraf-Nonius CAD-4 diffractometer with graphite monochromated Mo K α radiation. No

decay in the intensities of three standard reflections was observed during data collection. Lorentz and polarization corrections were applied. An absorption correction was applied by using psi-scan data. Experimental details of the X-ray diffraction study of **7** are given in Table 5.7.

Structure Solution and Refinement. All computations were performed on either a DEC VAXstation II or a DEC VAXstation 3100.

For Complex 3. The structures were solved by using the direct method option of SHELX-86.³³ Scattering factors for non-hydrogen atoms were taken from the literature.^{28,29} The structures were refined by using the full matrix least-squares program in TEXSAN.²⁷ Only iron and chlorine atoms were refined anisotropically in both cases. Oxygen and carbon atoms tend to become "not-positive definite" when refined anisotropically so isotropic thermal parameters were applied. No hydrogen atoms were included in the refinement of the triclinic structure. The best R value obtained for the triclinic structure was 0.119 with $R_w = 0.151$. The two solvent molecules in the lattice were disordered. In the case of the cubic structure, hydrogen atoms were generated with C-H distances set equal to 0.95 Å. All hydrogens were allowed to ride on the appropriate carbon [$B(H) = 1.2B_{eq}(C)$]. A theta angle cutoff was applied by using the criterion of $\sin(\theta)/\lambda < 0.498$. Reflections with $I > 2\sigma(I)$, instead of $I > 3\sigma(I)$, were used in the refinement owing to a shortage of strong reflections relative to the number of parameters. The final refinement on F used 155 parameters and converged at $R = 0.101$, $R_w = 0.121$ with the largest ratio of parameter shift to estimated standard deviation being 0.04. On the final difference Fourier map, the highest residual peak was $0.79 \text{ e}/\text{Å}^3$ and located in the center of cavities formed by molecule packing in the lattice. Atomic coordinates and isotropic thermal parameters are listed in Table 5.8a and Table 5.8b for the triclinic and cubic

structure, respectively. Final thermal parameters are given in Table 5.9a and Table 5.9b for both structures. Selected bond lengths and angles are listed in Table 5.10a and 5.10b.

For Complex 7. The structure was solved and refined in the same manner as 3. All nonhydrogen atoms were located on the difference Fourier map and refined anisotropically. Hydrogen atoms were generated with C-H distances set equal to 0.95 Å. The thermal parameters of hydrogen atoms were fixed at $1.2 \times B_{eq}$, where B_{eq} is the equivalent isotropic thermal parameters of the attached carbon atom. The final refinement converged at $R = 0.034$ and $R_w = 0.037$ with the largest ratio of parameter shift to estimated standard deviation being 0.027. On the final difference Fourier map, the highest residual peak was $0.42 \text{ e}/\text{Å}^3$ and was located near the bromide in BzPh₃PBr salt. Atomic coordinates and isotropic thermal parameters for non-hydrogen atoms in 7 are listed in Table 5.11. Final thermal parameters are given in Table 5.12. Selected bond lengths and angles are listed in Table 5.13.

Redox Titration of 3. Redox titrations were employed to assess the assignment of ligand oxidation states of the ligands in 3. Table 5.14 lists all of the oxidants, indicators, solvents and reaction conditions used for the titration. The end-point was determined by using either a redox indicator or an Orion Research 960 Autochemistry potentiometric titrator equipped with a redox combination electrode (Pt vs Ag/AgCl). All experiments were carried out under inert atmosphere (N₂ or Ar) at room temperature. In the cases where ceric ion or dichromate was used as the oxidant, the system was calibrated by using the primary standard 4. For the iodometric titration, I₂ was prepared as an aqueous I₃⁻ solution, the concentration of which was determined by using the primary standard As₂O₃. The titration of free

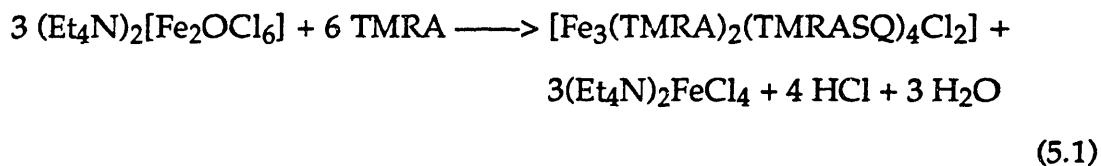
TMRA was always used as a control to examine the validity of the method employed. For the potentiometric titration, the titration was usually carried out in 0.72 N H₂SO₄ aqueous solution. A three-necked flask was used as reaction vessel, equipped with a redox combination electrode and Ar gas supply line. The temperature of the system was maintained at 30 °C by using an oil bath. Titrant was added with a Gilson pipette (accurate to 0.001 ml).

Reactivity Studies of 3. All reactions were carried out at 30 °C in acetone with dried air as the oxygen source and cyclohexane as substrate. Methyl benzoate (1.6×10^{-5} M) was used as an internal standard. The reaction was monitored by examining aliquots of the reaction mixture by HP5890 GC and HP5971 GC-Mass spectrometers at periodic time intervals. Three sets of experiments were carried out to examine the reactivity of 3 toward air oxidation of cyclohexane. An *in situ* system prepared from 5/TMRA was used as the control. (i) A small portion (15-20 mg) of crystalline or a microcrystalline complex 3 was weighed out under N₂ and dissolved in acetone. Substrate and standard were added and the reaction was initiated by opening the solution to air. (ii) One equivalent of 3 was dissolved in CH₃CN in the drybox and 7 equivalents of acid were added to the purple solution. When HBF₄·Et₂O and p-toluene-sulfonic acid were added, the color of the solution faded immediately and a white precipitate formed. In the case of benzoic acid, the purple color persisted. The substrate and standard were then added and the system was exposed to air. (iii) One equivalent of 3 was dissolved in acetone and ~40 equivalents of TMRA were added to the solution. The system was opened to air after the substrate and standard were added.

Mössbauer Studies of Reactions Between Ascorbic Acid or Ascorbate and Iron in Aqueous Solution. Sample 1 was prepared by dissolving 0.196 g (0.5 mmol) of $(\text{NH}_4)_2\text{Fe}(\text{SO}_4)_2 \cdot 6\text{H}_2\text{O}$ in a 0.1 mM MOPS (MOPS = 4-morpholinepropanesulfonic acid) aqueous solution (2 ml) under argon. 0.198 g (1.0 mmol) of NaAA were added with stirring. The solution remained colorless. The flask was opened to air for five minutes and the air was subsequently removed by the freeze-pump-thaw procedure. An intense purple color developed. The solution was transferred by syringe into a sample holder and frozen to -78°C immediately. Sample 2 was prepared in a similar manner by dissolving 0.368 g of 5 in 2 ml 0.1 mM MOPS solution. 0.244 g of NaAA was added under argon with stirring.

Results and Discussion

Synthesis. A proposed reaction scheme for the formation of 3 is shown in eq. 5.1. The 47% isolated yield reported in the experimental



section of this chapter was based on this reaction scheme. It is difficult to measure accurately the true yield due to the high solubility of 3 in most solvents. When microcrystals were separated from the solution, a fair amount of 3 remained in the mother liquor.

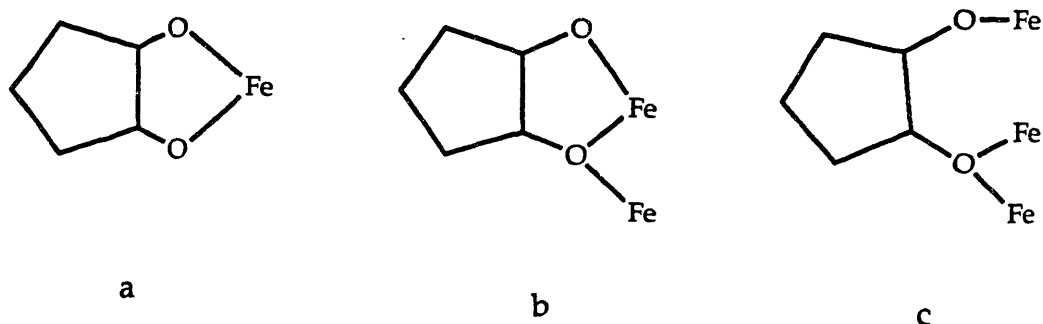
As previously described, a large quantity of a green precipitate was formed during the reaction. Efforts have been made to identify this

byproduct. The UV-vis spectrum of this green species contains three peaks at 364, 314 and 244 nm, identical to those observed for the spectrum of $(\text{Et}_4\text{N})[\text{FeCl}_4]$.³⁴ Recrystallization of this species yielded both crystalline Et_4NCl and a green crystal. A preliminary X-ray diffraction study of the green crystal failed to provide any structural information due to the poor quality of the data. In the hope of obtaining better crystals of both the trinuclear iron complex and its byproduct, **6**, a bromide analog of **5**, was used as the starting material in the synthesis. The red compound isolated after ether extraction revealed a UV-vis spectrum with a peak at 262 nm in methylene chloride, similar to that reported for $(\text{Et}_4\text{N})_2[\text{FeBr}_4]$.³⁴ The spectrum of the compound changed dramatically upon exposure to air, with new peaks appearing at 270, 316, 390 and 468 nm, in accordance with the published spectrum of **7**.³⁴ This complex was recrystallized from acetonitrile/ether/methylene chloride and was proved to be **7** by an X-ray diffraction study. This result provides the supporting evidence for the reaction scheme in shown eq. 5.1. The failure to observe the formation of $[\text{FeCl}_4^{2-}]$ may be attributed to its instability in the presence of even a trace amount of oxygen.

Structure of 3. Figures 5.5a and b show the molecular structure of **3** determined from the triclinic and cubic data set, respectively. The structures obtained from the two data sets are virtually identical. The molecular structure obtained from the cubic data set, however, is more precise owing to the better quality of the data.

In the structure determined from the cubic crystal data set, three iron centers in the molecule form an isosceles triangle with a crystallographic two-fold axis passing through Fe1 and the center of the Fe2...Fe2* edge. The longer edge of the triangle (Fe1... Fe2) measures 3.49 (1) Å and the shorter

one ($\text{Fe2}\cdots\text{Fe2}^*$), 3.24 (1) Å. The shorter distance arises because of the presence of two alkoxide bridges. Correspondingly, the $\text{Fe2} - \text{O} - \text{Fe2}$ angle of $104 (1)^\circ$ is significantly smaller than the $\text{Fe1} - \text{O} - \text{Fe2}$ angle, $113(1)^\circ$. All three iron atoms have a distorted octahedral geometry, with the $\text{O} - \text{Fe} - \text{O}$ or $\text{Cl} - \text{Fe} - \text{O}$ angles ranging from 83° to 97.7° . There are three types of ligand coordination to the iron atoms (Scheme 5.2). One is chelating (Scheme 5.2a) as exemplified by the ligand bonded to Fe2 . The second is chelating but also bridges to a second iron atom by using its central hydroxyl group (Scheme 5.2b). The third bridges all three iron atoms by using two hydroxyl groups (Scheme 5.2c). All three binding patterns have been observed in a

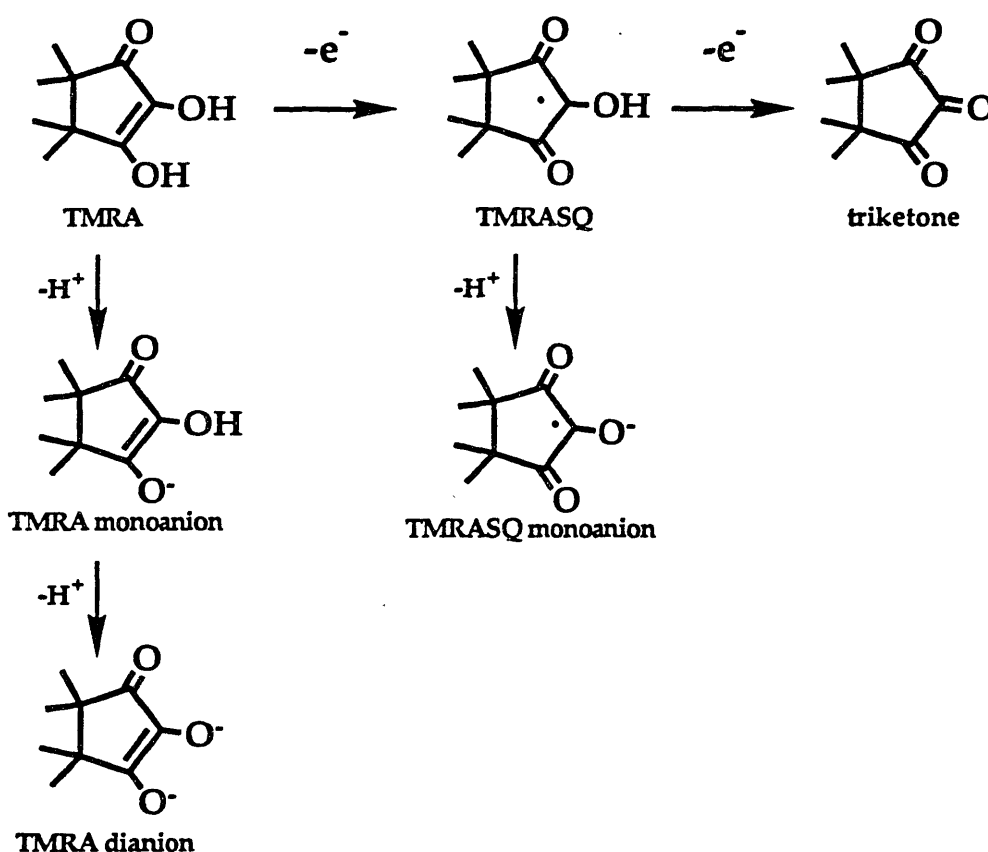


Scheme 5.2

tetranuclear iron complex with 3,5-di-*t*-butyl-1,2-benzoquinone as the ligand.³⁵ There are two terminal chloride ligands bonded to two Fe2 atoms and arranged in an *anti* configuration across the $\text{Fe}_2(\text{OR})_2$ four membered ring.

There are two ferric and one ferrous ions in the structure, the oxidation states of which were determined by Mössbauer spectroscopy as described below. From symmetry considerations, one can assign Fe1 as the ferrous ion and Fe2 as the ferric ion. Thus the six ligands have to bear a

total of six negative charges to maintain charge neutrality in the complex. This requirement can be satisfied by the proper distribution among three possible redox states and three forms of deprotonation of the ligands (Scheme 5.3). Given the C_2 symmetry of the molecule, there are two possible combinations. One requires that all six ligands be monoanions, while the other demands two neutral, two monoanionic and two dianionic ligands.



Scheme 5.3

It has been demonstrated in the literature that, by a detailed analysis of bond lengths, it is sometimes possible to assign oxidation states for ligand such as TMRA, as has been found for metal catechol complexes.³⁵ In the fully reduced form, both C=C bonds in the enediol fragment should be

shorter than the corresponding bonds in the semiquinone form due to the different distribution of electron density in the two redox states. Close examination of the appropriate distances in **3** reveals that C1-C2 (1.29 Å) in the ligand chelated to Fe2 is much shorter than the corresponding bonds in the other two ligands (C6-C7 = 1.36 Å and C11-C12 = 1.38 Å). A comparison of the C-O bond lengths in the enediol fragments of such ligands can also reveal the oxidation states. This comparison, however, may not be apply to this structure because of the different coordination environments. Based on this analysis, the two ligands chelated to Fe2 and Fe2* were tentatively assigned as TMRA monoanions and the remaining four ligands as TMRASQ monoanions.

In the structure determined from the triclinic data set, the pseudo-isosceles triangle formed by three iron atoms has a short edge of 3.241 Å between Fe1 and Fe2 and two long, slightly asymmetric edges of 3.446 Å (Fe1...Fe3) and 3.507 Å (Fe2...Fe3). The Fe1-O1-Fe2 and Fe1-O2-Fe2 angles on the doubly bridged edges (106.8 and 106.5°) are significantly smaller than the singly bridged edges (Fe1-O5-Fe3 (113.1°) and Fe2-O8-Fe3 (115.6°)), as was observed for the cubic structure. because of the poor quality of the data set, the resolution of the triclinic structure is not high enough to make accurate redox state assignments for the ligands based on a bond length analysis.

The packing of molecules in the lattice is dramatically different in the two structures. Figure 5.6 portrays a PLUTO drawing showing the unit cell packing of **3** in the cubic crystal lattice. One interesting feature is the large empty cavity. This result may account for the calculated density of the crystal, only 0.934 g/cm³, an unexpectedly small value for a molecule with several heavy atoms in it. The highest residual peak on the difference

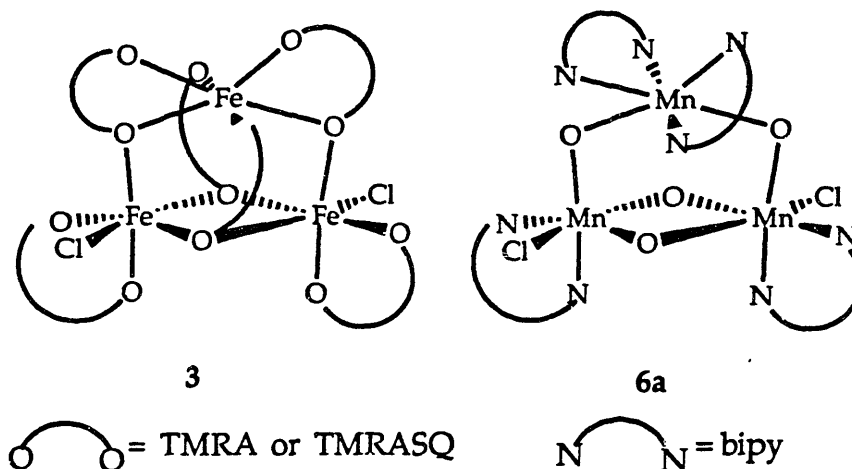
Fourier map after the final refinement is situated in the middle of the cavity (the circle in Figure 5.6), and could be the trapped residual solvent. The diameter of these cavities was estimated to be 8 Å. This type of hole was not observed in the triclinic lattice. Figure 5.7 shows two molecules in the asymmetric unit of the $P\bar{1}$ lattice. These two molecules are interlocked with one another through hydrogen bonding interactions between the hydroxyl group on TMRASQ of one molecule and the carbonyl group of the TMRASQ of the other molecule. This result further supports the assignment of the chelating ligands as TMRA monoanions, which must contain a proton required to form the hydrogen bonds (O15...O401, 2.59(2) Å; O18...O301, 2.63(2)Å).

Complex 3 is the first example of an iron complex with an ascorbate analog as ligand to be structurally characterized. The corresponding iron-AA complex may be quite similar. Ascorbate is capable of forming chelates like TMRA, as previously suggested (Scheme 5.1). An iron-ascorbate complex with a similar structure to that of 3 would be consistent with the observations obtained from previous Mössbauer and spectroscopic studies.¹⁵

The core geometry of 3 is unique among the trinuclear iron clusters with oxygen bridges. Among such known trinuclear iron clusters, the most common structural motif is that of the basic iron acetate, which contains an equilateral triangular array of iron atoms.³⁶⁻³⁸ This core distorts toward an isosceles triangle when one of the irons is reduced to the ferrous form. A trinuclear iron(III) complex, $[\text{Fe}_3\text{O}(\text{TIEO})_2(\text{O}_2\text{CPh})_2\text{Cl}_3]\cdot 2\text{C}_6\text{H}_6$ (TIEOH = 1,1,2-tris(N-methyl-2-imidazolyl)ethanol), also has an isosceles triangular core.³⁹ Recently, a novel trinuclear mixed-valent iron complex, $[\text{Fe}_3\text{O}(\text{OAc})_6(\text{TACN})]$, was characterized, the isosceles triangular core of which differs from that of the classical mixed-valent basic iron acetate.⁴⁰ All

of these complexes have a $\{\text{Fe}_3\text{O}\}^{6+,7+}$ unit with only small variations in their core geometry from that of the basic iron acetate. In addition, a linear trinuclear iron cluster has recently appeared in the literature.⁴¹ Among the iron complexes with a triangular structural motif, complex **3** provides the sole example of a core geometry with only alkoxo bridges. The double alkoxide bridge between the two Fe2 atoms observed in **3** is also uncommon among the iron trinuclear clusters.

Many of the structural features of **3** are shared by the trinuclear manganese complex, $[\text{Mn}_3\text{O}_4(\text{bipy})_4\text{X}_2]^{n+}$ ($\text{X} = \text{Cl}$, $n = 2$, **6a**; $\text{X} = \text{H}_2\text{O}$, $n = 4$, **6b**) (Scheme 5.4).^{42,43} As depicted in Scheme 5.4, complex **6a** has the same



Scheme 5.4

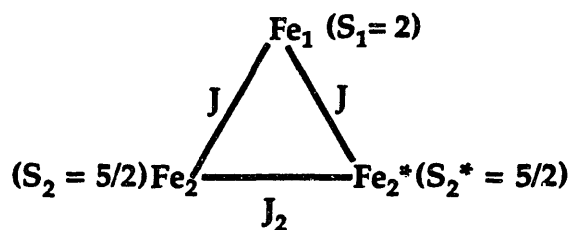
triangular metal cluster as that observed in **3**, with oxo-bridges between manganese centers, instead of the alkoxo bridges between iron centers found in **3**. Two chloride atoms in **6a** also bind to the manganese in an *anti* configuration. The other trinuclear manganese analog **6b**, in which the two chloride ligands in **6a** are replaced by two water molecules, was recently found to be an active catalyst for hydroxylating alkanes with the use of *t*BuOOH as the oxidant.^{44,45}

Spectroscopic and Magnetic Studies. The optical spectrum of **3** in acetonitrile exhibits a broad peak at 554 (ϵ 4460 $\text{cm}^{-1}\text{mol}^{-1}$) nm, a shoulder at 358 nm, and a peak at 280 nm. The peak at 540 nm quickly diminishes to a shoulder and then disappears when the solution of **3** is exposed to air. No band was observed in the near IR region. Similar low energy bands (501 nm ~ 650 nm) were reported for many AA-iron species^{19-23,46} and for several iron semiquinone complex.^{47,48} This resonance was proposed as a d-d transition (${}^6A_1 \rightarrow {}^4T_2$) of iron.²¹

Figure 5.8 shows the resonance Raman spectrum of a sample of **3** in chloroform solution. The only distinguishable bands are the peaks at 280 and 314 cm^{-1} . The latter feature has been observed for other binuclear iron complexes containing chloride ligands,⁴⁹ and is assigned as the Fe-Cl stretch in **3**. It may provide a useful probe for kinetic studies. Assuming that the chloride site might be the site of oxygen binding during the catalytic cycle, the kinetics of the oxygen binding process can thus be monitored by measuring the change in Fe-Cl stretch on proper time scale. The feature at 280 cm^{-1} has not yet been assigned.

The molar magnetic susceptibility and effective moment of a solid sample of **3** vary as a function of temperature, as shown in Figure 5.9. Due to the complexity of the possible coupling pathways among the three iron centers and the irons and the radical ligands, an exact theoretical treatment of the data was not possible. A simplified model was used for approximate fit by neglecting spin coupling between the iron centers and radical ligands. The theoretical model adopted was reported in the literature for trinuclear mixed-valent basic iron acetate.⁴⁵ Based on the C_2 symmetry of **3**, it is assumed that there are two different magnetic coupling interactions

between the two high spin iron(III) ($S = 5/2$) centers and one high spin



Scheme 5.5

iron(II) ($S = 2$) centers with $J_2 > J$ as indicated in scheme 5.5. Equation 5.2 is the exchange Hamiltonian which describes these interactions. The expression derived from this Hamiltonian can be found in the literature.⁴⁵

$$H = -2J (S_2 \cdot S_1 + S_1 \cdot S_2^*) - J (S_2 \cdot S_2^*) \quad (5.2)$$

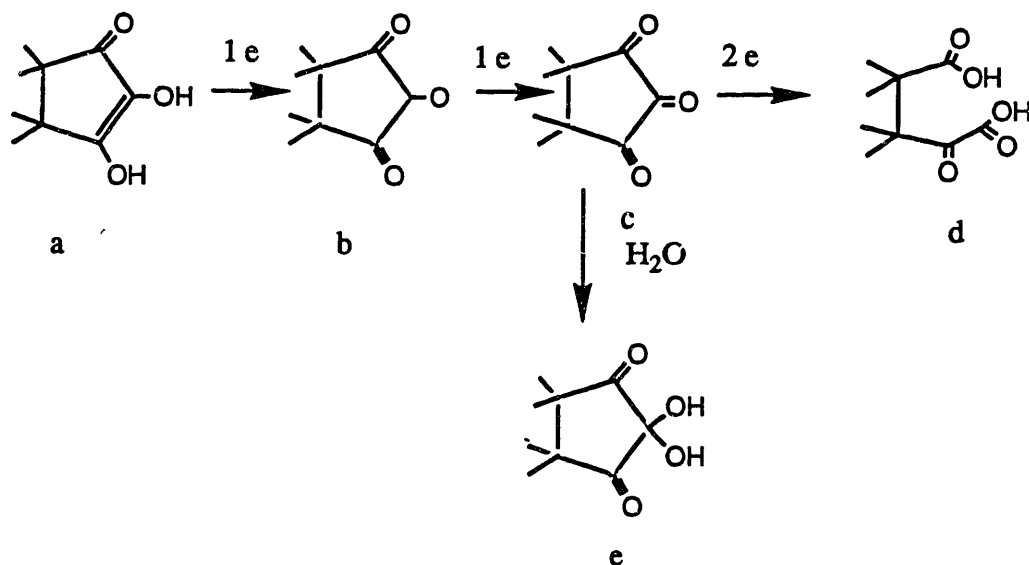
With the g value for Fe(III) fixed at 2.00 and the g value for Fe(II) (g_2) allowed to vary, a non-linear least-squares fit was determined. The best fit gave: $J_2 = -16 \text{ cm}^{-1}$, $J = -9 \text{ cm}^{-1}$, $g_2 = 1.93$, TIP = -1.4%. Figure 5.9 also shows the curve calculated by using this model. The TIP term (temperature independent paramagnetism) is unreasonably large and negative, which may reflect the existence of a small amount of diamagnetic impurity, e.g. free TMRA, in the sample. Such a impurity may not be large enough to affect the results of the elemental analysis and other physical measurements performed on this sample but is large enough to affect the magnetic study. Ultimately, purer sample is needed for a better data set. Extrapolation of the effective moment to 0 K gives a value 2.39 B.M.. This value suggests a $S=1$ ground state ($\mu_{\text{eff}} = 2.82 \text{ B.M.}$). Such a system could be the result of partial coupling between all unpaired electrons which gives a total spin of one for the cluster.

Figure 5.10 shows the Mössbauer spectra of solid and frozen solution samples of **3** at 80 K in zero magnetic field. The fitting parameters are listed in Table 5.15. Spectra taken at different temperatures showed very little temperature dependence. There are two different iron sites. The isomer shifts of the two sites are typical for iron(II) and iron(III), respectively, with a relative ratio of Fe(II):Fe(III) of 1:2. To examine the integrity of **3** in solution, a solution spectrum was taken. Both Mössbauer parameters (δ and ΔE_Q), as well as the ratio of ferric to ferrous ion, were very similar to the solid sample. This result is consistent with **3** having a similar structure in both solid and solution state.

Figure 5.11 shows the EPR spectra of **3** at different temperatures. A temperature dependence of the line shape was observed, which indicates either the presence of an impurity in the sample or a multi-spin state system. All features disappear above 16 K. The significant observation from EPR experiment is that there is no free organic radical signal which would be expected for a classical semiquinone radical. This indicates possible coupling between unpaired electrons on TMRASQ ligands and high spin iron centers.

Redox and Reactivity Studies. TMRA (**1**) can be oxidized under appropriate conditions to form $1e$, $2e$ and $4e$ oxidation products as shown in scheme 5.6.⁵⁰ Under the proper titration conditions, oxidation of **1** can be halted at a given stage. By determining the number of redox equivalents required to oxidize all ligands in **3** to a certain oxidation state, for example the triketone form, the redox states of the ligands in **3** can in principle be assigned. There were two major difficulties encountered in carrying out such a titration when Ce^{4+} was used as the oxidant in a 0.72 N H_2SO_4 aqueous solution with N-phenylanthranilic acid as the indicator. First of

all, the end-point was not stable, possibly due to reaction between 1 and the indicator. When 1 was titrated, the clear solution become cloudy upon the addition of a few drops of indicator solution. To circumvent this problem,

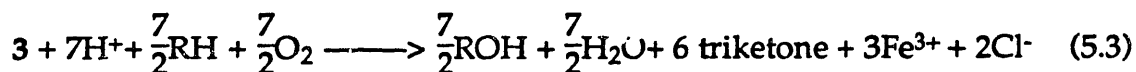


Scheme 5.6

another indicator, O-dianisidine (ODA), was employed, which generates a stable and distinct orange color at the end-point. The use of a potentiometric titrator also avoided the aforementioned problem by eliminating the use of indicators. Secondly, the results obtained were irregular and not reproducible. Further oxidation of the triketone to a higher oxidation product by the strong oxidant Ce^{4+} was suspected. The use of a milder oxidant, I_2 , alleviated this problem. I_2 was used for the quantitation of TMRA in the literature by oxidizing the fully reduced form exclusively to the triketone (c in Scheme 5.6).⁵¹ The titration results for both 1 and 3 are given in Table 5.16. The total number of oxidation equivalents required to titrate the ligands in 1 equivalent of 3 is 9 ± 1 , which is consistent with the oxidation of two fully reduced TMRA ligands ($4e^-$), four

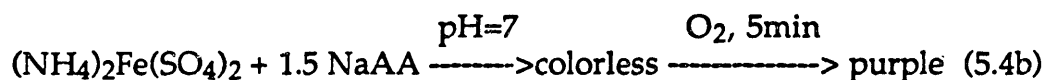
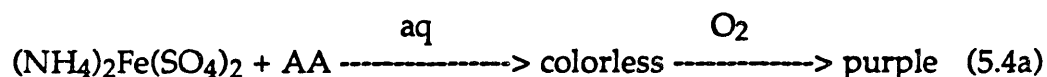
semiquinone ligands ($4e^-$) and one ferrous ion ($1e^-$). This result is in agreement with the assignments of the X-ray crystal structure and the Mössbauer spectrum.

Reactivity of 3. The role of **3** in the catalytic hydroxylation of alkanes by dioxygen is of interest. Equation 5.3 presents a postulated reaction



stoichiometry for a single turnover experiment, assuming that **3** is the active species. To test this hypothesis, the catalytic activity of **3** in the air oxidation of cyclohexane was examined by using (i) only **3** and O_2 ; (ii) **3**, acid, and O_2 ; and (iii) **3**, extra TMRA, and O_2 . In case (i), conversion of cyclohexane to cyclohexanol is very slow. Cyclohexanol was formed with an overall yield of about 40% and an alcohol/ketone ratio of 2/1 in 24 hours. The addition of excess protons accelerated the oxidation reaction slightly and gave a total yield of 52%. With extra TMRA, complex **3** catalyzed the oxidation reaction with a rate and overall yield comparable to those found for the *in situ* system.⁵² A change in the product distribution pattern was observed, however. The ratio of cyclohexanol to cyclohexanone was 7/1, much lower than that observed in the *in situ* system. This result suggests that the presence of excess TMRA does affect the selectivity of the system. If an alkyl hydroperoxide is formed during the catalytic cycle as a precursor of alcohol or ketone (see chapter 4 for detailed discussion), TMRA may act as an oxygen atom acceptor during the decomposition of such an alkyl hydroperoxide, inhibiting the ketone formation.

Mössbauer Studies of the Ascorbate Analog of 3. It is very difficult to prepare and crystallize the ascorbate analog of 3 from non-aqueous solvents owing to the limited solubility of ascorbic acid. The formation of a purple complex between ferrous sulfate and ascorbic acid (eq. 5.4a) was observed in aqueous solution, but the lifetime of the complex was quite short; at room temperature the color bleached within a few minutes. Attempts to crystallize a complex formed between an iron salt and AA have not succeeded to date. A solution Mössbauer study was therefore undertaken to offer some insight into the nature of the complex.



The pH of the medium was found to be crucial for stabilizing the complex. At pH 7, the purple complex was stable in air for an hour and stable indefinitely in the absence of air. A 0.1 mM MOPS buffer and monosodium ascorbate were employed to maintain the pH of the solution at 7. Samples prepared according to equations (5.4b) and (5.4c) were frozen at -78°C and their Mössbauer spectra were taken. The Mössbauer parameters listed in Table 5.17 clearly indicate the presence of a mixed-valent species. Differences in the $\text{Fe}^{2+}/\text{Fe}^{3+}$ ratio between different preparations may be due to the incomplete oxidation of the sample prepared via route (b). The UV-Vis spectrum of the solution prepared as in (5.4c) showed a peak at 475 nm and a

shoulder at 550 nm. It is interesting to note that there is more Fe^{2+} than Fe^{3+} , which is just the opposite of what was observed in complex 3. The result obtained with sample b is very similar to that reported for the purple complex formed upon exposure of a $\text{FeCl}_2 \cdot 4\text{H}_2\text{O}$ and 10-fold NaAA mixture to oxygen, which has a ferrous to ferric ion ratio of 3 to 1.²³ It is interesting that the existence of excess reductant seems to have little effect on the Mössbauer properties of the iron centers and the relative ratio of Fe(II) to Fe(III) in the complex.

III. X-Ray Diffraction Study of a Tetranuclear Iron Complex [$\text{Fe}_4(\text{TMRA})_8(\text{H}_2\text{O})_4$] (8)

Experimental

Crystallization and X-ray Diffraction Study. Compound 8 was crystallized from an acetone solution prepared as described for the synthesis of 3. The solution was kept at $-20\text{ }^\circ\text{C}$ for a longer period of time (>1 year) compared to that of crystallization of 3. A crystal ($0.4\text{ mm} \times 0.35\text{ mm} \times 0.08\text{ mm}$) was mounted on a glass fiber under low temperature nitrogen stream. The data were collected at $-78\text{ }^\circ\text{C}$ on an Enraf-Nonius CAD-4 diffractometer with graphite monochromated Mo $\text{K}\alpha$ radiation. Very little decay (av. 2.5%) of the intensities of three standard reflections was observed throughout the data collection. The data set was corrected for absorption by using the analytical method. Both Lorentz and polarization corrections were also applied to both data sets. Experimental details of the X-ray diffraction studies of 8 are given in Table 5.18.

Structure Solution and Refinement. The structure of **8** was solved and refined as described in previous sections. All nonhydrogen atoms were located on Fourier difference maps and refined anisotropically except for the solvent acetone molecule. Hydrogen atoms of one water ligand which coordinates to an iron center and that of an unbound hydroxyl group of the fully reduced TMRA were located on the difference map. Other hydrogen atoms were generated with the C-H distance set equal to 0.95 Å. All hydrogens were allowed to ride on the appropriate carbon [$B(H) = 1.2B_{eq}(C)$]. The refinement on F converged at $R = 0.056$, $R_w = 0.060$ with the largest ratio of parameter shift to estimated standard deviation being 0.4. On the final difference Fourier map, the highest residual peak was $0.57 \text{ e}/\text{Å}^3$ and was located near the solvent water molecule. Atomic coordinates and isotropic thermal parameters are listed in Table 5.19 and Table 5.20 gives the final thermal parameters for non-hydrogen atoms. Selected bond lengths and angles are listed in Table 5.21.

Results and Discussion

Structure of 8. Figure 5.12 depicts the molecular structure of **8**. There is a crystallographically imposed inversion center located at the center of the parallelogram comprised of the two Fe2 and two μ -O atoms. The $\text{Fe}_4(\mu\text{-O})_6$ core can be viewed as two $\text{Fe}_3(\mu\text{-O})_4$ triangular cores of **3** joined with a shared edge. The coordination sphere of Fe2 is completed by a water or hydroxyl ligand, instead of a chloride ligand as in **3**. These water or hydroxyl groups retain the *anti* configuration.

It is difficult to distinguish water from hydroxyl ligation by the structural analysis alone. The overall of ligand iron ratio is 2 to 1, as

observed in **3**. Two of the three binding patterns of TMRA coordination observed in **3**, type b and c in Scheme 5.2, are preserved in **8** while the chelating type of binding (type a in Scheme 5.2) is absent. Instead, two of the ligands are coordinated to iron in a monodentate fashion. The remaining hydroxyl group of this ligand forms an intramolecular hydrogen bond with one of the carbonyl groups of the neighboring TMRASQ ligand (Figure 5.13). There is only one ligand bound to Fe1 in **8** that bridges to all three iron atoms (type c), compared to two of such ligand on Fe1 in **3**. As a result, a water molecule coordinates to Fe1 to complete the coordination sphere. The Fe1...Fe2 and Fe2...Fe2 distances, 3.640(2), 3.681(1) Å and 3.140(2) Å, are very similar to those observed in **3**.

No assignment of the oxidation state was made for irons due to the lack of sufficient material for Mössbauer study. The oxidation states of the ligands, however, can be assigned by a detailed bond length analysis, owing to the high resolution of the structure. Two criteria were used for this purpose. The terminal C-O bond in the fully reduced form of the ligand is longer than in the semiquinone form. Thus, the difference (Δ) between the two C-O bonds should be less within the semiquinone than in the fully reduced form of the ligand. Table 5.22 gives the Δ value for each ligand. The second criterion is that the C=C bonds in the five-membered ring should be much shorter in the fully reduced than in the semiquinone form. The results are given in Table 5.22. It is reasonably clear from these results that two monodentate ligands attached to Fe1 are in the fully reduced form while the other six ligands are in the semiquinone form. The ratio of the fully reduced to the semiquinone form is therefore 1 to 3, compared to 1 to 2 observed in **3**. Because of the difficulty of assessing the degree of protonation of each ligand (Scheme 5.3) and the ambiguity concerning the

nature of the oxygen ligand on Fe²⁺, as well as the absence of Mössbauer data, the oxidation states of irons remain unassigned. If all the ligands are monoanions, then two possibilities still remain depending on the nature of the oxygen ligand on Fe²⁺. If a water molecule is coordinated to Fe²⁺, then all irons are divalent. If it is an hydroxyl group, then **8** is mixed valent with two ferric and two ferrous ions.

The Formation of **8 and Its Possible Significance to the Catalytic Mechanism.** Similarity of structural features in **3** and **8** suggests that both the trinuclear and tetranuclear clusters are derived from the same building blocks, possibly a mono- or dinuclear iron moiety. Perhaps when **1** reacts with **5**, both dinuclear and mononuclear precursors are formed, which subsequently react with one another to form trinuclear (1:1) or tetranuclear (1:2) clusters. The former case has precedent in the literature, the trinuclear manganese cluster **6b** being synthesized from a dinuclear precursor.⁴⁴ The yield realized in the synthesis of **3** and the solution Mössbauer spectrum suggest that **3** is the major product of the reaction. The reaction conditions under which tetramer formation is favored still need to be explored more

Conclusions

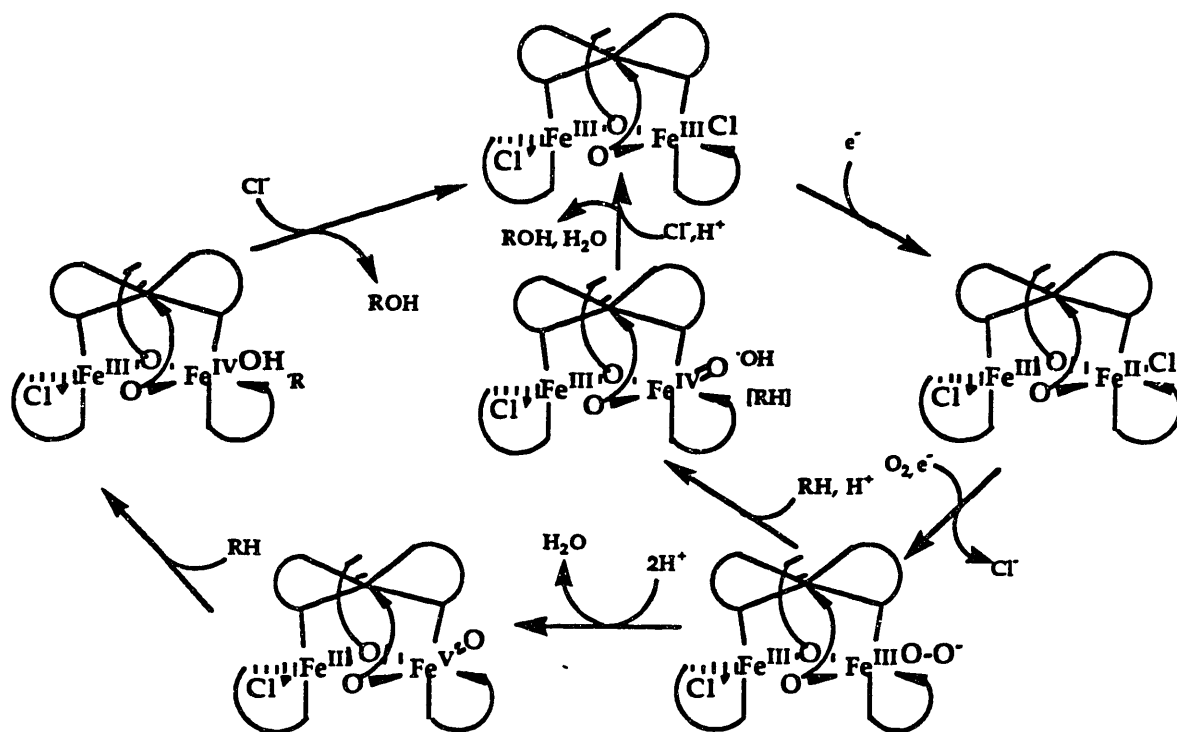
The structural characterization of **1** was completed and affords some interesting observations concerning the reactivity of this compound. There are extensive intermolecular hydrogen bonding patterns in the crystal lattice, the nature of which is dependent upon the crystallization solvent. The delocalization of the electron density in the enediol fragment is clearly manifested by its planarity and the deviation of both the C-C and C=O bond

lengths from conventional values. This delocalization makes the terminal hydroxyl group more acidic than the central one.

A trinuclear mixed-valent iron complex of TMRA, **3**, was isolated and structurally characterized. The molecule has a unique core geometry with three iron atoms, one ferrous and two ferric, forming an isosceles triangle. The oxidation states of the ligands were determined by detailed bond length analysis and redox titrations to be two fully reduced and four semiquinone TMRA. Two chloride ions, coordinated to two of the Fe(III) centers, may provide coordination sites for oxygen binding and activation in the catalytic chemistry. It has been demonstrated in **6a**, a related manganese structural analog of **3**, that the chloride ligands can be replaced by water, and the water derivative has been shown to catalyze the oxidation of alkanes.⁴⁴ As the first structurally characterized iron complex with an ascorbate analog, the structure of **3** provides considerable insight into the possible coordination geometry of iron-AA complexes. A preliminary Mössbauer study of a solution sample containing a purple iron-AA complex prepared at pH 7 indicates the existence of a multinuclear mixed-valent cluster. The optical spectrum of **3** shows a band at 540 nm, a feature similar to that reported for iron-AA complexes in the literature. The lack of an organic free radical signal in the ESR spectrum may be due to the rapid relaxation or effective coupling between the radical ligands and iron.

When crystals of **3** were used to catalyze the oxidation of cyclohexane by dioxygen without excess proton source or reductant, the yield of alcohol and ketone formation was 40%, and its alcohol-to-ketone ratio was 2 to 1. When 20-fold of excess TMRA was added, the catalytic system gave a yield comparable to that of the *in situ* system with a lower selectivity for alcohol formation (cyclohexanol:cyclohexanone=7:1). These results suggest that **3** is

involved in the catalytic cycle, either directly or indirectly. It is more likely that **3** acts as a precursor from which the real active species is generated. The catalytically active species, most likely an activated oxygenating agent, can be generated by coordinating dioxygen to one of the irons after the dissociation of labile ligand chloride. In Scheme 5.7, a proposed catalytic cycle parallel to that of the cytochrome P-450 system is depicted. In this scheme, the role of the ferrous center in **3** is to maintain the trinuclear core. The reactive moiety is located at the two ferric centers. The possibility that **3** dissociates into a Fe(III)-Fe(III) dimer and a monomer prior to the oxygen activation cannot be ruled out, however. The dimer and the monomer could regenerate **3** in the presence of excess reductants, a hypothesis supported by the formation of **8**. The different distribution pattern of the reaction products of **3**, as compared to the *in situ* system, maybe attributed to the existence of some independent minor oxidation routes in which the alcohol formation is favored. These routes may utilize the mononuclear iron salt present in *in situ* preparation.



Scheme 5.7

References

- (1) *The Vitamins: Chemistry, Physiology, Pathology, Methods*; Sebrell, J., W. H.; Harris, R. S., Ed.; Academic: New York, 1967; Vol. 1.
- (2) Sharman, I. M. In *Vitamin C: Recent Aspects of Its Physiological and Technological Importance*; G. C. Birch and K. J. Parker, Ed.; Applied Science: London, 1974; pp 1-15.
- (3) Hallberg, L. In *Vitamin C (Ascorbic acid)*; J. N. Counsell and D. H. Hornig, Ed.; Applied Science: London, 1981; pp 49-61.
- (4) Gorman, J. E.; Clydesdale, F. M. *J. Food. Sci.* **1983**, *48*, 1217-1221.
- (5) Martell, A. E. In *Ascorbic Acid: Chemistry, Metabolism and uses.*; P. A. Seib and B. M. Tolbert, Ed.; American Chemical Society: Washington, D.C., 1982; pp 153-178.
- (6) Purr, A. *Biochem. J.* **1933**, *27*, 1703.
- (7) Purr, A. *Biochem. J.* **1935**, *29*, 13.
- (8) Purr, A. *Biochem. J.* **1935**, *27*, 5.
- (9) McFarlane, W. D. *Biochem. J.* **1936**, *30*, 1472.
- (10) Mawson *Biochem. J.* **1935**, *29*, 569.
- (11) Lund, L. G.; Aust, A. E. *Arch. Biochem. Biophys.* **1990**, *278*, 60-64.
- (12) Fodor, I.; Marx, J. J. M. *Biochem. Biophys. Acta* **1988**, *961*, 96-102.
- (13) Wang, Y.; Ness, B. V. *Nucleic Acid Res.* **1989**, *17*, 6915.
- (14) Pijoan, M. *Science* **1937**, *86*, 2221-2222.
- (15) Lynch, S. R.; Cook, J. D. *Ann. New York Acad. Sci.* **1980**, *355*, 32.
- (16) Conrad, M. E.; Schade, S. G. *Gastroenterology* **1968**, *55*, 35-45.
- (17) Taqui Khan, M. M.; Martell, A. E. *J. Am. Chem. Soc.* **1967**, *89*, 4176-4185.

- (18) Taqui Khan, M. M.; Martell, A. E. *J. Am. Chem. Soc.* **1967**, *89*, 7104-7111.
- (19) Stolyarov, K. P.; Amantova, I. A. *Talanta* **1967**, *14*, 1237-1244.
- (20) Laurence, G. S.; Ellis, K. J. *J. Chem. Soc., Dalton Trans.* **1972**, 1667-1670.
- (21) Kurbatova, G. T.; Kriss, E. E.; Grigor'eva, A. S. *Russ. J. Inorga. Chem.* **1981**, *26*, 982-983.
- (22) Martinez, P.; Uribe, D. Z. *Naturforsch.* **1982**, *37b*, 1446-1449.
- (23) Hamed, M. Y.; Keypour, H.; Silver, J.; Wilson, M. T. *Inorga. Chim. Acta* **1988**, *152*, 227-231.
- (24) Hughes, D. L. *J. Chem. Soc., Dalton Trans.* **1973**, 2209.
- (25) Kriss, E. E. *Rus. J. Inorga. Chem.* **1978**, *23*, 1004-1008.
- (26) Hollis, L. S.; Stern, E. W.; Amundsen, A. R.; Miller, A. V.; Doran, S. L. *J. Am. Chem. Soc.* **1987**, *109*, 3596-3602.
- (27) *TEXSAN: Single Crystal Structure Analysis Software Version 5.0*; Molecular Structure Corporation: Woodlands, TX, 1989.
- (28) Ibers, J. A.; Hamilton, W. C. *International Tables for X-ray Crystallography*; Kynoch Press: Birmingham, 1974; Vol. IV, pp 71-98.
- (29) Steward, R. F.; Davison, E. R.; Simpson, W. T. *J. Chem. Phys.* **1965**, *42*, 3175.
- (30) Semmingsen, D. *Acta Chem. Scand.* **1977**, *B31*, 81-85.
- (31) Perrin, D. D.; Armrages, W. L. F.; Perrin, D. R. *Purification of Laboratory Chemicals*; 2nd ed.; Pergamon: Oxford, 1980.
- (32) Bassett, J.; Denney, R. C.; Jeffery, G. H.; Mendham, J. *Vogel's Textbook of Quantitative Inorganic Analysis*; 4 ed.; Wiley: New York, 1978, pp 351.
- (33) Sheldrick, G. M. In *Crystallographic Computing 3*; G. M. Sheldrick, C. Krüger and R. Goddard, Ed.; Oxford University Press: Oxford, England, 1985; pp 175-189.

- (34) Day, P.; Jorgensen, C. K. *J. Chem. Soc.* **1964**, 6234.
- (35) Boone, S. R.; Purser, G. H.; Chang, H.-R.; Lowery, M. D.; Hendrickson, D. N.; Pierpont, C. G. *J. Am. Chem. Soc.* **1989**, *111*, 2292.
- (36) Christou, G. *Acc. Chem. Res.* **1989**, *22*, 328-335.
- (37) Cannon, R. D.; White, R. P. *Prog. Inorg. Chem.* **1988**, *36*, 195.
- (38) Lippard, S. J. *Angew. Chem. Int. Ed. Engl.* **1988**, *27*, 344-361.
- (39) Gorun, S. M.; Papaefthymiou, G. C.; Frankel, R. B.; Lippard, S. J. *J. Am. Chem. Soc.* **1987**, *109*, 4244.
- (40) Poganiuch, P.; Liu, S.; Papaefthymiou, G. C.; Lippard, S. J. *J. Am. Chem. Soc.* **1991**, *113*, 4645-4651.
- (41) Rardin, R. L.; Bino, A.; Poganiuch, P.; Tolman, W. B.; Liu, S.; Lippard, S. J. *Angew. Chem. Int. Ed. Engl.* **1990**, *29*, in press.
- (42) Sarneski, J. E.; Thorp, H. H.; Brudvig, G. W.; Crabtree, R. H.; Schulte, G. K. *J. Am. Chem. Soc.* **1990**, *112*, 7255-7260.
- (43) Auger, N.; Girerd, J.-J.; Corbella, M.; Gleizes, A.; Zimmermann, J.-L. *J. Am. Chem. Soc.* **1990**, *112*, 448.
- (44) Sarneski, J. E.; Michos, D.; Thorp, H. H.; Didiuk, M.; Poon, T.; Blewitt, J.; Brudvig, G. W.; Crabtree, R. H. *Tetrahedron Lett.* **1991**, *32*, 1153-1156.
- (45) Dziobkowski, C. T.; Wroblewski, J. T.; Brown, D. B. *Inorg. Chem.* **1981**, *20*, 679.
- (46) Keypour, H.; Silver, J.; Wilson, M. T.; Hamed, M. Y. *Inorg. Chim. Acta* **1986**, *125*, 97-106.
- (47) Anderson, B. F.; Webb, J.; Buckingham, D. A.; Robertson, G. B. *J. Inorg. Biochem.* **1982**, *16*, 21-32.
- (48) Funabiki, T.; Konishi, T.; TADA, S.; Yoshida, S. *Chem. Lett.* **1987**, 1803-1806.

- (49) Solbrig, R. M.; Duff, L. L.; Shriver, D. F.; Klotz, I. M. *Inorga. Biochem.* 1982, 17, 69.
- (50) Inbar, S.; Ehret, A.; Norland, K. *Abstrate of Papers; National Meeting of the Society of Photographic Sciences: Minneapolis, 1987.*
- (51) Hesse, G.; Wehling, B. *Liebigs. Ann. Chem.* 1964, 679, 100.
- (52) Roth, M. E. Thesis, Massachusetts Institute of Technology, 1988.

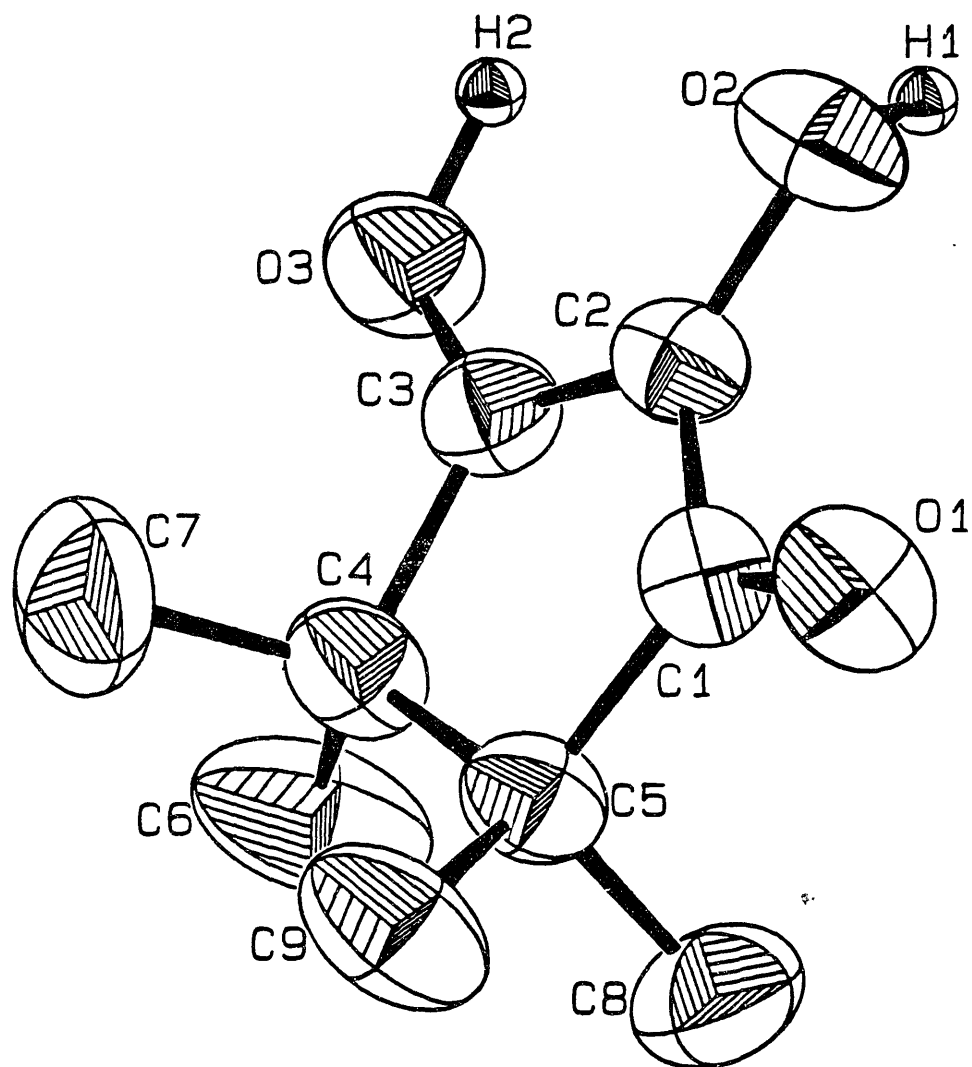


Figure 5.1a. ORTEP drawing of molecule 1 of 1 (24 °C) showing the atomic numbering scheme.

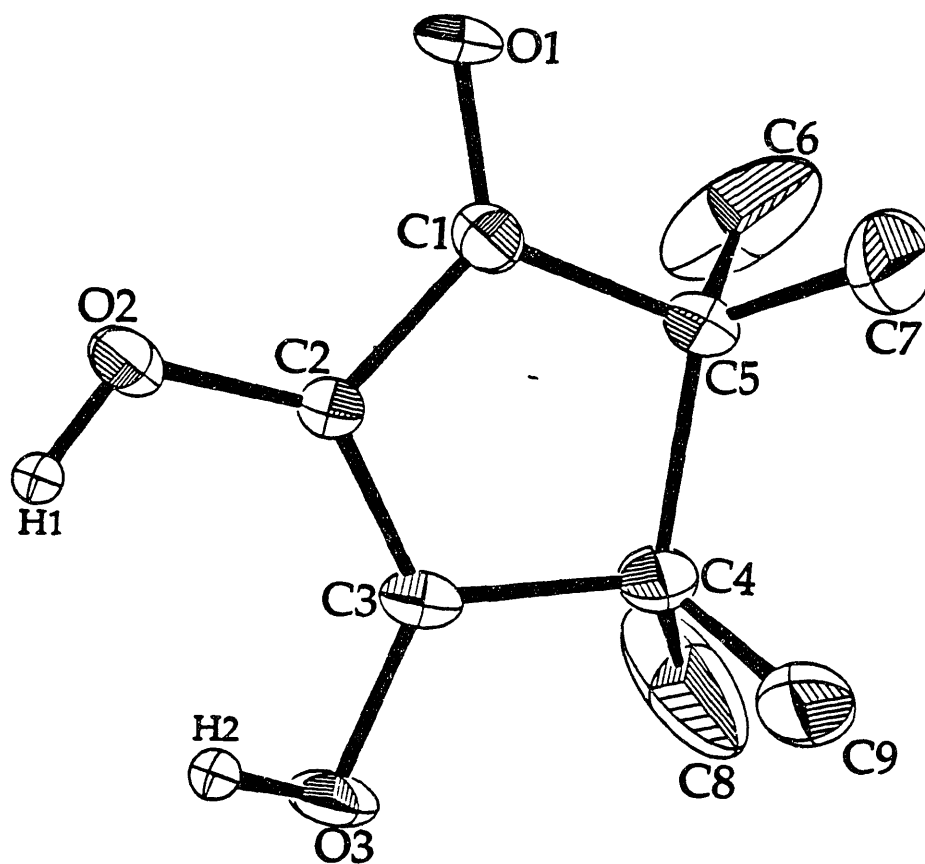


Figure 5.1b. ORTEP drawing of **1** (-78.5 °C) showing the atomic numbering scheme.

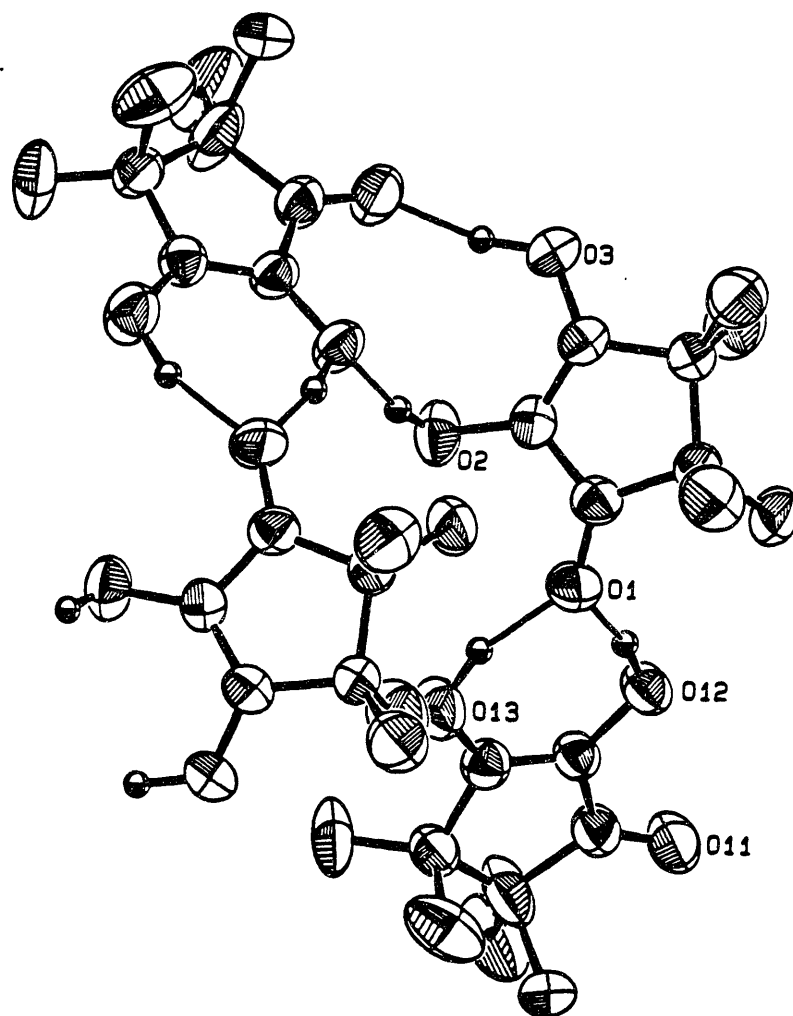


Figure 5.2a. Two asymmetric units in the structure of **1** (24 °C) showing the various modes of hydrogen bonding. Only one of two disordered sets of carbon atoms is depicted for molecule **2**.

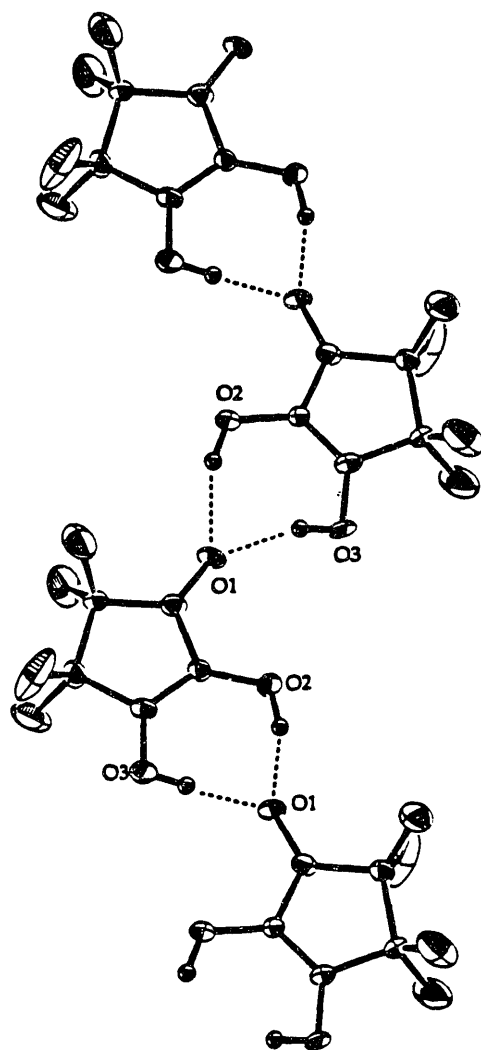


Figure 5.2b. Part of the packing diagram in the unit cell of 1-CHCl₃ showing hydrogen bonding scheme (see text for detailed discussions).

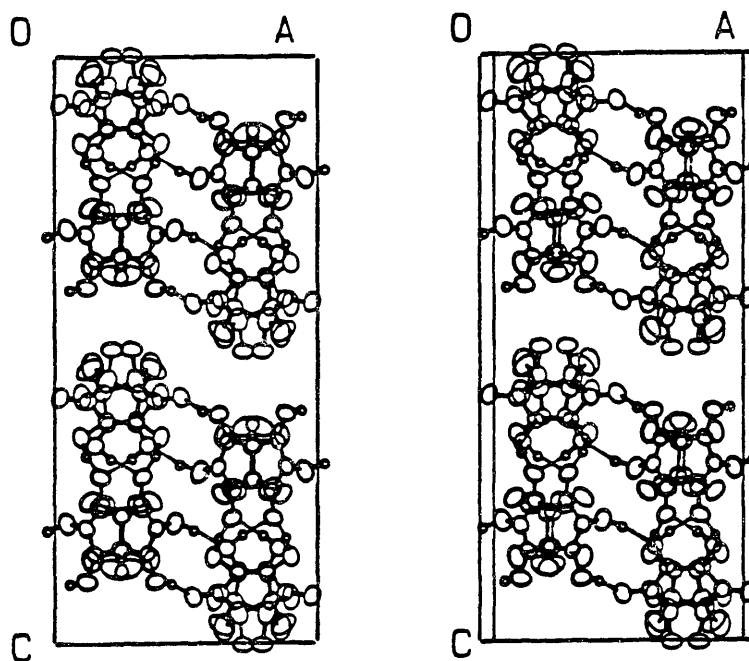


Figure 5.3a. Stereoview of the unit cell packing structure of **1** (24°C).

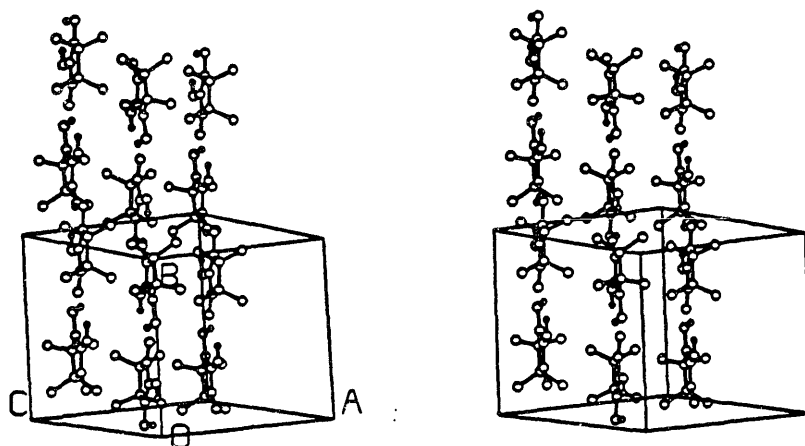


Figure 5.3b. Stereoview of the unit cell packing structure of 1 (-78 °C).

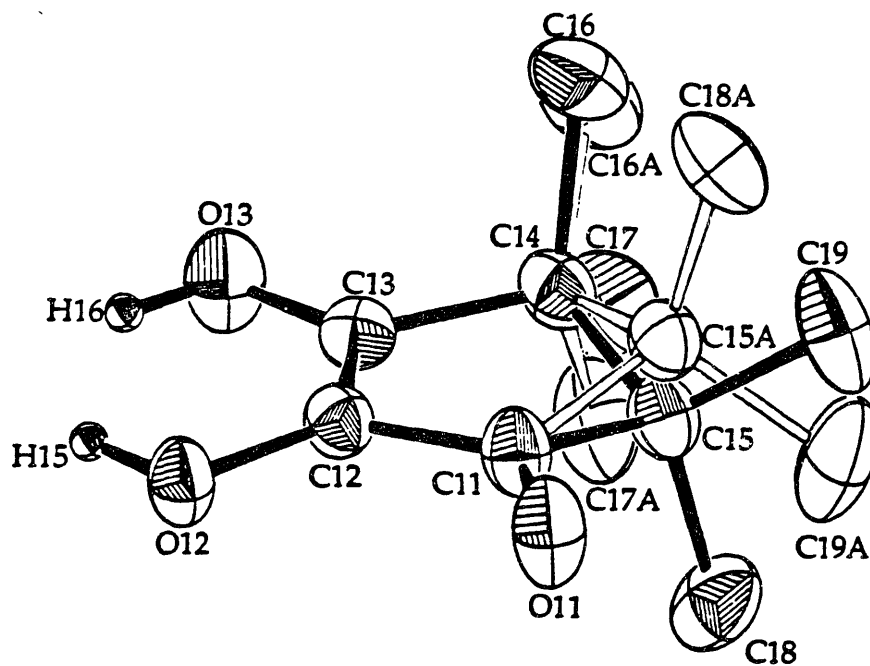


Figure 5.4. Structure of molecule 2 showing the atomic numbering scheme and the model used to define the disordered carbon atoms in the structure of 1 (24 °C).

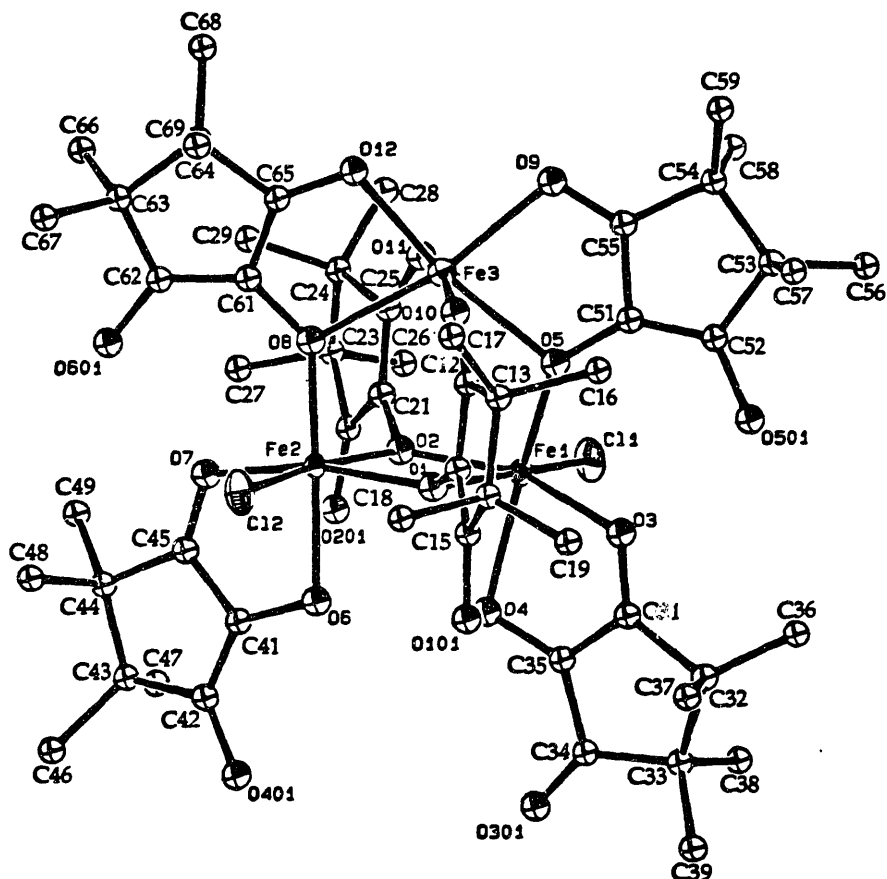


Figure 5.5a. ORTEP drawing of molecule 1 in the structure of 3 determined from the triclinic data set showing 40% probability thermal ellipsoids and atom labelling scheme for non-hydrogen atoms.

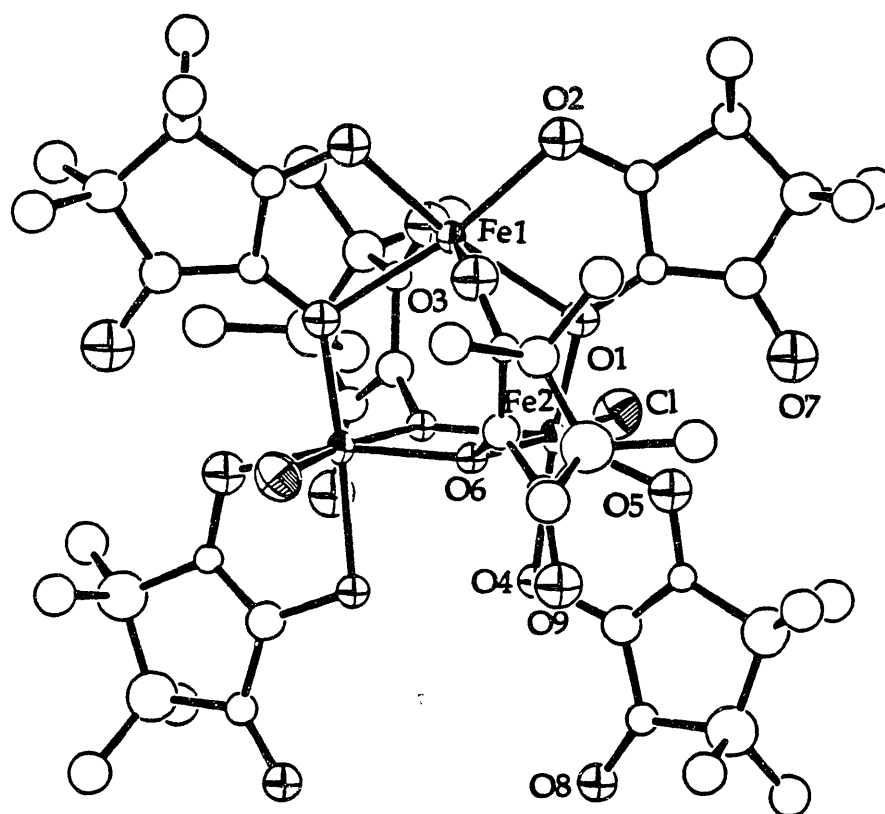


Figure 5.5b. ORTEP drawing of **3** determined from the cubic data set showing 40% probability thermal ellipsoids and atom labelling scheme for non-hydrogen atoms.

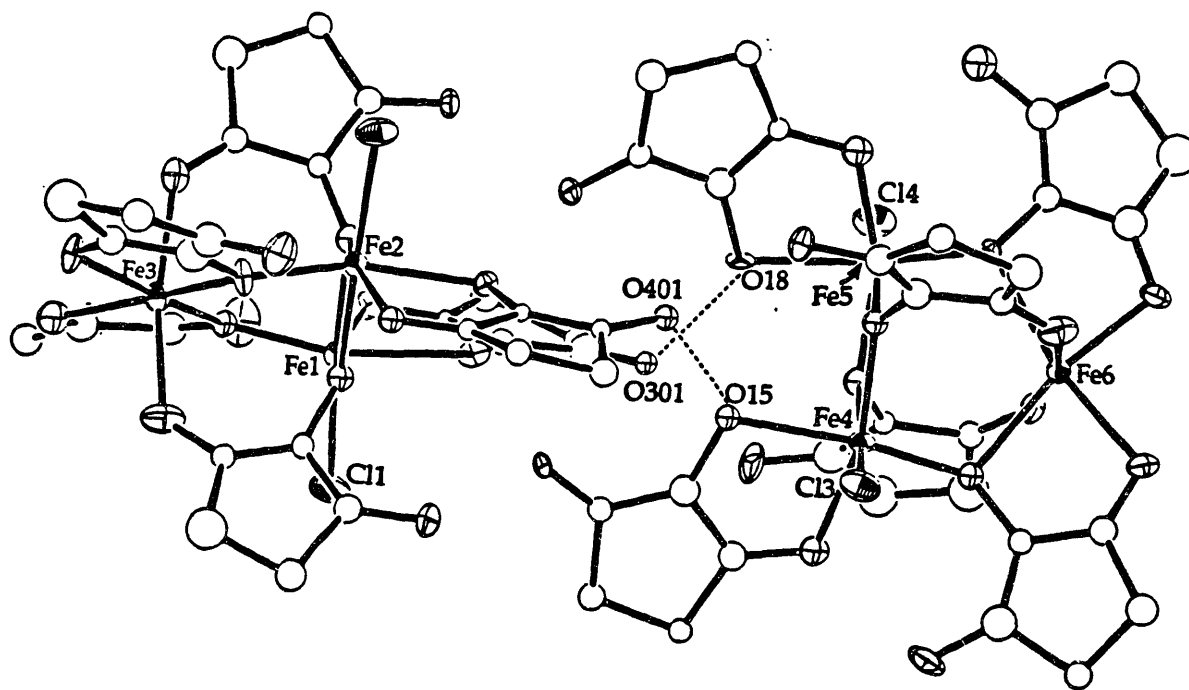


Figure 5.6. ORTEP drawing of two molecules of **3** in the triclinic unit cell showing the packing pattern and hydrogen bonding scheme.

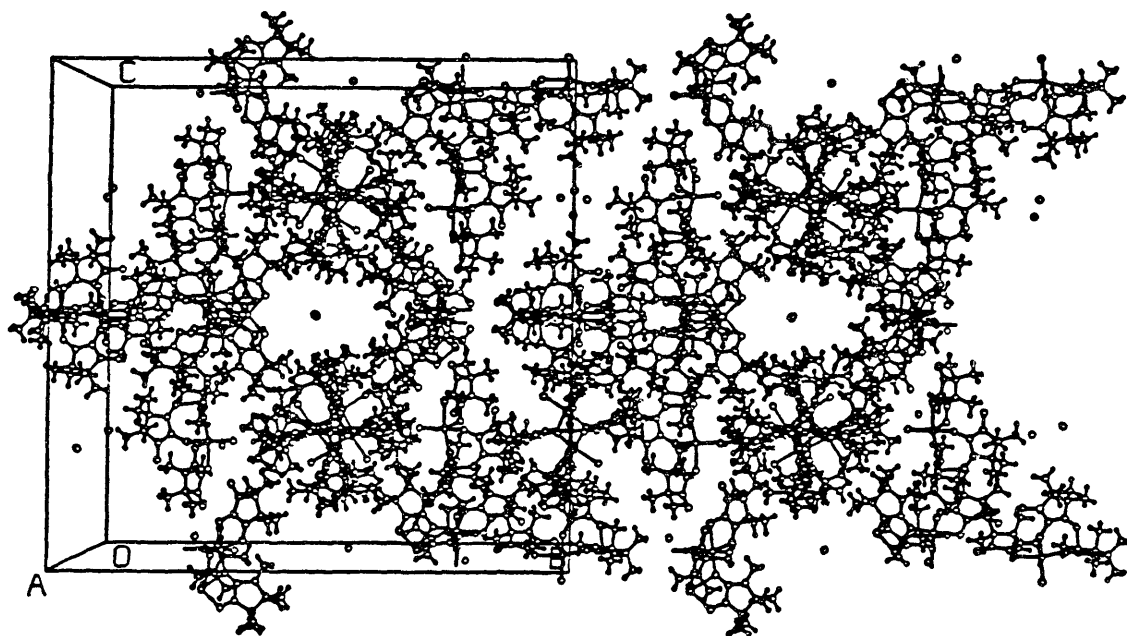


Figure 5.7. Packing diagram of 3 in the cubic unit cell.

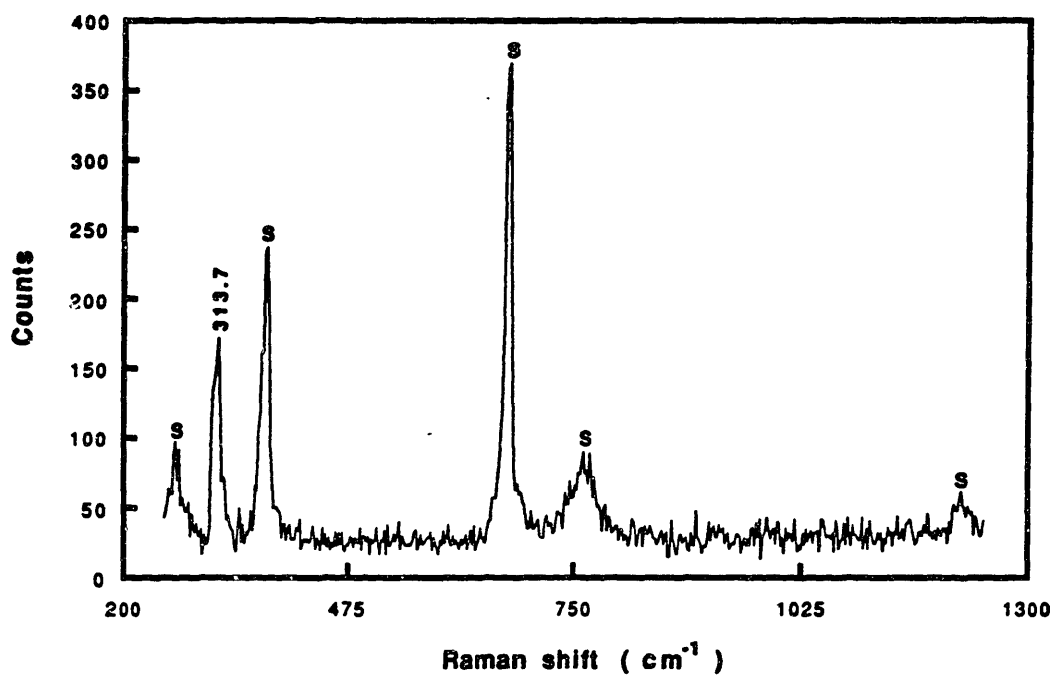


Figure 5.8. Raman spectrum of 3 in chloroform solution. Laser line with the wavelength of 406.7 nm was used and the power incidented at the sample was 60 mW. The peaks labelled as S are the solvent peaks.

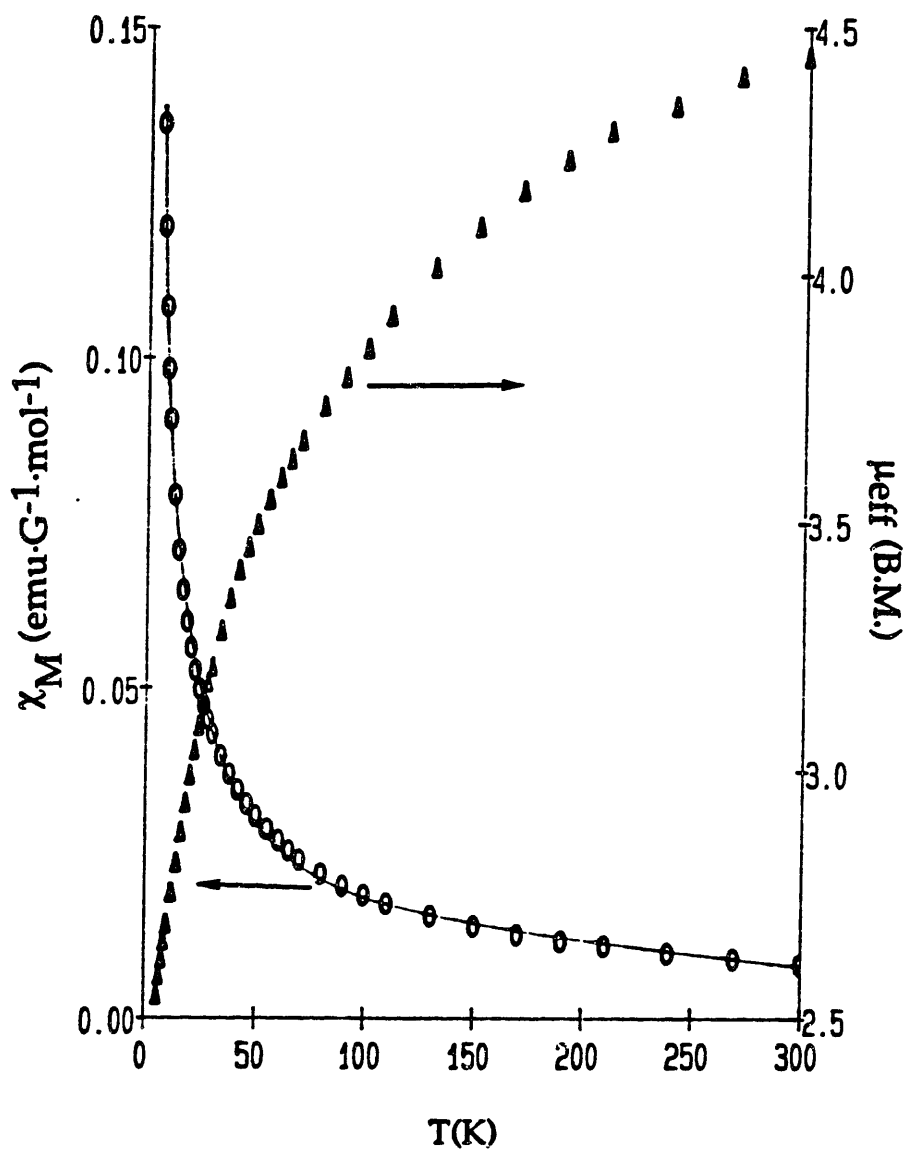


Figure 5.9. Plot of molar susceptibility (o) and effective moment (Δ) for 3.

The solid line shows the best result from the least-squares fits of eq. 5.2. to the data (see text for details).

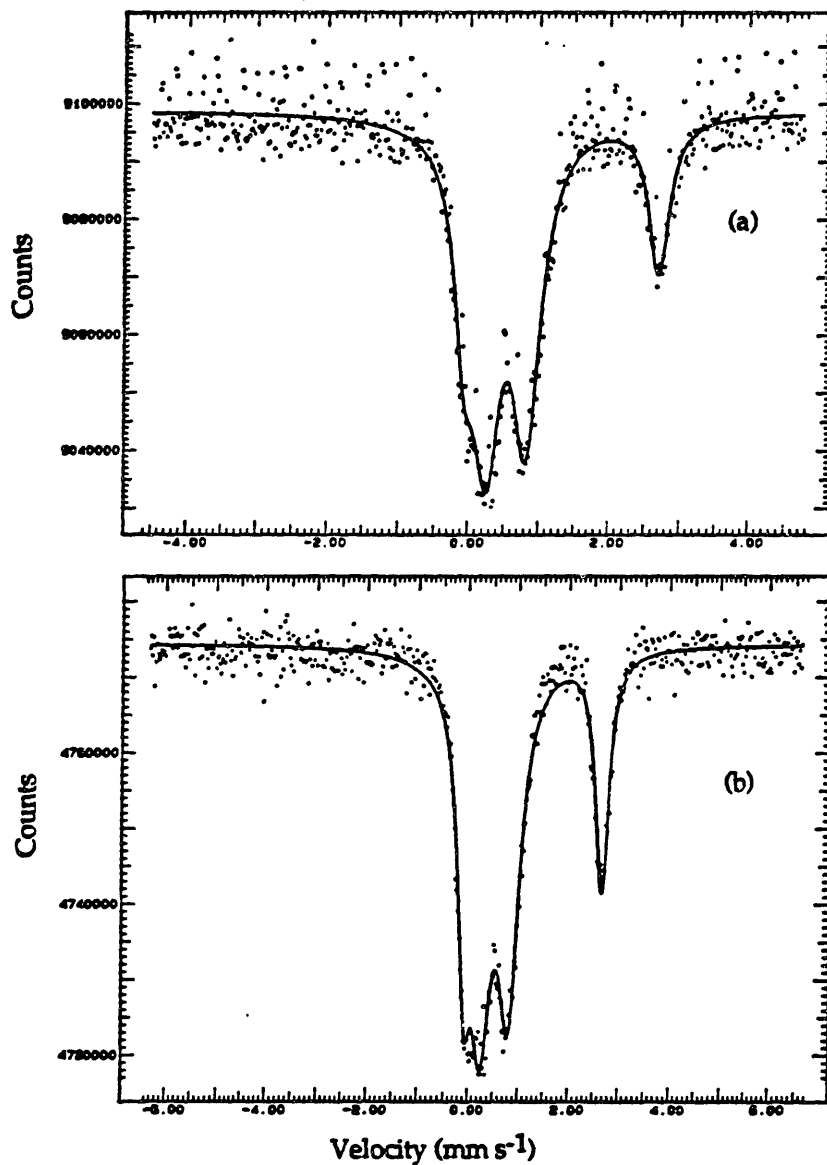


Figure 5.10. Zero field Mössbauer spectra at 80 K for (a) a solid sample and (b) a solution of 3. The solid lines are the least-squares fits to the data.

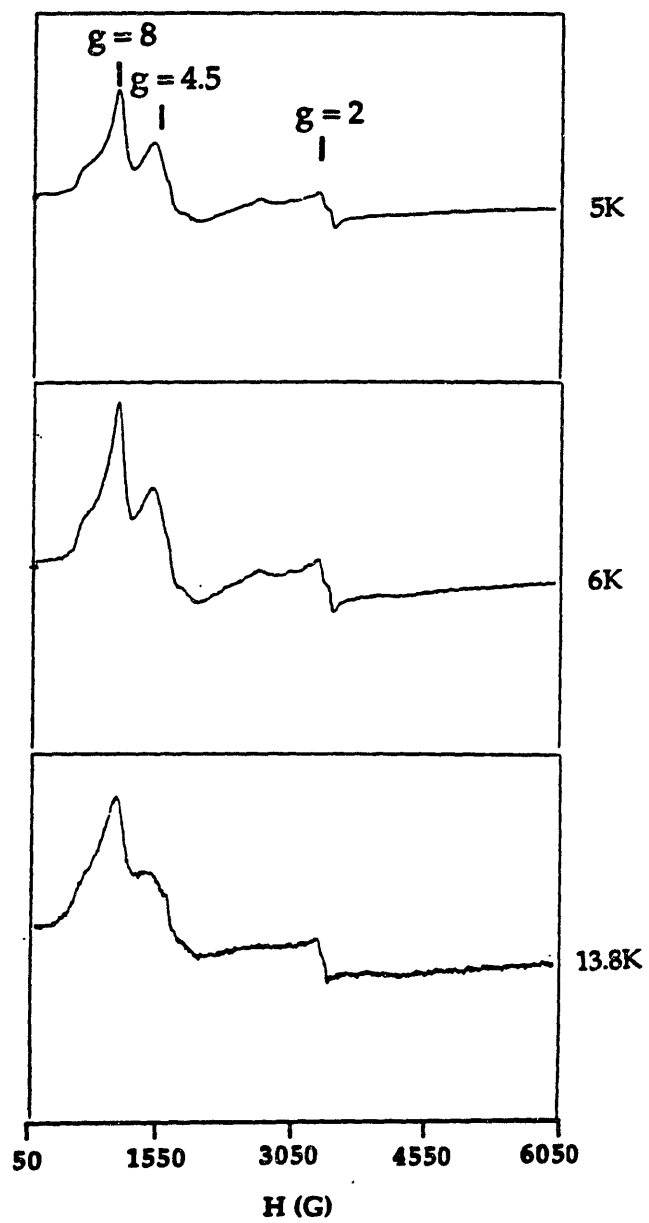


Figure 5.11. EPR spectra of 3 in frozen hexane glass at different temperatures.

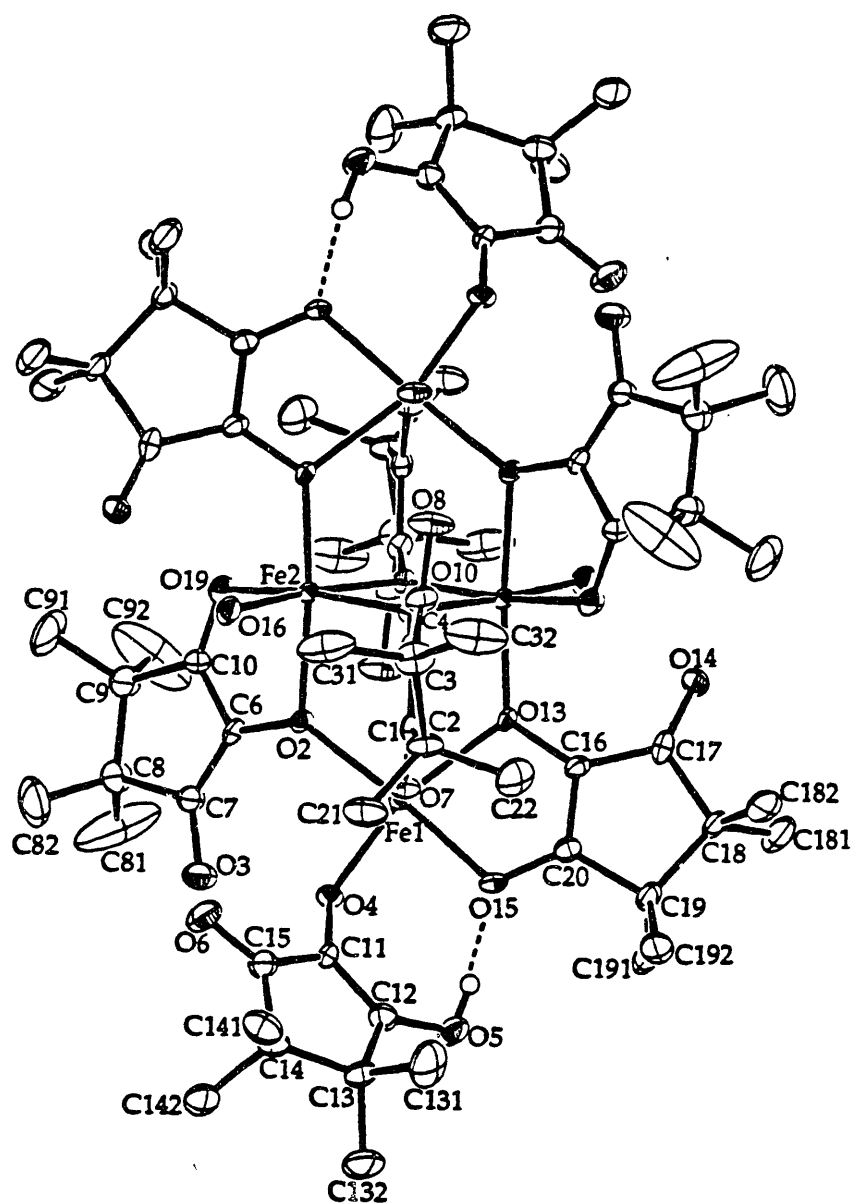


Figure 5.12. ORTEP drawing of **8** showing 40% probability thermal ellipsoids and atom labelling scheme for non-hydrogen atoms. Dotted lines indicate the intramolecular hydrogen bonds.

Table 5.1. Experimental Details of the X-ray Diffraction Studies of TMRA, 1 and TMRA·CHCl₃, 1·CHCl₃.^a

| compound | 1 | 1·CHCl ₃ |
|---|---|--|
| radiation | Cu K α ($\lambda = 1.5418 \text{ \AA}$) | Mo K α ($\lambda = 0.71069 \text{ \AA}$) |
| formula | C ₉ H ₁₄ O ₃ | C ₁₀ H ₁₅ O ₃ Cl ₃ |
| formula weight, g mol ⁻¹ | 170.21 | 289.59 |
| crystal system | orthorhombic | monoclinic |
| space group | Pbca | P2 ₁ /c |
| a, \AA | 11.651 (2) | 10.436 (4) |
| b, \AA | 12.279 (2) | 10.521 (1) |
| c, \AA | 26.257 (4) | 12.498 (5) |
| β , ° | | 102.91 (2) |
| V, \AA^3 | 3756 | 1337 |
| Z | 16 | 4 |
| temperature, °C | 24 | -70 |
| ρ_{calcd} , g cm ⁻³ | 1.204 | 1.44 |
| crystal dimensions, mm | 0.3x0.35x0.5 | 0.12x0.18x0.25 |
| transmission factor range | | 0.958 - 1.000 |
| linear absorption coefficient, cm ⁻¹ | 7.01 | 6.77 |
| 2 θ range | 2° \leq 2 θ \leq 130°, +h, +k, \pm l | 3° \leq 2 θ \leq 46°, \pm h, +k, +l |
| total no. of data collected | 4655 | 2141 |
| R _{merge} ^b | 0.015 | 0.059 |
| no. of independent data | 3627 | 1532 |

Table 5.1, contd. Experimental Details of the X-ray Diffraction Studies of
 TMRA, 1 and TMRA·CHCl₃, 1·CHCl₃.

| compound | 1 | 1·CHCl ₃ |
|------------------------------------|-------|---------------------|
| no. of unique data with F>6σ(F) | 2152 | 1443 |
| no. of variables | 278 | 145 |
| R ^c | 0.051 | 0.063 |
| R _w ^d | 0.069 | 0.084 |
| p ^d | 0.05 | 0.05 |

^a All measurements were made on an Enraf-Nonius CAD4-F diffractometer.

^b $R_{(\text{merge})} = \frac{\sum_{i=1}^n \sum_{j=1}^m | \langle F_i^2 \rangle - F_{ij}^2 |}{\sum_{i=1}^n m \times \langle F_i^2 \rangle}$ where n = numbers of unique reflections which were measured more than once during data collection, m = number of times a given reflection was measured and $\langle F_i^2 \rangle$ is the average value of F² for the reflection. ^c $R = \frac{\sum | |F_o| - |F_c| |}{\sum |F_o|}$. ^d $R_w = [\sum w (|F_o| - |F_c|)^2 / \sum w |F_o|^2]^{1/2}$, where $w = 1/\sigma^2(F)$, $\sigma^2(F) = [S^2(C+4B) + (pI)^2] / [(Lp)^2 4F^2]$ with S = scan rate, C = peak count, B = sum of left and right background counts, Lp = Lorentz-polarization factor, and p = fudge factor.

Table 5. 2a. Final Positional and Equivalent Isotropic Thermal Parameters of Non-Hydrogen Atoms in TMRA, 1 at 24 °C.^a

| Atom ^b | x | y | z | B(eq) |
|-------------------|--------|---------|--------|---------|
| O1 | 0.1719 | 0.1148 | 0.2147 | 5.08(8) |
| O2 | 0.0491 | 0.2269 | 0.2939 | 5.21(9) |
| O3 | 0.1220 | 0.1182 | 0.3922 | 5.29(9) |
| O11 | 0.4771 | 0.2304 | 0.5803 | 5.9(1) |
| O12 | 0.3480 | 0.3195 | 0.6617 | 4.56(7) |
| O13 | 0.1020 | 0.2340 | 0.6476 | 5.8(1) |
| C1 | 0.1776 | 0.0885 | 0.2606 | 3.9(1) |
| C2 | 0.1196 | 0.1397 | 0.3014 | 3.8(1) |
| C3 | 0.1539 | 0.0942 | 0.3454 | 3.8(1) |
| C4 | 0.2458 | 0.0089 | 0.3388 | 4.4(1) |
| C5 | 0.2469 | -0.0073 | 0.2798 | 4.1(1) |
| C6 | 0.2234 | -0.0914 | 0.3705 | 7.8(2) |
| C7 | 0.3596 | 0.0640 | 0.3569 | 8.1(2) |
| C8 | 0.1796 | -0.1091 | 0.2638 | 6.9(2) |
| C9 | 0.3659 | -0.0115 | 0.2550 | 6.2(1) |
| C11 | 0.3727 | 0.2125 | 0.5857 | 4.4(1) |
| C12 | 0.3023 | 0.2539 | 0.6250 | 3.70(9) |
| C13 | 0.1945 | 0.2166 | 0.6189 | 3.9(1) |
| C14 | 0.1813 | 0.1466 | 0.5723 | 4.4(1) |
| C15 | 0.3089 | 0.1208 | 0.5587 | 4.2(2) |
| C15A | 0.2971 | 0.1595 | 0.5441 | 4.2(2) |
| C16A | 0.0748 | 0.1685 | 0.5417 | 7.5(4) |
| C16 | 0.1270 | 0.2270 | 0.5321 | 8.3(5) |
| C17 | 0.1013 | 0.0539 | 0.5782 | 7.1(4) |
| C17A | 0.1603 | 0.0296 | 0.5947 | 7.2(4) |
| C18 | 0.3453 | 0.0112 | 0.5812 | 6.3(3) |
| C18A | 0.2854 | 0.2379 | 0.4982 | 6.1(3) |
| C19A | 0.3578 | 0.0565 | 0.5263 | 8.0(5) |
| C19 | 0.3394 | 0.1241 | 0.5022 | 7.8(5) |

^aNumbers in parentheses are errors in the last significant digit. ^bSee Figure 5.1a for atom labelling scheme. C15A, C16A,, C19A are disordered carbon atoms on the ring with an occupancy of 0.5.

Table 5.2b. Final Positional and Equivalent Isotropic Thermal Parameters of Non-Hydrogen Atoms in TMRA·CHCl₃, 1·CHCl₃ at -70 °C.^a

| Atom ^b | x | y | z | B(eq) |
|-------------------|-----------|-----------|------------|--------|
| O1 | 0.5347(4) | 0.9067(3) | -0.1933(3) | 3.2(2) |
| O2 | 0.4501(3) | 0.6633(3) | -0.2784(3) | 2.5(1) |
| O3 | 0.6321(3) | 0.4717(3) | -0.1304(3) | 3.1(2) |
| C1 | 0.8013(5) | 0.2126(6) | 0.2037(5) | 3.6(3) |
| C2 | 0.5879(5) | 0.8063(5) | -0.1510(4) | 2.2(2) |
| C3 | 0.5518(4) | 0.6816(4) | -0.1892(4) | 1.9(2) |
| C4 | 0.6299(5) | 0.5976(5) | -0.1234(4) | 2.2(2) |
| C5 | 0.7246(5) | 0.6577(5) | -0.0286(4) | 3.0(2) |
| C6 | 0.6987(5) | 0.8040(5) | -0.0509(4) | 2.5(2) |
| C7 | 0.6530(8) | 0.8719(7) | 0.0422(5) | 5.9(4) |
| C8 | 0.8144(7) | 0.8752(9) | -0.0775(7) | 7.8(4) |
| C9 | 0.8623(7) | 0.6130(8) | -0.0260(8) | 8.5(5) |
| C10 | 0.686(1) | 0.6149(7) | 0.0789(5) | 7.5(4) |
| Cl1 | 0.9010(2) | 0.0786(2) | 0.2257(2) | 6.1(1) |
| Cl2 | 0.8947(2) | 0.1583(2) | 0.7726(2) | 6.7(1) |
| Cl3 | 0.7449(2) | 0.2451(2) | 0.0663(2) | 5.9(1) |

^aNumbers in parentheses are errors in the last significant digit. ^bSee Figure 5.1b for atom labelling scheme.

Table 5.3a. Final Thermal Parameters of Non-Hydrogen Atoms for
TMRA, 1 at 24 °C.^a

| Atom | U ₁₁ | U ₂₂ | U ₃₃ | U ₁₂ | U ₁₃ | U ₂₃ |
|------|-----------------|-----------------|-----------------|-----------------|-----------------|-----------------|
| O1 | 0.067(1) | 0.079(1) | 0.048(1) | 0.0081(9) | 0.0081(8) | 0.0178(8) |
| O2 | 0.059(1) | 0.052(1) | 0.087(1) | 0.0128(8) | 0.012(1) | 0.0151(9) |
| O3 | 0.073(1) | 0.080(1) | 0.048(1) | 0.022(1) | 0.0050(8) | -0.0062(9) |
| O11 | 0.056(1) | 0.097(1) | 0.073(1) | -0.017(1) | 0.0121(9) | -0.035(1) |
| O12 | 0.052(1) | 0.067(1) | 0.055(1) | -0.0047(8) | 0.0007(7) | -0.0198(8) |
| O13 | 0.052(1) | 0.091(1) | 0.077(1) | -0.010(1) | 0.0069(9) | -0.024(1) |
| C1 | 0.046(1) | 0.052(1) | 0.049(1) | -0.003(1) | 0.004(1) | 0.006(1) |
| C2 | 0.044(1) | 0.042(1) | 0.057(1) | 0.000(1) | 0.006(1) | 0.005(1) |
| C3 | 0.047(1) | 0.048(1) | 0.049(1) | -0.001(1) | 0.008(1) | -0.002(1) |
| C4 | 0.057(1) | 0.062(1) | 0.047(1) | 0.015(1) | 0.003(1) | 0.003(1) |
| C5 | 0.055(1) | 0.052(1) | 0.048(1) | 0.007(1) | 0.007(1) | 0.003(1) |
| C6 | 0.147(4) | 0.081(2) | 0.069(2) | 0.044(3) | 0.030(2) | 0.027(2) |
| C7 | 0.057(2) | 0.152(4) | 0.098(3) | 0.023(2) | -0.021(2) | -0.042(3) |
| C8 | 0.116(3) | 0.051(2) | 0.095(2) | 0.002(2) | -0.021(2) | -0.010(1) |
| C9 | 0.071(2) | 0.095(2) | 0.070(2) | 0.033(2) | 0.021(1) | 0.018(2) |
| C11 | 0.055(1) | 0.058(1) | 0.055(1) | -0.010(1) | 0.003(1) | -0.013(1) |
| C12 | 0.051(1) | 0.045(1) | 0.045(1) | -0.004(1) | -0.002(1) | -0.0041(9) |
| C13 | 0.049(1) | 0.047(1) | 0.051(1) | -0.002(1) | -0.001(1) | 0.003(1) |
| C14 | 0.057(1) | 0.059(1) | 0.052(1) | -0.008(1) | -0.011(1) | -0.004(1) |
| C15 | 0.056(3) | 0.054(3) | 0.049(3) | -0.011(2) | -0.001(2) | -0.009(3) |
| C15A | 0.059(3) | 0.049(3) | 0.052(3) | -0.005(2) | -0.002(2) | -0.007(3) |
| C16A | 0.070(4) | 0.143(8) | 0.071(5) | -0.015(4) | -0.015(3) | -0.005(5) |
| C16 | 0.127(7) | 0.104(6) | 0.086(5) | 0.024(6) | -0.054(5) | -0.012(4) |
| C17 | 0.066(4) | 0.084(5) | 0.118(6) | -0.028(4) | -0.007(4) | -0.009(4) |
| C17A | 0.148(7) | 0.050(3) | 0.077(4) | -0.035(4) | 0.014(5) | -0.009(3) |
| C18 | 0.078(4) | 0.047(3) | 0.112(5) | 0.002(3) | -0.011(4) | -0.018(3) |
| C18A | 0.089(4) | 0.095(5) | 0.048(3) | -0.024(4) | -0.000(3) | 0.007(3) |
| C19A | 0.086(5) | 0.082(5) | 0.136(7) | 0.001(4) | 0.003(5) | -0.055(6) |
| C19 | 0.099(6) | 0.133(8) | 0.064(4) | -0.035(5) | 0.004(4) | -0.043(5) |

^aSee footnote a and b in Table 5.2a. The anisotropic temperature factors are of the form $\exp[-2\pi^2(U_{11}h^2a^2 + 2U_{12}hka^*b^* + \dots)]$.

Table 5.3b. Final Thermal Parameters of Non-Hydrogen Atoms for
TMRA, C₉O₃H₁₄·CHCl₃, 1·CHCl₃ at -70 °C.^a

| Atom | U ₁₁ | U ₂₂ | U ₃₃ | U ₁₂ | U ₁₃ | U ₂₃ |
|------|-----------------|-----------------|-----------------|-----------------|-----------------|-----------------|
| O1 | 0.061(2) | 0.012(2) | 0.042(2) | 0.004(2) | -0.000(2) | 0.004(2) |
| O2 | 0.037(2) | 0.018(2) | 0.035(2) | 0.002(2) | -0.002(2) | -0.004(2) |
| O3 | 0.044(2) | 0.013(2) | 0.053(2) | 0.008(2) | -0.007(2) | 0.001(2) |
| C1 | 0.040(3) | 0.029(3) | 0.069(4) | -0.002(3) | 0.014(3) | -0.004(3) |
| C2 | 0.039(3) | 0.020(3) | 0.026(3) | -0.002(2) | 0.009(2) | -0.002(2) |
| C3 | 0.028(2) | 0.018(3) | 0.023(2) | 0.003(2) | 0.004(2) | -0.000(2) |
| C4 | 0.030(3) | 0.018(3) | 0.034(3) | 0.004(2) | 0.009(2) | 0.003(2) |
| C5 | 0.043(3) | 0.024(3) | 0.038(3) | 0.012(2) | -0.008(2) | -0.001(2) |
| C6 | 0.042(3) | 0.018(3) | 0.032(3) | -0.003(2) | 0.003(2) | -0.001(2) |
| C7 | 0.122(6) | 0.055(5) | 0.040(4) | 0.029(5) | 0.000(4) | -0.012(3) |
| C8 | 0.054(4) | 0.113(7) | 0.108(7) | -0.040(5) | -0.024(4) | 0.074(6) |
| C9 | 0.051(4) | 0.081(6) | 0.160(9) | 0.020(4) | -0.038(5) | -0.073(6) |
| C10 | 0.20(1) | 0.034(4) | 0.040(4) | -0.016(5) | 0.007(5) | 0.008(3) |
| Cl1 | 0.087(1) | 0.046(1) | 0.088(1) | 0.019(1) | -0.002(1) | -0.004(1) |
| Cl2 | 0.101(2) | 0.051(1) | 0.095(2) | 0.019(1) | 0.003(1) | 0.027(1) |
| Cl3 | 0.104(1) | 0.041(1) | 0.067(1) | -0.002(1) | -0.005(1) | 0.0094(9) |

^aSee footnote a and b for table 5.2b. The anisotropic temperature factors are of the form $\exp[-2\pi^2(U_{11}h^2a^2 + 2U_{12}hka^*b^* + \dots)]$.

Table 5.4a. Selected Interatomic Distances (Å) and angles (°) for TMRA, 1
at 24 °C.^a

| Molecule 1 | | Molecule 2 | |
|---------------------|----------|----------------|----------|
| <u>Bond Lengths</u> | | | |
| Atoms | Distance | Atoms | Distance |
| O(1)--C(1) | 1.251(3) | O(11)--C(11) | 1.243(3) |
| O(2)--C(2) | 1.363(3) | O(12)--C(12) | 1.365(3) |
| O(3)--C(3) | 1.318(3) | O(13)--C(13) | 1.333(3) |
| C(1)--C(2) | 1.413(3) | C(11)--C(12) | 1.414(4) |
| C(1)--C(5) | 1.514(3) | C(11)--C(15) | 1.525(9) |
| | | C(11)-C(15A) | 1.55(1) |
| C(2)--C(3) | 1.345(3) | C(12)--C(13) | 1.346(3) |
| C(3)--C(4) | 1.507(3) | C(13)--C(14) | 1.503(3) |
| C(4)--C(5) | 1.563(4) | C(14)--C(15) | 1.56(1) |
| | | C(14)-C(15A) | 1.55(1) |
| C(4)--C(6) | 1.509(4) | C(14)--C(16) | 1.577(9) |
| | | C(14)-C(16A) | 1.502(9) |
| C(4)--C(7) | 1.563(5) | C(14)--C(17) | 1.479(9) |
| | | C(14)-C(17A) | 1.573(8) |
| C(5)--C(8) | 1.534(4) | C(15)--C(18) | 1.53(1) |
| | | C(15A)--C(18A) | 1.55(1) |
| C(5)--C(9) | 1.532(4) | C(15A)--C(19A) | 1.52(1) |
| | | C(15)--C(19) | 1.53(1) |
| O(2)--H(1) | 0.89(4) | O(12)--H(15) | 0.83(3) |
| O(3)--H(2) | 0.96(4) | O(13)--H(16) | 0.84(4) |
| O(1)···O(12) | 2.606(3) | O(11)···O(3) | 2.612(3) |
| O(1)···O(13) | 2.685(3) | O(12)···O(2) | 2.677(3) |

Table 5.4a, contd. Selected Interatomic Distances (Å) and angles (°) for
TMRA, 1 at 24 °C.

| Molecule 1 | | Molecule 2 | |
|--------------------|----------|---------------------|----------|
| <u>Bond Angles</u> | | | |
| O(1)-C(1)-C(2) | 126.2(2) | O(11)-C(11)-C(12) | 125.9(2) |
| O(1)-C(1)-C(5) | 123.4(2) | O(11)-C(11)-C(15) | 123.7(4) |
| | | O(11)-C(11)-C(15A) | 123.5(4) |
| C(2)-C(1)-C(5) | 110.4(2) | C(12)-C(11)-C(15) | 108.8(4) |
| | | C(12)-C(11)-C(15A) | 109.6(4) |
| O(2)-C(2)-C(1) | 121.9(2) | O(12)-C(12)-C(11) | 120.1(2) |
| O(2)-C(2)-C(3) | 129.0(2) | O(12)-C(12)-C(13) | 130.5(2) |
| C(1)-C(2)-C(3) | 108.9(2) | C(11)-C(12)-C(13) | 109.4(2) |
| O(3)-C(3)-C(2) | 128.6(2) | O(13)-C(13)-C(12) | 129.2(2) |
| O(3)-C(3)-C(4) | 117.6(2) | O(13)-C(13)-C(14) | 118.0(2) |
| C(2)-C(3)-C(4) | 113.7(2) | C(12)-C(13)-C(14) | 112.8(2) |
| C(3)-C(4)-C(5) | 102.0(2) | C(13)-C(14)-C(15) | 101.8(4) |
| | | C(13)-C(14)-C(15A) | 103.9(4) |
| C(3)-C(4)-C(6) | 112.4(2) | C(13)-C(14)-C(16) | 103.2(4) |
| | | C(13)-C(14)-C(16A) | 114.7(4) |
| C(3)-C(4)-C(7) | 105.6(2) | C(13)-C(14)-C(17) | 114.8(4) |
| | | C(13)-C(14)-C(17A) | 103.5(3) |
| C(5)-C(4)-C(6) | 116.3(2) | C(15)-C(14)-C(16) | 110.8(5) |
| | | C(15A)-C(14)-C(16A) | 116.6(5) |
| C(5)-C(4)-C(7) | 110.4(2) | C(15)-C(14)-C(17) | 117.8(5) |
| | | C(15A)-C(14)-C(17A) | 114.1(5) |
| C(6)-C(4)-C(7) | 109.4(3) | C(16)-C(14)-C(17) | 107.5(6) |
| | | C(16A)-C(14)-C(17A) | 103.7(6) |
| C(1)-C(5)-C(4) | 103.1(2) | C(11)-C(15)-C(14) | 102.0(5) |
| | | C(11)-C(15A)-C(14) | 101.8(6) |
| C(1)-C(5)-C(8) | 105.6(2) | C(11)-C(15)-C(18) | 109.6(6) |
| | | C(11)-C(15A)-C(18A) | 109.7(6) |

Table 5.4a, contd. Selected Interatomic Distances (Å) and angles (°) for
TMRA, 1 at 24 °C.

| Molecule 1 | | Molecule 2 | |
|---------------------------|----------|----------------------|----------|
| <u>Bond Angles, contd</u> | | | |
| C(1)-C(5)-C(9) | 111.5(2) | C(11)-C(15)-C(19) | 108.6(6) |
| | | C(11)-C(15A)-C(19A) | 107.5(7) |
| C(4)-C(5)-C(8) | 111.8(2) | C(14)-C(15)-C(18) | 110.7(6) |
| | | C(14)-C(15A)-C(18A) | 111.0(6) |
| C(4)-C(5)-C(9) | 115.7(2) | C(14)-C(15)-C(19) | 115.9(7) |
| | | C(14)-C(15A)-C(19A) | 117.9(7) |
| C(8)-C(5)-C(9) | 108.6(2) | C(18)-C(15)-C(19) | 109.6(8) |
| | | C(18A)-C(15A)-C(19A) | 108.5(8) |

^a Numbers in parentheses are errors in the last significant digit(s). See Figure 5.1a for atom labelling scheme.

Table 5.4b. Selected Interatomic Distances (Å) and angles (°) for
 TMRA·CHCl₃ (C₉O₃H₁₄·CHCl₃), 1·CHCl₃ at -70 °C.^a

| <u>Bond Lengths</u> | | | |
|---------------------|----------|----------------|----------|
| Atoms | Distance | Atoms | Distance |
| O(1)--C(1) | 1.254(6) | | |
| O(2)--C(2) | 1.370(5) | O(3)--C(3) | 1.328(6) |
| C(1)--C(2) | 1.418(7) | C(1)--C(5) | 1.502(7) |
| C(2)--C(3) | 1.350(7) | C(3)--C(4) | 1.503(7) |
| C(4)--C(5) | 1.577(8) | | |
| C(4)--C(8) | 1.506(9) | C(4)--C(9) | 1.551(9) |
| C(5)--C(6) | 1.530(9) | C(5)--C(7) | 1.519(8) |
| O(2)--H(1) | 0.891 | O(3)--H(2) | 0.898 |
| <u>Bond Angles</u> | | | |
| Atoms | Angles | Atoms | Angles |
| O(1)-C(1)-C(2) | 125.4(4) | O(1)-C(1)-C(5) | 123.4(4) |
| O(2)-C(2)-C(1) | 120.2(4) | O(2)-C(2)-C(3) | 131.0(4) |
| O(3)-C(3)-C(2) | 129.1(5) | O(3)-C(3)-C(4) | 117.0(4) |
| C(2)-C(1)-C(5) | 111.2(4) | C(1)-C(2)-C(3) | 108.8(4) |
| C(2)-C(3)-C(4) | 113.9(4) | C(3)-C(4)-C(5) | 102.4(4) |
| C(3)-C(4)-C(8) | 110.0(5) | C(3)-C(4)-C(9) | 108.0(5) |
| C(5)-C(4)-C(8) | 115.7(6) | C(5)-C(4)-C(9) | 111.7(5) |
| C(8)-C(4)-C(9) | 108.6(7) | C(1)-C(5)-C(4) | 103.2(4) |
| C(1)-C(5)-C(6) | 108.2(5) | C(1)-C(5)-C(7) | 108.2(4) |
| C(4)-C(5)-C(6) | 113.0(5) | C(4)-C(5)-C(7) | 114.0(5) |
| C(6)-C(5)-C(7) | 109.5(6) | | |

^aNumbers in parentheses are errors in the last significant digit(s). See Figure 5.1b for atom labelling scheme.

Table 5.5. Deviations (Å) of Non-hydrogen Atoms From the Least-squares Planes Through Different Parts of the Molecules of TMRA, 1.^a

| <u>TMRA, 1 (24 °C)</u> | | | | | | |
|---|------------|-----------|------|------------|-----------|-----------|
| | Molecule 1 | | | Molecule 2 | | |
| C1 | 0.0543 | -0.0315 | C11 | -0.0324 | 0.0352 | -0.0033 |
| C2 | -0.0119 | -0.0270 | C12 | 0.0030 | -0.0159 | -0.0078 |
| C3 | -0.0342 | -0.0023 | C13 | 0.0210 | -0.0015 | -0.0064 |
| C4 | 0.0897 | (0.0864) | C14 | -0.0434 | 0.0211 | (-0.0427) |
| C5 | -0.0834 | (-0.1679) | C15 | 0.2974 | | (0.3360) |
| | | | C15A | | -0.2018 | (-0.2889) |
| O1 | (0.1730) | 0.0304 | O11 | (-0.0444) | (0.0490) | 0.0085 |
| O2 | (0.0556) | (0.0539) | O12 | (0.0335) | (-0.0493) | (0.0073) |
| O3 | (-0.0823) | 0.0206 | O13 | (0.0747) | (-0.0160) | 0.0105 |
| <u>TMRA .CHCl₃, 1-CHCl₃</u> | | | | | | |
| C1 | | -0.0036 | | | 0.0017 | |
| C2 | | -0.0085 | | | -0.0071 | |
| C3 | | 0.0179 | | | -0.0111 | |
| C4 | | -0.0267 | | | (-0.0760) | |
| C5 | | 0.0164 | | | (-0.0087) | |
| O1 | | (-0.0272) | | | 0.0036 | |
| O2 | | (-0.0578) | | | (-0.0314) | |
| O3 | | (0.0516) | | | 0.0086 | |

^aDeviations of atoms which do not define the plane are listed in parentheses. See Figure 5.1a and b for atom labelling scheme.

Table 5.6 Experimental Details of the X-ray Diffraction Studies of
 $[\text{Fe}_3\text{Cl}_2(\text{C}_9\text{H}_{12}\text{O}_3)_4(\text{C}_9\text{H}_{13}\text{O}_3)_2]$, **3**.^a

| compound | 3·2CH ₃ CN | 3 |
|---|--|---|
| formula | Fe ₃ Cl ₂ O ₁₈ C ₅₈ N ₂ H ₈₀ | Fe ₃ Cl ₂ O ₁₈ C ₅₄ H ₇₄ |
| formula weight, g mol ⁻¹ | 1331.83 | 1249.63 |
| crystal system | triclinic | cubic |
| space group | P $\bar{1}$ | I $\bar{4}3d$ |
| a, Å | 19.106(3) | 37.631(8) |
| b, Å | 24.794(4) | |
| c, Å | 15.085(3) | |
| α , ° | 107.31(2) | |
| β , ° | 91.96(1) | |
| γ , ° | 79.58(1) | |
| V, Å ³ | 6708 | 53289 |
| Z | 4 | 24 |
| temperature, °C | -78 | -79 |
| ρ_{calcd} , g cm ⁻³ | 1.295 | 0.934 |
| linear absorption coefficient, cm ⁻¹ | 7.81 | 5.87 |
| 2 θ range | 4° ≤ 2 θ ≤ 44°, +h, ±k, ±l | 2° ≤ 2 θ ≤ 45°, +h,+k,+l h+k+l=2n, h>k>l |
| total no. of data collected | 16928 | 3493 |
| R _{merge} ^b | 0.177 | 1.067 |
| no. of independent data | 16322 | 3296 |

Table 5.6, contd. Experimental Details of the X-ray Diffraction Studies of
 $[\text{Fe}_3\text{Cl}_2(\text{C}_9\text{H}_{12}\text{O}_3)_4(\text{C}_9\text{H}_{13}\text{O}_3)_2]$, **3**.

| compound | 3·2CH ₃ CN | 3 |
|--------------------------------------|-----------------------|-------|
| no. of unique data with F > 6σ(F) | 7714 | 1001 |
| no. of variables | 685 | 168 |
| R ^c | 0.118 | 0.101 |
| R _w ^d | 0.151 | 0.121 |
| p ^d | 0.05 | 0.05 |

^a All measurements were made on an Enraf-Nonius CAD4-F diffractometer with Mo Kα radiation (λ = 0.70926 Å). ^{b-d} See corresponding footnotes of Table 5.1.

Table 5.7 Experimental Details of the X-ray Diffraction Study of
 (BzPh₃P)[FeBr₄]·[BzPh₃PBr], 7·BzPh₃Br.^a

| compound | 7·BzPh ₃ Br |
|---|--|
| formula | FeBr ₅ P ₂ C ₅₀ H ₄₄ |
| formula weight, g mol ⁻¹ | 1162.34 |
| crystal system | triclinic |
| space group | P $\bar{1}$ |
| a, Å | 9.980(1) |
| b, Å | 13.245(1) |
| c, Å | 19.337(2) |
| α , ° | 98.550(9) |
| β , ° | 103.90(1) |
| γ , ° | 102.077(9) |
| V, Å ³ | 2372 |
| Z | 2 |
| temperature, °C | -78 |
| ρ_{calcd} , g cm ⁻³ | 1.627 |
| linear absorption coefficient, cm ⁻¹ | 45.87 |
| 2 θ range | 3° ≤ 2 θ ≤ 47° |
| total no. of data collected | 7314 |
| R _{merge} | 0.026 |
| no. of independent data | 6984 |

Table 5.7, contd. Experimental Details of the X-ray Diffraction Study of
(BzPh₃P)[FeBr₄]·[BzPh₃PBr], 7·BzPh₃Br.

| compound | 7·BzPh ₃ Br |
|--|------------------------|
| no. of unique data with $F > 6\sigma(F)$ | 4367 |
| no. of variables | 523 |
| R | 0.0340 |
| R _w | 0.0370 |
| p | 0.03 |

^a See footnotes of Table 5.6.

Table 5. 8a. Final Positional and Equivalent Isotropic Thermal Parameters of Non-Hydrogen Atoms in
 $[\text{Fe}_3\text{Cl}_2(\text{C}_9\text{O}_3\text{H}_{12})_4(\text{C}_9\text{O}_3\text{H}_{13})_2] \cdot 2\text{CH}_3\text{CN}, 3 \cdot 2\text{CH}_3\text{CN}^{\text{a}}$

| Atom | x | y | z | B(eq) |
|------|-----------|------------|------------|--------|
| Fe1 | 0.2600(2) | 0.1229(1) | 0.4368(2) | 1.1(2) |
| Fe2 | 0.1784(2) | 0.1338(1) | 0.2487(2) | 1.0(1) |
| Fe3 | 0.1944(2) | 0.2596(1) | 0.4262(2) | 1.6(2) |
| Fe4 | 0.3698(2) | -0.2306(1) | 0.0782(2) | 1.3(2) |
| Fe5 | 0.2217(2) | -0.2389(1) | 0.1688(2) | 1.3(2) |
| Fe6 | 0.3263(2) | -0.3672(1) | 0.0419(2) | 1.4(2) |
| Cl1 | 0.3762(3) | 0.1135(3) | 0.4744(5) | 2.5(3) |
| Cl2 | 0.0658(3) | 0.1327(3) | 0.1980(4) | 2.4(3) |
| Cl3 | 0.4010(3) | -0.2190(3) | -0.0563(4) | 2.4(3) |
| Cl4 | 0.1927(3) | -0.2492(3) | 0.3079(4) | 2.8(3) |
| O1 | 0.1612(8) | 0.1276(6) | 0.373(1) | 1.6(3) |
| O2 | 0.2765(7) | 0.1308(5) | 0.3123(9) | 0.5(3) |
| O3 | 0.2260(8) | 0.0921(6) | 0.536(1) | 1.8(3) |
| O4 | 0.2712(7) | 0.0307(6) | 0.363(1) | 1.3(3) |
| O5 | 0.2276(7) | 0.1996(6) | 0.510(1) | 1.0(3) |
| O6 | 0.2054(7) | 0.0422(6) | 0.207(1) | 1.2(3) |
| O7 | 0.2228(7) | 0.1176(6) | 0.119(1) | 1.1(3) |
| O8 | 0.1789(8) | 0.2140(6) | 0.277(1) | 1.8(3) |
| O9 | 0.2093(8) | 0.3191(7) | 0.559(1) | 2.1(3) |
| O10 | 0.0950(8) | 0.2515(6) | 0.460(1) | 1.7(3) |
| O11 | 0.2958(9) | 0.2532(7) | 0.377(1) | 2.6(4) |
| O12 | 0.1472(8) | 0.3298(6) | 0.376(1) | 1.9(3) |
| O13 | 0.3231(8) | -0.2366(6) | 0.197(1) | 1.7(3) |
| O14 | 0.2685(7) | -0.2295(6) | 0.050(1) | 1.2(3) |
| O15 | 0.3395(7) | -0.1383(6) | 0.142(1) | 1.3(3) |
| O16 | 0.4601(8) | -0.2112(6) | 0.147(1) | 1.5(3) |
| O17 | 0.4077(8) | -0.3100(6) | 0.050(1) | 1.3(3) |
| O18 | 0.2104(8) | -0.1457(6) | 0.226(1) | 1.6(3) |
| O19 | 0.1237(8) | -0.2127(6) | 0.129(1) | 1.6(3) |
| O20 | 0.2199(7) | -0.3156(6) | 0.096(1) | 1.0(3) |

Table 5. 8a, contd. Final Positional and Equivalent Isotropic Thermal Parameters of Non-Hydrogen Atoms in
[Fe₃Cl₂(C₉O₃H₁₂)₄(C₉O₃H₁₃)₂]·2CH₃CN, 3·2CH₃CN.

| Atom | x | y | z | B(eq) |
|------|-----------|------------|-----------|--------|
| O22 | 0.2875(8) | -0.3514(7) | -0.078(1) | 2.3(3) |
| O23 | 0.4108(8) | -0.4264(7) | -0.043(1) | 2.2(3) |
| O24 | 0.2712(8) | -0.4330(6) | 0.046(1) | 1.9(3) |
| O100 | 0.1369(8) | -0.0204(6) | 0.267(1) | 1.4(3) |
| O101 | 0.0567(8) | 0.0612(6) | 0.406(1) | 1.5(3) |
| O110 | 0.0617(8) | -0.2990(7) | 0.147(1) | 2.4(3) |
| O120 | 0.5599(9) | -0.2908(7) | 0.042(1) | 2.4(3) |
| O201 | 0.4005(8) | 0.0698(7) | 0.187(1) | 2.3(3) |
| O301 | 0.2942(7) | -0.0966(6) | 0.354(1) | 1.0(3) |
| O401 | 0.2453(7) | -0.0783(6) | 0.065(1) | 0.9(3) |
| O501 | 0.2347(9) | 0.1687(7) | 0.695(1) | 2.8(4) |
| O601 | 0.155(1) | 0.2096(7) | 0.071(1) | 3.1(4) |
| O701 | 0.3898(9) | -0.1834(7) | 0.375(1) | 2.5(4) |
| O801 | 0.1896(8) | -0.1595(6) | -0.060(1) | 1.9(3) |
| O901 | 0.3662(8) | -0.0156(6) | 0.234(1) | 1.5(3) |
| N1S | 0.2814 | 0.4059 | 0.4747 | 9(1) |
| N2S | 0.9111 | 0.4341 | 0.5366 | 34(5) |
| N4S | 0.0467 | 0.4286 | 0.5645 | 21(2) |
| N6S | 0.6352 | 0.5176 | 0.3384 | 18(3) |
| C1S | 0.3143 | 0.4679 | 0.3586 | 20(2) |
| C2S | 0.3020 | 0.4347 | 0.4257 | 33(5) |
| C3S | 0.7012 | 0.4960 | 0.1827 | 13(1) |
| C5S | 0.6725 | 0.5113 | 0.2764 | 18(2) |
| C7S | 0.0858 | 0.4652 | 0.5870 | 21(3) |
| C8S | 0.0870 | 0.5042 | 0.7020 | 31(5) |
| C11 | 0.098(1) | 0.150(1) | 0.421(2) | 1.3(4) |
| C11S | 0.834(5) | 0.436(4) | 0.514(6) | 22(3) |
| C12 | 0.068(1) | 0.210(1) | 0.463(2) | 1.2(4) |
| C12S | 0.764(4) | 0.412(3) | 0.530(5) | 16(2) |
| C13 | -0.001(1) | 0.214(1) | 0.515(2) | 2.1(5) |

Table 5. 8a, contd. Final Positional and Equivalent Isotropic Thermal Parameters of Non-Hydrogen Atoms in
 $[\text{Fe}_3\text{Cl}_2(\text{C}_9\text{O}_3\text{H}_{12})_4(\text{C}_9\text{O}_3\text{H}_{13})_2] \cdot 2\text{CH}_3\text{CN}, 3 \cdot 2\text{CH}_3\text{CN}.$

| Atom | x | y | z | B(eq) |
|------|-----------|------------|-----------|--------|
| C14 | -0.018(1) | 0.153(1) | 0.482(2) | 1.2(4) |
| C15 | 0.048(1) | 0.118(1) | 0.431(2) | 1.2(4) |
| C16 | 0.019(1) | 0.231(1) | 0.617(2) | 3.2(6) |
| C17 | -0.058(1) | 0.260(1) | 0.496(2) | 3.0(6) |
| C18 | -0.077(1) | 0.146(1) | 0.406(2) | 2.6(5) |
| C19 | -0.039(1) | 0.128(1) | 0.558(2) | 2.6(5) |
| C21 | 0.329(1) | 0.156(1) | 0.289(2) | 1.2(4) |
| C22 | 0.385(1) | 0.124(1) | 0.227(2) | 1.5(5) |
| C23 | 0.434(1) | 0.164(1) | 0.214(2) | 2.2(5) |
| C24 | 0.390(1) | 0.224(1) | 0.256(2) | 3.4(6) |
| C25 | 0.332(1) | 0.212(1) | 0.319(2) | 1.6(5) |
| C26 | 0.503(1) | 0.147(1) | 0.264(2) | 2.8(6) |
| C27 | 0.453(2) | 0.148(1) | 0.108(2) | 4.8(7) |
| C28 | 0.435(2) | 0.271(1) | 0.316(2) | 4.2(7) |
| C29 | 0.348(1) | 0.247(1) | 0.183(2) | 3.2(6) |
| C31 | 0.242(1) | 0.0374(9) | 0.516(1) | 0.6(4) |
| C32 | 0.231(1) | 0.002(1) | 0.582(2) | 1.7(5) |
| C33 | 0.275(1) | -0.0598(9) | 0.522(1) | 0.8(4) |
| C34 | 0.280(1) | -0.058(1) | 0.425(2) | 2.2(5) |
| C35 | 0.266(1) | 0.003(1) | 0.430(2) | 1.3(4) |
| C36 | 0.262(1) | 0.027(1) | 0.678(2) | 3.0(6) |
| C37 | 0.150(1) | 0.001(1) | 0.582(2) | 3.0(6) |
| C38 | 0.352(1) | -0.069(1) | 0.559(2) | 2.1(5) |
| C39 | 0.239(1) | -0.110(1) | 0.526(2) | 2.7(6) |
| C41 | 0.229(1) | 0.0225(8) | 0.111(1) | 0.4(4) |
| C42 | 0.248(1) | -0.0304(8) | 0.052(1) | 0.6(4) |
| C43 | 0.282(1) | -0.026(1) | -0.033(2) | 1.8(5) |
| C44 | 0.257(1) | 0.038(1) | -0.028(2) | 1.6(5) |
| C45 | 0.237(1) | 0.065(1) | 0.073(2) | 1.2(4) |
| C46 | 0.258(1) | -0.070(1) | -0.125(2) | 2.2(5) |

Table 5. 8a, contd. Final Positional and Equivalent Isotropic Thermal Parameters of Non-Hydrogen Atoms in
 $[\text{Fe}_3\text{Cl}_2(\text{C}_9\text{O}_3\text{H}_{12})_4(\text{C}_9\text{O}_3\text{H}_{13})_2] \cdot 2\text{CH}_3\text{CN}, 3 \cdot 2\text{CH}_3\text{CN}.$

| Atom | x | y | z | B(eq) |
|------|----------|-----------|-----------|--------|
| C47 | 0.363(1) | -0.042(1) | -0.030(2) | 2.9(6) |
| C48 | 0.185(1) | 0.053(1) | -0.082(2) | 3.3(6) |
| C49 | 0.316(1) | 0.071(1) | -0.059(2) | 3.2(6) |
| C51 | 0.230(1) | 0.230(1) | 0.601(2) | 1.9(5) |
| C52 | 0.233(1) | 0.220(1) | 0.680(2) | 2.1(5) |
| C53 | 0.223(1) | 0.272(1) | 0.762(2) | 2.4(5) |
| C54 | 0.232(1) | 0.322(1) | 0.720(2) | 1.8(5) |
| C55 | 0.221(1) | 0.293(1) | 0.620(2) | 2.5(5) |
| C56 | 0.278(1) | 0.265(1) | 0.844(2) | 2.5(5) |
| C57 | 0.148(1) | 0.280(1) | 0.807(2) | 2.7(5) |
| C58 | 0.308(2) | 0.333(1) | 0.726(2) | 3.8(6) |
| C59 | 0.183(1) | 0.376(1) | 0.761(2) | 3.3(6) |
| C61 | 0.153(1) | 0.256(1) | 0.237(2) | 1.9(5) |
| C62 | 0.139(1) | 0.255(1) | 0.147(2) | 2.3(5) |
| C63 | 0.111(1) | 0.311(1) | 0.135(2) | 1.8(5) |
| C64 | 0.095(1) | 0.353(1) | 0.238(2) | 2.8(6) |
| C65 | 0.135(1) | 0.312(1) | 0.292(2) | 1.3(4) |
| C66 | 0.170(1) | 0.331(1) | 0.089(2) | 3.0(6) |
| C67 | 0.044(2) | 0.307(1) | 0.072(2) | 4.1(7) |
| C68 | 0.121(2) | 0.407(1) | 0.259(2) | 4.9(8) |
| C69 | 0.011(2) | 0.363(1) | 0.261(2) | 3.9(7) |
| C71 | 0.363(1) | -0.265(1) | 0.253(2) | 1.4(4) |
| C72 | 0.390(1) | -0.237(1) | 0.335(2) | 2.2(5) |
| C73 | 0.430(1) | -0.278(1) | 0.389(2) | 3.3(6) |
| C74 | 0.431(2) | -0.336(1) | 0.313(2) | 3.8(6) |
| C75 | 0.381(1) | -0.327(1) | 0.237(2) | 1.6(5) |
| C76 | 0.505(2) | -0.265(1) | 0.419(2) | 5.1(8) |
| C77 | 0.381(2) | -0.271(1) | 0.472(3) | 5.8(9) |
| C78 | 0.508(2) | -0.357(1) | 0.260(2) | 4.7(7) |
| C79 | 0.421(2) | -0.390(2) | 0.342(2) | 5.7(8) |

Table 5. 8a, contd. Final Positional and Equivalent Isotropic Thermal Parameters of Non-Hydrogen Atoms in
 $[\text{Fe}_3\text{Cl}_2(\text{C}_9\text{O}_3\text{H}_{12})_4(\text{C}_9\text{O}_3\text{H}_{13})_2]\cdot 2\text{CH}_3\text{CN}, 3\cdot 2\text{CH}_3\text{CN}.$

| Atom | x | y | z | B(eq) |
|------|-----------|------------|-----------|--------|
| C81 | 0.244(1) | -0.249(1) | -0.038(2) | 1.6(5) |
| C82 | 0.209(1) | -0.215(1) | -0.089(2) | 1.7(5) |
| C83 | 0.193(1) | -0.248(1) | -0.191(2) | 1.6(5) |
| C84 | 0.229(1) | -0.311(1) | -0.195(2) | 2.8(6) |
| C85 | 0.257(1) | -0.307(1) | -0.098(2) | 1.5(5) |
| C86 | 0.221(2) | -0.222(1) | -0.256(2) | 5.8(9) |
| C87 | 0.109(1) | -0.239(1) | -0.197(2) | 3.2(6) |
| C88 | 0.296(2) | -0.330(2) | -0.259(3) | 9(1) |
| C89 | 0.189(2) | -0.355(2) | -0.235(3) | 8(1) |
| C91 | 0.399(1) | -0.116(1) | 0.184(2) | 1.5(5) |
| C92 | 0.410(1) | -0.061(1) | 0.230(2) | 1.4(4) |
| C93 | 0.483(1) | -0.065(1) | 0.269(2) | 1.4(4) |
| C94 | 0.519(1) | -0.1270(9) | 0.226(1) | 0.9(4) |
| C95 | 0.459(1) | -0.155(1) | 0.182(2) | 1.8(5) |
| C96 | 0.520(1) | -0.020(1) | 0.251(2) | 2.8(6) |
| C97 | 0.469(1) | -0.047(1) | 0.375(2) | 2.6(5) |
| C98 | 0.573(1) | -0.134(1) | 0.146(2) | 2.0(5) |
| C99 | 0.559(1) | -0.159(1) | 0.297(2) | 2.3(5) |
| C101 | 0.142(1) | -0.123(1) | 0.202(2) | 1.8(5) |
| C102 | 0.111(1) | -0.063(1) | 0.219(2) | 1.3(4) |
| C103 | 0.042(1) | -0.062(1) | 0.165(2) | 2.0(5) |
| C104 | 0.030(1) | -0.127(1) | 0.134(2) | 1.3(4) |
| C105 | 0.100(1) | -0.1579(9) | 0.151(1) | 1.0(4) |
| C106 | 0.052(1) | -0.039(1) | 0.088(2) | 2.4(5) |
| C107 | -0.020(1) | -0.020(1) | 0.226(2) | 2.7(6) |
| C108 | -0.027(1) | -0.140(1) | 0.187(2) | 2.5(5) |
| C109 | 0.013(1) | -0.149(1) | 0.025(2) | 2.5(5) |
| C111 | 0.181(1) | -0.355(1) | 0.108(2) | 1.7(5) |
| C112 | 0.110(1) | -0.346(1) | 0.132(2) | 2.5(5) |
| C113 | 0.088(1) | -0.403(1) | 0.131(2) | 2.5(5) |

Table 5. 8a, contd. Final Positional and Equivalent Isotropic Thermal Parameters of Non-Hydrogen Atoms in
 $[\text{Fe}_3\text{Cl}_2(\text{C}_9\text{O}_3\text{H}_{12})_4(\text{C}_9\text{O}_3\text{H}_{13})_2] \cdot 2\text{CH}_3\text{CN}, 3 \cdot 2\text{CH}_3\text{CN}.$

| Atom | x | y | z | B(eq) |
|------|----------|------------|-----------|--------|
| C114 | 0.156(2) | -0.445(1) | 0.105(2) | 3.6(6) |
| C115 | 0.210(1) | -0.413(1) | 0.082(2) | 2.3(5) |
| C116 | 0.063(2) | -0.397(1) | 0.230(2) | 5.2(8) |
| C117 | 0.024(2) | -0.414(1) | 0.061(2) | 4.2(7) |
| C118 | 0.186(3) | -0.469(2) | 0.184(4) | 10(1) |
| C119 | 0.160(2) | -0.502(2) | 0.044(3) | 9(1) |
| C121 | 0.466(1) | -0.3457(9) | 0.000(2) | 1.1(4) |
| C122 | 0.533(1) | -0.335(1) | -0.004(2) | 2.3(5) |
| C123 | 0.582(1) | -0.392(1) | -0.058(2) | 1.4(4) |
| C124 | 0.531(1) | -0.429(1) | -0.102(2) | 2.4(5) |
| C125 | 0.463(1) | -0.401(1) | -0.047(2) | 1.6(5) |
| C126 | 0.630(1) | -0.412(1) | 0.015(2) | 2.3(5) |
| C127 | 0.634(2) | -0.375(1) | -0.121(2) | 3.7(6) |
| C128 | 0.514(2) | -0.430(1) | -0.203(2) | 4.0(7) |
| C129 | 0.552(1) | -0.495(1) | -0.101(2) | 2.8(6) |

^aNumbers in parentheses are errors in the last significant digit. ^bSee Figure 5.5a for atom labelling scheme.

Table 5. 8b. Final Positional and Equivalent Isotropic Thermal Parameters of Non-Hydrogen Atoms in $[\text{Fe}_3\text{Cl}_2(\text{C}_9\text{O}_3\text{H}_{12})_4(\text{C}_9\text{O}_3\text{H}_{13})_2]$, **3**.^a

| Atom ^b | x | y | z | B(eq) |
|-------------------|------------|-----------|-----------|--------|
| Fe1 | 0.0684(2) | 1.0000 | 1/4 | 2.8(5) |
| Fe2 | -0.0139(2) | 1.0083(2) | 0.2077(2) | 1.9(3) |
| Cl1 | -0.0152(3) | 1.0589(3) | 0.1759(3) | 3.8(7) |
| O1 | 0.0355(7) | 0.9967(7) | 0.2002(8) | 2.3(6) |
| O2 | 0.1064(7) | 1.0041(8) | 0.2088(8) | 3.1(7) |
| O3 | 0.0627(8) | 0.9455(8) | 0.2488(8) | 3.4(7) |
| O4 | -0.0711(6) | 1.0083(7) | 0.2138(7) | 1.9(6) |
| O5 | -0.0295(8) | 0.9764(8) | 0.1667(7) | 3.1(7) |
| O6 | -0.0138(6) | 0.9665(6) | 0.2449(7) | 1.6(6) |
| O7 | 0.0216(8) | 0.9796(8) | 0.1199(8) | 4.0(8) |
| O8 | -0.1492(7) | 0.9961(8) | 0.1898(7) | 2.3(6) |
| O9 | -0.0524(8) | 0.9048(8) | 0.2199(8) | 3.7(8) |
| C1 | -0.064(1) | 0.975(1) | 0.162(1) | 1.3(9) |
| C2 | -0.085(1) | 0.992(1) | 0.182(1) | 3(1) |
| C3 | -0.122(1) | 0.985(1) | 0.175(1) | 2(1) |
| C4 | -0.121(1) | 0.957(1) | 0.144(1) | 4(1) |
| C5 | -0.082(1) | 0.955(1) | 0.132(1) | 4(1) |
| C6 | 0.091(1) | 1.001(1) | 0.178(1) | 2(1) |
| C7 | 0.056(1) | 0.994(1) | 0.173(1) | 1.6(9) |
| C8 | 0.052(1) | 0.987(1) | 0.138(1) | 3(1) |
| C9 | 0.085(1) | 0.988(1) | 0.117(1) | 3(1) |
| C10 | 0.114(1) | 0.997(1) | 0.144(1) | 2(1) |
| C11 | 0.038(1) | 0.925(1) | 0.240(1) | 1.4(8) |
| C12 | 0.003(1) | 0.935(1) | 0.238(1) | 2(1) |
| C13 | -0.016(1) | 0.908(1) | 0.226(1) | 2(1) |
| C14 | 0.007(1) | 0.878(1) | 0.214(1) | 4(1) |
| C15 | 0.041(1) | 0.890(1) | 0.232(1) | 3(1) |
| C41 | -0.150(1) | 0.967(1) | 0.119(1) | 4(1) |
| C42 | -0.132(1) | 0.923(2) | 0.159(1) | 6(2) |
| C51 | -0.075(1) | 0.983(1) | 0.102(1) | 5(1) |

Table 5. 8b, contd. Final Positional and Equivalent Isotropic Thermal Parameters of Non-Hydrogen Atoms in
 $[\text{Fe}_3\text{Cl}_2(\text{C}_9\text{O}_3\text{H}_{12})_4(\text{C}_9\text{O}_3\text{H}_{13})_2]_3$

| Atom | x | y | z | B(eq) |
|------|-----------|----------|----------|-------|
| C91 | 0.083(1) | 1.012(1) | 0.086(1) | 4(1) |
| C92 | 0.090(1) | 0.950(1) | 0.102(1) | 5(1) |
| C101 | 0.132(2) | 1.032(2) | 0.140(2) | 7(2) |
| C102 | 0.144(1) | 0.971(1) | 0.150(1) | 4(1) |
| C141 | -0.008(2) | 0.846(2) | 0.234(2) | 12(3) |
| C142 | 0.010(2) | 0.876(2) | 0.172(2) | 8(2) |
| C151 | 0.051(2) | 0.872(2) | 0.268(2) | 9(2) |
| C152 | 0.074(2) | 0.884(2) | 0.209(2) | 10(2) |

^aNumbers in parentheses are errors in the last significant digit. ^bSee Figure 5.5b for atom labelling scheme.

Table 5.9a. Final Thermal Parameters of Non-Hydrogen Atoms for
 $[\text{Fe}_3\text{Cl}_2(\text{C}_9\text{H}_{12}\text{O}_3)_4(\text{C}_9\text{H}_{13}\text{O}_3)] \cdot 2\text{CH}_3\text{CN}, 3 \cdot 2\text{CH}_3\text{CN}.$ ^a

| Atom ^b | U ₁₁ | U ₂₂ | U ₃₃ | U ₁₂ | U ₁₃ | U ₂₃ |
|-------------------|-----------------|-----------------|-----------------|-----------------|-----------------|-----------------|
| Fe1 | 0.016(2) | 0.016(2) | 0.009(2) | -0.001(1) | 0.001(2) | 0.003(1) |
| Fe2 | 0.016(2) | 0.013(2) | 0.010(2) | -0.002(1) | 0.002(1) | 0.004(1) |
| Fe3 | 0.025(2) | 0.018(2) | 0.017(2) | -0.004(2) | -0.000(2) | 0.005(2) |
| Fe4 | 0.012(2) | 0.018(2) | 0.021(2) | -0.003(1) | -0.004(2) | 0.006(2) |
| Fe5 | 0.014(2) | 0.011(2) | 0.024(2) | -0.000(1) | -0.003(2) | 0.004(2) |
| Fe6 | 0.014(2) | 0.016(2) | 0.021(2) | -0.004(1) | 0.002(2) | 0.003(2) |
| Cl1 | 0.020(4) | 0.048(4) | 0.031(4) | -0.012(3) | -0.014(3) | 0.014(3) |
| Cl2 | 0.018(4) | 0.049(4) | 0.022(4) | -0.003(3) | -0.005(3) | 0.008(3) |
| Cl3 | 0.025(4) | 0.044(4) | 0.030(4) | -0.014(3) | -0.002(3) | 0.018(3) |
| Cl4 | 0.027(4) | 0.052(5) | 0.025(4) | -0.012(3) | 0.011(3) | 0.006(3) |
| O1 | 0.020(4) | | | | | |
| O2 | 0.007(3) | | | | | |
| O3 | 0.023(4) | | | | | |
| O4 | 0.017(4) | | | | | |
| O5 | 0.013(4) | | | | | |
| O6 | 0.015(4) | | | | | |
| O7 | 0.014(4) | | | | | |
| O8 | 0.023(4) | | | | | |
| O9 | 0.026(4) | | | | | |
| O10 | 0.022(4) | | | | | |
| O11 | 0.033(5) | | | | | |
| O12 | 0.024(4) | | | | | |
| O13 | 0.022(4) | | | | | |
| O14 | 0.015(4) | | | | | |
| O15 | 0.016(4) | | | | | |
| O16 | 0.019(4) | | | | | |
| O17 | 0.017(4) | | | | | |
| O18 | 0.021(4) | | | | | |
| O19 | 0.021(4) | | | | | |
| O20 | 0.013(4) | | | | | |

Table 5.9a, contd. Final Thermal Parameters of Non-Hydrogen Atoms for
 $[\text{Fe}_3\text{Cl}_2(\text{C}_9\text{H}_{12}\text{O}_3)_4(\text{C}_9\text{H}_{13}\text{O}_3)] \cdot 2\text{CH}_3\text{CN}, 3 \cdot 2\text{CH}_3\text{CN}.$

| Atom | U_{11} | Atom | U_{11} | Atom | U_{11} |
|------|----------|------|----------|------|----------|
| O21 | 0.021(4) | C13 | 0.026(6) | C46 | 0.028(6) |
| O22 | 0.030(4) | C14 | 0.015(5) | C47 | 0.037(7) |
| O23 | 0.027(4) | C15 | 0.016(5) | C48 | 0.042(8) |
| O24 | 0.023(4) | C16 | 0.040(7) | C49 | 0.041(8) |
| O100 | 0.017(4) | C17 | 0.039(7) | C51 | 0.024(6) |
| O101 | 0.018(4) | C18 | 0.033(7) | C52 | 0.026(6) |
| O110 | 0.030(4) | C19 | 0.033(7) | C53 | 0.030(7) |
| O120 | 0.031(4) | C21 | 0.016(6) | C54 | 0.023(6) |
| O201 | 0.030(4) | C22 | 0.019(6) | C55 | 0.032(7) |
| O301 | 0.013(4) | C23 | 0.027(6) | C56 | 0.031(7) |
| O401 | 0.012(3) | C24 | 0.042(8) | C57 | 0.034(7) |
| O501 | 0.035(5) | C25 | 0.020(6) | C58 | 0.048(8) |
| O601 | 0.039(5) | C26 | 0.035(7) | C59 | 0.042(8) |
| O701 | 0.032(4) | C27 | 0.06(1) | C61 | 0.025(6) |
| O801 | 0.024(4) | C28 | 0.053(9) | C62 | 0.029(7) |
| O901 | 0.019(4) | C29 | 0.040(8) | C63 | 0.023(6) |
| N1S | 0.11(2) | C31 | 0.008(5) | C64 | 0.036(7) |
| N2S | 0.42(6) | C32 | 0.022(6) | C65 | 0.017(6) |
| N4S | 0.26(3) | C33 | 0.011(5) | C66 | 0.038(7) |
| N6S | 0.22(3) | C34 | 0.028(6) | C67 | 0.051(9) |
| C1S | 0.25(3) | C35 | 0.017(6) | C68 | 0.06(1) |
| C2S | 0.42(7) | C36 | 0.038(7) | C69 | 0.050(8) |
| C3S | 0.16(2) | C37 | 0.038(7) | C71 | 0.017(6) |
| C5S | 0.22(3) | C38 | 0.026(6) | C72 | 0.028(7) |
| C7S | 0.27(4) | C39 | 0.035(7) | C73 | 0.042(8) |
| C8S | 0.39(6) | C41 | 0.005(5) | C74 | 0.048(8) |
| C11 | 0.016(6) | C42 | 0.008(5) | C75 | 0.021(6) |
| C11S | 0.27(4) | C43 | 0.023(6) | C76 | 0.07(1) |
| C12 | 0.016(5) | C44 | 0.020(6) | C77 | 0.07(1) |
| C12S | 0.21(3) | C45 | 0.015(5) | C78 | 0.06(1) |

**Table 5.9a, contd. Final Thermal Parameters of Non-Hydrogen Atoms for
[Fe₃Cl₂(C₉H₁₂O₃)₄(C₉H₁₃O₃)]·2CH₃CN, 3·2CH₃CN.**

| Atom | U ₁₁ | Atom | U ₁₁ | Atom | U ₁₁ |
|------|-----------------|------|-----------------|------|-----------------|
| C79 | 0.07(1) | C97 | 0.033(7) | C115 | 0.029(7) |
| C81 | 0.020(6) | C98 | 0.025(6) | C116 | 0.07(1) |
| C82 | 0.021(6) | C99 | 0.029(7) | C117 | 0.053(9) |
| C83 | 0.020(6) | C101 | 0.022(6) | C118 | 0.13(2) |
| C84 | 0.036(7) | C102 | 0.016(6) | C119 | 0.11(2) |
| C85 | 0.019(6) | C103 | 0.025(6) | C121 | 0.014(5) |
| C86 | 0.07(1) | C104 | 0.016(6) | C122 | 0.030(7) |
| C87 | 0.040(7) | C105 | 0.012(5) | C123 | 0.018(6) |
| C88 | 0.11(2) | C106 | 0.031(7) | C124 | 0.030(7) |
| C89 | 0.10(1) | C107 | 0.035(7) | C125 | 0.021(6) |
| C91 | 0.019(6) | C108 | 0.032(7) | C126 | 0.029(7) |
| C92 | 0.017(6) | C109 | 0.032(7) | C127 | 0.046(8) |
| C93 | 0.018(6) | C111 | 0.022(6) | C128 | 0.051(8) |
| C94 | 0.011(5) | C112 | 0.032(7) | C129 | 0.035(7) |
| C95 | 0.022(6) | C113 | 0.031(7) | | |
| C96 | 0.036(7) | C114 | 0.045(8) | | |

^aNumbers in parentheses are errors in the last significant digit(s). ^bSee Figure 5.5a for atom labelling scheme.

Table 5.9b. Final Thermal Parameters of Non-Hydrogen Atoms for
 $[\text{Fe}_3\text{Cl}_2(\text{C}_9\text{H}_{12}\text{O}_3)_4(\text{C}_9\text{H}_{13}\text{O}_3)], 3^{\text{a}}$

| Atom | U ₁₁ | U ₂₂ | U ₃₃ | U ₁₂ | U ₁₃ | U ₂₃ |
|------|-----------------|-----------------|-----------------|-----------------|-----------------|-----------------|
| Fe1 | 0.020(6) | 0.066(8) | 0.020(6) | 0 | 0 | -0.010(6) |
| Fe2 | 0.025(4) | 0.032(5) | 0.014(4) | -0.000(4) | 0.002(3) | 0.002(3) |
| Cl1 | 0.06(1) | 0.044(9) | 0.046(9) | 0.006(8) | -0.008(8) | 0.014(7) |
| O1 | 0.029(8) | | | | | |
| O2 | 0.039(8) | | | | | |
| O3 | 0.043(9) | | | | | |
| O4 | 0.024(7) | | | | | |
| O5 | 0.039(9) | | | | | |
| O6 | 0.020(7) | | | | | |
| O7 | 0.05(1) | | | | | |
| O8 | 0.029(8) | | | | | |
| O9 | 0.05(1) | | | | | |
| C1 | 0.02(1) | | | | | |
| C2 | 0.03(1) | | | | | |
| C3 | 0.02(1) | | | | | |
| C4 | 0.05(2) | | | | | |
| C5 | 0.05(2) | | | | | |
| C6 | 0.02(1) | | | | | |
| C7 | 0.02(1) | | | | | |
| C8 | 0.03(1) | | | | | |
| C9 | 0.04(1) | | | | | |
| C10 | 0.03(1) | | | | | |
| C11 | 0.02(1) | | | | | |
| C12 | 0.03(1) | | | | | |
| C13 | 0.03(1) | | | | | |
| C14 | 0.06(2) | | | | | |
| C15 | 0.04(1) | | | | | |
| C41 | 0.05(1) | | | | | |
| C42 | 0.07(2) | | | | | |
| C51 | 0.06(2) | | | | | |

Table 5.9b, contd. Final Thermal Parameters of Non-Hydrogen Atoms for
[Fe₃Cl₂(C₉H₁₂O₃)₄(C₉H₁₃O₃)], 3.

| Atom | U ₁₁ | U ₂₂ | U ₃₃ | U ₁₂ | U ₁₃ | U ₂₃ |
|------|-----------------|-----------------|-----------------|-----------------|-----------------|-----------------|
| C52 | 0.08(2) | | | | | |
| C91 | 0.05(1) | | | | | |
| C92 | 0.07(2) | | | | | |
| C101 | 0.09(2) | | | | | |
| C102 | 0.05(2) | | | | | |
| C141 | 0.15(3) | | | | | |
| C142 | 0.10(2) | | | | | |
| C151 | 0.12(3) | | | | | |
| C152 | 0.12(3) | | | | | |

^aSee footnotes of Table 5.9a. ^b See figure 5.5b for atom labelling scheme.

Table 5.10a. Selected Interatomic Distances (Å) and Angles (deg) for
 $[\text{Fe}_3\text{Cl}_2(\text{C}_9\text{H}_{12}\text{O}_3)_4(\text{C}_9\text{H}_{13}\text{O}_3)_2] \cdot 2\text{CH}_3\text{CN}, 3 \cdot 2\text{CH}_3\text{CN}.$ ^a

| <u>Coordination Sphere</u> | | | |
|----------------------------|----------|---------------|----------|
| Fe1- Cl1 | 2.261(7) | Fe4- Cl3 | 2.245(7) |
| Fe1- O1 | 2.09(2) | Fe4- O13 | 2.08(2) |
| Fe1- O2 | 1.99(1) | Fe4- O14 | 1.97(1) |
| Fe1- O3 | 2.04(2) | Fe4- O15 | 2.18(1) |
| Fe1- O4 | 2.20(1) | Fe4- O16 | 2.04(1) |
| Fe1- O5 | 1.90(1) | Fe4- O17 | 1.90(1) |
| Fe2- Cl2 | 2.261(7) | Fe5- Cl4 | 2.286(7) |
| Fe2- O1 | 1.97(2) | Fe5- O13 | 1.98(2) |
| Fe2- O2 | 2.07(1) | Fe5- O14 | 2.12(1) |
| Fe2- O6 | 2.14(1) | Fe5- O18 | 2.18(1) |
| Fe2- O7 | 2.05(1) | Fe5- O19 | 2.00(2) |
| Fe2- O8 | 1.91(1) | Fe5- O20 | 1.90(1) |
| Fe3- O5 | 2.23(1) | Fe6- O17 | 2.26(1) |
| Fe3- O8 | 2.24(2) | Fe6- O20 | 2.23(1) |
| Fe3- O9 | 2.16(2) | Fe6- O21 | 2.07(2) |
| Fe3- O10 | 2.04(2) | Fe6- O22 | 2.05(2) |
| Fe3- O11 | 2.06(2) | Fe6- O23 | 2.14(2) |
| Fe3- O12 | 2.14(2) | Fe6- O24 | 2.11(2) |
| Cl1- Fe1- O1 | 167.7(5) | Cl3- Fe4- O13 | 170.1(5) |
| Cl1- Fe1- O2 | 94.8(4) | Cl3- Fe4- O14 | 95.8(5) |
| Cl1- Fe1- O3 | 97.1(5) | Cl3- Fe4- O15 | 92.2(4) |
| Cl1- Fe1- O4 | 91.9(4) | Cl3- Fe4- O16 | 96.1(5) |
| Cl1- Fe1- O5 | 99.5(5) | Cl3- Fe4- O17 | 97.4(5) |
| O1- Fe1- O2 | 73.4(6) | O13- Fe4- O14 | 74.7(6) |
| O1- Fe1- O3 | 93.3(6) | O13- Fe4- O15 | 84.5(6) |
| O1- Fe1- O4 | 83.6(5) | O13- Fe4- O16 | 92.4(6) |
| O1- Fe1- O5 | 86.9(6) | O13- Fe4- O17 | 87.6(6) |
| O2- Fe1- O3 | 159.5(6) | O14- Fe4- O15 | 85.9(6) |

Table 5.10a, contd. Selected Interatomic Distances (Å) and Angles (deg) for
 $[\text{Fe}_3\text{Cl}_2(\text{C}_9\text{H}_{12}\text{O}_3)_4(\text{C}_9\text{H}_{13}\text{O}_3)_2]\cdot 2\text{CH}_3\text{CN}, 3\cdot 2\text{CH}_3\text{CN}.$

| <u>Coordination Sphere, contd</u> | | | |
|-----------------------------------|----------|---------------|----------|
| O2- Fe1- O4 | 84.6(5) | O14- Fe4- O16 | 160.7(6) |
| O2- Fe1- O5 | 103.4(6) | O14- Fe4- O17 | 103.1(6) |
| O3- Fe1- O4 | 78.4(6) | O15- Fe4- O16 | 78.5(6) |
| O3- Fe1- O5 | 91.0(6) | O15- Fe4- O17 | 166.0(6) |
| O4- Fe1- O5 | 165.3(6) | O16- Fe4- O17 | 90.3(6) |
| Cl2- Fe2- O1 | 97.2(5) | Cl4- Fe5- O13 | 95.6(5) |
| Cl2- Fe2- O2 | 171.0(4) | Cl4- Fe5- O14 | 169.1(4) |
| Cl2- Fe2- O6 | 92.8(4) | Cl4- Fe5- O18 | 92.7(4) |
| Cl2- Fe2- O7 | 94.9(4) | Cl4- Fe5- O19 | 98.9(5) |
| Cl2- Fe2- O8 | 99.2(5) | Cl4- Fe5- O20 | 96.9(5) |
| O1- Fe2- O2 | 74.0(6) | O13- Fe5- O14 | 73.5(6) |
| O1- Fe2- O6 | 85.8(6) | O13- Fe5- O18 | 83.0(6) |
| O1- Fe2- O7 | 160.7(6) | O13- Fe5- O19 | 156.9(6) |
| O1- Fe2- O8 | 101.1(6) | O13- Fe5- O20 | 105.0(6) |
| O2- Fe2- O6 | 84.7(5) | O14- Fe5- O18 | 86.2(5) |
| O2- Fe2- O7 | 93.1(5) | O14- Fe5- O19 | 91.5(6) |
| O2- Fe2- O8 | 84.7(6) | O14- Fe5- O20 | 86.1(6) |
| O6- Fe2- O7 | 78.6(5) | O18- Fe5- O19 | 78.4(6) |
| O6- Fe2- O8 | 165.3(6) | O18- Fe5- O20 | 166.7(6) |
| O7- Fe2- O8 | 91.7(6) | O19- Fe5- O20 | 91.1(6) |
| O5- Fe3- O8 | 112.8(5) | O17- Fe6- O20 | 111.2(5) |
| O5- Fe3- O9 | 79.1(6) | O17- Fe6- O21 | 82.6(6) |
| O5- Fe3- O10 | 82.3(6) | O17- Fe6- O22 | 90.7(6) |
| O5- Fe3- O11 | 94.4(6) | O17- Fe6- O23 | 79.0(6) |
| O5- Fe3- O12 | 165.4(6) | O17- Fe6- O24 | 165.9(6) |
| O8- Fe3- O9 | 167.7(6) | O20- Fe6- O21 | 91.7(6) |
| O8- Fe3- O10 | 90.9(6) | O20- Fe6- O22 | 81.3(6) |
| O8- Fe3- O11 | 81.6(6) | O20- Fe6- O23 | 163.8(6) |
| O8- Fe3- O12 | 78.9(6) | O20- Fe6- O24 | 79.4(5) |

Table 5.10a,contd. Selected Interatomic Distances (Å) and Angles (deg) for
 $[\text{Fe}_3\text{Cl}_2(\text{C}_9\text{H}_{12}\text{O}_3)_4(\text{C}_9\text{H}_{13}\text{O}_3)_2]\cdot 2\text{CH}_3\text{CN}, 3\cdot 2\text{CH}_3\text{CN}.$

| <u>Coordination Sphere, contd</u> | | | |
|-----------------------------------|---|---------------|-------------|
| O9- Fe3- O10 | 93.9(6) | O21- Fe6- O22 | 167.8(6) |
| O9- Fe3- O11 | 94.8(6) | O21- Fe6- O23 | 102.3(6) |
| O9- Fe3- O12 | 89.9(6) | O21- Fe6- O24 | 88.1(6) |
| O10- Fe3- O11 | 169.9(6) | O22- Fe6- O23 | 86.3(6) |
| O10- Fe3- O12 | 89.1(6) | O22- Fe6- O24 | 100.3(6) |
| O11- Fe3- O12 | 96.0(6) | O23- Fe6- O24 | 92.8(6) |
| <u>Cluster</u> | | | |
| Fe1- O1- Fe2 | 106.3(7) | Fe4- O13- Fe5 | 106.5(7) |
| Fe1- O2- Fe2 | 106.2(6) | Fe4- O14- Fe5 | 105.2(7) |
| Fe1- O5- Fe3 | 113.0(7) | Fe4- O17- Fe6 | 115.1(7) |
| Fe2- O8- Fe3 | 115.4(7) | Fe5- O20- Fe6 | 114.6(6) |
| <u>Ligand</u> | | | |
| | <i>min</i> | <i>max</i> | <i>mean</i> |
| | $\text{C}_9\text{H}_{14}\text{O}_3$ (fully reduced) | | |
| C- O (Terminal) ^b | 1.27(2) | 1.32(3) | 1.29(3) |
| C- O (Central) | 1.40(3) | 1.43(3) | 1.41(3) |
| C=O | 1.21(3) | 1.27(2) | 1.25(3) |
| C-C | 1.34(3) | 1.68(3) | 1.52(3) |
| C=C | 1.35(3) | 1.37(3) | 1.36(3) |
| | $\text{C}_9\text{H}_{12}\text{O}_3$ (semiquinone) | | |
| C- O (Terminal) | 1.21(3) | 1.28(3) | 1.25(3) |
| C- O (Central) | 1.35(3) | 1.39(3) | 1.37(3) |
| C=O | 1.29(2) | 1.35(3) | 1.31(3) |
| C-C | 1.30(3) | 1.63(3) | 1.52(5) |
| C=C | 1.34(3) | 1.49(3) | 1.41(3) |
| Fe -O _{chelate} -C | 105(1) | 118(1) | 110(1) |

Table 5.10a, contd. Selected Interatomic Distances (Å) and Angles (deg) for
 $[\text{Fe}_3\text{Cl}_2(\text{C}_9\text{H}_{12}\text{O}_3)_4(\text{C}_9\text{H}_{13}\text{O}_3)_2] \cdot 2\text{CH}_3\text{CN}, 3 \cdot 2\text{CH}_3\text{CN}.$

| <u>Ligand, contd</u> | | | |
|---------------------------------------|------------|------------|-------------|
| C - C - C | 106(2) | 115(2) | 110(2) |
| C - C _{sp3} - C ^c | 98(2) | 107(2) | 103(2) |
| C _{Me} - C - C _{Me} | 89(3) | 123(2) | 111(3) |
| <u>Solvent</u> | | | |
| | <i>min</i> | <i>max</i> | <i>mean</i> |
| N - C | 1.1505(2) | 1.5(1) | 1.3(1) |
| C - C | 1.4489(3) | 1.7179(4) | 1.58(9) |

^aNumbers in parentheses are standard deviations in the last significant digit. ^bSee the first section of this chapter for the definition of terminal versus central hydroxyl groups in the ene-diol fragment of ligands. ^cC_{sp3} stands for the carbon atoms that are not involved in the conjugation of the ene-diol fragment.

Table 5.10b. Selected Interatomic Distances (Å) and Angles (deg) for
 $[\text{Fe}_3\text{Cl}_2(\text{C}_9\text{H}_{12}\text{O}_3)_4(\text{C}_9\text{H}_{13}\text{O}_3)_2], 3^{\text{a}}$

| <u>Coordination Sphere</u> | | | |
|------------------------------|------------|--------------|-------------|
| Fe1- O1 | 2.25(3) | Fe2- Cl1 | 2.25(1) |
| | | Fe2- O1 | 1.93(3) |
| Fe1- O2 | 2.12(3) | Fe2- O4 | 2.16(2) |
| | | Fe2- O5 | 2.04(3) |
| Fe1- O3 | 2.06(3) | Fe2- O6 | 2.10(3) |
| | | Fe2- O6 | 2.02(3) |
| O1- Fe1- O1* ^b | 113(1) | Cl1- Fe2- O1 | 97.7(9) |
| O1- Fe1- O2 | 76(1) | Cl1- Fe2- O4 | 92.0(8) |
| O1*- Fe1- O2 | 168(1) | Cl1- Fe2- O5 | 95.1(9) |
| O1- Fe1- O3 | 83(1) | Cl1- Fe2- O6 | 170.3(8) |
| O1*- Fe1- O3 | 91(1) | Cl1- Fe2- O6 | 94.1(8) |
| O1*- Fe1- O2 | 168(1) | O1- Fe2- O4 | 167(1) |
| O1- Fe1- O2 | 76(1) | O1- Fe2- O5 | 92(1) |
| O2- Fe1- O2* | 95(2) | O1- Fe2- O6 | 86(1) |
| O2- Fe1- O3 | 97(1) | O1- Fe2- O6 | 104(1) |
| O2- Fe1- O3* | 91(1) | O4- Fe2- O5 | 78(1) |
| O3- Fe1- O3* | 168(2) | O4- Fe2- O6 | 86(1) |
| Fe1- O2- Fe2 | 123.8(2) | O4- Fe2- O6 | 85(1) |
| Fe2- O10- Fe2 | 104.6(2) | O5- Fe2- O6 | 94(1) |
| | | O5- Fe2- O6 | 161(1) |
| | | O6- Fe2- O6 | 76(1) |
| <u>Ligand, TMRA</u> | | | |
| | <i>min</i> | <i>max</i> | <i>mean</i> |
| C- O (terminal) ^c | | | 1.30(4) |
| C- O (central) | | | 1.46(5) |
| C= O | | | 1.26(4) |

Table 5.10b,contd. Selected Interatomic Distances (Å) and Angles (deg) for
 $[\text{Fe}_3\text{Cl}_2(\text{C}_9\text{H}_{12}\text{O}_3)_4(\text{C}_9\text{H}_{13}\text{O}_3)_2], 3.$

| <u>Ligand, TMRA, contd</u> | | | |
|---------------------------------------|------------|------------|-------------|
| | <i>min</i> | <i>max</i> | <i>mean</i> |
| C=C | | | 1.28(5) |
| C-C | 1.40(5) | 1.56(6) | 1.49(6) |
| <u>Ligand, TMRASO</u> | | | |
| C- O (terminal) | 1.24(4) | 1.30(4) | 1.27(4) |
| C- O (central) | 1.27(4) | 1.38(4) | 1.33(4) |
| C=O | 1.38(5) | 1.38(4) | 1.38(5) |
| C=C | 1.37(5) | 1.39(5) | 1.38(5) |
| C-C | 1.33(5) | 1.58(7) | 1.49(7) |
| Fe -O -C | 106(2) | 115(3) | 111(3) |
| C -C -C | 99(4) | 116(4) | 108(4) |
| C - C _{sp3} - C ^d | 104(4) | 119(4) | 109(4) |

^aNumbers in parentheses are errors in the last significant digits. ^bAtoms with "*" are generated by symmetry operation. ^{c,d}See footnote b and c in Table 5.10a.

Table 5.11. Final Positional and Equivalent Isotropic Thermal Parameters of Non-Hydrogen Atoms in [(BzPh₃P)FeBr₄]·BzPh₃PBr, 7·BzPh₃PBr.^a

| Atom | x | y | z | B(eq) |
|------|---------------------|-------------|------------|---------|
| Br | 0.03512(7) | 0.44863(5) | 0.84133(4) | 2.60(3) |
| Br1 | -0.36383(8) | 0.17671(6) | 0.21056(4) | 2.80(3) |
| Br2 | -0.49798(8) | 0.13946(6) | 0.37790(4) | 2.85(3) |
| Br3 | -0.39509(8) | -0.08374(5) | 0.26983(4) | 2.74(3) |
| Br4 | -0.11159(8) | 0.15743(6) | 0.39091(4) | 3.29(3) |
| Fe | -0.3428(<i>i</i>) | 0.09846(7) | 0.31212(5) | 1.86(3) |
| P1 | 0.1377(2) | 0.3003(1) | 0.04770(9) | 1.70(6) |
| P2 | 0.6727(2) | 0.3017(1) | 0.63504(9) | 1.88(6) |
| C1 | 0.2892(7) | 0.4105(5) | 0.0665(3) | 2.0(2) |
| C2 | 0.4231(7) | 0.3937(5) | 0.0736(4) | 2.7(3) |
| C3 | 0.5422(7) | 0.4769(6) | 0.0946(4) | 3.5(3) |
| C4 | 0.5284(8) | 0.5792(6) | 0.1090(4) | 3.3(3) |
| C5 | 0.3957(8) | 0.5973(5) | 0.1012(4) | 3.1(3) |
| C6 | 0.2758(7) | 0.5144(5) | 0.0815(3) | 2.5(2) |
| C7 | 0.1576(6) | 0.1984(5) | -0.0184(3) | 1.7(2) |
| C8 | 0.1838(7) | 0.2276(5) | -0.0809(4) | 2.3(2) |
| C9 | 0.1974(7) | 0.1532(5) | -0.1353(3) | 2.9(3) |
| C10 | 0.1850(7) | 0.0495(5) | -0.1281(4) | 2.9(3) |
| C11 | 0.1557(7) | 0.0200(5) | -0.0665(4) | 2.9(3) |
| C12 | 0.1435(7) | 0.0948(5) | -0.0117(4) | 2.3(2) |
| C13 | 0.1335(6) | 0.2538(5) | 0.1295(3) | 1.7(2) |
| C14 | 0.2340(7) | 0.2008(5) | 0.1585(3) | 2.5(2) |
| C15 | 0.2351(8) | 0.1674(6) | 0.2220(4) | 3.1(3) |
| C16 | 0.1390(8) | 0.1869(6) | 0.2587(4) | 3.0(3) |
| C17 | 0.0412(7) | 0.2414(5) | 0.2328(3) | 2.8(3) |
| C18 | 0.0390(7) | 0.2762(5) | 0.1682(3) | 2.2(2) |
| C19 | -0.0221(6) | 0.3400(5) | 0.0100(3) | 1.9(2) |
| C20 | -0.1577(6) | 0.2506(5) | -0.0154(3) | 1.9(2) |
| C21 | -0.1869(7) | 0.1764(5) | -0.0795(4) | 2.7(3) |
| C22 | -0.3141(8) | 0.0976(6) | -0.1034(4) | 3.6(3) |

Table 5. 11, contd. Final Positional and Equivalent Isotropic Thermal Parameters of Non-Hydrogen Atoms in [(BzPh₃P)FeBr₄]·BzPh₃PBr, 7·BzPh₃PBr.

| Atom | x | y | z | B(eq) |
|------|------------|-----------|------------|--------|
| C23 | -0.4099(7) | 0.0918(6) | -0.0634(4) | 3.5(3) |
| C24 | -0.3849(7) | 0.1653(6) | -0.0003(4) | 3.1(3) |
| C25 | -0.2578(7) | 0.2442(5) | 0.0235(3) | 2.4(2) |
| C26 | 0.7512(7) | 0.4051(5) | 0.5962(3) | 2.2(2) |
| C27 | 0.7021(7) | 0.4052(5) | 0.5221(4) | 2.7(3) |
| C28 | 0.7731(8) | 0.4834(6) | 0.4935(4) | 3.3(3) |
| C29 | 0.8929(8) | 0.5575(5) | 0.5369(4) | 3.2(3) |
| C30 | 0.9426(8) | 0.5565(5) | 0.6093(4) | 3.2(3) |
| C31 | 0.8733(7) | 0.4810(5) | 0.6397(3) | 2.5(2) |
| C32 | 0.7931(7) | 0.2190(5) | 0.6514(3) | 1.9(2) |
| C33 | 0.8900(8) | 0.2146(5) | 0.6106(4) | 2.9(3) |
| C34 | 0.9848(8) | 0.1527(6) | 0.6235(4) | 4.0(3) |
| C35 | 0.9834(8) | 0.0944(6) | 0.6770(4) | 3.7(3) |
| C36 | 0.8868(8) | 0.0970(6) | 0.7172(4) | 3.6(3) |
| C37 | 0.7922(7) | 0.1598(5) | 0.7047(4) | 2.9(3) |
| C38 | 0.5045(7) | 0.2268(5) | 0.5750(3) | 1.8(2) |
| C39 | 0.4698(7) | 0.1162(5) | 0.5619(3) | 2.3(2) |
| C40 | 0.3360(7) | 0.0582(5) | 0.5195(4) | 2.5(2) |
| C41 | 0.2362(7) | 0.1100(6) | 0.4886(4) | 3.0(3) |
| C42 | 0.2701(7) | 0.2189(6) | 0.5006(4) | 3.0(3) |
| C43 | 0.4027(7) | 0.2779(5) | 0.5440(4) | 2.6(2) |
| C44 | 0.6487(7) | 0.3555(5) | 0.7208(3) | 2.2(2) |
| C45 | 0.5377(7) | 0.4192(5) | 0.7141(3) | 2.0(2) |
| C46 | 0.5753(7) | 0.5259(5) | 0.7159(4) | 2.7(3) |
| C47 | 0.4735(9) | 0.5850(5) | 0.7123(4) | 3.8(3) |
| C48 | 0.3351(8) | 0.5355(6) | 0.7086(4) | 3.7(3) |
| C49 | 0.2960(7) | 0.4294(6) | 0.7070(4) | 3.1(3) |
| C50 | 0.3965(8) | 0.3711(5) | 0.7090(4) | 3.0(3) |

^aNumbers in parentheses are errors in the last significant digit.

Table 5.12. Final Thermal Parameters of Non-Hydrogen Atoms in
(BzPh₃P)[FeBr₄].[BzPh₃PBr], 7·BzPh₃Br.^a

| Atom | U ₁₁ | U ₂₂ | U ₃₃ | U ₁₂ | U ₁₃ | U ₂₃ |
|------|-----------------|-----------------|-----------------|-----------------|-----------------|-----------------|
| Br | 0.0303(4) | 0.0380(4) | 0.0317(4) | 0.0126(3) | 0.0084(3) | 0.0057(3) |
| Br1 | 0.0458(5) | 0.0371(4) | 0.0319(4) | 0.0187(4) | 0.0151(3) | 0.0146(3) |
| Br2 | 0.0419(5) | 0.0470(5) | 0.0293(4) | 0.0240(4) | 0.0163(3) | 0.0098(3) |
| Br3 | 0.0421(5) | 0.0244(4) | 0.0406(4) | 0.0070(3) | 0.0198(4) | 0.0045(3) |
| Br4 | 0.0252(4) | 0.0447(5) | 0.0450(5) | 0.0008(4) | -0.0021(3) | 0.0102(4) |
| Fe | 0.0223(6) | 0.0236(5) | 0.0253(5) | 0.0079(4) | 0.0062(4) | 0.0047(4) |
| P1 | 0.018(1) | 0.023(1) | 0.023(1) | 0.0045(8) | 0.0055(7) | 0.0037(7) |
| P2 | 0.023(1) | 0.023(1) | 0.025(1) | 0.0063(8) | 0.0048(8) | 0.0040(8) |
| C1 | 0.022(4) | 0.028(4) | 0.021(4) | 0.003(3) | 0.006(3) | 0.003(3) |
| C2 | 0.029(4) | 0.035(4) | 0.033(4) | 0.004(4) | 0.006(3) | -0.002(3) |
| C3 | 0.021(4) | 0.060(6) | 0.047(5) | 0.004(4) | 0.013(4) | 0.002(4) |
| C4 | 0.027(5) | 0.046(5) | 0.034(4) | -0.019(4) | 0.006(4) | 0.001(4) |
| C5 | 0.047(5) | 0.029(4) | 0.032(4) | -0.005(4) | 0.010(4) | 0.003(3) |
| C6 | 0.032(4) | 0.028(4) | 0.032(4) | 0.005(3) | 0.006(3) | 0.001(3) |
| C7 | 0.018(4) | 0.022(4) | 0.022(4) | 0.002(3) | 0.004(3) | 0.002(3) |
| C8 | 0.033(4) | 0.021(4) | 0.039(4) | 0.011(3) | 0.016(3) | 0.007(3) |
| C9 | 0.032(4) | 0.053(5) | 0.026(4) | 0.009(4) | 0.016(3) | 0.002(4) |
| C10 | 0.028(4) | 0.036(5) | 0.038(4) | 0.008(4) | 0.010(3) | -0.012(4) |
| C11 | 0.037(5) | 0.027(4) | 0.041(5) | 0.008(4) | 0.005(4) | 0.004(4) |
| C12 | 0.029(4) | 0.024(4) | 0.036(4) | 0.009(3) | 0.008(3) | 0.005(3) |
| C13 | 0.019(4) | 0.024(4) | 0.019(3) | 0.001(3) | 0.001(3) | 0.006(3) |
| C14 | 0.029(4) | 0.038(4) | 0.030(4) | 0.013(3) | 0.008(3) | 0.010(3) |
| C15 | 0.041(5) | 0.049(5) | 0.034(5) | 0.019(4) | 0.005(4) | 0.022(4) |
| C16 | 0.041(5) | 0.041(5) | 0.026(4) | -0.000(4) | 0.001(4) | 0.015(4) |
| C17 | 0.034(5) | 0.042(5) | 0.027(4) | 0.000(4) | 0.012(3) | 0.007(4) |
| C18 | 0.031(4) | 0.032(4) | 0.021(4) | 0.009(3) | 0.008(3) | 0.002(3) |
| C19 | 0.026(4) | 0.022(4) | 0.026(4) | 0.012(3) | 0.006(3) | 0.007(3) |
| C20 | 0.013(4) | 0.029(4) | 0.031(4) | 0.008(3) | 0.004(3) | 0.011(3) |
| C21 | 0.021(4) | 0.044(5) | 0.036(4) | 0.012(4) | 0.004(3) | 0.002(4) |
| C22 | 0.032(5) | 0.046(5) | 0.039(5) | 0.001(4) | -0.003(4) | -0.012(4) |

Table 5.12, contd. Final Thermal Parameters of Non-Hydrogen Atoms in
(BzPh₃P)[FeBr₄].[BzPh₃PBr], 7·BzPh₃Br.

| Atom | U ₁₁ | U ₂₂ | U ₃₃ | U ₁₂ | U ₁₃ | U ₂₃ |
|------|-----------------|-----------------|-----------------|-----------------|-----------------|-----------------|
| C23 | 0.023(4) | 0.042(5) | 0.056(5) | -0.001(4) | -0.004(4) | 0.010(4) |
| C24 | 0.026(4) | 0.041(5) | 0.050(5) | 0.002(4) | 0.013(4) | 0.012(4) |
| C25 | 0.027(4) | 0.036(4) | 0.027(4) | 0.009(3) | 0.008(3) | 0.004(3) |
| C26 | 0.034(4) | 0.021(4) | 0.027(4) | 0.005(3) | 0.008(3) | 0.004(3) |
| C27 | 0.036(4) | 0.030(4) | 0.029(4) | 0.005(3) | 0.003(3) | 0.001(3) |
| C28 | 0.050(5) | 0.048(5) | 0.034(4) | 0.010(4) | 0.020(4) | 0.019(4) |
| C29 | 0.059(6) | 0.025(4) | 0.054(5) | 0.015(4) | 0.035(5) | 0.015(4) |
| C30 | 0.041(5) | 0.030(4) | 0.050(5) | 0.004(4) | 0.016(4) | 0.007(4) |
| C31 | 0.034(4) | 0.029(4) | 0.028(4) | 0.007(3) | 0.006(3) | 0.005(3) |
| C32 | 0.023(4) | 0.020(4) | 0.028(4) | 0.010(3) | 0.005(3) | -0.003(3) |
| C33 | 0.039(5) | 0.033(4) | 0.048(5) | 0.015(4) | 0.023(4) | 0.005(4) |
| C34 | 0.040(5) | 0.054(6) | 0.063(6) | 0.017(4) | 0.027(4) | 0.001(5) |
| C35 | 0.032(5) | 0.037(5) | 0.063(6) | 0.018(4) | -0.001(4) | -0.005(4) |
| C36 | 0.049(5) | 0.044(5) | 0.046(5) | 0.024(4) | 0.006(4) | 0.017(4) |
| C37 | 0.034(5) | 0.041(5) | 0.042(4) | 0.022(4) | 0.010(4) | 0.012(4) |
| C38 | 0.023(4) | 0.027(4) | 0.021(3) | 0.004(3) | 0.010(3) | 0.006(3) |
| C39 | 0.022(4) | 0.036(4) | 0.030(4) | 0.008(3) | 0.005(3) | 0.007(3) |
| C40 | 0.031(4) | 0.025(4) | 0.036(4) | 0.002(3) | 0.012(3) | 0.004(3) |
| C41 | 0.024(4) | 0.039(5) | 0.038(4) | -0.003(4) | 0.005(3) | -0.005(4) |
| C42 | 0.024(4) | 0.043(5) | 0.041(5) | 0.012(4) | 0.000(4) | 0.002(4) |
| C43 | 0.032(4) | 0.025(4) | 0.036(4) | 0.008(3) | 0.003(3) | 0.002(3) |
| C44 | 0.030(4) | 0.025(4) | 0.028(4) | 0.009(3) | 0.007(3) | 0.007(3) |
| C45 | 0.028(4) | 0.027(4) | 0.022(4) | 0.013(3) | 0.005(3) | 0.003(3) |
| C46 | 0.028(4) | 0.029(4) | 0.039(4) | 0.005(3) | 0.002(3) | -0.005(3) |
| C47 | 0.052(6) | 0.023(4) | 0.064(6) | 0.021(4) | 0.006(4) | -0.000(4) |
| C48 | 0.041(5) | 0.049(5) | 0.044(5) | 0.022(4) | -0.002(4) | -0.004(4) |
| C49 | 0.024(4) | 0.049(5) | 0.040(5) | 0.013(4) | 0.005(3) | -0.003(4) |
| C50 | 0.038(5) | 0.038(4) | 0.041(5) | 0.014(4) | 0.015(4) | 0.009(4) |

^aNumbers in parentheses are errors in the last significant digit. The anisotropic temperature factors are of the form $\exp[-2\pi^2(U_{11}h^2a^2 + 2U_{12}hka^*b^* + U_{22}k^2b^2)]$.

Table 5.13. Selected Interatomic Distances (Å) and Angles (deg) for
 [(BzPh₃P)FeBr₄]·BzPh₃Br, 7·BzPh₃Br.^a

| <u>Coordination Sphere</u> | | | |
|--------------------------------------|------------|--------------|-------------|
| Br1- Fe | 2.340(1) | Br3- Fe | 2.334(1) |
| Br2- Fe | 2.325(1) | Br4- Fe | 2.336(1) |
| Br1- Fe- Br2 | 111.06(4) | Br2- Fe- Br3 | 110.36(4) |
| Br1- Fe- Br3 | 107.53(4) | Br2- Fe- Br4 | 107.46(4) |
| Br1- Fe- Br4 | 111.17(5) | Br3- Fe- Br4 | 109.27(4) |
| <u>BzPh₃P⁺</u> | | | |
| | <i>min</i> | <i>max</i> | <i>mean</i> |
| P-C | 1.782(6) | 1.804(6) | 1.792(6) |
| C-C | 1.520(8) | 1.521(8) | 1.521(8) |
| C=C | 1.365(9) | 1.404(9) | 1.384(9) |
| C-P-C | 107.6(3) | 111.9(3) | 109.5(3) |
| P-C-C | 113.7(4) | 124.3(5) | 119.4(5) |
| C-C-C | 118.6(6) | 121.2(6) | 120.0(6) |

^aNumbers in parentheses are errors in the last significant digit.

Table 5.14. Reaction Conditions for the Redox Titration Experiment

| Oxidant | Solvent | Medium | End-pt Reading |
|--|---|-------------------------------|----------------|
| $(\text{NH}_4)_2\text{Ce}(\text{NO}_3)_6$ in $0.72\text{NH}_2\text{SO}_4$ | H_2O | $0.72\text{NH}_2\text{SO}_4$ | titrator |
| | | $0.288\text{NH}_2\text{SO}_4$ | titrator |
| | CH_3CN 50% $\text{CH}_3\text{CN}/\text{H}_2\text{O}$ | $2.2\text{M H}_3\text{PO}_4$ | O-dianisidine |
| | | 0.1N KCl | titrator |
| | | 0.1NTBAP | titrator |
| $\text{K}_2\text{Cr}_2\text{O}_7$ in H_2O | H_2O | 0.1N TBAP | titrator |
| | | $10\% \text{HCl}$ | titrator |
| | | 2.4N HCl | titrator |
| | | 0.48N HCl | titrator |
| | | $0.72\text{N H}_2\text{SO}_4$ | titrator |
| I_2 with KI in H_2O | H_2O | | starch |

Table 5.15. Mössbauer Parameters of Solid and Solution Samples of **3** at 80 K and Zero Magnetic Field

| Sample | Site | δ (mm s ⁻¹) | ΔE_Q (mm s ⁻¹) | % |
|----------|---------|--------------------------------|------------------------------------|----|
| solid | Fe(II) | 1.297 | 2.752 | 30 |
| | Fe(III) | 0.525 | 0.480 | 70 |
| solution | Fe(II) | 1.297 | 2.742 | 31 |
| | Fe(III) | 0.534 | 0.550 | 69 |

Table 5.16. Results from the Redox Titration of Free TMRA and 3

| Oxidant | Solvent/medium | End-point | TMRA | 3 |
|--|--|---------------|-----------|-----------|
| $(\text{NH}_4)_2\text{Ce}(\text{NO}_3)_6/$ 0.72 N H_2SO_4 | $\text{H}_2\text{O}/2.2\text{MH}_3\text{PO}_4$ | o-dianisidine | 1.93 | 10.7, 9.9 |
| | $\text{CH}_3\text{CN}/0.1\text{MTBAP}$ | titrator | 2.00,2.00 | 8.4, 8.2 |
| $\text{K}_2\text{Cr}_2\text{O}_7$ in H_2O | $\text{H}_2\text{O}/10\% \text{HCl}$ | titrator | 1.91,1.93 | 2.03,2.09 |
| I_3^- in H_2O | H_2O | starch | 1.97,1.95 | 9.1, 9.9 |

Table 5.17. Mössbauer Parameters for the Solution Samples of Analogous Ascorbate Complexes of **3**

| Sample | Fe(II) | | | Fe(III) | | |
|--|-----------------|---------------------|------|-----------------|---------------------|------|
| | δ (mm/s) | ΔE_Q (mm/s) | % | δ (mm/s) | ΔE_Q (mm/s) | % |
| 5 + 2NaAA | 1.390 | 3.246 | 66.8 | 0.513 | 0.613 | 33.2 |
| Fe ²⁺ +1.5NaAA + O ₂ | 1.364 | 3.135 | 74.4 | 0.523 | 0.522 | 25.6 |
| Fe ²⁺ +10NaAA + O ₂ ^a | 1.34 | 2.94 | 77 | 0.36 | 0.29 | 23 |

^aSee ref. 23.

Table 5.18 Experimental Details of the X-ray Diffraction Study of
 $[\text{Fe}_4(\text{H}_2\text{O})_4(\text{TMRA})_8] \cdot 1.5\text{CH}_3\text{COCH}_3 \cdot \text{H}_2\text{O}, 8 \cdot 1.5\text{CH}_3\text{COCH}_3 \cdot \text{H}_2\text{O}^{\text{a}}$

| compound | 8 |
|---|---|
| formula | $\text{Fe}_4\text{O}_{30.5}\text{C}_{76.5}\text{H}_{117}$ |
| formula weight, g mol^{-1} | 1748.13 |
| crystal system | triclinic |
| space group | $\text{P}\bar{1}$ |
| $a, \text{\AA}$ | 13.521(3) |
| $b, \text{\AA}$ | 13.673(2) |
| $c, \text{\AA}$ | 13.234(2) |
| $\alpha, ^\circ$ | 97.88(1) |
| $\beta, ^\circ$ | 93.94(2) |
| $\gamma, ^\circ$ | 106.31(2) |
| $V, \text{\AA}^3$ | 2311 |
| Z | 1 |
| temperature, $^\circ\text{C}$ | -78 |
| $\rho_{\text{calcd}}, \text{g cm}^{-3}$ | 1.256 |
| linear absorption coefficient, cm^{-1} | 6.90 |
| 2θ range | $3^\circ \leq 2\theta \leq 46^\circ$ |
| total no. of data collected | 7016 |
| R_{merge} | 0.036 |
| no. of independent data | 6405 |

Table 5.18, contd. Experimental Details of the X-ray Diffraction Study of
[Fe₄(H₂O)₄(TMRA)₈].1.5CH₃COCH₃·H₂O,
8·1.5CH₃COCH₃·H₂O.

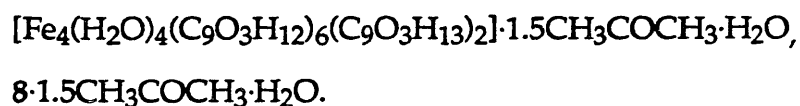
| compound | 8 |
|--|--------|
| no. of unique data with $F > 6\sigma(F)$ | 4067 |
| no. of variables | 543 |
| R | 0.0555 |
| R _w | 0.0595 |
| p | 0.03 |

^a See footnotes of Table 5.6.

Table 5.19. Final Positional and Equivalent Isotropic Thermal Parameters of Non-Hydrogen Atoms in $[\text{Fe}_4(\text{H}_2\text{O})_4(\text{C}_9\text{O}_3\text{H}_{12})_6(\text{C}_9\text{O}_3\text{H}_{13})_2] \cdot 1.5\text{CH}_3\text{COCH}_3 \cdot \text{H}_2\text{O}, 81.5\text{CH}_3\text{COCH}_3 \cdot \text{H}_2\text{O}^{\text{a}}$

| Atom ^b | x | y | z | B(eq) |
|-------------------|-------------|------------|------------|---------|
| Fe1 | 0.10610(8) | 0.41012(7) | 0.30388(7) | 1.38(4) |
| Fe2 | -0.10544(7) | 0.41535(7) | 0.45844(7) | 1.28(3) |
| O1S | 0.8537(5) | 0.4206(4) | 0.9467(4) | 3.8(2) |
| O2 | 0.1682(3) | 0.5457(3) | 0.4043(3) | 1.4(2) |
| O3S | 0.6222(5) | 0.4822(6) | 0.4632(5) | 8.2(4) |
| O3 | 0.3311(4) | 0.6046(4) | 0.2479(4) | 3.2(2) |
| O4 | 0.2333(3) | 0.4202(3) | 0.2409(3) | 1.6(2) |
| O4S | 0.383(2) | 0.445(2) | 0.986(2) | 10.0(5) |
| O5 | 0.1808(4) | 0.2213(4) | 0.0914(4) | 3.1(2) |
| O6 | 0.4287(4) | 0.4327(4) | 0.3575(4) | 4.1(2) |
| O7 | 0.1424(4) | 0.3274(3) | 0.3986(3) | 1.8(2) |
| O8 | 0.0281(4) | 0.3480(4) | 0.7264(4) | 3.0(2) |
| O10 | 0.0334(3) | 0.4379(3) | 0.5375(3) | 1.3(2) |
| O13 | -0.0545(3) | 0.3639(3) | 0.3320(3) | 1.5(2) |
| O14 | -0.2894(4) | 0.2402(4) | 0.2747(4) | 2.6(2) |
| O15 | 0.0474(4) | 0.2843(3) | 0.1913(3) | 1.9(2) |
| O16 | -0.2368(3) | 0.4185(3) | 0.3817(3) | 2.0(2) |
| O19 | -0.1610(4) | 0.2706(3) | 0.4908(3) | 2.1(2) |
| O100 | 0.0582(4) | 0.5032(3) | 0.2122(3) | 2.0(2) |
| C1S | 0.8423(6) | 0.4791(6) | 1.0199(6) | 2.5(3) |
| C1 | 0.1264(5) | 0.3131(5) | 0.4906(5) | 1.5(2) |
| C2S | 0.8819(7) | 0.5928(6) | 1.0250(6) | 3.8(3) |
| C2 | 0.1556(6) | 0.2272(5) | 0.5346(5) | 2.2(3) |
| C3 | 0.1401(6) | 0.2500(5) | 0.6510(5) | 2.5(3) |
| C3S | 0.7894(7) | 0.4382(6) | 1.1069(6) | 3.5(3) |
| C4S | 0.474(2) | 0.491(3) | 1.002(3) | 6.7(6) |
| C4 | 0.0738(6) | 0.3250(5) | 0.6515(5) | 2.1(3) |
| C5 | 0.0769(5) | 0.3624(5) | 0.5584(5) | 1.6(2) |

Table 5. 19, contd. Final Positional and Equivalent Isotropic Thermal
Parameters of Non-Hydrogen Atoms in



| Atom | x | y | z | B(eq) |
|------|------------|-----------|-----------|---------|
| C5S | 0.517(4) | 0.578(4) | 1.088(4) | 14(2) |
| C6 | -0.2254(5) | 0.3618(5) | 0.6196(5) | 1.6(2) |
| C7 | 0.2955(6) | 0.6625(5) | 0.3126(5) | 2.2(3) |
| C8 | 0.3422(6) | 0.7795(5) | 0.3198(6) | 2.8(3) |
| C8S | 0.548(4) | 0.455(3) | 0.934(3) | 11(2) |
| C9 | -0.2815(6) | 0.1759(5) | 0.5986(6) | 2.8(3) |
| C10 | -0.2170(5) | 0.2706(5) | 0.5639(5) | 1.8(2) |
| C11 | 0.2884(5) | 0.3507(5) | 0.2279(5) | 1.6(2) |
| C12 | 0.2650(6) | 0.2627(5) | 0.1579(5) | 2.1(3) |
| C13 | 0.3447(6) | 0.2048(5) | 0.1607(6) | 2.6(3) |
| C14 | 0.4339(6) | 0.2799(6) | 0.2401(6) | 2.5(3) |
| C15 | 0.3857(6) | 0.3626(6) | 0.2847(5) | 2.4(3) |
| C16 | -0.1062(5) | 0.2777(5) | 0.2620(5) | 1.5(2) |
| C17 | -0.2125(6) | 0.2224(5) | 0.2398(5) | 2.0(3) |
| C18 | -0.2236(6) | 0.1255(5) | 0.1593(5) | 2.2(3) |
| C19 | -0.1132(5) | 0.1442(5) | 0.1196(5) | 1.9(3) |
| C20 | -0.0503(6) | 0.2386(5) | 0.1932(5) | 1.7(2) |
| C21 | 0.0779(7) | 0.1264(6) | 0.4771(6) | 3.6(4) |
| C22 | 0.2652(7) | 0.2260(6) | 0.5138(6) | 3.6(3) |
| C31 | 0.0896(9) | 0.1563(7) | 0.6992(7) | 5.3(5) |
| C32 | 0.2415(8) | 0.3102(8) | 0.7171(6) | 4.9(4) |
| C81 | -0.4616(8) | 0.1955(8) | 0.640(1) | 7.4(5) |
| C82 | 0.336(1) | 0.8087(8) | 0.2170(8) | 11.9(8) |
| C91 | -0.206(1) | 0.125(1) | 0.646(1) | 11.0(9) |
| C92 | -0.348(1) | 0.1013(8) | 0.5086(9) | 9.8(6) |
| C131 | 0.2944(7) | 0.1011(6) | 0.1957(7) | 4.7(4) |
| C132 | 0.3752(7) | 0.1808(7) | 0.0522(7) | 4.2(4) |
| C141 | 0.4735(6) | 0.2309(6) | 0.3252(6) | 3.5(3) |

Table 5. 19, contd. Final Positional and Equivalent Isotropic Thermal Parameters of Non-Hydrogen Atoms in
 $[\text{Fe}_4(\text{H}_2\text{O})_4(\text{C}_9\text{O}_3\text{H}_{12})_6(\text{C}_9\text{O}_3\text{H}_{13})_2] \cdot 1.5\text{CH}_3\text{COCH}_3 \cdot \text{H}_2\text{O},$
 $8 \cdot 1.5\text{CH}_3\text{COCH}_3 \cdot \text{H}_2\text{O}.$

| Atom | x | y | z | B(eq) |
|------|------------|-----------|-----------|--------|
| C142 | 0.5283(6) | 0.3364(6) | 0.1914(6) | 3.1(3) |
| C181 | -0.2530(6) | 0.0333(5) | 0.2178(6) | 3.3(3) |
| C182 | -0.3140(6) | 0.1145(6) | 0.0773(6) | 3.7(3) |
| C191 | -0.0651(6) | 0.0557(5) | 0.1243(6) | 3.3(3) |
| C192 | -0.1115(7) | 0.1688(6) | 0.0099(6) | 3.5(3) |

^aNumbers in parentheses are errors in the last significant digit. ^bSee Figure 5.12 for atom labelling scheme.

Table 5. 20. Final Thermal Parameters of Non-Hydrogen Atoms in
 $[\text{Fe}_4(\text{H}_2\text{O})_4(\text{C}_9\text{O}_3\text{H}_{12})_6(\text{C}_9\text{O}_3\text{H}_{13})_2] \cdot 1.5\text{CH}_3\text{COCH}_3 \cdot \text{H}_2\text{O}$,
 $8 \cdot 1.5\text{CH}_3\text{COCH}_3 \cdot \text{H}_2\text{O}$.^a

| Atom ^b | U ₁₁ | U ₂₂ | U ₃₃ | U ₁₂ | U ₁₃ | U ₂₃ |
|-------------------|-----------------|-----------------|-----------------|-----------------|-----------------|-----------------|
| Fe1 | 0.0197(6) | 0.0151(5) | 0.0186(5) | 0.0071(4) | 0.0033(4) | 0.0007(4) |
| Fe2 | 0.0180(6) | 0.0117(5) | 0.0187(5) | 0.0050(4) | 0.0036(4) | 0.0001(4) |
| O1S | 0.071(5) | 0.042(3) | 0.039(3) | 0.025(3) | 0.020(3) | 0.012(3) |
| O2 | 0.023(3) | 0.011(2) | 0.019(2) | 0.005(2) | 0.004(2) | 0.001(2) |
| O3S | 0.043(5) | 0.180(8) | 0.075(5) | 0.064(5) | -0.019(4) | -0.076(5) |
| O3 | 0.050(4) | 0.022(3) | 0.050(3) | 0.005(3) | 0.030(3) | 0.003(3) |
| O4 | 0.022(3) | 0.015(2) | 0.029(3) | 0.011(2) | 0.008(2) | 0.003(2) |
| O4S | 0.126(7) | | | | | |
| O5 | 0.028(3) | 0.040(3) | 0.045(3) | 0.015(3) | -0.003(3) | -0.017(3) |
| O6 | 0.032(4) | 0.061(4) | 0.052(4) | 0.022(3) | -0.010(3) | -0.031(3) |
| O7 | 0.028(3) | 0.025(3) | 0.021(3) | 0.015(2) | 0.008(2) | 0.005(2) |
| O8 | 0.057(4) | 0.051(3) | 0.026(3) | 0.041(3) | 0.019(3) | 0.016(2) |
| O10 | 0.018(3) | 0.010(2) | 0.022(2) | 0.007(2) | 0.001(2) | 0.003(2) |
| O13 | 0.017(3) | 0.013(2) | 0.023(2) | 0.001(2) | 0.001(2) | -0.005(2) |
| O14 | 0.016(3) | 0.033(3) | 0.049(3) | 0.010(2) | 0.006(3) | -0.009(3) |
| O15 | 0.025(3) | 0.023(3) | 0.025(3) | 0.009(2) | 0.008(2) | -0.005(2) |
| O16 | 0.021(3) | 0.024(3) | 0.028(3) | 0.006(2) | -0.005(2) | -0.003(2) |
| O19 | 0.034(3) | 0.013(2) | 0.031(3) | 0.004(2) | 0.008(2) | 0.002(2) |
| O100 | 0.033(3) | 0.029(3) | 0.021(2) | 0.021(2) | 0.008(2) | 0.003(2) |
| C1S | 0.030(5) | 0.038(5) | 0.033(4) | 0.012(4) | 0.004(4) | 0.019(4) |
| C1 | 0.018(4) | 0.013(3) | 0.026(4) | 0.003(3) | -0.000(3) | 0.005(3) |
| C2S | 0.072(7) | 0.044(5) | 0.028(4) | 0.013(5) | 0.007(4) | 0.009(4) |
| C2 | 0.041(5) | 0.029(4) | 0.023(4) | 0.022(4) | 0.009(3) | 0.006(3) |
| C3 | 0.052(6) | 0.031(4) | 0.026(4) | 0.027(4) | 0.004(4) | 0.019(3) |
| C3S | 0.058(6) | 0.040(5) | 0.044(5) | 0.020(4) | 0.024(5) | 0.016(4) |
| C4S | 0.084(8) | | | | | |
| C4 | 0.035(5) | 0.021(4) | 0.027(4) | 0.015(3) | 0.006(4) | 0.005(3) |
| C5 | 0.022(4) | 0.017(4) | 0.021(4) | 0.008(3) | -0.003(3) | 0.003(3) |
| C5S | 0.18(3) | | | | | |
| C6 | 0.023(4) | 0.011(3) | 0.022(4) | 0.002(3) | -0.001(3) | -0.002(3) |

Table 5. 20, contd. Final Thermal Parameters of Non-Hydrogen Atoms in
 $[\text{Fe}_4(\text{H}_2\text{O})_4(\text{C}_9\text{O}_3\text{H}_{12})_6(\text{C}_9\text{O}_3\text{H}_{13})_2] \cdot 1.5\text{CH}_3\text{COCH}_3 \cdot \text{H}_2\text{O}$,
 $8 \cdot 1.5\text{CH}_3\text{COCH}_3 \cdot \text{H}_2\text{O}$.

| Atom | U ₁₁ | U ₂₂ | U ₃₃ | U ₁₂ | U ₁₃ | U ₂₃ |
|------|-----------------|-----------------|-----------------|-----------------|-----------------|-----------------|
| C7 | 0.034(5) | 0.015(4) | 0.033(4) | 0.002(3) | 0.015(4) | 0.003(3) |
| C8 | 0.046(6) | 0.018(4) | 0.041(5) | -0.001(4) | 0.020(4) | 0.012(3) |
| C8S | 0.30(7) | 0.10(3) | 0.09(2) | 0.14(4) | 0.13(4) | 0.06(2) |
| C9 | 0.045(6) | 0.017(4) | 0.044(5) | 0.004(4) | 0.017(4) | 0.005(3) |
| C10 | 0.023(4) | 0.025(4) | 0.019(4) | 0.006(3) | 0.005(3) | 0.001(3) |
| C11 | 0.021(4) | 0.013(4) | 0.022(4) | 0.002(3) | 0.002(3) | -0.001(3) |
| C12 | 0.026(5) | 0.025(4) | 0.032(4) | 0.010(3) | 0.005(4) | 0.004(3) |
| C13 | 0.035(5) | 0.024(4) | 0.040(4) | 0.015(4) | 0.008(4) | -0.006(3) |
| C14 | 0.030(5) | 0.033(4) | 0.037(4) | 0.016(4) | 0.008(4) | 0.003(4) |
| C15 | 0.023(5) | 0.038(5) | 0.026(4) | 0.010(4) | -0.001(4) | -0.003(4) |
| C16 | 0.026(4) | 0.015(3) | 0.017(3) | 0.006(3) | 0.004(3) | 0.000(3) |
| C17 | 0.026(5) | 0.016(4) | 0.028(4) | -0.000(3) | -0.005(3) | 0.003(3) |
| C18 | 0.027(5) | 0.019(4) | 0.033(4) | 0.007(3) | -0.003(3) | -0.010(3) |
| C19 | 0.026(4) | 0.015(4) | 0.028(4) | 0.004(3) | 0.000(3) | -0.002(3) |
| C20 | 0.024(5) | 0.019(4) | 0.022(4) | 0.008(3) | 0.003(3) | 0.003(3) |
| C21 | 0.061(7) | 0.024(4) | 0.054(5) | 0.015(4) | 0.008(5) | 0.006(4) |
| C22 | 0.048(6) | 0.056(6) | 0.045(5) | 0.035(5) | 0.014(4) | 0.006(4) |
| C31 | 0.11(1) | 0.066(7) | 0.061(6) | 0.070(7) | 0.046(6) | 0.045(5) |
| C32 | 0.085(8) | 0.093(8) | 0.032(5) | 0.070(7) | -0.001(5) | 0.002(5) |
| C81 | 0.027(6) | 0.065(7) | 0.17(1) | 0.001(5) | 0.015(7) | -0.029(7) |
| C82 | 0.37(2) | 0.035(6) | 0.063(7) | 0.06(1) | 0.09(1) | 0.024(6) |
| C91 | 0.14(1) | 0.11(1) | 0.26(2) | 0.09(1) | 0.13(1) | 0.16(1) |
| C92 | 0.14(1) | 0.072(8) | 0.084(8) | -0.079(8) | 0.066(8) | -0.041(6) |
| C131 | 0.063(7) | 0.024(5) | 0.085(7) | 0.008(4) | 0.002(6) | 0.005(5) |
| C132 | 0.046(6) | 0.059(6) | 0.055(6) | 0.027(5) | 0.009(5) | -0.016(5) |
| C141 | 0.034(5) | 0.056(6) | 0.051(5) | 0.023(4) | 0.010(4) | 0.012(4) |
| C142 | 0.039(5) | 0.034(5) | 0.048(5) | 0.019(4) | 0.005(4) | -0.003(4) |
| C181 | 0.052(6) | 0.018(4) | 0.052(5) | 0.010(4) | 0.014(4) | -0.003(4) |
| C182 | 0.035(5) | 0.043(5) | 0.054(5) | 0.016(4) | -0.015(4) | -0.024(4) |
| C191 | 0.034(5) | 0.024(4) | 0.067(6) | 0.013(4) | 0.016(4) | -0.004(4) |

Table 5. 20, contd. Final Thermal Parameters of Non-Hydrogen Atoms in
 $[\text{Fe}_4(\text{H}_2\text{O})_4(\text{C}_9\text{O}_3\text{H}_{12})_6(\text{C}_9\text{O}_3\text{H}_{13})_2] \cdot 1.5\text{CH}_3\text{COCH}_3 \cdot \text{H}_2\text{O}$,
 $8 \cdot 1.5\text{CH}_3\text{COCH}_3 \cdot \text{H}_2\text{O}$.

| Atom | U_{11} | U_{22} | U_{33} | U_{12} | U_{13} | U_{23} |
|------|----------|----------|----------|-----------|-----------|-----------|
| C192 | 0.054(6) | 0.031(4) | 0.034(5) | -0.002(4) | -0.000(4) | -0.008(4) |

^aNumbers in parentheses are errors in the last significant digit. The anisotropic temperature factors are of the form $\exp[-2\pi^2(U_{11}h^2a^2 + 2U_{12}hka^*b^* + \dots)]$. ^bSee Figure 5.12 for atom labelling scheme.

Table 5.21. Selected Interatomic Distances (Å) and Angles (deg) for
 $[\text{Fe}_4(\text{H}_2\text{O})_4(\text{C}_9\text{O}_3\text{H}_{12})_6(\text{C}_9\text{O}_3\text{H}_{13})_2] \cdot 1.5\text{CH}_3\text{COCH}_3 \cdot \text{H}_2\text{O}$,
 $8 \cdot 1.5\text{CH}_3\text{COCH}_3 \cdot \text{H}_2\text{O}$.^a

| <u>Coordination Sphere</u> | | | |
|----------------------------|------------|---------------|-------------|
| Fe1- O2 | 2.051(4) | Fe2- O2 | 2.122(4) |
| Fe1- O4 | 1.941(4) | Fe2- O10 | 2.008(4) |
| Fe1- O7 | 1.925(4) | Fe2- O10 | 1.960(4) |
| Fe1- O13 | 2.158(4) | Fe2- O13 | 1.969(4) |
| Fe1- O15 | 2.044(4) | Fe2- O16 | 2.000(5) |
| Fe1- O100 | 2.071(4) | Fe2- O19 | 2.027(4) |
| O2- Fe1- O4 | 93.7(2) | O2- Fe2- O10 | 90.8(2) |
| O2- Fe1- O7 | 93.5(2) | O2- Fe2- O10 | 89.3(2) |
| O2- Fe1- O13 | 103.4(2) | O2- Fe2- O13 | 174.0(2) |
| O2- Fe1- O15 | 173.8(2) | O2- Fe2- O16 | 87.5(2) |
| O2- Fe1- O100 | 84.0(2) | O2- Fe2- O19 | 82.2(2) |
| O4- Fe1- O7 | 91.6(2) | O10- Fe2- O10 | 75.4(2) |
| O4- Fe1- O13 | 162.3(2) | O10- Fe2- O13 | 90.4(2) |
| O4- Fe1- O15 | 83.3(2) | O10- Fe2- O16 | 170.5(2) |
| O4- Fe1- O100 | 93.5(2) | O10- Fe2- O19 | 92.8(2) |
| O7- Fe1- O13 | 92.0(2) | O10- Fe2- O13 | 96.7(2) |
| O7- Fe1- O15 | 92.1(2) | O10- Fe2- O16 | 95.2(2) |
| O7- Fe1- O100 | 174.5(2) | O10- Fe2- O19 | 165.4(2) |
| O13- Fe1- O15 | 79.3(2) | O13- Fe2- O16 | 92.3(2) |
| O13- Fe1- O100 | 83.9(2) | O13- Fe2- O19 | 91.8(2) |
| O15- Fe1- O100 | 90.8(2) | O16- Fe2- O19 | 96.3(2) |
| Fe1- O2- Fe2 | 123.8(2) | Fe2- O10- Fe2 | 104.6(2) |
| Fe1- O13- Fe2 | 123.7(2) | | |
| <u>Ligand, TMRA</u> | | | |
| | <i>min</i> | <i>max</i> | <i>mean</i> |
| C=O | 1.242(8) | 1.242(8) | 1.242(8) |

Table 5.21, contd. Selected Interatomic Distances (Å) and Angles (deg) for
 $[\text{Fe}_4(\text{H}_2\text{O})_4(\text{C}_9\text{O}_3\text{H}_{12})_6(\text{C}_9\text{O}_3\text{H}_{13})_2] \cdot 1.5\text{CH}_3\text{COCH}_3 \cdot \text{H}_2\text{O}$,
 $8 \cdot 1.5\text{CH}_3\text{COCH}_3 \cdot \text{H}_2\text{O}$.

| <u>Ligand, TMRA, contd</u> | | | |
|------------------------------------|------------|------------|-------------|
| | <i>min</i> | <i>max</i> | <i>mean</i> |
| C-O (Central) ^b | 1.363(7) | 1.363(7) | 1.363(7) |
| C-O (Terminal) | 1.325(8) | 1.325(8) | 1.325(8) |
| C-C | 1.51(1) | 1.56(1) | 1.53(1) |
| C=C | 1.358(9) | 1.358(9) | 1.358(9) |
| C-C ^c | 1.426(9) | 1.426(9) | 1.426(9) |
| Fe-O-C | 129.4(4) | 129.4(4) | 129.4(4) |
| C-C-C | 108.2(6) | 114.4(6) | 111.1(6) |
| C-C-C ^d | 102.5(5) | 103.4(6) | 103.0(6) |
| C _{Me} -C-C _{Me} | 107.1(6) | 107.6(6) | 107.4(6) |
| <u>Ligand, TMRASO</u> | | | |
| | <i>min</i> | <i>max</i> | <i>mean</i> |
| C=O | 1.236(8) | 1.295(8) | 1.216(8) |
| C-O (Terminal) ^b | 1.372(7) | 1.375(7) | 1.373(7) |
| C-O (Central) | 1.269(7) | 1.296(8) | 1.283(8) |
| C-C | 1.47(1) | 1.51(1) | 1.53(1) |
| C-C ^c | 1.355(9) | 1.413(9) | 1.388(9) |
| C=C | 1.370(9) | 1.396(9) | 1.379(9) |
| Fe-O-C | 129.4(4) | 129.4(4) | 129.4(4) |
| C-C-C | 108.4(6) | 114.2(6) | 110.9(6) |
| C-C-C ^d | 101.6(5) | 104.4(5) | 102.9(5) |
| C _{Me} -C-C _{Me} | 107.6(6) | 108.8(9) | 108.2(9) |

Table 5.21, cond. Selected Interatomic Distances (Å) and Angles (deg) for
 $[\text{Fe}_4(\text{H}_2\text{O})_4(\text{C}_9\text{O}_3\text{H}_{12})_6(\text{C}_9\text{O}_3\text{H}_{13})_2] \cdot 1.5\text{CH}_3\text{COCH}_3 \cdot \text{H}_2\text{O}$,
 $8 \cdot 1.5\text{CH}_3\text{COCH}_3 \cdot \text{H}_2\text{O}$.

| | <u>Solvent</u> | | |
|-------|----------------|------------|-------------|
| | <i>min</i> | <i>max</i> | <i>mean</i> |
| O-C | 1.21(3) | 1.216(8) | 1.21(3) |
| C-C | 1.48(7) | 1.53(5) | 1.50(7) |
| O-C-C | 119(4) | 122(4) | 121(4) |
| C-C-C | 118.6(7) | 119(3) | 119(3) |

^aNumbers in parentheses are errors in the last significant digit(s). See Figure 5.12 for atom labelling scheme. ^bSee section I of this chapter for definitions of terminal versus central hydroxyl group. ^cThis is the C-C on the five membered ring involved in the conjugation system in the ene-diol fragment. ^dThis is the angle around the carbon atom that is not involved in the conjugated enediol fragment.

Table 5.22. Assignment of the Oxidation States for Ligands in **3**

| Ligand ^a | C-O (c, Å) ^b | C-O (s, Å) ^b | Δ (Å) | C=C (Å) | Oxidation State ^c |
|---------------------|-------------------------|-------------------------|--------------|----------|------------------------------|
| C11 - C15 | 1.363 | 1.325 | 0.038 | 1.358(9) | fully reduced |
| C1 - C5 | 1.373 | 1.283 | 0.090 | 1.370(9) | semiquinone |
| C6 - C10 | 1.375 | 1.269 | 0.106 | 1.396(9) | semiquinone |
| C16 - C20 | 1.372 | 1.296 | 0.076 | 1.370(9) | semiquinone |

^aSee Figure 5.5b for atom labelling scheme. ^bc = central; s = side. ^cSee Scheme 5.5 for definitions of fully reduced and semiquinone type of ligands.

Appendix
Manometric Measurement of Oxygen Consumption by the
Catalytic Alkane Oxidation System

Experimental

A home-made manometer was used in this study. The apparatus, designed for the accurate measurement of gas intake, was calibrated assuming the ideal gas law by using a known amount of gas. At a certain temperature, each reading on the U-tube (mm Hg) corresponds to a particular pressure which, in turn, corresponds to a certain amount of gas in terms of number of moles inside of the system. In a typical experiment, the apparatus except for the reaction flask was completely evacuated and the solution in the reaction flask was then degassed at least twice to remove any gases dissolved in the solution. After letting a certain amount of O₂ into the system, the reaction was allowed to proceed. Upon the completion of the reaction, the system was allowed to stand for two to three hours to reach the full equilibrium, depending on the vapor pressure of the solvent. A reading was taken at this point. Subtraction of this reading from that of a control run in which the above experiment was carried out under exactly the same condition with solvent alone gave the amount of the O₂ consumed by the reactant. [Ir(CO)(Ph₃P)₂I] (**1**) was used as a standard to examine the accuracy of the system. It was synthesized according to a literature procedure and characterized by ³¹P NMR and IR spectroscopy.¹ Oxidation of this compound was carried out in toluene, using pure O₂ from the cylinder. The reaction was completed within two hours. All measurements were made at 25°± 1°C.

Methylbenzoate was chosen as the solvent in which to measure oxygen uptake of the (Et₄N)₂[Fe₂OCl₆]/TMRA system. This solvent is inert under the reaction conditions and has a low vapor pressure. Adamantane was used as the substrate. A control run was carried out by using only TMRA in methylbenzoate. The result obtained in the control run accounts for the

amount of oxygen consumed by the autoxidation of TMRA and dissolved in the solvent.

Results and Discussion

MMO is a mixed-function oxygenase that incorporates only one of the oxygen atoms of dioxygen into the substrate and uses the other one to produce water, as indicated in equation 4.1. This characteristic can be established for any model system by measuring the oxygen uptake during the reaction. In a monooxygenase-type of oxidation, one mole of dioxygen consumed should give one mole of oxygen incorporated into product and one mole of water.

The reliability of the manometer was examined by using **1** as a standard. This complex binds one equivalent of molecular oxygen irreversibly in benzene.¹ In an experiment, toluene was used in place of benzene because the higher vapor pressure of benzene results in unstable manometer readings. Table A.1 summarizes the experimental results. Compound **1** is extremely air-sensitive. Even though it was kept in the dry box, prolonged storage caused partial oxidation which resulted in the discrepancy between different runs in Table A.1. For the catalytic oxidation reaction, the amount of oxygen consumed by oxidation of substrate was obtained by subtracting the amount of oxygen used for the autoxidation of the reductant from the total amount of oxygen consumption. In a preliminary run for the oxidation reaction of adamantane, 2.55×10^{-2} mmol of dioxygen were consumed by the oxidation of the substrate while only 8.63×10^{-3} mmol of oxidation products were formed. Only 34% of the oxygen consumed was incorporated into the substrate to form the products. Even though this result

is preliminary, it is unlikely that our system operates by a dioxygenase mechanism which should yield two moles of products per mole of oxygen consumed.

References

- (1) McGinnety, J. A.; Doedens, R. J.; Ibers, J. A. *Inorg. Chem.* 1967, 6, 2234.

Table A.1. Manometric Measurements of Oxygen Uptakes by the Oxygen Binding Reaction of **1**.^a

| Run No. | 1 (mg/mmol) | O ₂ used (mmol) | %Conversion |
|-----------|--------------------|----------------------------|-------------|
| XF-IV-95 | 30.6/0.0351 | 0.0350 | 100 |
| XF-IV-107 | 30.0/0.0344 | 0.0310 | 90 |
| XF-IV-109 | 27.6/0.0317 | 0.0237 | 75 |

^aThe reaction was carried out in toluene at 25 °C.